Dynamics in polymer blends and polymer-solvent blends close to the glass transition

Grégoire Julien

THÈSE DE DOCTORAT DE
l'UNIVERSITÉ CLAUDE BERNARD LYON I

Spécialité

Physique

Ecole doctorale matériaux de Lyon

Présentée par

Grégoire JULIEN

Pour obtenir le grade de

Docteur de l'université Claude Bernard Lyon I

Sujet de la thèse :

Dynamics in polymer blends and polymer-solvent blends close to the glass transition

Soutenue le 09 Octobre 2014 devant le jury composé de :

M. Jörg Baschnagel	Rapporteur
M. Thierry Biben	Examinateur
M. Jean-Yves Delannoy	Examinateur
M. Masao Doi	Examinateur
M. Jean-François Joanny	Examinateur
M. Albert Johner	Rapporteur
M. Didier Long	Directeur de thèse

Remerciements

Tout d'abord, je remercie Ludovic Odoni, Jean-Yves Delannoy et Didier Long pour m'avoir accueilli au sein du Laboratoire Polymères et Matériaux Avancés qu'ils dirigent. Je souhaiterais tout particulièrement exprimer ma gratitude à Didier Long, mon directeur de thèse, pour m'avoir formé et appris la physique des polymères et des systèmes vitreux. Son approche de la physique et de la théorie de la matière molle m'ont énormément apporté en maturité scientifique. Je retiendrai aussi nos discussions politiques et économiques. Enfin, un grand merci à Messieurs J. Baschnagel et A. Johner pour avoir accepté d'être rapporteur de cette thèse. Merci également aux autres membres du jury, T. Biben, J-F. Joanny et M. Doi pour avoir accepté d'être examinateurs.
Je voudrais remercier également le service d'Informatique Scientifique et Technique de Solvay qui m'a permis d'avoir accès aux ressources numériques nécessaires à l'exécution de ce travail. Merci à Philippe pour toutes nos pauses café et Anthony pour nos discussions sur la physico-chimie des polymères. Je voudrais aussi remercier tous les membres permanents et administratifs du laboratoire pour leur accueil et soutient. Un grand merci aux thèsards et post-docs du laboratoires à qui je souhaite tous mes vœux de réussite pour la suite. Enfin, merci au CNRS et Solvay pour leur engagement financier dans ce projet de recherche.

Mes remerciements vont aussi à ma famille et mes amis qui, avec cette question récurrente, « est-ce que tu as une date de soutenance ? », bien qu'angoissante en période de doutes, m'ont permis de ne jamais dévier de mon objectif final. Enfin, merci du fond cœur à Nastassja, mon Amie, qui m'a soutenue au quotidien et grâce à qui j'ai pu garder confiance et patience tout au long de ces années. Je lui dédie cette thèse.

Abstract

We propose a model for describing the dynamics in polymer blends or polymer-solvent blends close to the glass transition. In the case of polymer blends, we focus on situations where at least one of the species corresponds to molecular weight below the entanglement threshold. Our model incorporates the strong heterogeneous nature of the dynamics close to T_g on a scale of dynamical heterogeneities of size ξ of order 3-5 nm. Dynamical heterogeneities are enhanced in blends as compared to pure polymers. We assume that spatial distributions of relaxation times are the consequence of concentration fluctuations. We apply this model to study interdiffusion of both components close to and below T_g.

We have proposed a Gibbs free energy model (which is an extension of the Flory-Huggins model) for compressible blends, which allows for calculating the driving forces. The spatial dynamics follows then from an Onsager like description. The evolution of concentrations is calculated by Langevin equations on the scale of dynamical heterogeneities. This model takes into account a "facilitation mechanism" which describes the relaxation of slow dynamic heterogeneities when surrounded by faster subunits as due to free volume diffusion or diffusion of different components. This model is solved on a 2D lattice.

In case of polymer blends, we apply this model to study phase separation close to and below T_g. During phase separation *e.g.* after cooling the system, we observe the formation of complex morphologies where slow domains are in coexistence with faster ones. At early stages of the process, the size of the domains grows regularly like the logarithm of time. At later stages, domains evolution is observed to be much more irregular (on a logarithmic scale though) due to the huge difference in dynamics of fast domains and slow ones: the fast fluid phase melts partially the slow domains. We compare the phase separation dynamics to the reverse process, when the temperature is increased again in the totally miscible range. This process is analogous to the rejuvenating process described by Kovacs in pure polymers. In this situation, we observe a temporal asymmetry between the aging and the rejuvenation dynamics: the slow domains melt much faster than the elapsed time required to built them during the separation process and total miscibility is recovered after a much shorter time. The melting of slow glassy structures during the rejuvenation process is the consequence of interpenetration mechanisms of the very mobile component and free volume diffusion inside them.

For studying solvent diffusion, we consider the case of polymer solvent systems in contact with a reservoir of pure solvent. We consider situations where the activity of the solvent reservoir is varied in order to describe either thin films drying, or swelling of a glassy polymer matrix by a penetrating solvent. Our model allows for explaining case-II diffusion -i.e. solvent propagation at constant velocity with a well defined front- in glassy polymers during swelling. It allows e.g. for calculating the front velocity as a function of the plasticizing power of the solvent and the dynamical state of the glassy matrix. The mechanism is the following: the solvent penetrates first through fast path within the glassy matrix, and then melts the polymer under the osmotic pressure it exerts. Regarding the process of film drying, we show that films up to a few thousands of nanometer thick can be almost completely dried in an accessible experimental time, even at temperatures well below the polymer glass transition temperature. This is a consequence: 1- of the presence of the fast path through which the solvent evaporates 2- the separation of time scales between solvent evaporation (fast path) and the subsequent film contraction (controlled by the α-relaxation process). When drying a thicker film, we show that a glassy crust appears on the free surface, as shown experimentally.

Keywords: glass transition, polymer blends, polymer-solvent systems, diffusion heterogeneous dynamics

Résumé

Dans ce travail, nous proposons un modèle mesoscopique permettant de décrire la dynamique dans les mélanges de polymères et polymère-solvant proche de la température de transition vitreuse (T_g). Ce modèle incorpore l'aspect hétérogène de la dynamique à l'échelle d'une hétérogénéité dynamique (3-5 nm) ce qui permet de décrire la diffusion rapide de petites molécules dans l'état vitreux. De plus, nous proposons un modèle thermodynamique qui rend compte de la compressibilité des mélanges binaires afin d'implémenter les forces physiques nécessaires qui pilotent la dynamique dans ces mélanges. Enfin, le modèle dynamique prend en compte le mécanisme de facilitation qui permet de décrire la relaxation d'hétérogénéités lentes par la diffusion de volume libre et l'inter-diffusion des différentes composantes en leur sein.
Nous appliquons ce notre modèle dans le cas des mélanges de polymères, dont au moins une des composantes est sous le seuil d'enchevêtrement, dans le but d'étudier les phénomènes de séparation de phase proche et en dessous de Tg. Nous observons dans ce cas, après avoir refroidi le système, l'apparition de morphologies vitreuses se formant lentement (processus logarithmique) en coexistence avec des morphologies rapides. Nous montrons qu'il est ainsi possible d'obtenir des matériaux polymériques composites très stables dans le temps, dont les morphologies vitreuses peuvent atteindre la taille de quelques dizaines de nanomètres. Nous avons également comparé la cinétique de séparation de phase proche de Tg avec la cinétique de rajeunissement du matériau e.g. après avoir réchauffé le système. Nous observons -1- que les morphologies vitreuses fondent plus rapidement que le temps nécessaire pour les former lors du processus de séparation de phase et -2- que la fusion de ces morphologies est pilotée par le mécanisme de facilitation. Dans le cas des systèmes de polymère-solvant, nous avons étudié les mécanismes de séchage et gonflement lorsque que le système est sous la Tg du polymère pur et en contact avec un réservoir de solvant. Nous montrons que le séchage –i.e. évaporation du solvant après avoir baissé le potentiel chimique du réservoir est la conséquence -1- de la présence de zones rapides au sein du matériau dans lesquelles le solvant diffuse et -2- d'une séparation d'échelles de temps entre la diffusion du solvant et la relaxation mécanique du matériau. Nous observons aussi qu'il est possible de sécher entièrement des films d'une épaisseur allant jusqu'à quelques centaines de nanomètres dans le cas de séchages à atmosphère sèche. Pour des films de taille micrométrique en revanche, on observe l'apparition d'une croûte vitreuse qui se forme au niveau de la surface du matériau empêchant ainsi la fuite du solvant dans les régions plus profondes. Notre modèle permet également d'expliquer la diffusion « cas II » -i.e. pénétration du solvant sous la forme d'un front invariant se propageant à vitesse constante lors du gonflement d'une matrice de polymère-solvant vitreuse par pénétration de solvant. Enfin, il permet de calculer la vitesse du front de diffusion « cas II » en fonction du pouvoir de plastification du solvant ou de l'état dynamique de la matrice.

Mots-clé: transition vitreuse, mélanges de polymères, systèmes polymère-solvant diffusion, dynamique hétérogène

Contents

State of the art **12**

Etat de l'art en français **24**

1 Modelling of binary mixtures close to and below T_g **34**
1.1 Résumé en français 34
1.2 Introduction 34
1.3 Physical model 35
1.4 Solving the model 47
1.5 Equilibrium in polymer blend and polymer solvent systems 57
1.6 Conclusion 60

Appendices **61**
Appendix 1.A Thermodynamics 61
1.A.1 Comparisons with experimental results: semi-quantitative agreement . . 61
1.A.2 Composition fluctuations distribution 64
1.A.3 Small angle neutron scattering in polymer blends 65
Appendix 1.B Derivation of Fick laws for diffusion 67
Appendix 1.C Derivation of some basics for interface theory 68
Appendix 1.D Method for determining the time steps 70
Appendix 1.E Paires correlation function: size of morphologies 71
Appendix 1.F Time correlation functions: composition fluctuations and relaxation times 72

2 Dynamics in polymer blends close to and below the glass transition temperature: phase separation and rejuvenation **75**
2.1 Résumé en français 75
2.2 Introduction 76
2.3 Phase separation and aging in polymer blends close to and below T_g 77
2.4 Rejuvenation and high temperature remixing dynamics for aged and phase separated blends close to T_g 84
2.5 Conclusion 93

Appendices **95**

Appendix 2.A Phase separation in dynamically homogeneous polymer blends ("Standard case") . . . 95

Appendix 2.B Aging and rejuvenation in symmetrical polymer blends . . . 99

Appendix 2.C Violation of the Stokes-Einstein relation for diffusion . . . 101

Appendix 2.D Non symmetric phase diagrams: phase separation close to T_g and rejuvenation . . . 102

3 Dynamics in polymer-solvent systems close to and below the glass transition temperature **110**

3.1 Résumé en français . . . 110

3.2 Introduction . . . 111

3.3 Thermodynamics of polymer-solvent systems in contact with a pure solvent reservoir . . . 112

3.4 Standard Fickian diffusion in polymer-solvent systems . . . 115

3.5 Drying of polymer-solvent films close to T_g at non zero activity . . . 118

3.5.1 Conclusion on film drying close to T_g at non zero activity . . . 125

3.6 Drying of polymer-solvent films close to T_g at very low activity . . . 126

3.6.1 Prediction of cavity formation . . . 126

3.6.2 New ansatz for calculating kinetic coefficients . . . 129

3.6.3 Low activity drying without cavity formation . . . 130

3.6.4 Low activity drying with cavity formation . . . 134

3.6.5 Conclusion on low activity drying . . . 137

3.7 Swelling of polymer-solvent films close to T_g . . . 138

3.7.1 Conclusion on thin and thick films swelling . . . 150

Appendices **153**

Appendix 3.A Effect of activity on drying . . . 153

Appendix 3.B Effect of activity on swelling . . . 154

Appendix 3.C Numerical method for studying thick films swelling . . . 156

General conclusion **159**

Conclusion générale en français **165**

Table des matières

Etat de l'art (version Anglaise) **12**

Etat de l'art (version Française) **24**

1 Modélisation de mélanges binaires proche de T_g **34**
1.1 Résumé en français . . . 34
1.2 Introduction . . . 35
1.3 Modèle physique . . . 35
1.4 Résolution du modèle . . . 47
1.5 Equilibre thermodynamique dans les mélanges de polymères et polymère-solvant 57
1.6 Conclusion . . . 60

Appendices **61**
Appendix 1.A Thermodynamique . . . 61
1.A.1 Comparaison avec des résultats expérimentaux . . . 61
1.A.2 Distribution des fluctuations de compositions . . . 64
1.A.3 Diffusion de neutrons aux petits angles dans les mélanges de polymères . 65
Appendix 1.B Dérivation des lois de Fick pour la diffusion . . . 67
Appendix 1.C Résultats standards de la théorie des interfaces . . . 68
Appendix 1.D Méthode pour déterminer le pas de temps . . . 70
Appendix 1.E Fonction de correlation de paires: taille des morphologies . . . 71
Appendix 1.F Fonctions de corrélation temporelles: fluctuations de compositions et temps de relaxation . . . 72

2 Dynamique dans les mélanges de polymères proches et en dessous de la température de transition vitreuse: séparation de phase et rajeunissement **75**
2.1 Résumé en français . . . 75
2.2 Introduction . . . 76
2.3 Séparation de phase et vieillissement dans les mélanges de polymères proches de T_g . . . 77
2.4 Rajeunissement et dynamique de remélangeage pour des mélanges vieillis et séparés de phase proche de T_g . . . 84
2.5 Conclusion . . . 93

Appendices **95**

Appendix 2.A Séparation de phase dans les mélanges de polymères dynamiquement homogènes ("Situation Standard") 95

Appendix 2.B Aging and rejuvenation in symmetrical polymer blends 99

Appendix 2.C Violation de la loi de Stockes-Einstein 101

Appendix 2.D Mélanges de polymères non symétriques: séparation de phase proche de T_g et rajeunissement 102

3 Mélanges polymère-solvant **110**

3.1 Résumé 110

3.2 Introduction 111

3.3 Thermodynamique des mélanges polymère-solvant en contact avec un réservoir de solvant 112

3.4 Diffusion Fickienne dans les mélanges polymère-solvant 115

3.5 Séchage de films de polymère-solvant proche de T_g à activité non nulle 118

3.5.1 Conclusion sur le séchage de films proche de T_g à activité non nulle . . . 125

3.6 Séchage de films polymère-solvant proche de T_g à très basse activité 126

3.6.1 Prediction de la formation de cavités 126

3.6.2 Nouvel anzatz pour calculer les coefficients cinétiques 129

3.6.3 Séchage à basse activité sans formation de cavités 130

3.6.4 Séchage à basse activité avec formation de cavités 134

3.6.5 Conclusion sur le séchage à basse activité 137

3.7 Gonflement de films de polymère-solvant proche de T_g 138

3.7.1 Conclusion sur le gonflement de films minces et épais 150

Appendices **153**

Appendix 3.A Effet de l'activité sur le séchage 153

Appendix 3.B Effet de l'activité sur le gonflement 154

Appendix 3.C Méthode numérique pour étudier le gonglement de films épais 156

Conclusion générale (version Anglaise) **159**

Conclusion générale (version Française) **165**

State of the art

Basics on polymers

In every day life, polymers are everywhere and play an important role. From chemical point of view, they are macromolecules composed of identical repeated units called monomers (From the greek, *pollus*=several and *meros*=parts). They are either present in nature: DNA, proteins, cellulose or again elastomers, or they can be manufactured by human technologies, like carbon-based polymers. From the material physics point of view, polymers are very interesting because of their viscoelastic properties. The behaviour of such materials is correlated to dynamical processes and structural properties occurring at the microscopic scale, and one of the most active field in polymer physics nowadays, is to develop a multi-scale approach to make progress in the understanding of macroscopic behaviour by microscopic considerations. Polymers are complex systems which are characterized by a broad range of different time scales and associated length scales due to their chain conformation. Intrinsically, their dynamics is slow and most of polymeric materials undergo a glass transition at a given temperature called the glass transition temperature (T_g). The glass transition is a phenomenon characterized by a sharp increase of the viscosity and very long dominant α-relaxation times (macroscopic time scales). Above T_g the polymer is in a molten state and below it is glassy, which is a solid-like state where there is no apparent order at the microscopic level. The glass transition is still not fully understood so far, and solving such a problem represents one of the most important challenge of modern physics.

Diffusion

Diffusion process of particles in a material environment tend to make the composition of its constituent homogeneous. The description of diffusion was first attempted by Brown and Einstein. From a phenomenological point of view diffusion responds to the Fick's laws. The first of them stipulates that the flux (J) of matter through a unit area is controlled by the local gradient of concentration (c) in the media and the diffusion kinetics is controlled by a diffusion constant D. This law reads (in 1D):

$$J = -D\frac{\partial c}{\partial x} \qquad .$$

In the Fick's description of diffusion, the diffusion coefficient does not depend on local concentration. Moreover, the time variation of the local concentration, following Fick description, is given by:

$$\frac{\partial c}{\partial t} = -\frac{\partial J}{\partial x} = D\frac{\partial^2 c}{\partial x^2}$$

This is the second Fick's law.
The Fick's law are nowadays the most commonly used description for diffusive phenomena. However, it appears that the diffusion is multi faceted and Fickian theory breaks down in many situations. Indeed, the diffusion in a large number of material environment, depends on local concentration of species, and in this case, diffusion is described by the following equation:

$$\frac{\partial c}{\partial t} = \frac{\partial}{\partial x} D(c) \frac{\partial c}{\partial x}$$

where the diffusion constant is, a priori, a non trivial function of local concentration, and is also a function of system's history. It is for instance the case in the context of small penetrant molecules (sorption) within a hard polymeric matrix (glassy). Theoretical studies performed by Crank in the 50's [1] were among the first to describe the dependance of species' diffusion in term of local concentration. This approach describes non linear effects in the diffusion process by taking formally into account molecular rearrangements due to the diffusion of penetrant molecules within the material. In these systems, a common experimental technics consists in measuring the mass intake (M) of penetrant molecules within the media. In its general formulation, the time variation of the mass intake can be expressed as follows:

$$M \sim t^n$$

When $n = 1/2$, small molecules sorption mechanisms follows a pure Fickian diffusion process, but it is rarely observed. However, in many other cases [2], observed regimes correspond to:

-$0 < n < 1/2$ and $1/2 < n < 1$: Anomalous diffusion (Non Fickian)
-$n = 1$: case II diffusion (non Fickian)

Case II diffusion is a particular diffusive phenomenon which has been extensively [3, 4, 5, 6] studied experimentally. Notably, Kramer et al. [7, 8, 9, 10, 11] performed experiments in order to study solvent penetration front in glassy polymer films by using Rutherford Backscattering technics. The latter can give dynamical information as well as time evolution of concentration profiles as a function of film depth. Case II diffusion is characterised by the presence of an invariant solvent front moving at constant velocity which separates the system between a highly swollen region from a hard glassy dried one (See Figure 0.0.1). In addition, a strong gradient of solvent concentration is observed between both regions. This corresponds to a Fickian front precursor which propagates in the dried region ahead of the case II front. Thomas and Windle made a major advance in the understanding of the case II diffusion of solvent in a polymeric

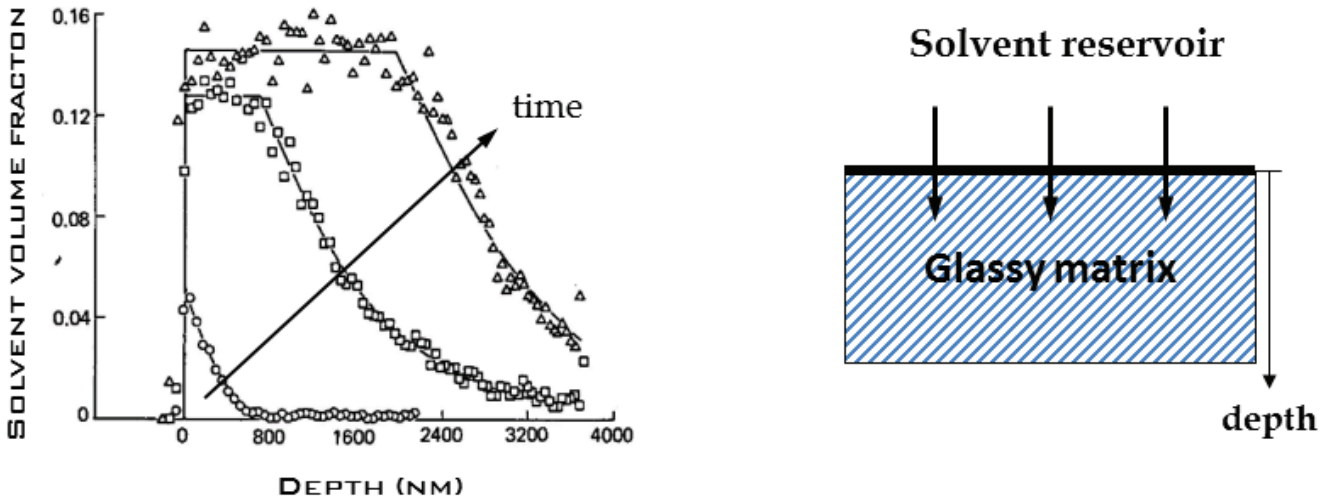

Figure 0.0.1: Iodohexane (solvent) penetration in glassy PolyStyrene(PS) at T= 295,5K from reference [11]. The system is far the pure PS glass transition temperature which is equal to $368K$. An invariant case II diffusion front moving at constant velocity is observed. It is preceded by an exponential like Fickian front. The front takes place at time $t_{ind} = 4 \times 10^5 s$ to establish. Time t_{ind} corresponds to the induction time.

matrix [12, 13]. They introduced the osmotic effect induced by solvent molecules on contracted glassy polymer chains at the origin of the polymer deformation during the swelling process. The Thomas and Windle model also predicts the existence of an induction times as observed experimentally by Kramer et al.. Following the authors, case II diffusion results from the coupling between an osmotic pressure driven viscous response of the polymer (polymer chain relaxation) and a Fickian diffusion process. Nevertheless the major limitation of this model lies in the fact that it considers the induction times and the front velocity as adjustable parameters and are inputs of the model to fit experimental data. Moreover, this model is unable to predict effect of system's history on case II diffusion , which has been observed experimentally. Experiments dealing with the revers process (drying of polymer-solvent systems) [14, 15, 16, 17] show that it is possible to dry completely a thin polymer films (a few hundred of nanometers thick), even at temperatures much below the pure polymer glass transition temperature. It is observed that the film ages during drying, and that the aging process depends on the way the film was dried. This supports the idea that solvent diffusion depends strongly on the history of the system like for case II diffusion. Molecular dynamics have also been performed [18] regarding freestanding and supported thin films drying above T_g and close to T_g. Above T_g, the solvent is found to evaporate from the film with a constant diffusion coefficient. Close to T_g, in contrast, the diffusion of solvent "far" from the interface is found to drop due to the dynamics slowing down induced by the decreasing solvent concentration. Moreover, according to the authors, solvent evaporation rate is very important at early stages, and the system contracts a little. At later stages, on the other hand, the film thickness decreases strongly converging slowly toward the final dried state. This suggests that solvent evaporation and the mechanical response of the system are both strongly connected to each other. Experiments on micrometric film drying

was performed by Macosko et al. [19] using "spin coating" technics . The authors observed a glassy crust forming at the film/reservoir interface with a low solvent concentration while a large quantity of solvent is trapped deeper in the film. Results presented here highlight the existence of complex diffusive phenomenon of solvent molecules within a glassy matrix (either in solvent penetration mechanisms or in drying conditions) which have been only partially understood so far, and for which Fickian description for diffusion breaks down.

In polymeric media, because of chains conformations, geometrical aspects must be taken into account in diffusion and rheological process. There exist models dealing with polymer chains dynamics at the microscopic level: the Rouse and the Reptation model [20, 21]. The Rouse model describes the visco-elastic behavior of relatively small gaussian chains. It thus does not take into account entanglement effect, unlike the reptation model which describes long chain diffusion process. These models tell us that diffusion at the scale of a polymer chain is highly affected by its molecular mass. In this work, we are mainly focused on relaxation dynamics at the monomeric scale at which it exists a continuum spectrum of relaxation times [29]. The Rouse/Reptation models however consider the dynamics of chains segments, and they assume that the relaxation time at the scale of a monomer is unique. These models would then require further development so they can take into account the spectrum of monomeric relaxation times, which has not been done so far. In this work, effect of molecular mass on diffusion is reproduced through a phenomenological adjustable parameter. Finally, spinodal decomposition in molten polymer blends has been extensively studied. It is observed that domains size R grow like $R \sim t^{1/3}$ [22, 23, 24, 26, 25]). This growth law is recovered from a semi quantitative point of view by assuming that diffusion coefficient is constant and does not depend on concentration.

Heterogeneous dynamics in polymer liquids close to T_g

The WLF (William-Landel-Ferry) law is known to reproduce the time-temperature equivalence in case of glass forming systems. This law reads:

$$\log\Big(\frac{\tau_\alpha(T)}{\tau}\Big) = -\frac{C_1(T-T_0)}{C_2+(T-T_0)} \tag{0.0.1}$$

where C_1 and C_2 are constants and T_0 is a reference temperature. The time τ_α is called the α-relaxation time, and is referred to a "global" relaxation process related to the viscosity of the system. This law is known to be correct for temperature close to the glass transition up to 100K above T_g. Far above T_g , typical relaxation times are 10^{-9}s and becomes much larger as the temperature decreases close to T_g. At T_g, characteristic times is equal to 100s and the viscosity is equal to 10^{12} Pa.s [27]. Many years ago, it has been evidenced experimentally that the dynamics of a glass forming system is not governed by a unique relaxation time, but by a whole spectrum of relaxation times at the monomeric scale [28, 29, 30, 31, 33, 32, 34, 35]. The presence of a distribution of relaxation times has been evidenced experimentally by dielectric measurements. Other studies using NMR or probe molecules translational diffusion gives a

spatial aspect to the relaxation time distribution, and these experiments highlight the presence of dynamic heterogeneities of a typical size of 3-5 nm. Probes experiments were performed from temperature comprised between $T_g + 100$K down to $T_g - 10$K in a glass forming liquids. The diameter of the probe molecules is smaller than 2 nm. The well known Stokes-Einstein relation which relates the diffusion constant D of a diffusing object of size R, and the viscosity (η) of the system at temperature T is:

$$\frac{D\eta}{T} = \frac{k_B}{6\pi R} \tag{0.0.2}$$

where k_B is the Boltzmann constant. Down to $T_g + 50$K typically, the Stokes-Einstein relation is verified by probes diffusion experiments. However, it was observed that this law is violated for lower temperature and the amplitude of the violation is typically of 2 to 3 decades at T_g in the context of pure polymeric super cooled liquids: the diffusion coefficient of probes D is observed to be 100 times larger than that predicted by the Stockes Einstein D_{SE} relation, i.e. $(\log\Big(D/D_{SE}\Big) \sim 2$. The violation amplitude of the Stokes-Einstein relation is reduced when the probe size increases. This is another proof of the spatial nature of heterogeneous dynamics. Indeed, in the heterogeneous dynamic picture, there are fast dynamic heterogeneities of size 3-5 nm in coexistence with much slower ones. If the probe is smaller than a dynamic heterogeneity, it would preferentially diffuse through faster dynamic heterogeneities and much faster than the macroscopic time (α-relaxation time) obtained from the measured viscosity (see Figure 0.0.2). Thus, in this context, probes translational diffusion is not related to α-relaxation, but is driven by faster relaxation times in the system. Nevertheless, if the probe is larger than a dynamic heterogeneity, the latter interacts with slower regions and its diffusion is controlled by α-relaxation times: the Stokes relation is recovered. From all this, in case of small diffusive probes, the fact that quantity $\log\Big(D/D_{SE}\Big)$ increases when approaching T_g, means that the relative difference between α-relaxation times and fast relaxation times is large in these systems. Moreover, the Stokes-Einstein violation proves that the relaxation times spectrum widens when approaching Tg (see Figure 0.0.2). Finally, even if the viscous response is driven by long times close to the glass transition temperature, heterogeneous dynamics makes the system not "frozen" and allows for diffusion. This is a very important feature of glass forming liquids. In the context of binary mixtures such as polymer-solvent systems, it has been observed that the stokes law is violated by up to 6 decades which means that relaxation times distributions are much larger than in pure polymeric glass forming liquids. Indeed, it has been observed [14] that solvent diffusion constant is equal to $10^{-15} m^2.s^{-1}$ [14] at T_g, which gives a fast relaxation time responsible for diffusion are equal to 10^{-4}s at the scale of a monomer, whereas at T_g the α relaxation monomeric relaxation time is equal to $\tau_\alpha = 100$s. From a theoretical point of view, the model developed by Long and Lequeux [36, 37] gives a phenomenological approach to the glass transition phenomenon in polymeric liquids. This model assumes the existence of a spatial distribution of relaxation times which widens when approaching T_g. This assumption is justified by experimental results described above. The presence of dynamic heterogeneities are explained by density fluctuations within the material and are controlled by the bulk modulus ($K_{bulk} \sim 10^9$Pa) in case of pure polymeric liquids. In this idea, a dynamic heterogeneity,

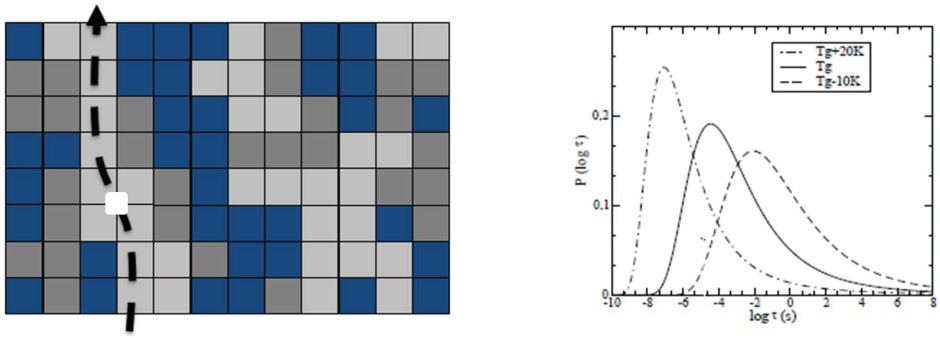

Figure 0.0.2: (Left) Probe (white square) diffusion in a heterogeneous media. Light gray subunits represent fast dynamics heterogeneity, while dark gray subunits represent slow ones. The size of the probe is smaller than a dynamic heterogeneity and diffuse through path composed of fast dynamic heterogeneities. (Right) Distribution of relaxation times in Polystyrene at $T_g + 20K$, T_g and $T_g - 10K$. The lower the temperature, the larger the distribution and the longer the relaxation times.

whose internal relaxation times is related to the average free volume accessible for monomers to move, is slow when the dynamics heterogeneity is dense and fast when it is less dense. Hence a relaxation time is associated to a density fluctuation by means of the WLF relation which is assumed to be correct at the monomeric level. At the scale of the whole system, a density fluctuation distribution gives rise to a spatial relaxation time distribution. In binary systems, when a fast component is mixed with a slow one, relaxation times distribution are related to composition fluctuations which are controlled by the osmotic modulus $K_{osm} \sim 10^7$ Pa. As it is much smaller than the bulk modulus, relaxation times distribution are larger in case of binary system in a glassy state than in pure polymeric glass forming liquids.

- **Facilitation mechanisms**

Spatial distribution of dynamics heterogeneities allows for describing melting process of slow subunits of size ξ (with internal relaxation time τ_{slow}) by the presence of fast surrounding ones (with internal relaxation time τ_{fast}) [38]. This process is illustrated by diffusion mechanisms of monomers at the interface between the slow subunit and fast surrounding ones, and the life time of such density fluctuation is

$$\tau_{life} = N^{2/3}\tau_{fast}$$

where $N = \xi^3 \times \rho_0$ is the dimensionless size of a dynamic heterogeneity in term of number of monomers, and ρ_0 the close packing density (See Figure 0.0.3). More recently, this mechanism has been referred to as facilitation mechanism in the literature [39]. In binary systems, when a slow dynamic heterogeneity, dense and highly composed of slow monomers, is surrounded by fast ones composed of fast monomers, facilitation mechanism is the consequence of diffusion of slow monomers out of the slow domains while in the same time fast monomers diffuse

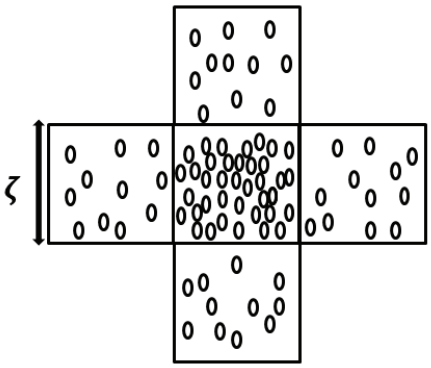

Figure 0.0.3: Representation of a spatial density fluctuation on a typical size $\xi \sim 3-5nm$ (dynamic heterogeneity): The cell in the center is denser than surrounding ones: the relaxation time of the central cell, noted τ_{slow}, is much longer than that of surrounding cells. Relaxation time of surrounding cells is noted τ_{fast}. Monomers which belong to the dense cell diffuse toward fast cells through their common interface. The life time , noted τ_{life}, of such a density fluctuation is $\tau_{life} = N^{2/3}\tau_{fast}$. N is the dimensionless volume of a cell: $\xi^3 = N/\rho_0$ with ρ_0 the close packing density. Hence a slow dynamic heterogeneity can melt in a time τ_{life}, and this internal melting process is driven by fast dynamic heterogeneities.

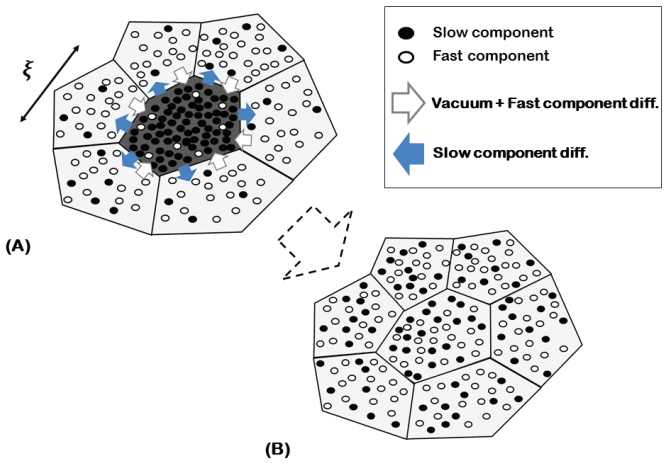

Figure 0.0.4: Representation of the facilitation mechanism in case of binary a systems. The central (dark) slow dynamic heterogeneity, with a relaxation time τ_{slow}, is mainly composed of slow monomers and is dense. Surrounding dynamic heterogeneities are less dense and are mainly composed of fast component: they have fast relaxation times τ_{fast}. The relaxation of the central slow subunit is the consequence of inter diffusion of slow and fast monomer from its interface. The diffusion of fast monomers inside the slow domain is also accompanied by the diffusion of free volume which accelerates the dynamics at the monomeric level. Finally, like in case of pure simple liquids, the life time τ_{life} of such composition fluctuation is given by $\tau_{life} = N^{2/3}\tau_{fast}$.

inside from the interface. The diffusion of fast monomers is also accompanied with a diffusion of vacuum which tends to accelerate the dynamics at the monomeric level. See 0.0.4 for an illustration of this. As in case of pure polymeric liquids, facilitation mechanisms are kinetically controlled by relaxation times of fast surrounding subunits, and the diffusion scaling factor $N^{2/3}\tau_{fast}$ is still relevant here. We will see that such mechanisms are fundamental for describing the melting of slow glassy structures during rejuvenation mechanism in polymer blends.

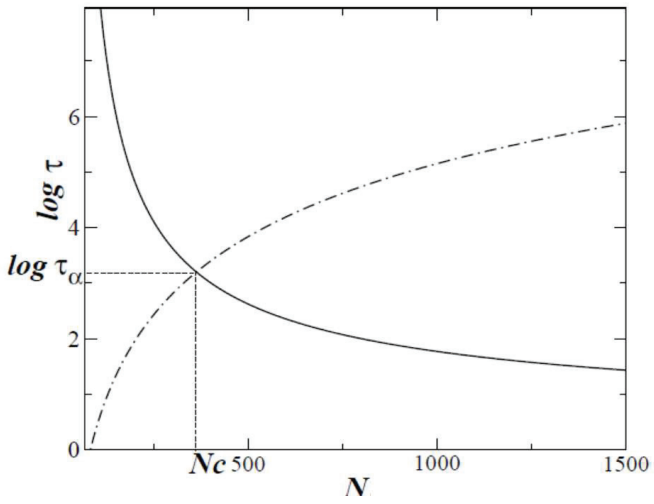

Figure 0.0.5: Schematic representation for the evolution of the internal monomeric relaxation time (full line) and the time τ_{life} (dotted-dashed line) as a function of the volume N at which we consider density fluctuations. The intersection of these curves gives the scale of a dynamic heterogeneity N_c.

For determining N_c, the procedure is the following. Let us note N the dimensionless volume of a dynamic heterogeneity. When N is small, the slow density fluctuation relaxes mainly by exchanging monomers in the fast surrounding domains (short-live density fluctuation). On the other hand, for large N, slow subunits relaxes mostly with the internal relaxation process associated to monomeric jumps process (long-live density fluctuation).
As it shown in Figure 0.0.5, the competition between internal relaxation process and facilitation mechanisms gives rise to the relevant size N_c for a dynamical heterogeneity (dimensionless). At size N_c, $\tau_{life} = N_c^{2/3}\tau_{fast}$ corresponds to the longest density fluctuation relaxation time in the system. This can also be seen as the competition between local free volume rearrangement so that monomers can move at fixed density in a dynamic heterogeneity, and density fluctuation relaxation by free volume exchange with nearest neighbors heterogeneities.
α-relaxation process in glass forming systems are associated to mechanical relaxation process of the material, though its precise origin is still under debate nowadays. In reference [36], authors interpret the mechanical behavior of a glass forming sample as the following. Close to T_g and on certain observation time scale t_{obs} related to macroscopic time scales, some dynamic heterogeneities have time to relax because their relaxation time is smaller than t_{obs}: they are fluid-like. On the other hand, much slower dynamic heterogeneities with relaxation times longer than t_{obs} do not have time to relax (see Figure 0.0.6): they are solid-like. The mechanical behaviour

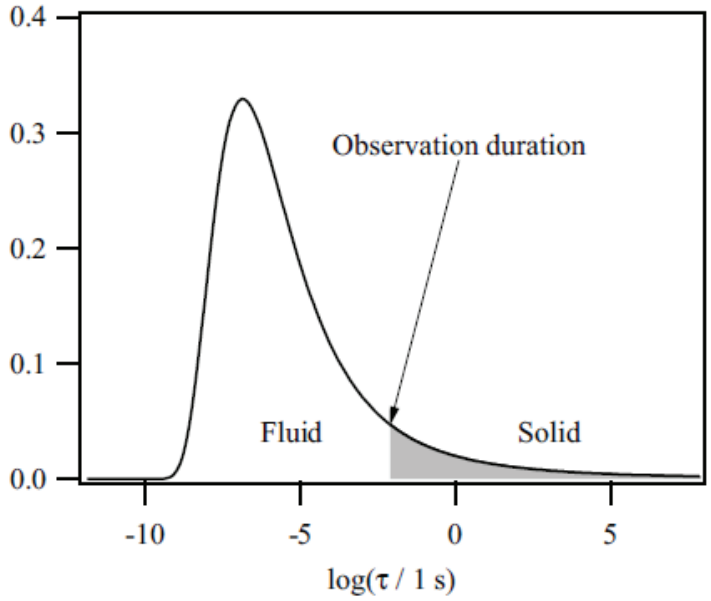

Figure 0.0.6: Typical relaxation time distribution at temperature above T_g. Distribution shifts towards long times when the temperature decreases. Dynamic heterogeneities of relaxation times longer than t_{obs} are solid like. Sub-units with lower relaxation times are fluid like.

of the sample is then conditioned by the proportion of fluid and solid-like heterogeneities on the time scale t_{obs} (see Figure 0.0.7): the system is fluid if the proportion of solid-like heterogeneities is low, whereas it is solid as a whole when the proportion of solid-like heterogeneities is high enough so that they percolate. Finally, the transition between the fluid and the solid-like behaviour of the sample takes place when the proportion of solid-like heterogeneities reaches a certain percolation threshold p_c. Following this interpretation, α-relaxation process is related to the percolation of a small fraction ($p_c \sim 10\%$) of most rigid subunits and the α relaxation time is defined as the following:

$$\int_{\tau_\alpha}^{+\infty} P(\tau)d\tau = p_c$$

where P is the relaxation times distribution. Note that the value $p_c \sim 10\%$ is taken following the bond percolation criterion and allows to recover very satisfying T_g shifts in thin polymer films [40]. At equilibrium, parameter N_c satisfies to the following equation:

$$\tau_\alpha = N_c^{2/3}\tau_{fast} \tag{0.0.3}$$

Size N_c is thus the smallest scale for which the density fluctuation relaxation process is at least equal to τ_α at equilibrium. N_c is typically equal to $100 - 500$ at T_g [38].
In reference [41] authors study the case of aging in out of equilibrium conditions after a temperature quench down to or below T_g. They show that, in these conditions, the relaxation times distribution changes permanently and that the dynamical state of the system depends on its history. It has been observed notably that during aging, relaxation times distributions widen and relax toward longer relaxation times.

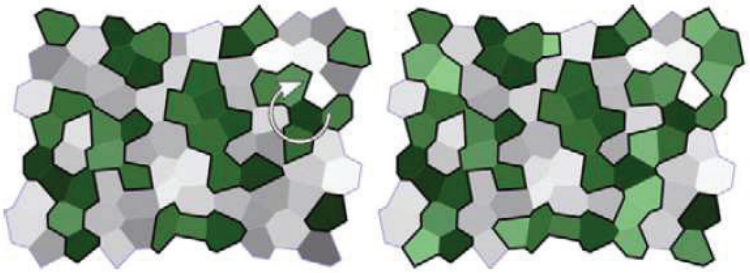

Figure 0.0.7: Representation of spatial dynamic heterogeneities in the system at a certain temperature. Left: On the observation duration, slow dynamic heterogeneities (dark green) behave like solids and form clusters. These clusters are surrounded by fast (fluid) dynamic heterogeneities because the proportion of slow (solid-like) heterogeneities is below the percolation threshold. The system behaves as a viscous fluid. Right: On much shorter times than the observation duration, a more important proportion of dynamic heterogeneities behave as rigid like units and a clusters begin to percolate. On this time scale, the whole system behaves like a solid.

Objectives

The main objectives of this work is to study inter diffusion mechanisms of small molecules in the glassy state, either at equilibrium or in out of equilibrium conditions. We consider two kinds of systems:

- **Polymer blends** with components of different T_g's, for which at least one of the two polymers has a mass smaller than entanglement threshold.
- **Polymer-solvent** systems in contact with a solvent reservoir at temperatures far below the pure polymer glass transition temperature. In these systems, the total number of solvent molecules can vary when changing the solvent reservoir chemical potential.

A model is designed for describing dynamics of these systems. It incorporates the heterogeneous nature of the dynamics on a scale of 3-5nm and takes into account the evolution of the dynamical state of the systems with respect to the history they have followed. In polymer blends, we are particularly interested in describing phase decomposition process close to T_g occurring during aging. We also consider rejuvenation process of phase separated polymer blends close to T_g after increasing the temperature. In polymer solvent systems, we are first interested in drying phenomenons of polymeric materials maintained far below the pure polymer glass transition temperature. We also study swelling phenomenons in order to understand how a hard (glassy) polymer film can be diluted by solvent molecules.

This manuscript is organized as follow:

- In chapter 1, we describe the spatial model and methods followed to solve it and to implement dynamics in polymer blends and polymer-solvent systems. Important ingredients of the model are exposed, as well as the dynamical model by introducing diffusion equations and equations responsible for dilatation and contraction of the system. The mapping from physical equations to equations solved numerically is also made. Finally, we discuss about the implementation of facilitation mechanisms.

- In chapter 2, we apply the spatial model described in chapter 1 to the case of polymer blends, and especially in the context of phase separation close to and below T_g. In a first step, we look at phase separation process close to or below T_g in case where composition fluctuations are coupled to the blend glass transition temperature. After that, we study rejuvenation mechanisms, which occur when the temperature is increased again. Effect of the history of the system on rejuvenation kinetics are also studied.

- In chapter 3 we study the drying and swelling of polymer solvent system in contact with a solvent reservoir, and the same spatial model used for polymer blends is adapted in this sense. Whether it is in case of drying or swelling, we consider films of size varying from ten nanometers up to a few micrometers, and at temperatures much lower than the pure polymer glass transition temperature. For drying processes, we consider situations where the system is drying at non zero and at very low activity. Finally, the influence of the history of the system on swelling kinetics is also studied.

Etat de l'art

Notion générales sur les polymères

Dans la vie de tous les jours, les polymères nous entourent partout et jouent un rôle fondamental. D'un point de vue chimique, ce sont des macromolécules composés de sous unités identiques appelés monomères. Ils sont soit naturellement présents dans la nature (ADN, protéines, cellulose ou encore les caoutchoucs), ou ils peuvent être conçues par des technologies humaines comme les polymères à base carbonée. Du point de vue de la physique des matériaux, les polymères possèdent de bonnes propriétés viscoélastiques, et un des domaines les plus actifs dans la physique des polymères actuellement est le développement d'une approche multi échelle afin de comprendre le comportement macroscopique des matériaux polymériques en considérant l'aspect microscopique. Les polymères sont des systèmes complexes caractérisés par un large spectre d'échelles de temps et de longueurs associés du fait de leurs conformations. Leur dynamique est lente et la plupart des polymères subissent une transition vitreuse à partir d'une certaine température appelée la température de transition vitreuse (T_g). La transition vitreuse est un phénomène qui se traduit par une augmentation brutale de la viscosité du matériau proche de T_g. Les temps de relaxation dominants appelés temps de relaxation α, qui caractérisent les échelles de temps macroscopiques du matériau, sont très longs. Au-dessus de T_g, le polymère est dans un état dit fondu, et en dessous, il est vitreux. Dans l'état vitreux le matériau est solide et fragile, et il n'y a pas d'ordre apparent à l'échelle microscopique. Enfin, la transition vitreuse est un phénomène toujours incompris, et résoudre ce problème représente un des challenges les plus importants de la physique moderne.

Diffusion

Les processus de diffusion de particules dans un environnement matériel tendent à rendre homogène la composition de ses constituants. Brown et Einstein ont été les premiers à décrire la diffusion. D'un point de vue phénoménologique, au premier ordre, la diffusion répond aux lois de Fick. La première d'entre elles que le flux (J) de matière à travers une surface est contrôlé par le gradient local de concentration (c) dans le milieu, et que la cinétique de diffusion est pilotée par la constant de diffusion D:

$$J = -D\frac{\partial c}{\partial x} \quad .$$

De plus, la variation temporelle de la concentration locale, dans une description Fickienne suit la loi suivante

$$\frac{\partial c}{\partial t} = -\frac{\partial J}{\partial x} = D\frac{\partial^2 c}{\partial x^2}$$

C'est la seconde loi de Fick.
Les lois de Fick sont les plus utilisées encore actuellement et elles supposent que le coefficient D ne dépend pas de la concentration locale. Cependant, il semble que la diffusion dans un cadre plus global a plusieurs facettes, et que la théorie de Fick n'est plus valable dans un grand nombre de cas où notamment elle dépend de la concentration locale, i.e.

$$\frac{\partial c}{\partial t} = \frac{\partial}{\partial x}D(c)\frac{\partial c}{\partial x}$$

La constante de diffusion ici est à priori une fonction complexe de la concentration locale, et dépend de l'histoire du système. C'est par exemple le cas lorsque de petites molécules pénètrent (phénomène de sorption) au sein d'une matrice vitreuse. Des études théoriques effectuées par Cranks dans les années 50 [1] ont été les premières à décrire la dépendance de la concentration locale dans les processus de diffusion. Cette approche décrit la diffusion par des effets non linéaires en prenant en compte les réarrangements moléculaires à l'échelle locale du fait de la pénétration des petites molécules au sein du matériau. Dans ces systèmes, une technique expérimentale communément utilisée consiste à mesurer la prise en masse (M) du matériau. De façon générale, la variation temporelle de la prise en masse du matériau peut être exprimée comme suit:

$$M \sim t^n$$

Lorsque $n = 1/2$, les mécanismes de sorption des molécules suivent une loi de Fick. Dans plusieurs autres cas [2], les régimes observés sont:

-$0 < n < 1/2$ and $1/2 < n < 1$ diffusion anormale (Non Fickien)
-$n = 1$: diffusion cas II (non Fickien)

La diffusion cas II est un processus de diffusion assez particulier qui a beaucoup été étudié expérimentalement [3, 4, 5, 6]. Notamment Kramer et al. [7, 8, 9, 10, 11] ont effectués des expériences dans le but d'étudier la pénétration d'espèces de solvant dans des films de polymères vitreux en utilisant la technique de la rétro diffusion Rutherford. Cette dernière permet d'obtenir des informations dynamiques sur le déplacement du front de solvant, ainsi que l'évolution temporelle des profils de concentrations en fonction de la profondeur dans le film. La diffusion cas II est caractérisée par la présence d'un front de solvant invariant se propageant à vitesse constante qui sépare le système en une région gonflée en solvant située en amont, et une région dure et vitreuse située en aval. Voir la Figure 0.0.8. De plus, on observe la présence d'un gradient de concentration entre les deux régions. Ceci correspond à un pied Fickien qui se propage dans la région vitreuse. Thomas and Windle ont effectués une avancée majeure dans la compréhension de ce phénomène [12, 13]. Ils ont notamment introduit les effets osmotiques

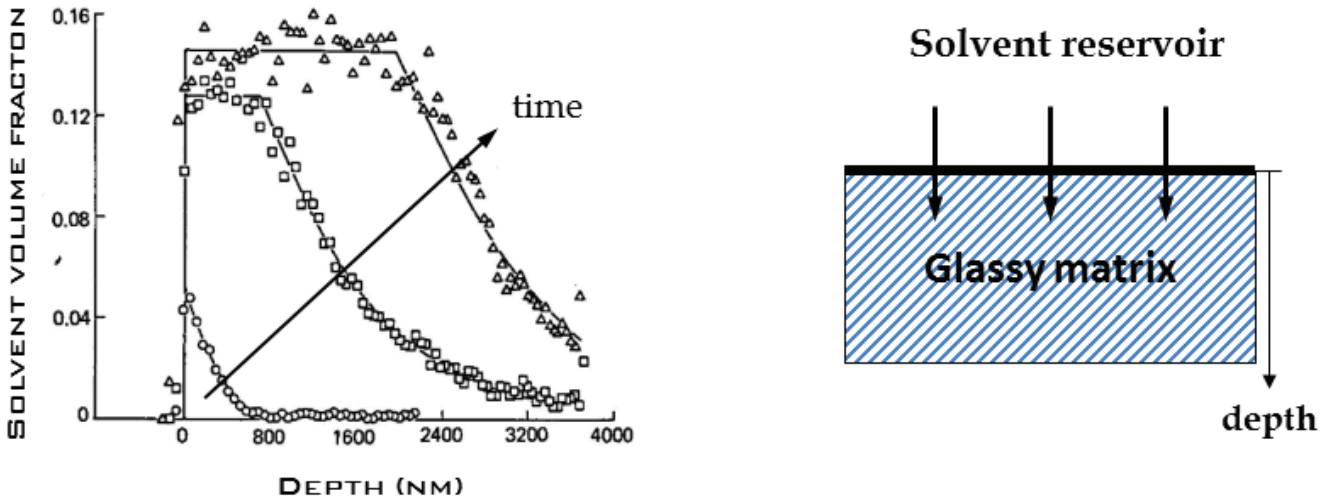

Figure 0.0.8: Pénétration d'Iodohexane (solvant) dans du PolyStyrène(PS) vitreux à T= 295,5K (issue de la référence [11]). Le system est en dessous de la T_g du polymère pure qui vaut $368K$. On observe un front de diffusion cas II précédé par un front Fickian qui décroit exponentiellement. Le front cas II s'établit à l'instant $t_{ind} = 4 \times 10^5 s$ qui correspond au temps d'induction.

induits par les molécules de solvant sur les chaînes de polymères comme étant à l'origine de la déformation de la matrice. Le modèle de Thomas et Windle prédit aussi l'existence d'un temps d'induction comme il a été observé par Kramer et al.. Cependant, il est limité dans le sens qu'il considère le temps d'induction et la vitesse du front comme étant des paramètres ajustables. De plus ce modèle ne permet pas de prédire l'effet de l'histoire du système sur la diffusion cas II. Des expériences portant sur les phénomènes de séchage (évaporation du solvant) [14, 15, 16, 17] ont montré qu'il est possible de sécher complétement un film mince de polymères de quelque centaines de nanomètres d'épaisseur, même si ce dernier est bien en dessous de la T_g du polymère pur. Il est observé notamment que le séchage induit un vieillissement du film, et que le processus de vieillissement dépend de la façon dont le film a été séché. Ceci suggère donc que la diffusion du solvant est fonction de l'histoire du système comme c'est le cas pour la diffusion cas II. Des simulations de dynamique moléculaire de séchage on été effectuées [18] dans le cas de films très mince supportés et non supportés au-dessus et proche de T_g. Au-dessus de T_g, il est observé que le solvant s'évapore du film avec un coefficient de diffusion constant. Proche de T_g au contraire, la diffusion du solvant loin de l'interface est réduite du fait du ralentissement de la dynamique. De plus, aux premiers instants, le taux d'évaporation du solvant est très important, et le système se contracte un peu. Bien après, en revanche, l'épaisseur du film décroît et le système converge lentement vers l'état séché final. Ceci suggère donc que l'évaporation du solvant et la réponse mécanique du système sont liés l'un l'autre. Enfin, des expériences de séchage sur des films de taille micrométrique [19] montrent qu'une croûte vitreuse se forme proche de l'interface sèche, alors qu'une grande quantité de solvant reste piégée dans le fond du film. Tous les résultats décrits ici, mettent en lumières l'existence de phénomènes de diffusion complexes dans le cadre de la sorption et l'évaporation de petite molécules dans des matrices de polymères vitreux. Ce sont des phénomènes qui n'ont pas encore été pleinement compris et

pour lesquels la diffusion de Fick ne permet pas de donner une interprétation convenable.

Dans les matériaux de polymères, du fait de la conformation des chaînes, des aspects géométriques doivent d'être pris en compte pour décrire les processus de diffusion et rhéologiques. Il éxiste des modèles traitants de ces questions en considérant la dynamique des chaînes au niveau microscopique: les modèle dits de "Rouse" et de "reptation" [20, 21]. Le modèle de Rouse décrit le comportement viscoélastique de matériaux composés de petites chaînes de polymères gaussiennes. Il ne prend donc pas en compte d'effet d'enchevêtrement comme c'est le cas pour le modèle de reptation qui lui décrit les processus de diffusion des longues chaînes. En conséquence, ces modèle prédisent que la diffusion à l'échelle du chaine de polymère est fortement affectée par sa masse moléculaire. Dans le cadre de notre travail, on se focalise principalement sur la dynamique de relaxation à l'échelle du monomère à laquelle il existe un spectre continu de temps de relaxation [29]. Or les modèles de Rouse/Reptation consièrent la dynamique de segments de chaînes, et ils supposent que le temps de relaxation à l'échelle d'un monomère est unique. Il serait donc nécessaire de développer ces modèles de sorte à ce qu'ils tiennent compte du spectre des temps de relaxation monomèriques, ce qui n'a pas été encore fait. Dans ce travail, l'effet de la masse moléculaire des chaînes sur la diffusion est pris en compte par le biais d'un paramètre ajustable phénoménologique. Enfin, la décomposition spinodale dans les mélanges de polymères fondus a été largement étudié. Il est en particulier observé dans ce contexte que les tailles R des domaines qui se forment croissent comme $R \sim t^{1/3}$ [22, 23, 24, 26]). Cette loi de croissance, décrite par le modèle de Ostwald [25], est retrouvée d'un point de vue semi quantitatif en supposant que la diffusion est Fickienne.

Dynamique hétérogène

La loi WLF (William-Landel-Ferry) permet de reproduire l'équivalence temps-températures dans le cas des systèmes devenant vitreux. Elles s'exprime comme:

$$\log\Big(\frac{\tau_\alpha(T)}{\tau}\Big) = -\frac{C_1(T-T_0)}{C_2+(T-T_0)} \tag{0.0.4}$$

où C_1 et C_2 sont des constantes et T_0 est une température de référence. Le temps τ_α est le temps de relaxation α. Le domaine de validité de cette loi s'étend entre des températures proches et en dessous de T_g jusqu'à 100K au dessus de T_g. A haute température, le temps de relaxation est de 10^{-9}s typiquement et de 1 à 100 s proche de T_g. Enfin, la viscosité à T_g est égale à 10^{12} Pa.s [27]. Il y a un certain nombre d'années, il a été montré que la dynamique dans les système devenant vitreux n'est pas gouvernée par un temps de relaxation unique, mais par un spectre entier de temps de relaxation à l'échelle du monomère [28, 29, 30, 31, 33, 32, 34, 35]. La présence d'une distribution de temps de relaxations a été observée par de mesures diélectriques. D'autres études utilisant la RMN où la diffusion de molécules sondes ont permis de décrire l'aspect spatial des distribution de temps de relaxation, et ces résultats montrent la présence d'hétérogénéités dynamiques de 3-5 nm dans les polymères. La loi de Stokes-Einstein qui relie le coefficient de

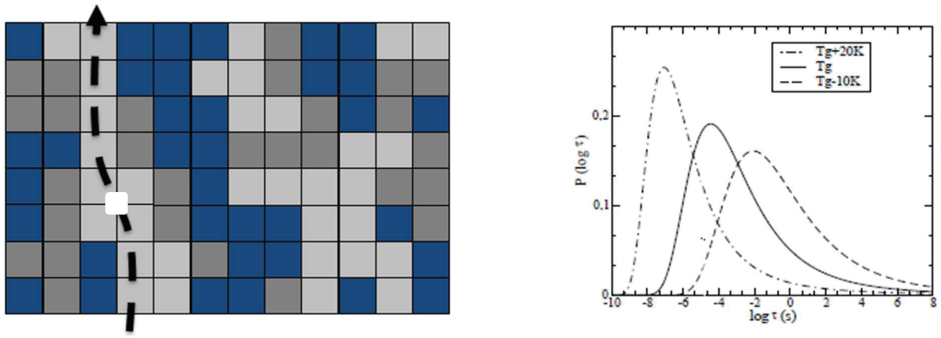

Figure 0.0.9: (Gauche) Diffusion d'une molécules sonde (carré blanc) dans un milieu hétérogène. Les sous unités en gris clair représentent les hétérogénéités rapides, alors que celle en noir représentent les lentes. La taille de la sonde est plus petite qu'une hétérogénéité et diffuse à travers les zones rapides (flèche). (Droite) Distributions de temps de relaxation dans le Polystyrène à $T_g + 20K$, T_g et $T_g - 10K$. Plus la température est basse, plus la distribution est large et les temps de relaxation sont longs.

diffusion D d'une molécules sonde de taille R et la viscosité η du milieu à la température T est:

$$\frac{D\eta}{T} = \frac{k_B}{6\pi R} \tag{0.0.5}$$

avec k_B la constante de Boltzmann. Jusqu'à $T_g + 50$K environ, la loi de Stokes-Einstein est retrouvée par l'expérience de diffusion de petites sondes. En dessous en revanche, il a été observé qu'elle était violée. L'amplitude de la violation est typiquement de 2-3 décades proche de T_g dans les matériaux de polymères simples, i.e. $\log\Big(D/D_{SE}\Big) \sim 2-3$ où D_{SE} est le coefficient de diffusion prédit par la loi de Stokes-Einstein. Malgré cela, l'amplitude de violation de la loi est moins prononcée lorsque la taille de la sonde augmente ce qui prouve l'aspect spatial des hétérogéneités dynamiques. En effet, dans un milieu hétérogène, il y a des sous unités lentes en coexistence avec des sous unités rapides. Si la sonde est plus petite que ces sous unités, elle diffusera principalement au sein des sous unités rapides, et son temps de diffusion sera plus rapide que le temps α obtenue par des mesures de viscosité (see Figure 0.0.9). Donc, dans ce contexte, ces processus de diffusion ne sont pas reliés au temps α. Si au contraire, la sonde est plus large qu'une sous unité, elle interagira avec les sous unités lentes et sa diffusion sera contrôlée par les temps α qui contrôlent la viscosité du milieu. Dans ce cas la relation de Stokes-Einstein est retrouvée. En conséquence, dans le cas de petites sondes, le fait que la quantité $\log\Big(D/D_{SE}\Big)$ augmente lorsqu'on approche T_g signifie que la distribution des temps de relaxation s'élargie (Cf. Figure 0.0.9). Enfin, même si la réponse visqueuse du système est pilotée par les temps longs, la dynamique hétérogène fait que le système n'est pas "gelé" et rend possible la diffusion de molécules dans l'état vitreux. Dans le contexte des systèmes binaires tels que les systèmes polymères-solvant, il a été observé que la loi de Stokes-Einstein est violée de 6 décades au moins, ce qui signifie que les distributions de temps de relaxation sont bien plus large dans ces systèmes que dans les systèmes vitreux de polymères purs. En effet, des observations éxpérimantales [14] montrent que la constante de diffusion du solvant à T_g est égale à $10^{-15} m^2.s^{-1}$ [14] ce qui fait

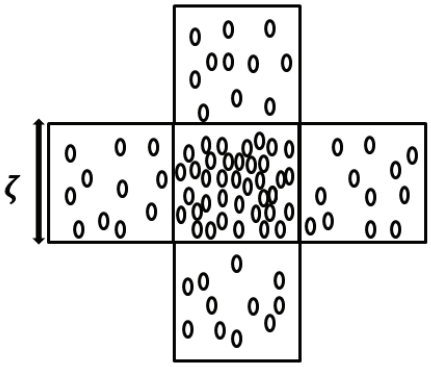

Figure 0.0.10: Représentation d'une fluctuation de densité à l'échelle $\xi \sim 3-5nm$: la cellule centrale, avec un temps de relaxation noté τ_{slow}, is plus dense que ces voisines ayant un temps de relaxation noté τ_{fast}. Les monomères qui appartiennent à la cellule centrale peuvent diffuser vers les cellules rapides par leur interface commune. Le temps de vie, noté τ_{life} d'une telle fluctuation de densité vaut $\tau_{life} = N^{2/3}\tau_{fast}$. N is le volume adimensionné d'une cellule tel que $\xi^3 = N/\rho_0$ avec ρ_0 la densité de close packing. En conséquence, une hétérogénéité lente peut fondre en un temps τ_{life}, et ce processus de fusion est piloté par la cellules rapides.

que les temps de relaxation responsables de la diffusion valent 10^{-4}s à l'échelle d'un monomère. En considérant que $\tau_\alpha = 100$s, on obtient une distribution large de 6 décades proche de T_g. D'un point de vue théorique, le modèle de Long et Lequeux [36, 37] donne une interprétation phénoménologique de la transition vitreuse. Il suppose l'existence d'une distribution spatiale des temps de relaxation, ce qui est justifié par les résultats expérimentaux décrits plus haut. La présence d'hétérogénéités dynamiques sont expliqués par les fluctuations de densité qui sont contrôlés par le module du bulk ($K_{bulk} \sim 10^9$Pa) dans le cas des matériaux de polymères purs. Selon cette interprétation, une hétérogénéité dynamique, dont le temps de relaxation interne est relié au volume libre moyen accessible aux monomères, est lente quand la densité est grande, et rapide quand la densité est basse. En conséquence, on peut associer un temps à une fluctuation de densité par le biai de la relation WLF qui est supposée valide à l'échelle des monomères. Enfin, à l'échelle du matériau, la distribution des fluctuations de densité donne naissance à une distribution spatiale des temps de relaxation. Dans les systèmes binaires, lorsqu'une composante rapide est mélangé à une composante lente, la distribution de temps de relaxation sont reliées aux fluctuations de composition qui sont contrôlées par le module osmotique $K_{osm} \sim 10^7$ Pa.

- **Mécanismes de facilitation**

La distribution spatiales des hétérogénéités dynamiques permettent de décrire des processus de fusion de sous unités lentes de taille ξ (temps de relaxation τ_{slow}) par la présence des sous unités rapides (temps de relaxation τ_{fast})[38]. Dans le cas des systèmes pures, ce processus s'illustre par des mécanismes de diffusion à l'interface entre les sous unités rapides et lentes, et

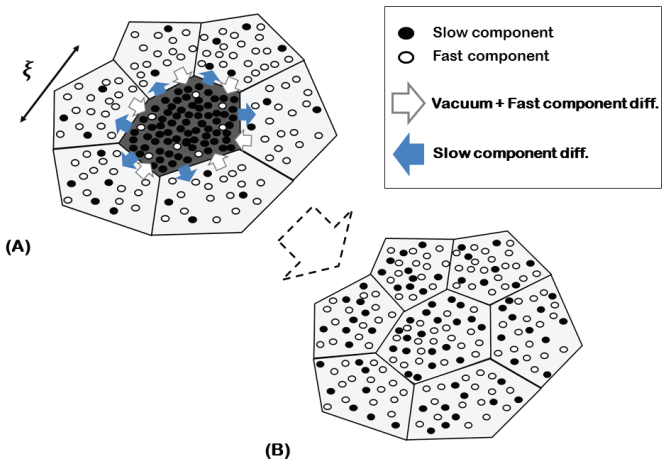

Figure 0.0.11: Représentation du mécanisme de facilitation dans le cas d'un système binaire. La sous unité centrale lente et dense (noir), avec un temps de relaxation τ_{slow}, est principalement composée de monomères lents. Les sous unités voisines sont elles rapides, avec un temps de relaxation τ_{fast}, et composées en majorité de monomères rapides. Grâce au mécanisme de facilitation, la relaxation de la sous unité lente est la conséquence de l'inter diffusion de monomères rapides et lents à l'interface. La diffusion des monomères rapides au sein de la cellule centrale est aussi accompagné de la diffusion de volume libre qui tend à accélérer la dynamique des monomères. Enfin, comme dans le cas des liquides de polymères purs, le temps de vie τ_{life} d'une telle fluctuation de composition vaut $\tau_{life} = N^{2/3}\tau_{fast}$.

le temps de vie d'une telle fluctuation de densité vaut

$$\tau_{life} = N^{2/3}\tau_{fast}$$

où $N = \xi^3 \times \rho_0$ est le volume adimensionné d'une hétérogénéité dynamique et ρ_0 la densité de close packing (Cf. Figure 0.0.10). Dans le cas des systèmes binaires, quand une hétérogénéité lente, dense et composée en majorité de monomères lents, est entourée de sous unités rapides composées de monomères rapides, le mécanisme de facilitation est la conséquence de la diffusion de monomères lents vers les sous unités rapides, et de la diffusion de monomères rapides qui diffusent au sein de la sous unité lente. La diffusion de monomères rapides est aussi accompagnée de la diffusion de volume libre. Ce dernier tend à accélérer la dynamique et donc à faciliter l'inter-diffusion des monomères. Comme dans le cas des liquides simples, le temps de vie de cette fluctuation de composition est $\tau_{life} = N^{2/3}\tau_{fast}$ (Cf. Figure 0.0.11). Comme nous le verrons, ces mécanismes sont fondamentaux pour décrire la fusion de structures vitreuses lentes au cours de phénomène de rajeunissement dans le mélange de polymères.

Les temps de relaxation α sont associés au processus de relaxation mécanique des matériaux vitreux, mais son origine précise n'est pas encore comprise. Il est dit dans la référence [36] que les temps α sont reliés à la percolation d'une petite fraction (10% typiquement) des sous unités les plus lentes et rigides. Enfin, le couplage entre les processus de relaxation α et le mécanisme de facilitation permet de donner une interprétation de la taille d'une hétérogénéité dynamique N_c.

Proche de T_g, N_c est estimé à quelques centaines de monomères ce qui donne $\xi = 3-5$nm comme il est montré expérimentalement. Dans la référence [41] les auteurs étudient le vieillissement après une trempe en température proche de T_g. Il a été observé que la distribution des temps de relaxation change de façon permanente, et l'état dynamique du système à un instant précis dépend de son histoire.

Objectifs

L'objectif principal de ce travail est d'étudier les mécanismes d'inter-diffusion de petites molécules dans l'état vitreux que ce soit à l'équilibre ou hors d'équilibre. Nous allons considérer deux sortes de systèmes:

- **Mélanges de polymères** avec des composantes ayant des T_gs différentes, pour lesquelles au moins une d'elles est en dessous du seuil d'enchevêtrement.
- **Systèmes polymères-solvant** en contact avec un réservoir de solvant. Le système sera sous la T_g du polymère pur et le nombre total de particules de solvant pourra changer en modifiant le potentiel chimique du réservoir.

Un modèle est construit pour décrire la dynamique de ces systèmes. Il incorpore la nature hétérogène de la dynamique à l'échelle de 3-5 nm, et prend en compte l'évolution de l'état dynamique des systèmes par rapport à leur histoire suivie. Dans les mélanges de polymères, nous serons particulièrement intéressé au processus de décomposition de phase proche ou sous la T_g du mélange pendant le vieillissement du système. Nous considèrerons aussi les processus de rajeunissement en réchauffant le système après qu'il ait été séparé de phase proche de T_g. Dans les systèmes polymère-solvant, nous étudierons les phénomènes de séchage et de gonflement.

Ce mémoire est composé des chapitres suivants

- Dans le chapitre 1, nous introduisons le modèle utilisé pour décrire la dynamique dans les mélanges de polymères et les mélanges polymères-solvant. Les ingrédients importants du modèle sont exposés ainsi que le modèle dynamique. Le passage entre les équations physiques et celles qui seront résoluent numériquement est aussi traité. Enfin, nous présentons la méthode suivie pour implémenter le mécanisme de facilitations numériquement.

- Dans le chapitre 2, nous appliquons le modèle introduit dans le chapitre 1 au cas des mélanges de polymères se séparant de phase proche ou en dessous de T_g. Nous discutons également du processus inverse lorsque le système se réchauffe et se remélange.

- Dans le chapitre 3, nous appliquons le modèle introduit dans le chapitre 1 afin d'étudier le séchage et le gonflement de films de polymères solvant sous la T_g du polymère pur en contact avec un réservoir de solvant.

Chapter 1

Modelling of binary mixtures close to and below T_g

1.1 Résumé en français

Dans ce chapitre, nous proposons l'implémentation d'un model spatiale adapté pour les deux systèmes: mélanges de polymères et systèmes polymères-solvant. Ce modèle coarse grainé est résolu sur un réseau carré et intègre le caractère hétérogène de la dynamique à l'échelle d'une hétérogénéité dynamique. Cette dernière correspond à la résolution spatiale du système (3-5nm). Un modèle thermodynamique décrivant les mélanges compressibles est conçu pour calculer les forces permettant de piloter la dynamique du système. Ces dernières sont égales au gradient de potentiel chimique entre deux site voisins. Comme une composante lente est mélangé avec une composante rapide la température de transition de la solution dépend explicitement de la composition. Ainsi par le biais de la loi WLF, nous calculons les temps de relaxation monomérique qui dépendent également de la composition. En conclusion, en couplant les fluctuations de composition et la température de transition vitreuses, on obtient une distribution spatiale des temps de relaxation à l'échelle d'une hétérogénéité dynamique. Ainsi les temps de relaxation sur un site riche en composante lente (resp rapide) est long (resp. court). Il faut noter que les temps de relaxation prennent en compte le volume libre présent dans chaque sites afin de traiter les situations hors d'équilibre. Enfin, afin de prendre en compte le mécanisme de facilitation, le coefficient cinétiques qui contrôle les échanges de matière entre un site et un de ses proches voisins est pris comme le plus court des deux . Enfin, nous prenons en compte également la relaxation mécanique du système en plus de la diffusion. En conclusion, suivant ce modèle, la relaxation d'un site est la conséquence de mécanismes de diffusion non linéaires entre le site lui-même et ses proches voisins, et de la relaxation mécanique du système.

1.2 Introduction

A theoretical work performed by Souche and Long [42] was aimed at studying the diffusion of solvent in glassy polymer films after the system is experiencing an arbitrary activity change.

This work shows notably that heterogeneous nature of the dynamics is very important for describing the solvent diffusion in glassy media. Indeed, in this scheme and as it is represented in Figure 0.0.2, solvent molecules could diffuse through fast dynamic heterogeneities in much shorter time than the mechanical relaxation driven by α-like relaxation times. However, this model proposed by Souche and Long does not incorporate any spatial aspects for solvent diffusion. We thus propose to extend it and to design a spatial diffusion model which incorporates the heterogeneous nature of the dynamics at the scale of a dynamic heterogeneity. Non linear constitutive equations for polymer and solvent diffusion are then solved at this scale on a 2D square lattice. Finally, we integrate explicitly the mechanical relaxation of the system in this model.

1.3 Physical model

- **Thermodynamics of pure polymer melts**

The diffusion of molecules is a relaxation process toward a state representing a minimum of free enthalpy. A free enthalpy model is then required to define such a state, and also to describe the composition fluctuations statistics in order to create dynamical heterogeneities.
We first consider a mean field thermodynamical model describing pure polymer melts. Quantities of interest are calculated based on the mean state of the system. In this context, the most relevant distance to consider between two neighboring particles of radius d is the mean intermolecular distance σ. The interaction energy is a Lennard-Jones potential: the attractive part is a potential that decreases with the distance r between the center of mass of particles like $-1/r^6$. To this potential, a repulsive part which varies like $1/r^{12}$ is added (see Figure 1.3.1 (b)). In our model we consider the same $1/r^6$ part that accounts for van der Waals attractive interactions, but in contrast, we only consider a pure Hard-Core (HC) repulsive potential (See Figure 1.3.1 (a)).
The attractive energy between two monomers i, j at a distance $r_{i,j}$ from each other reads:

$$U(i,j) = \frac{-C}{r_{i,j}^6}$$

where C is the Hamaker constant of the considered monomers and is typically of order 10^{-77} J m^6 [63]. The attractive interaction per monomer can be written as

$$W = \frac{1}{2}\sum_{j\neq i} U(i,j)$$

In the mean field picture, this sum has to be calculated by assuming that the particles are located at a typical distance σ from each other, which is directly related to the density of the

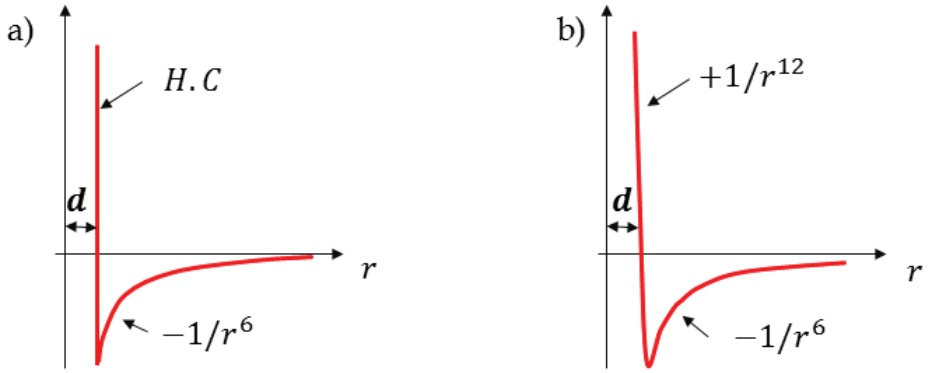

Figure 1.3.1: (a)Schematic of the potential that we use in our model. It has a $1/r^6$ attractive part and a Hard-Core (HC) part that accounts for the repulsive interactions. (b) Representation of the 6-12 Lennard-Jones potential used in the Cell Model by Prigogine et al [54, 55, 56, 57]. This model considers the same attractive potential than ours. Nevertheless, it considers a $1/r^{12}$ part at small distances for modelling repulsive interactions between particles.

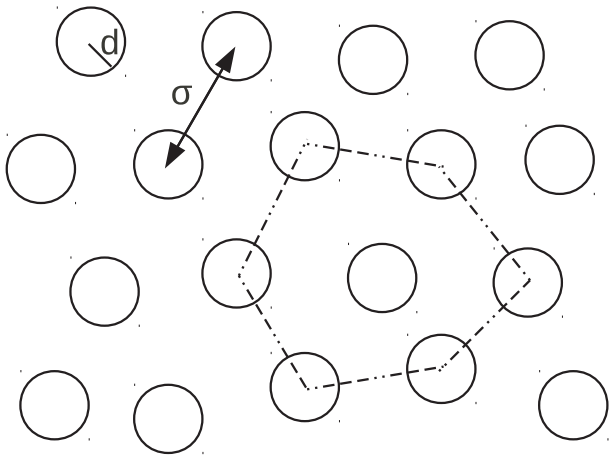

Figure 1.3.2: Schematic representation of a liquid in a mean field picture. The interaction energy has to be calculated assuming an average distance σ between particles. Similarly, the confinement entropy has to be calculated assuming an average volume in which the molecules can move. This volume, per molecule, is $(V - V_0)/N_A$, where N_A is the number of molecules, V is the total volume, $V_0 = N_A v_0$ is the total excluded volume due to the hard-core repulsion between the molecules. v_0 is the volume of one molecule.

sample. As a function of the number of monomers per unit volume ρ, one obtains

$$W = -\Phi C \rho^2 \tag{1.3.1}$$

with $\Phi \approx 4$. The quadratic dependence of the attractive energy is similar to that of the Prigogine model [55]. This dependence results from the r^{-6} decay of the interaction, and from the mean field picture.

Let us consider a molecular liquid constituted by small molecules of radius d for which we assume a hard-core repulsion. In the mean field picture, the entropy is the logarithm of the volume in which the molecules can move. The total volume of the liquid is V. Let us denote by V_0 the total volume of the molecules themselves. The available volume for motion per molecule is $v - v_0$ where $v = V/N_A$ and $v_0 = V_0/N_A$ and N_A is the number of molecules. The entropy per molecule reads then $S = \ln(v - v_0)$ [64]. The entropy may be written as

$$S = \ln(1 - v_0/v) + \ln v \tag{1.3.2}$$

The second term of the right hand side of Eq. (1.3.2) is the translational entropy per molecule when no restriction due to hard core or repulsive potentials are present. That corresponds to the perfect gas entropy. The first term is the contribution of confinement to the entropy. In the context of polymers, the translational entropy must be calculated per chain, whereas the confinement contribution is not modified. One obtains thus

$$S = \ln(1 - v_0/v) + \frac{1}{X_A} \ln v \tag{1.3.3}$$

where X_A is the degree of polymerization of the chains. In the dense state limit (at low temperature), $\ln v$ is a slowly varying function, close to $\ln v_0$. The second term of the right hand side of Eq.(1.3.3) can thus be considered as an irrelevant constant in this regime. This is all the more true for large molecular weight polymers. However, the term $\frac{1}{X_A} \ln v$ must be kept when dealing with more diluted cases (molecular liquids at high temperature) or when dealing with blends as will be discussed in the next section. In the context of large molecular weight polymers in the dense molten state, the entropy (1.3.3) can be written

$$S = \ln(\rho_0 - \rho) \tag{1.3.4}$$

where $\rho_0 = 1/v_0$ and $\rho = 1/v$, where we have omitted an irrelevant constant $\ln v_0$. This expression was used in reference [36] for describing the thermodynamics of large molecular weight polymers in the dense molten state. Note that the entropy term introduced by Prigogine et al [55], and Flory-Orvoll and Vrij [51, 59, 60, 61, 62] is similar to that of Equation (1.3.2).

For dense polymer melts, the equilibrium density ρ_{eq} corresponds to a local minimum of the free energy $F_0 = W - TS$:

$$F_0(\rho) = -\Phi C \rho^2 - T \ln(\rho_0 - \rho) \tag{1.3.5}$$

A metastable solution is obtained with the equation $\frac{\partial F_0}{\partial \rho} = 0$ and with the condition $\frac{\partial^2 F_0}{\partial \rho^2} > 0$. That results in a quadratic equation which can be solved exactly. We define a temperature noted T_c for which one finds a solution corresponding to a metastable equilibrium state for the melt when $T < T_c$, whereas above T_c no such state exists :

$$T_c = \frac{\Phi}{2}\rho_0^2 C \tag{1.3.6}$$

The corresponding density is equal to $\rho_0/2$. This temperature sets the temperature scale below which the liquid may be considered as a dense liquid. The regime of dense polymer liquids corresponds thus to $T \ll T_c$. For usual polymers, T_c is typically of order 1000 K [36, 58].

- **Thermodynamics of the compressible binary mixture**

For calculating the free energy for a compressible binary mixtures, we extend the model proposed in [36]. In case of N_A and N_B particles in a volume N at temperature T and pressure P, we define the free energy as :

$$\begin{aligned} G(N, N_A, N_B, P, T) =& a\frac{(N_A + N_B)N_A^2}{N^2} + b\frac{(N_A + N_B)N_B^2}{N^2} + 2c\frac{(N_A + N_B)N_A N_B}{N^2}(I) \\ &+ T\left(\frac{N_A}{X_A}\ln\left(\frac{N_A}{N}\right) + \frac{N_B}{X_B}\ln\left(\frac{N_A}{N}\right)\right)(II) \\ &- T(N_A + N_B)\ln\left(1 - \frac{N_A}{N} - \frac{N_B}{N}\right) + \frac{PN}{\rho_0}(III) \end{aligned} \tag{1.3.7}$$

where term (I) corresponds to the internal energy with $a, b, c \sim -10^{-20}J$; the term (II) is a translation entropy term with X_A and X_B the polymerisation degrees of molecular species A and B; term (III) is a confinement entropy plus the external pressure term. The term $\rho_0 = 1/a^3 \sim 10^{28}m^{-3}$ is the close packing density with a the size of a monomer. The volume N is dimensionless and is related to physical volume V thanks to relation $V[m^3] = N/\rho_0$. This model can also describe polymer-solvent blends by putting $X_A = 1$ and $X_B > 1$. It is also usable in case of pure solvent systems. At equilibrium, the volume N adapts itself to the number of particles N_A and N_B contained in this volume. Formally, at equilibrium, the system satisfies equation:

$$\left(\frac{\partial G}{\partial N}\right)_{N_A, N_B, P, T} = 0 \tag{1.3.8}$$

with $N \gtrsim N_A + N_B$. We can define the Gibbs free energy per unit volume, $\overline{G} = G/N$. We obtain

$$\begin{aligned}\overline{G} = \frac{G}{N} =& a(\phi_A + \phi_B)\phi_A^2 + b(\phi_A + \phi_B)\phi_B^2 + 2c(\phi_A + \phi_B)\phi_A\phi_B \\ &+ T\left(\frac{\phi_A}{X_A}\ln\left(\phi_A\right) + \frac{\phi_B}{X_B}\ln\left(\phi_B\right)\right) \\ &- T(\phi_A + \phi_B)\ln\left(1 - \phi_A - \phi_B\right) + \frac{P}{\rho_0}\end{aligned} \tag{1.3.9}$$

Volume fractions $\phi_A = N_A/N$ and $\phi_B = N_B/N$ are two independent variables which verify

$$\phi_A + \phi_B < 1$$

and the free volume fraction ϕ_v is such that $\phi_v = 1 - \phi_A - \phi_B$ where $\phi_v \sim 0,1$ typically. For models such as the Flory-Huggins model describing incompressible systems, we have $\phi_v = 0$. In reference [70], where this model is published, it is shown that equation of state obtained by the free energy written in Equation 1.3.7 is very close from a quantitative point of view, to that of the Cell Model by Prigogine[54, 55, 56, 57] or again of the FOV model[44, 45, 46, 47]. It has also the advantage to be easily treatable analytically. This free energy model is used to compute thermodynamical forces $F_{A/B}$ which drive the dynamics at a scale of a dynamical heterogeneity in out equilibrium situations by considering ϕ_A and ϕ_B as independent degrees of freedom. As we will see later on, thermodynamical forces depend on the local gradient of chemical potential $\mu_{A/B}$ in the material which we define as:

$$\begin{aligned}\mu_A =& \left(\frac{\partial G}{\partial N_A}\right)_{N_B,N,P,T} = \left(\frac{\partial \overline{G}}{\partial \phi_A}\right)_{\phi_B,P,T} \\ =& a\Big(3(\phi_A)^2 + 2\phi_A\phi_B\Big) + b(\phi_B)^2 + 2c\Big(2\phi_A\phi_B + (\phi_B)^2\Big) \\ &+ T\left(\frac{1}{X_A}\ln(\phi_A) - \ln(1 - \phi_A - \phi_B) + \frac{1}{X_A} + \frac{\phi_A + \phi_B}{1 - \phi_A - \phi_B}\right)\end{aligned} \tag{1.3.10}$$

and

$$\begin{aligned}\mu_B =& \left(\frac{\partial G}{\partial N_B}\right)_{N_A,N,P,T} = \left(\frac{\partial \overline{G}}{\partial \phi_B}\right)_{\phi_A,P,T} \\ =& b\Big(3(\phi_B)^2 + 2\phi_A\phi_B\Big) + a(\phi_A)^2 + 2c\Big(2\phi_B\phi_A + (\phi_A)^2\Big) \\ &+ T\left(\frac{1}{X_B}\ln(\phi_B) - \ln(1 - \phi_A - \phi_B) + \frac{1}{X_B} + \frac{\phi_A + \phi_B}{1 - \phi_A - \phi_B}\right)\end{aligned} \tag{1.3.11}$$

where $\overline{G} = G/N$.

It is worth considering the excess of free energy ΔG induced by a composition fluctuation

$\delta\phi = \begin{pmatrix} \delta\phi_A \\ \delta\phi_B \end{pmatrix}$. We consider a composition fluctuation taking place in a volume N immersed in a bigger system which can be seen as a reservoir of particles. We write

$$\begin{aligned} \Delta G &= N \times \Big[\overline{G}(\phi_A + \delta\phi_A, \phi_B + \delta\phi_B) - \overline{G}(\phi_A, \phi_B)\Big] \\ &\cong \frac{N}{2}\delta\phi^t \partial^2\overline{G}\delta\phi \end{aligned} \tag{1.3.12}$$

with

$$\partial^2\overline{G} \;= \begin{pmatrix} \partial^2_{\phi_A^2}\overline{G} & \partial^2_{\phi_A\phi_B}\overline{G} \\ \partial^2_{\phi_B\phi_A}\overline{G} & \partial^2_{\phi_B^2}\overline{G} \end{pmatrix} \;= \begin{pmatrix} a_{11} & a_{12} \\ a_{21} & a_{22} \end{pmatrix} \tag{1.3.13}$$

a dimensionless matrix with coefficients taken at equilibrium. In the approximated relation 1.3.12, linear terms have been omitted as due to the closeness of chemical potentials between both systems.
Eigenvalues λ_1 and λ_2 of matrix 1.3.13 read:

$$\begin{aligned} \lambda_1 &= \tfrac{Tr(\partial^2\overline{G})+\sqrt{\Delta}}{2} \\ \lambda_2 &= \tfrac{Tr(\partial^2\overline{G})-\sqrt{\Delta}}{2} \end{aligned} \tag{1.3.14}$$

with Δ the discriminant of the characteristic polynomial of $\partial^2\overline{G}$ which reads:

$$\Delta = \Big(Tr(\partial^2\overline{G})\Big)^2 - 4\,det(\partial^2\overline{G})$$

where $Tr(\partial^2\overline{G})$ and $det(\partial^2\overline{G})$ are the trace and the determinant of the matrix respectively. In the low temperature regime of interest, which corresponds to dense polymer melts or blends (*i.e.* when the temperature is far below the critical temperature of each of the components $T \ll T_c^A, T_c^B$), terms a_{11}, a_{12}, a_{21} et a_{22} are very closed to each other. We hence have $det(\partial^2\overline{G}) \ll \Big(Tr(\partial^2\overline{G})\Big)^2$ which implies that $\lambda_1 \gg \lambda_2$ because

$$\lambda_1 \approx Tr(\partial^2\overline{G})\Big(1 - \frac{det(\partial^2\overline{G})}{\Big(Tr(\partial^2\overline{G})\Big)^2}\Big) \approx Tr(\partial^2\overline{G})$$

$$\lambda_2 \approx \frac{det(\partial^2\overline{G})}{Tr(\partial^2\overline{G})}$$

In can be shown [70] that λ_1 and λ_2 are related to the bulk (K_{bulk}) and the osmotic (K_{osm}) modulus respectively up to a factor ρ_0 , i.e.:

$$\begin{aligned} K_{bulk} &\sim \frac{1}{2}\rho_0\lambda_1 \\ K_{osm} &\sim 2\rho_0\lambda_2 \end{aligned}$$

with $K_{bulk} \sim 10^9$Pa and $K_{osm} \sim 10^7$Pa. The expression of the osmotic modulus which controls composition fluctuations at the scale N is:

$$\begin{aligned} K_{osm} =& \rho_0 \Big(2(a+b)(\phi_s+\phi_p) - 4c(\phi_s+\phi_p) \\ &+ T\Big(\frac{1}{\phi_s} + \frac{1}{X\phi_p}\Big)\Big) \end{aligned} \tag{1.3.15}$$

The definition for the bulk modulus K_{bulk} is:

$$K_{bulk} = \rho_0 N \left(\frac{\partial^2 G}{\partial N^2}\right)_{N_A,N_B}$$

which gives by using equation 1.3.7:

$$\begin{aligned} K_{bulk} =& + \rho_0 \Big(6a(\phi_A+\phi_B)\phi_s^2 + 6b(\phi_A+\phi_B)\phi_p^2 + 12c(\phi_A+\phi_B)\phi_A\phi_B \Big) \\ &+ \rho_0 T \Big(\frac{\phi_A}{X_A} + \frac{\phi_B}{X_B} + \frac{(\phi_A+\phi_B)^2}{(1-\phi_A-\phi_B)^2}(2-\phi_A-\phi_B) \Big) \end{aligned} \tag{1.3.16}$$

We observe that unlike the bulk modulus, the expression of the osmotic modulus does not contain any diverging term: $(1-\phi_A-\phi_B)^{-1}$ which holds in the incompressible limit *i.e.* $\phi_A+\phi_B \to 1$. Moreover, one can note that by taking $\phi_A+\phi_B = 1$, one obtains:

$$K_{osm} = \rho_0 \Big(2(a+b) - 4c + T\Big(\frac{1}{X_A\phi_A} + \frac{1}{X_B\phi_B}\Big)\Big) \quad , \tag{1.3.17}$$

which corresponds to the standard expression of the osmotic modulus in the Flory-Huggins theory [21]

The total composition fluctuations ($\delta\phi$) distribution P in a system of volume N is given by;

$$P(\delta\phi) \propto \exp\Big(- \frac{N\Delta\overline{G}}{T}\Big) \tag{1.3.18}$$

where $\delta\phi = \begin{pmatrix} \delta\phi_A \\ \delta\phi_B \end{pmatrix}$ with $\delta\phi_{A/B} = \phi_{A/B} - <\phi_{A/B}>$ where $<\phi_{A/B}>$ is the average volume fraction of species A/B in the volume N. By using equation(1.3.12)one finds:

$$P(\delta\phi_A, \delta\phi_B) \propto \exp\Big(- \frac{N}{2T}(\delta\phi_A, \delta\phi_B)\partial^2\overline{G} \begin{pmatrix} \delta\phi_A \\ \delta\phi_B \end{pmatrix} \Big) \tag{1.3.19}$$

We show in Appendix 1.A.2 that the fluctuations distribution $\tilde{P}$ for one species k in the volume N reads

$$\tilde{P}(\delta\phi_k) \propto \exp\Big(- \frac{N}{2T}\Big[\big(\partial^2_{\phi_k^2}\overline{G}\big) - \frac{\big(\partial^2_{\phi_k\phi_{k'}}\overline{G}\big)^2}{\partial^2_{\phi_{k'}^2}\overline{G}} \Big]\delta\phi_k^2 \Big) \tag{1.3.20}$$

where $(k, k') = (A, B)$. We show as well in Appendix 1.A.2 that $\tilde{P}$ can be expressed as

$$\tilde{P}(\delta\phi_{A/B}) \propto \exp\Big(- \frac{N}{T}\lambda_2 \delta\phi_{A/B}^2\Big) \tag{1.3.21}$$

Let us now discuss the metastability conditions for blends. A multi-components blend is metastable if its Gibbs free energy is a convex function of the set of its independent variables. For the two components compressible blends considered here, $\overline{G}$ is a function of two independent variables ϕ_A and ϕ_B. The condition for metastability is thus that both eigen-values satisfy to the conditions $\lambda_1 > 0$ and $\lambda_2 > 0$ [66, 69]. As λ_1 is always positive, the relevant condition for metastability is thus $\lambda_2 < 0$, i.e. $\det(\partial^2\overline{G}) < 0$. The spinodal line is given by the equations

$$\left(\frac{\partial G}{\partial N}\right)_{N_A,N_B,P,T} = 0 \tag{1.3.22}$$

and

$$\lambda_2 = 0 \tag{1.3.23}$$

As it is shown in appendix1.A.1, this model has been confronted to experiment regarding phase behaviors in PS/PB and PS/PVME blends at non zero pressure. We show that this model reproduce well in a semi quantitative way experimental results. Finally, this model can be also applied to the case of pure solvent systems when reduced to one component for obtaining an expression of the chemical potential of the solvent reservoir. This aims to define equilibrium conditions between the reservoir and the polymer-solvent system as we will see in section 1.A of Chapter 3.

- **Glass transition temperature and relaxation times**

In Figure 1.3.3(a)(Black curve), we give the variation of equilibrium α-relaxation times at $T = 298K$ as a function of polymer volume fraction (ϕ_p) in PMMA(Polymethyl Methacrylate / polymer) / DEP(Diethyl phthalate / solvent) mixtures. We see in Figure 1.3.3(a) that the system is glassy for $\phi_p \geqslant \phi_g^p \approx 0.75$ ($\tau_\alpha(\phi_g^p) = 100s$) whereas it is molten for $\phi_p < \phi_g^p$: the presence of solvent tends to accelerate the dynamics of the system. Wether it is in case of thermodynamically miscible polymer blends or polymer solvent systems [74, 76, 77, 78], the equilibrium blend glass transition temperature is a function of the average composition of the system. In our model, wether for polymer blends or polymer solvent systems, we consider the following expression for the blend T_g:

$$\frac{T_g^{blend}(\phi_A, \phi_B)}{T_g^A} = \alpha + \beta\phi_A + \gamma\phi_B \tag{1.3.24}$$

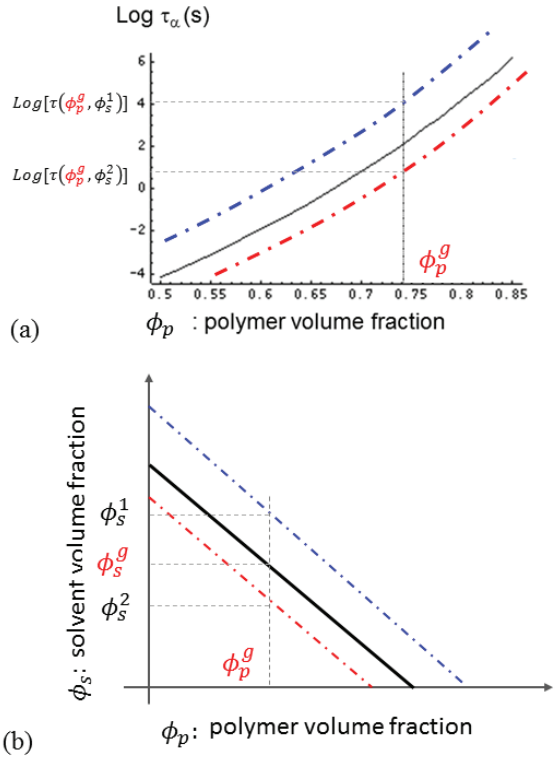

Figure 1.3.3: (a)Evolution of equilibrium α-relaxation times (black curve) in PMMA(Polymethyl Methacrylate: polymer)/DEP(Diethyl phthalate: solvent) system at $T = 298K$. Pure PMMA glass transition temperature is equal to $400K$. At fixed temperature, we see that the lower the polymer volume fraction, the faster the dynamics: the presence of solvent tends to accelerate the dynamics. Moreover, ϕ_g^p is the equilibrium PMMA volume fraction from which the system becomes glassy. The corresponding equilibrium solvent volume fraction is noted $\phi_s^g = \phi_s(\phi_g^p)$. (b) We schematize, in the phase space (ϕ_p, ϕ_s), the equilibrium curve(black curve) as well as two curves representing out of equilibrium situations (dashed red and blue curves). The Blue one corresponds to the situation where the solvent volume fraction is higher than its equilibrium value equilibrium $(\phi_s > \phi_s^g)$ at fixed polymer volume fraction ϕ_g^p. In contrast, the red curve corresponds to the situation where the solvent volume fraction is lower than its equilibrium value $(\phi_s < \phi_s^g)$ at fixed polymer volume fraction ϕ_g^p. In the first case, T_g^{blend} increases due to the free volume reduction (See Figure 1.3.4) and the dynamics slows down -i.e. $\tau(\phi_p^g, \phi_s^1) > \tau(\phi_p^g, \phi_s^g)$ as it is represented in Figure(a) and (b)-. In the second case though, T_g^{blend} decreases due to the free volume increase (See Figure 1.3.4) and the dynamics accelerates -i.e. $\tau(\phi_p^g, \phi_s^2) < \tau(\phi_p^g, \phi_s^g)$ as it is represented in Figure(a) and (b)-.

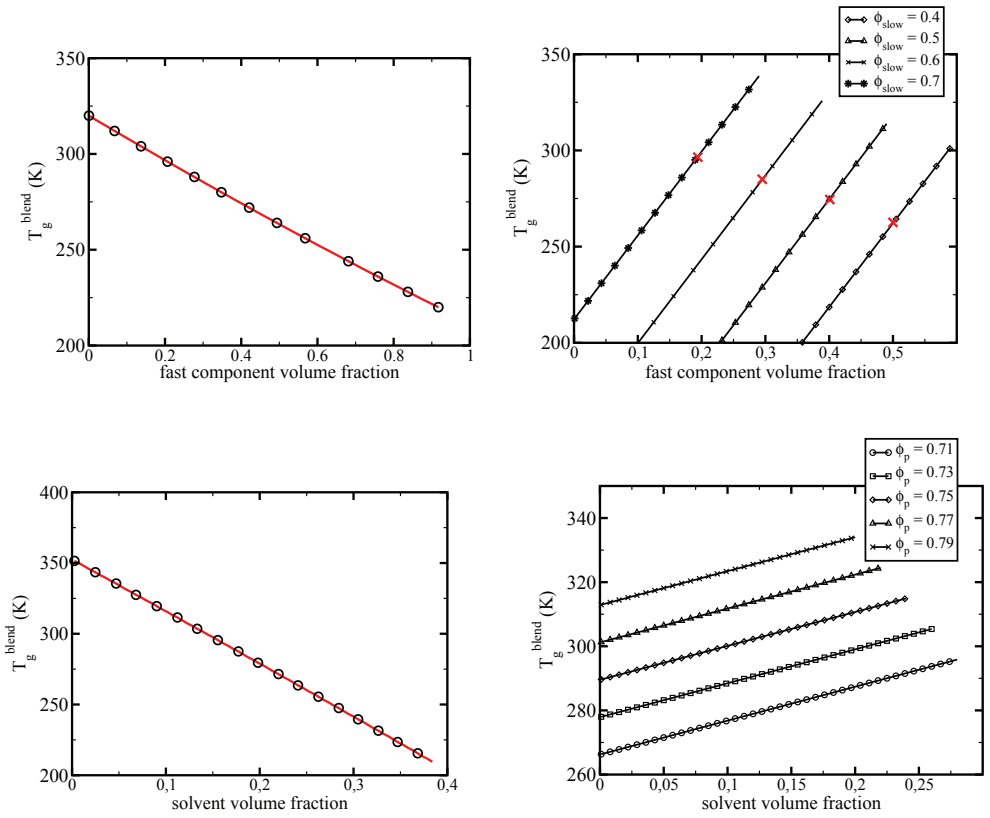

Figure 1.3.4: (UP-Left) Evolution of equilibrium blend glass transition temperature as a function of the fast component volume fraction in case of polymer blends. The T_g of the blend follows equation $T_g^{blend}(\phi_A, \phi_B)/T_g^A = \alpha + \beta\phi_A + \gamma\phi_B$ with $T_g^A = 320K$ and $T_g^B = 220K$. A and B are referred to the slow and fast component respectively and parameter are $\alpha = -1.27247$, $\beta = 2.5467$ and $\gamma = 1.9823$. (UP-Right) Evolution of the T_g^{blend} at fixed slow component volume fraction: 0,4; 0,5; 0,6 and 0,7 in case of polymer blends. Red cross correspond to the equilibrium fast component volume fraction given the fixed slow component volume fraction. (BOTTOM-Left) Evolution of the blend glass transition temperature as a function of the solvent component volume fraction in case of polymer-solvent systems. Parameters are $T_g^A = 352.5K$ (pure polymer T_g), $\alpha = -0.4184$, $\gamma = 1.6531$ and $\beta = 0.3$. (BOTTOM-Right) Evolution of the glass transition temperature versus solvent volume fraction at fixed slow component volume fraction in case of polymer blends and polymer-solvent systems. Either it is in case of polymer blends or polymer-solvent systems in Figure (UP-Right) or (BOTTOM-Right), T_g^{blend} decreases when the free volume fraction increases. This represent the plasticising effect of the free volume at the monomeric level.

where T_g^A is the T_g of the slow component and β (resp γ) is related to the plasticising effect of species A (resp B). Parameters α, β, γ are chosen such that $\alpha + \beta\phi_A(\phi_B = 0) = 1$ and $\alpha + \gamma\phi_B(\phi_A = 0) = T_g^B/T_g^A$ where T_g^B is the T_g of the fast component. Note that the quantity $T_g^{blend}(\phi_A, \phi_B)/T_g^A$ is an input of the model. Thus, the expression 1.3.24 has been chosen for simplicity and the latter represents the reference T_g for thermodynamically miscible mixtures (See Figure 1.3.4). We reformulate the WLF law written in equation0.0.1 as:

$$\ln\left(\frac{\tau(T)}{\tau_0}\right) = \frac{C_1 C_2}{T - T_0 + C_2} \tag{1.3.25}$$

where T_0 is a reference temperature. We chose $T_0 = T_g$ here, and $\tau(T_0) = 100$sec. Finally, we have $\tau_0 = 10^{-C_1}\tau(T_0)$. By making use of relation 1.3.24 one obtains relaxation times which depends on composition -i.e.

$$\tau(\phi_A, \phi_B) = \tau_{WLF}(T - T_g^{blend}(\phi_A, \phi_B)) \tag{1.3.26}$$

As we consider compressible mixtures, the relation 1.3.26 depends also on the free volume fraction. We see in Figure 1.3.4 that T_g^{blend} decreases (resp. increases) when the free volume fraction increases (resp. decreases). Hence, in out of equilibrium situations, as it is represented by the blue and red dashed curves in Figure 1.3.3(a) and (b), the dynamics may either accelerate or slow down when the free volume fraction increases or decreases respectively.
We can say from all this that the necessity of considering a compressible model lies essentially in the fact that: -1- both species volume fractions can fluctuate independently from each other which influences the out of equilibrium dynamics as it has just been discussed and -2- the compressibility of the material affects its global dynamics. Finally, we argued that composition fluctuations determine the width of the relaxation time spectrum [75]. Note that as K_{osm} is two orders of magnitudes smaller than K_{bulk}, the dynamics is more heterogeneous in binary systems than in a pure (simple or polymeric) glass forming liquid.

- **Equation of dynamics**

The total free energy in the system reads

$$G = \rho_0 \int \overline{G}(\phi_A, \phi_B; P, T) d^3x \tag{1.3.27}$$

at pressure P and temperature T. Here we have $[d^3x] = m^3$. For local variations of the concentration in A and B polymers $\delta\phi_A$ et $\delta\phi_B$, the variation of G reads

$$\delta G = \rho_0 \int \left[\left(\frac{\partial \overline{G}}{\partial \phi_A}\right)_{\phi_B,P,T} \delta\phi_A + \left(\frac{\partial \overline{G}}{\partial \phi_B}\right)_{\phi_A,P,T} \delta\phi_B \right] d^3x \tag{1.3.28}$$

By using the above definition for chemical potential and the conservation equations which read

$$\begin{aligned} \frac{\partial \phi_A}{\delta t} &= -\vec{\nabla} \cdot \vec{j}_A \qquad \Rightarrow \qquad \delta\phi_A = -\delta t \vec{\nabla} \cdot \vec{j}_A \\ \frac{\partial \phi_B}{\delta t} &= -\vec{\nabla} \cdot \vec{j}_B \qquad \Rightarrow \qquad \delta\phi_B = -\delta t \vec{\nabla} \cdot \vec{j}_B \end{aligned} \tag{1.3.29}$$

we obtain

$$\begin{aligned} \frac{\partial G}{\partial t} =& -\rho_0 \int \mu_A(\phi_A, \phi_B, P, T)\ \vec{\nabla} \cdot \vec{j}_A\ d^3x \\ & -\rho_0 \int \mu_B(\phi_A, \phi_B, P, T)\ \vec{\nabla} \cdot \vec{j}_B\ d^3x \end{aligned} \tag{1.3.30}$$

which yields

$$\begin{aligned} \frac{\partial G}{\partial t} =& \rho_0 \int \vec{\nabla}\mu_A(\phi_A, \phi_B, P, T)\ \cdot\ \vec{j}_A\ d^3x \\ & +\rho_0 \int \vec{\nabla}\mu_B(\phi_A, \phi_B, P, T)\ \cdot\ \vec{j}_B\ d^3x \end{aligned} \tag{1.3.31}$$

The general expression reads

$$\frac{\partial G}{\partial t} = -\rho_0 \int \left[\vec{F}_A \cdot \vec{j}_A + \vec{F}_B \cdot \vec{j}_B\right] d^3x \tag{1.3.32}$$

$\vec{F}_A$ and $\vec{F}_B$ are the thermodynamic forces which drive the relaxation of the system in the frame of Onsager's formalism. Within this formalism, the fluxes are proportional to the forces. We assume:

$$\begin{aligned} \vec{j}_A &= \lambda_A(\phi_A, \phi_B)\vec{F}_A = -\frac{\lambda_B(\phi_A, \phi_B)}{T}\vec{\nabla}\mu_A(\phi_A, \phi_B, P, T) \\ \vec{j}_B &= \lambda_B(\phi_A, \phi_B)\vec{F}_B = -\frac{\lambda_B(\phi_A, \phi_B)}{T}\vec{\nabla}\mu_B(\phi_A, \phi_B, P, T) \end{aligned} \tag{1.3.33}$$

Evolution equations finally read

$$\begin{aligned} \frac{\partial \phi_A}{\partial t} &= \vec{\nabla}\ \cdot \Big(\frac{\lambda_A(\phi_A, \phi_B)}{T}\vec{\nabla}\mu_A(\phi_A, \phi_B, P, T)\Big) \\ \frac{\partial \phi_B}{\partial t} &= \vec{\nabla}\ \cdot \Big(\frac{\lambda_B(\phi_A, \phi_B)}{T}\vec{\nabla}\mu_B(\phi_A, \phi_B, P, T)\Big) \end{aligned} \tag{1.3.34}$$

where the temperature T and the chemical potential are in Joules. Furthermore quantity $\lambda_{A/B}$ are diffusion coefficients ($[\lambda] = m^2.s^{-1}$) which depend on local relaxation times τ: $\lambda \sim a^2/\tau_{WLF}$ where a corresponds to the size of a monomer. We conclude from this that driving forces are given by chemical potential gradient ($\vec{F}_{A/B} = -\vec{\nabla}\mu_A(\phi_A, \phi_B, P, T)$) and currents are along chemical potential gradients, which is usual in diffusion theory. However, in our case, relaxation times are explicit functions of local composition, hence, diffusion coefficients

depend also on local composition and are not constant. This is a very important specificity of this diffusion model, which makes it different from the Fick model which assumes a constant diffusion coefficient. Finally, a derivation of Ficks laws from our model has been performed in appendix 1.B.

1.4 Solving the model

We give a representation in Figure 1.4.1 of the 2D square lattice on which the physical model described above is solved. The spatial resolution of the system is equal to the size of a dynamic heterogeneity $\xi \sim 3 - 5nm$ which reads:

$$\xi = \left(\frac{N_c}{\rho_0}\right)^{1/3} \tag{1.4.1}$$

where N_c is a input parameter of the model which is put equal to 500 in this work. Each site composed of both component volume volume fraction $\phi_A(i)$ and $\phi_B(i)$, exchange with its next neighbors, and driving forces which control the matter exchanges between sites is computed by means of the thermodynamical model described in previous section. The coupling between relaxation times and sites composition gives rise to a spatial distribution of relaxation times in the whole system. In case of polymer solvent system, the film is in contact with a solvent reservoir at one side and the opposite side is solid like. In other directions, we apply periodic boundary conditions. By changing the solvent reservoir activity(chemical potential equivalently), solvent molecules are allowed to penetrate or evaporate the system, but the polymer is not allowed to exchange with the reservoir. In case of polymer blends, we consider periodic boundary conditions in both directions. Note that in this case, the system will be always 30×30 cells large. According to the 2D-lattice model proposed above, we solve the discretized form of equations (1.3.34). We have at a site i:

$$\frac{\partial \phi_A(i)}{\partial t} = \sum_{<j>} \gamma_A^{(i,j)} \left[\left(\mu_A^{(j)} - \mu_A^{(i)} \right) \right] \tag{1.4.2}$$

$$\frac{\partial \phi_B(i)}{\partial t} = \sum_{<j>} \gamma_B^{(i,j)} \left[\left(\mu_B^{(j)} - \mu_B^{(i)} \right) \right] \tag{1.4.3}$$

where $< j >$ accounts for next neighboring sites. Following transformations have been performed to write equations 1.4.2 and 1.4.3:

$$\begin{aligned} \frac{\mu_{A/B}^i}{T} &\rightarrow \mu_{A/B}^i \\ \frac{\lambda_{A/B}^{(i,j)}}{\xi^2} &\rightarrow \gamma_{A/B}^{(i,j)} = 1/\tau_{WLF} \\ t/N_c^{2/3} &\rightarrow t \end{aligned}$$

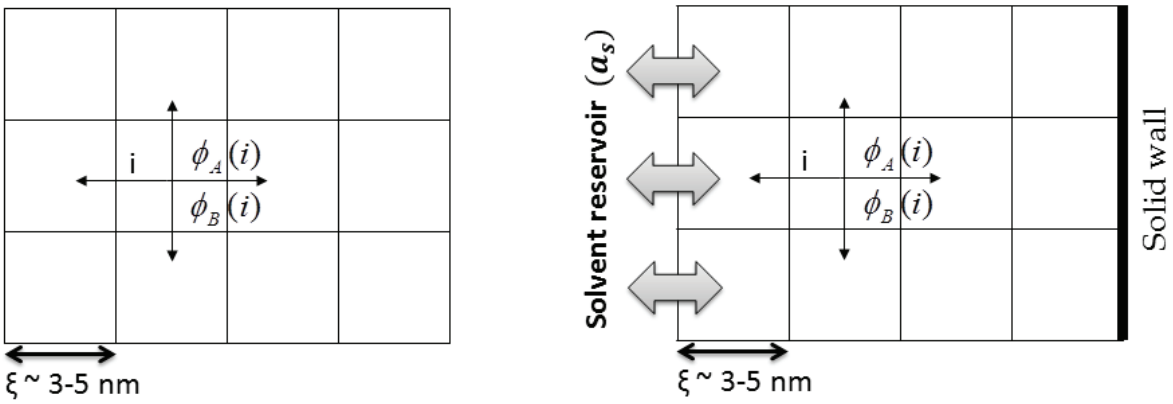

Figure 1.4.1: Schematic representation of the 2D-spatial model in case of polymer blends (Left) and polymer-solvent systems (Right). In both systems, every sites are of the size of a dynamic heterogeneity ($\xi \sim 3-5nm$) and exchange matter with their next neighbors. In case of polymer blends, we consider boundary conditions in both direction. In case of polymer-solvent systems, the left hand side is in contact with a pure solvent reservoir, and the right hand side is solid-like. We consider boundary condition in the other direction. The number of solvent molecules in the film depends on the activity of the reservoir (a_s). The latter can be changed arbitrarily in time, which makes that the quantity of solvent within the system can vary.

Note that dimensionless chemical potential $\mu^i_{A/B}$ are of order unity.
We will specify quantity γ later on. Moreover, α is a dimensionless parameter, smaller than one, which incorporates the difference of molecular weights between both species. We note:

$$\begin{aligned} \gamma^{i,j}_A &= \gamma^{i,j} \\ \gamma^{i,j}_B &= \alpha\gamma^{i,j} \end{aligned} \tag{1.4.4}$$

- **Composition fluctuations: Langevin formalism**

The aim now is to include fluctuations in equations (1.4.2) and (1.4.3). To do so, let us consider a very simple system, constituted only by one subunit i of volume N_c in contact with a reservoir denoted $i+1$. We consider the statistics and the dynamics of the fluctuations between the reservoir and the subunit. Note that in this discussion, we consider the dimensionless free energy -i.e. $\overline{G}/T \quad \rightarrow \quad \overline{G}$ - and dimensionless chemical potentials -i.e. $\mu^i_{A/B}/T \quad \rightarrow \quad \mu^i_{A/B}$-.
The evolution equations given in equations 1.4.2 and 1.4.3 for this simple system are

$$\begin{aligned} \frac{\partial\phi^i_A}{\partial t} &= \gamma^{i,i+1}(\mu^{i+1}_A - \mu^i_A) \\ \frac{\partial\phi^i_B}{\partial t} &= \alpha\gamma^{i,i+1}(\mu^{i+1}_B - \mu^i_B) \end{aligned} \tag{1.4.5}$$

One can then calculate the chemical potentials of both species in subunit i by the following approximation:

$$\begin{aligned}\mu_A^i &= \mu_A^{i+1} + \frac{\partial \mu_A^{i+1}}{\partial \phi_A}\Big(\phi_A^i - \phi_A^{i+1}\Big) + \frac{\partial \mu_A^{i+1}}{\partial \phi_B}\Big(\phi_B^i - \phi_B^{i+1}\Big) \\ \mu_B^i &= \mu_B^{i+1} + \frac{\partial \mu_B^{i+1}}{\partial \phi_A}\Big(\phi_A^i - \phi_A^{i+1}\Big) + \frac{\partial \mu_B^{i+1}}{\partial \phi_B}\Big(\phi_B^i - \phi_B^{i+1}\Big)\end{aligned} \tag{1.4.6}$$

where μ_A^{i+1} and μ_B^{i+1} are the chemical potentials of species A and B in the reservoir. One has then

$$\begin{aligned}\frac{\partial \phi_A^i}{\partial t} &= -\gamma^{i,i+1}\Big(\frac{\partial \mu_A^{i+1}}{\partial \phi_A}\delta\phi_A^i + \frac{\partial \mu_A^{i+1}}{\partial \phi_B}\delta\phi_B^i\Big) \\ \frac{\partial \phi_B^i}{\partial t} &= -\alpha\gamma^{i,i+1}\Big(\frac{\partial \mu_B^{i+1}}{\partial \phi_A}\delta\phi_A^i + \frac{\partial \mu_B^{i+1}}{\partial \phi_B}\delta\phi_B^i\Big)\end{aligned} \tag{1.4.7}$$

with $\delta\phi_A^i = \phi_A^i - \phi_A^{i+1}$ and $\delta\phi_B^i = \phi_B^i - \phi_B^{i+1}$. Above equation reads

$$\frac{\partial}{\partial t}\begin{pmatrix}\delta\phi_A^i \\ \delta\phi_B^i\end{pmatrix} = -\gamma^{i,i+1}\begin{pmatrix}1 & 0 \\ 0 & \alpha\end{pmatrix} \partial^2\overline{G}\begin{pmatrix}\delta\phi_A^i \\ \delta\phi_B^i\end{pmatrix} \tag{1.4.8}$$

where $\partial^2\overline{G}$ is the dimensionless version of the matrix given in equation 1.3.13 calculated with the concentrations ϕ_A^{i+1} and ϕ_B^{i+1} of the reservoir. The equation (1.4.8) is a relaxation equation without thermal fluctuations. $\delta\phi_A^i$ and $\delta\phi_B^i$ relax to zero which corresponds to the equality of concentrations between the subunit i and the reservoir $i+1$. Let us add here the effect of thermal noise $(\delta\psi_A, \delta\psi_B)$ regarding the evolution of the quantities $\delta\phi_A^i$ and $\delta\phi_B^i$. Let us write

$$\frac{\partial}{\partial t}\begin{pmatrix}\delta\phi_A^i \\ \delta\phi_B^i\end{pmatrix} = -\begin{pmatrix}\gamma^{i,j} & 0 \\ 0 & \alpha\gamma^{i,j}\end{pmatrix}\left[\partial^2\overline{G}\begin{pmatrix}\delta\phi_A^i \\ \delta\phi_B^i\end{pmatrix} - \begin{pmatrix}\delta\psi_A \\ \delta\psi_B\end{pmatrix}\right] \tag{1.4.9}$$

which we write as

$$\frac{\partial}{\partial t}\begin{pmatrix}\delta\phi_A^i \\ \delta\phi_B^i\end{pmatrix} = L\left[-\partial^2\overline{G}\begin{pmatrix}\delta\phi_A^i \\ \delta\phi_B^i\end{pmatrix} + \delta\psi\right] \tag{1.4.10}$$

with

$$L = \begin{pmatrix}\gamma^{i,j} & 0 \\ 0 & \alpha\gamma^{i,j}\end{pmatrix} \tag{1.4.11}$$

$\delta\psi = \begin{pmatrix}\delta\psi_A \\ \delta\psi_B\end{pmatrix}$ is the contribution of thermal noise. The thermal noise is introduced as a white noise. The statistics of $\delta\psi$ is chosen such that the distribution of concentration fluctuations in subunit i satisfies to the relation :

$$P(\delta\phi_A^i, \delta\phi_B^i) \propto exp\left(\frac{-N_c}{2}(\delta\phi_A^i, \delta\phi_B^i)\partial^2\overline{G}\begin{pmatrix}\delta\phi_A^i \\ \delta\phi_B^i\end{pmatrix}\right) \tag{1.4.12}$$

Then, the correlation must satisfy to the relation [20]

$$< \delta\psi_\alpha(t)\delta\psi_\beta(t') >= \frac{2(L^{-1})_{\alpha,\beta}}{N_c}\delta(t-t') \tag{1.4.13}$$

where $\delta(t-t')$ is the Dirac δ function. α and β design A or B. One obtains

$$\begin{aligned} < \delta\psi_A(t)\delta\psi_A(t') >&= \frac{2(\gamma^{i,j})^{-1}}{N_c}\delta(t-t') \\ < \delta\psi_B(t)\delta\psi_B(t') >&= \frac{2(\alpha\gamma^{i,j})^{-1}}{N_c}\delta(t-t') \\ < \delta\psi_A(t)\delta\psi_B(t) >&=< \delta\psi_B(t)\delta\psi_A(t) >= 0 \end{aligned} \tag{1.4.14}$$

The equations we have just written describe the dynamics of the fluctuations between one isolated subunit in contact with a single reservoir. Let us come back now to the spatial problem. A given subunit is in contact with several reservoirs, which are the neighboring subunits, those number we denote by p. In 3D, one must consider $p = 6$ such neighbors on a cubic lattice, or $p = 4$ in 2D on a square lattice. Each neighbor exchanges monomers with the considered subunit and these fluctuations contribute to the total concentration fluctuation of the considered subunit i. These are random and independent contributions.

$$\begin{aligned} &\frac{\partial}{\partial t}\begin{pmatrix}\delta\phi_A^i \\ \delta\phi_B^i\end{pmatrix} \quad = \\ &-\sum_{<j>}\begin{pmatrix}\gamma^{i,j} & 0 \\ 0 & \alpha\gamma^{i,j}\end{pmatrix} \quad \left[\partial^2\overline{G}\begin{pmatrix}\delta\phi_A^{i,j} \\ \delta\phi_B^{i,j}\end{pmatrix} \quad - \begin{pmatrix}\delta\psi_A^{i,j} \\ \delta\psi_B^{i,j}\end{pmatrix} \quad \right] \end{aligned} \tag{1.4.15}$$

where $\delta\phi_A^{i,j} = \phi_A^i - \phi_A^j$ and $\delta\phi_B^{i,j} = \phi_B^i - \phi_B^j$ and $\delta\psi_A^{i,j}$ and$\delta\psi_B^{i,j}$ are respectively the species A and B fluctuations from site j to site i. Close to equilibrium and on average, the concentration of sites j is the average concentration ϕ_A and ϕ_B. The evolution equations become

$$\frac{\partial}{\partial t}\begin{pmatrix}\delta\phi_A^i \\ \delta\phi_B^i\end{pmatrix} \quad = pL\left[-\partial^2\overline{G}\begin{pmatrix}\delta\phi_A^i \\ \delta\phi_B^i\end{pmatrix} \quad + \frac{1}{p}\sum_{<j>}\delta\psi^{i,j}\right] \tag{1.4.16}$$

The thermal fluctuations $\delta\psi^{i,j}$ are random variables independent from each other. We deduce that each of them satisfy the same correlations as those obtained when a single neighbor was present. Indeed, by writing

$$\delta\psi_\alpha = \frac{1}{p}\sum_{<j>}\delta\psi_\alpha^{i,j} \tag{1.4.17}$$

where α=A or B, and by using equations 1.4.13 we deduce

$$\begin{aligned} < \delta\psi_\alpha(t)\delta\psi_\beta(t') > &= \frac{1}{p^2}\sum_{<j>} < \delta\psi_\alpha^{i,j}(t)\delta\psi_\beta^{i,j}(t') > \\ &= \frac{2(pL)^{-1}_{\alpha\beta}}{N_c}\delta(t-t') \end{aligned} \tag{1.4.18}$$

and we obtain the correlation functions for the fluctuations:

$$\begin{aligned} &< \delta\psi_A^{i,j}(t)\delta\psi_A^{i,j}(t') >= \frac{2(\gamma^{i,j})^{-1}}{N_c}\delta(t-t') \\ &< \delta\psi_B^{i,j}(t)\delta\psi_B^{i,j}(t') >= \frac{2\alpha(\gamma^{i,j})^{-1}}{N_c}\delta(t-t') \\ &< \delta\psi_A^{i,j}(t)\delta\psi_B^{i,j}(t') >= 0 \end{aligned} \tag{1.4.19}$$

We take these fluctuations into account now in the evolution equations (1.4.2) and (1.4.3). The evolution equations for the concentration of monomers A and B at site i are then

$$\begin{aligned} \frac{\partial\phi_A(i)}{\partial t} &= \sum_{<j>}\gamma^{(i,j)}\Big(\mu_A^{(j)} - \mu_A^{(i)} + \delta\psi_A^{i,j}\Big) \\ \frac{\partial\phi_B(i)}{\partial t} &= \sum_{<j>}\gamma^{(i,j)}\Big(\alpha(\mu_B^{(j)} - \mu_B^{(i)}) + \delta\psi_B^{i,j}\Big) \end{aligned} \tag{1.4.20}$$

In order to perform numerical integration, equations 1.4.20 in the introduction are descritized *ie.*:

$$\frac{\Delta\phi_A(i)}{\delta t} = \sum_{<j>}\gamma^{(i,j)}\Big[\Big(\mu_A^{(j)} - \mu_A^{(i)}\Big) + \delta_A^{i,j}\Big] \tag{1.4.21}$$

$$\frac{\Delta\phi_B(i)}{\delta t} = \sum_{<j>}\gamma^{(i,j)}\Big[\alpha\Big(\mu_B^{(j)} - \mu_B^{(i)}\Big) + \delta_B^{i,j}\Big] \tag{1.4.22}$$

where δt is a time step and $\Delta\phi_\alpha(i) = \phi_\alpha(i)(t+\delta t) - \phi_\alpha(i)(t)$. The discretized thermal noise is a random variable which we write $\delta_A^{i,j} = \beta\sqrt{\frac{2}{N_c\gamma^{i,j}\delta t}}$ and $\delta_B^{i,j} = \beta\sqrt{\frac{2\alpha}{N_c\gamma^{i,j}\delta t}}$ where β a random variable that follows Gaussian distribution of variance unity. Note that the method followed for determining the time step is presented in Appendix 1.D.

In case of polymer solvent system, solvent is treated as a simple molecule, i.e. $X_A = 1$ and according to equations 1.4.20, solvent is the A species and the polymer the B species.

Sites located at the film/reservoir interface interact with the reservoir which imposes a chemical potential on the system $\mu_s^{res} = \ln(a_s)$ where a_s is the reservoir activity and μ_s^{res} the dimensionless reservoir chemical potential. We consider the following driving force $F_s^{film/res}$ for driving the matter exchange between the system and the reservoir:

$$F_s^{film/res} = (\ln(a_s) - \mu_s(i)) \tag{1.4.23}$$

The kinetic coefficient is taken equal to the relaxation time of the considered site i. Hence the flux of solvent molecules $j_s^{film/res}$ is:

$$j_s^{film/res} = \gamma(i)(\ln(a_s) - \mu_s(i)) \tag{1.4.24}$$

By inserting this term in equations 1.4.20 we obtain for sites i at the film/reservoir interface:

$$\begin{aligned}\frac{\partial \phi_s(i)}{\partial t} =& \sum_{<j>} \gamma^{(i,j)} \Big[\Big(\mu_s^{(j)} - \mu_s^{(i)} \Big) + \delta_s^{i,j} \Big] \\ &+ \gamma(i)(\ln(a_s) - \mu_s(i))\end{aligned} \tag{1.4.25}$$

$$\frac{\partial \phi_p(i)}{\partial t} = \sum_{<j>} \gamma^{(i,j)} \Big[\alpha \Big(\mu_p^{(j)} - \mu_p^{(i)} \Big) + \delta_p^{i,j} \Big] \tag{1.4.26}$$

- **Implementation of the facilitation mechanism**

Let us now discuss about kinetic coefficients $\gamma^{i,j} \sim 1/\tau^{i,j}$. According to facilitation mechanism, we assume that **the exchange kinetics between two sites is controlled by the faster relaxation time**, i.e.

$$\gamma^{i,j} = max\Big(\gamma(i) \ ; \ \gamma(j) \Big) \tag{1.4.27}$$

where $\gamma(i)$ and $\gamma(j)$ are calculated as function of the local concentration in site i and j. As an example, in Figure 1.4.2, we schematise two sites i and j, both having a certain composition in Slow species and Fast species. The site i have a faster internal relaxation time than site j according to the difference of composition between both sites. Hence, in this example, kinetic coefficient is $\gamma^{i,j} = \gamma^i$ thanks to 1.4.27 and the slow domain j would melt in time scales given by the relaxation times of site i: τ_{fast}. Note that the diffusion scale factor $N_c^{2/3}\tau_{fast}$ is included in kinetics coefficient $\gamma(i)$. Through this example, we show that taking the faster relaxation time to control the exchange between two sites is coherent with the facilitation mechanism.

- **Contraction and dilation of the system**

In order to integrate the mechanical relaxation in the system, one should define an evolution equation for the stress tensor $\overline{\sigma}_{i,j}$ coupled to the diffusion equations. This has not been done here because it is too complicated at this stage of the development of the model. In the view of the chosen geometry, we integrate the mechanical interaction at long distance by considering the system's deformation layer by layer. Since, physically, the stress tends to make the deformation homogeneous, layers deform homogeneously as schematized in Figure 1.4.3. In case of polymer blends, layers can deform in both directions, whereas in case of polymer solvent, we consider the deformation of layers parallel to the film/reservoir interface.
We write $N(l)$ the volume of a site on a given layer l. The evolution equation for $N(l)$ reads:

$$\frac{dN(l)}{dt} = -\frac{N(l)}{\tau_\alpha^{layer}} \frac{1}{n_{layer}} \sum_{layer} \frac{\partial G}{\partial N} \tag{1.4.28}$$

where n_{layer} is the number of sites on the layer, and the term

$$\frac{1}{n_{layer}} \times \sum_{layer} \frac{\partial G}{\partial N} = \langle \frac{\partial G}{\partial N} \rangle_{layer}$$

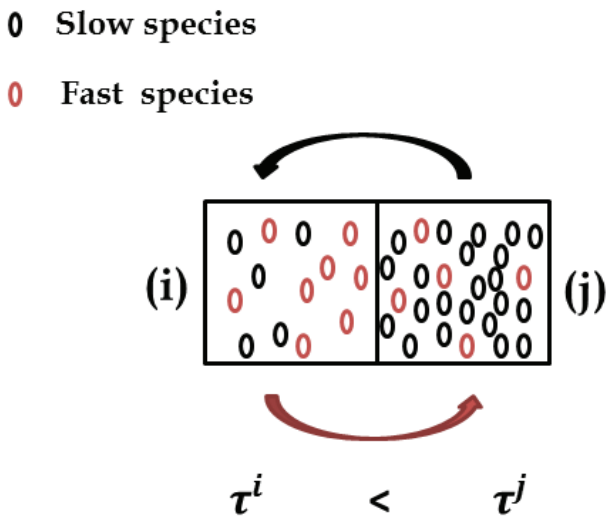

Figure 1.4.2: Schema representing two sites i and j which both have a certain composition in Slow and Fast component. Black arrow indicates the Slow component flux direction and the brown one the Fast componeent flux direction. Flux direction is determined by the difference $\Delta\mu_{fast/slow} = \mu^i_{fast/slow} - \mu^j_{fast/slow}$ of chemical potential between both sites:

$\Delta\mu_{fast} > 0 \quad \Rightarrow \quad \text{flux} : i \to j$
$\Delta\mu_{slow} < 0 \quad \Rightarrow \quad \text{flux} : j \to i$

Following 1.4.27, the exchange kinetics between site i and j is controlled by the relaxation time $\tau^i \sim 1/\gamma^i$
This is coherent regarding the facilitation mechanism.

is the driving force which controls the volume evolution. This term is statistically zero at thermodynamic equilibrium. Following equation 1.4.28, the deformation kinetics of a given layer, is controlled by α-relaxation times: τ_α^{layer}. The definition of τ_α^{layer} is given below.
The time derivative of $\phi_k(i) = \frac{N_k(i)}{N(i)}$ gives:

$$\frac{d\phi_k(i)}{dt} = \frac{d}{dt}\left(\frac{N_k(i)}{N(i)}\right) = -\frac{\phi_k(i)}{N(i)}\frac{dN(i)}{dt} \tag{1.4.29}$$

where $N_k(i)$ is the number of monomer k at site i which is assumed to be conserved. One then obtains for species A and B:

$$\begin{aligned}\frac{d\phi_A(i)}{dt} &= \phi_A(i)\frac{1}{\tau_\alpha^{layer} n_{layer}}\sum_{layer}\frac{\partial G}{\partial N}\\ \frac{d\phi_B(i)}{dt} &= \phi_B(i)\frac{1}{\tau_\alpha^{layer} n_{layer}}\sum_{layer}\frac{\partial G}{\partial N}\end{aligned} \tag{1.4.30}$$

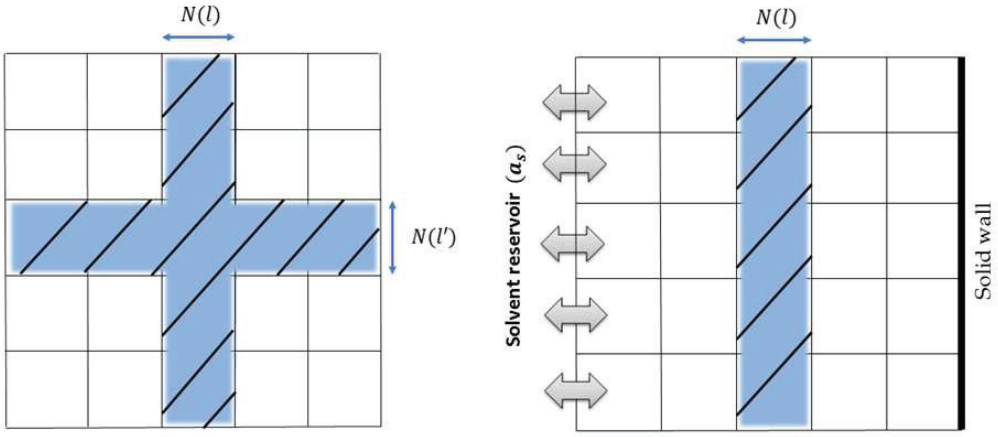

Figure 1.4.3: Schematic representation of the 2D-square lattice in case of polymer blends (Left) and polymer-solvent systems (Right). The total volume of the system can change by taking into account the contraction/dilatation of layers. Each of them can deform independently from each other, and the deformation of a given layer is homogeneous: the volume N(l) of a all sites on a layer l change the same way. In case of polymer blends, we consider the contraction/dilatation of layer in both directions, where as in the other case, only layers parallel to the film/resservoir interface can contract or dilate. Finally, the deformation kinetics is driven by the layer α-like relaxation times (τ_α^{layer}).

By adding such a contribution in equations 1.4.20, one finally has:

$$\frac{\partial \phi_A(i)}{\partial t} = \sum_{<j>} \gamma^{(i,j)} \left[\left(\mu_A^{(j)} - \mu_A^{(i)} \right) + \delta_A^{i,j} \right] + \phi_A(i) \frac{N_c^{2/3}}{\tau_\alpha^{layer} n_{layer}} \sum_{layer} \frac{\partial G}{\partial N} \tag{1.4.31}$$

$$\frac{\partial \phi_B(i)}{\partial t} = \sum_{<j>} \gamma^{(i,j)} \left[\alpha \left(\mu_B^{(j)} - \mu_B^{(i)} \right) + \delta_B^{i,j} \right] + \phi_B(i) \frac{N_c^{2/3}}{\tau_\alpha^{layer} n_{layer}} \sum_{layer} \frac{\partial G}{\partial N} \tag{1.4.32}$$

The tensorial expression for the osmotic stress reads:

$$\tilde{\sigma} = -P.I_d$$

where I_d is the identity matrix. The average osmotic stress in the layer is given by:

$$\langle \sigma \rangle_{layers} \equiv \frac{1}{n_{layer}} \sum_{layer} \frac{\partial G}{\partial N} \times \frac{T \rho_0}{N_c} \tag{1.4.33}$$

This quantity has the dimension of a pressure and is zero at thermodynamic equilibrium.

- **Distribution of relaxation times and α-relaxation times**

As already mentioned in the general introduction, distributions of relaxation times in binary systems are estimated to be spanning 6 decades. Numerically, dealing with such large distributions might be time consuming. In our model we get round this issue by computing sharper

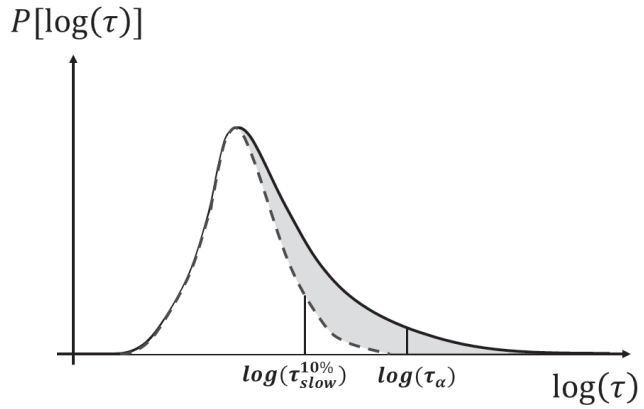

Figure 1.4.4: Schematic representation of a relaxation times distribution as it is obtained by experimental measurements (full black curve) and as it is obtained by numerical simulation (dashed black curve). Numerical distributions are typically 4 decades large whereas experimental distributions are estimated to be 6 decades large. We thus define the α-relaxation time (τ_α) as $\tau_\alpha = \kappa \times \tau_{slow}^{10\%}$ with $\kappa = 100 - 1000$ a numerical constant. In this work we take $\kappa = 500$ in order to obtain 6 decades large effective distributions to match physical situations.

distribution (3-4 decades typically) as compared to real ones as it is schematised in Figure 1.4.4. Distributions as they are computed numerically represent the fastest part of the real distribution which drives the diffusion of molecular species. In addition we define the α-relaxation times as

$$\tau_\alpha = \kappa \times \tau_{slow}^{10\%}$$

with κ a numerical constant of order 100-1000 and $\tau_{slow}^{10\%}$ the 10% slowest relaxation times of the numerical distribution. We thus obtain 6 decades large effective distributions in order to match physical situations. In this work, we take $\kappa = 500$ as an intermediate value between 100 and 1000.

- **Interfacial energy**

When studying phase separating systems, one needs to a include a non local spatial term in the total free energy to take into account the surface tension which drives the coarsening of domains which are forming. To do so, we make use of the "square gradient" model [89]. By considering such a non local contribution, the total free energy in the system reads

$$\begin{aligned} G =& \rho_0 \int \Big(\overline{G}(\phi_A, \phi_B, P, T) \\ &+ \widetilde{a} \left\| \vec{\nabla}\phi_A \right\|^2 + \widetilde{b} \left\| \vec{\nabla}\phi_B \right\|^2 + 2\widetilde{c}\vec{\nabla}\phi_A \cdot \vec{\nabla}\phi_B \Big) d^3x \end{aligned} \tag{1.4.34}$$

where $\overline{G}$ is given by 1.3.7 and positive coefficients $\widetilde{a}, \widetilde{b}$ and $\widetilde{c}$ are in Joules times square meter for homogeneity reasons.

We define $\widetilde{\mu}_i$ as the following:

$$\begin{aligned}\widetilde{\mu}_A &= \frac{\delta G}{\delta \phi_A} = \mu_A - 2\widetilde{a}\Delta\phi_A - 2\widetilde{c}\Delta\phi_B \\ \widetilde{\mu}_B &= \frac{\delta G}{\delta \phi_B} = \mu_B - 2\widetilde{b}\Delta\phi_B - 2\widetilde{c}\Delta\phi_A\end{aligned} \tag{1.4.35}$$

where $\mu_{A/B}$ are defined in equations 1.3.10 and 1.3.11. The quantity $\mu_{A/B}$ appearing in equations 1.4.20 is replaced by $\widetilde{\mu}_{A/B}$ when considering polymer blends. In this case, when performing numerical integrations of equations 1.4.20, quantities $\widetilde{\mu}_{A/B}$ are expressed in unit of T, the Laplacian operator appearing in expression 1.4.35 is descritized at the scale of the spatial resolution of the 2D square lattice, and we redefined $\widetilde{a}, \widetilde{b}$ and $\widetilde{c}$ as dimensionless quantities:

$$\begin{aligned}\widetilde{a} &= -\frac{a}{T} \times \frac{l^2}{\xi^2} \\ \widetilde{b} &= -\frac{b}{T} \times \frac{l^2}{\xi^2} \\ \widetilde{c} &= -\frac{c}{T} \times \frac{l^2}{\xi^2}\end{aligned} \tag{1.4.36}$$

with l the typical size of a monomer. By using the relation 1.4.1 one finally obtains

$$\begin{aligned}\widetilde{a} &= -\frac{a}{T} \times \frac{1}{N_c^{2/3}} = -\frac{a}{T} \times \frac{1}{L} \\ \widetilde{b} &= -\frac{b}{T} \times \frac{1}{N_c^{2/3}} = -\frac{b}{T} \times \frac{1}{L} \\ \widetilde{c} &= -\frac{c}{T} \times \frac{1}{N_c^{2/3}} = -\frac{c}{T} \times \frac{1}{L}\end{aligned} \tag{1.4.37}$$

where L is a parameter of order ten. Finally, a derivation from our model of some standard results of surface theory is performed in appendix 1.C.

1.5 Equilibrium in polymer blend and polymer solvent systems

In this section we illustrate our model by studying thermodynamic equilibrium in polymer blends and polymer solvent system using the spatial model described in previous sections. We also compare results provided from numerical resolution of the spatial model and the theory.

Let us first consider the case where relaxation times are fixed. Distributions of polymer and solvent composition are given in Figure 1.5.1. We observe a perfect fit between distributions obtained from the simulation and the ones obtain from theory. The system follows then a Boltzmann distribution at equilibrium when dynamics is homogeneous. Let us now consider the second situation where composition fluctuations are coupled with the glass transition temperature of the system. We observe that (see Figure 1.5.2) the distribution given by numerical simulation and theory match quite well, though numerical distributions are a little sharper than theoretical ones. Regarding equilibrium relaxation times distributions we observe in Figure 1.5.3 that the distribution of relaxations times at equilibrium widens and translates toward longer times when approaching T_g. Snapshots of the system in term of the logarithm of relaxation times and solvent composition at equilibrium given in Figure 1.5.4 show that relaxation times on a given are long if it contains an excess of slow components, while in contrast they are fast if the site contains an excess of fast components. Finally, the coupling between composition fluctuations and the blend T_g gives rise to a wide spatial distribution of relaxation times in the whole system where slowest subunits are forming a rigid network inside which solvent molecules diffuse through fastest subunits.

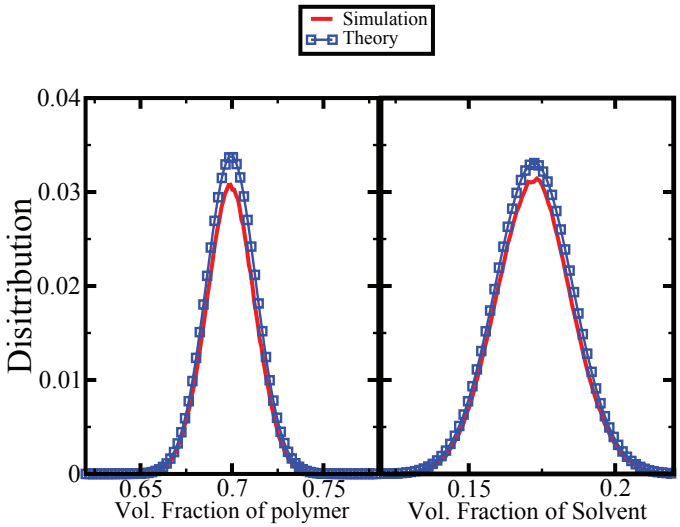

Figure 1.5.1: Distribution of solvent and polymer volume fraction for a system at equilibrium. $N_c = 500$ here, and relaxation times are equal to one second. Blue curve is the theoretical curve obtained from equation 1.A.8 in appendix 1.A.2. The red one is given when solving the spatial model. Accordance between theory and numerical results is very good.

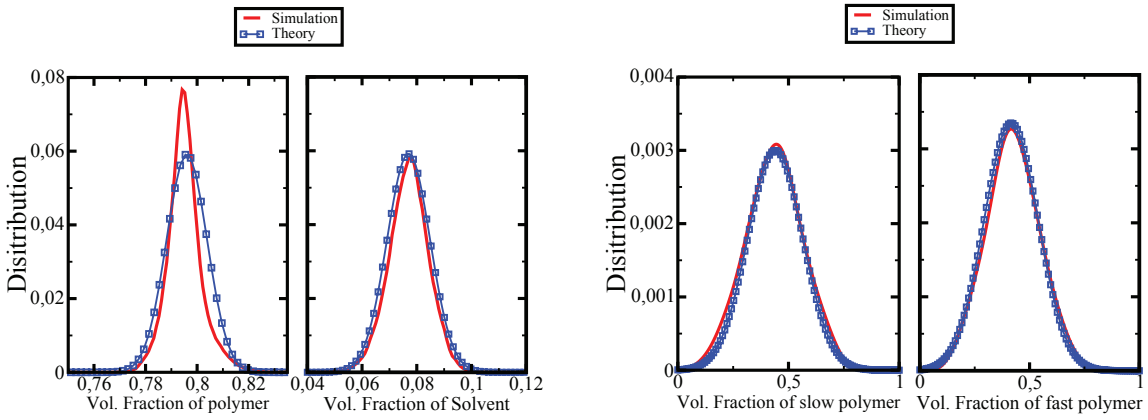

Figure 1.5.2: (Left) Distributions of polymer and solvent volume fraction fluctuations at equilibrium in polymer solvent system (Red curves). The system is at equilibrium with the solvent reservoir. (Right) Distributions of fast and slow polymer volume fraction in a polymer blend with symmetric composition. The system is in a homogeneous molten state 10K above the blend critical temperature. The phase diagram and the glass transition temperature of the blend are given in Figure 2.2.1. The numerical curves are compared to theoretical ones. Theoretical distributions are given by Equation 1.3.20. Wether it is for polymer-solvent system or for polymer blends, equilibrium composition fluctuations distributions obtained numerically and theoretically match in a satisfying way.

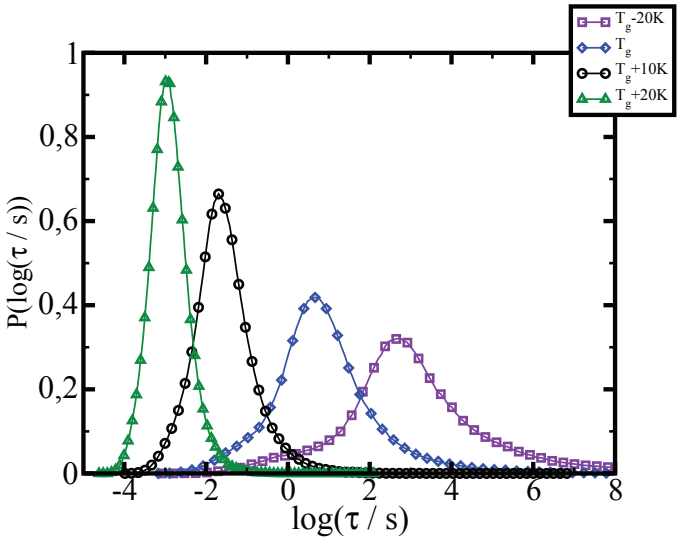

Figure 1.5.3: Distribution of relaxation times at different temperatures for a polymer solvent system equilibrated at activity 0.21. For this activity, $T_g^{blend} = 325.5$K.

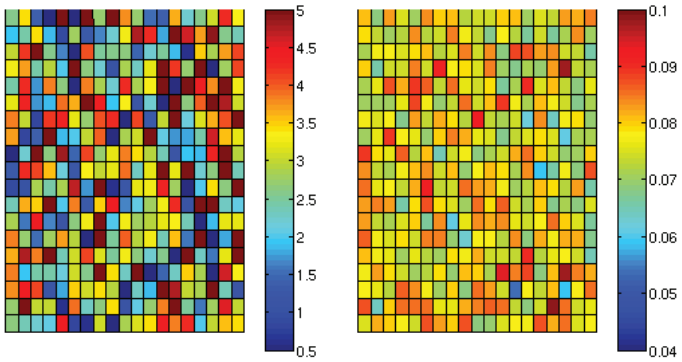

Figure 1.5.4: Snapshots in term the logarithm of relaxation times (Left panel) and solvent composition (Right panel) in a polymer solvent system at equilibrium at $Tg-10K$. Parameters of the system are that given in Figure 1.5.2. We see that at equilibrium, internal relaxation times on every sites of the system depend on their composition: the higher the solvent (resp. polymer) composition, the lower (resp. higher) the relaxation times.

1.6 Conclusion

In this section we have introduced the spatial model for describing diffusion in polymer blends or polymer-solvent systems close to or below T_g.
The 2-D spatial model incorporates the heterogeneous nature of the dynamics on the scale of a dynamic heterogeneity (spatial resolution of the model 3-5 nm) by coupling dynamics and composition fluctuations which allows for obtaining spatial distribution of relaxation times. Diffusion equations are explicitly solved on a scale of a dynamic heterogeneity ($\xi \sim 3 - 5nm$), and this diffusion model does not follow a Fick model which assumes that diffusion coefficients (related to relaxation times) are independent of composition.
We consider that matter exchanges, between a given site and its next neighbors, are driven by chemical potential gradient. Equation of dynamics follow an Onsager principle and the fluctuating term which controls spatial composition fluctuations in the system is written in a Langevin scheme. The fluctuating term is defined such that Boltzmann statistics is recovered at equilibrium. Finally we have seen that composition fluctuations gives rise to a very heterogeneous spatial distribution of relaxation times where slowest subunits form a rigid network inside which molecules diffuse through fastest subunits. In this model, contraction and the dilation of the system happens layers by layers and we consider that the deformation is homogeneous at this scale. Moreover, the deformation kinetics of a layer is controlled the α-relaxation times of a layer.

This spatial model and this formalism, which combines the diffusion of molecules and the mechanical relaxation of the system, allows for studying dynamics and relaxation mechanisms in polymer blends or polymer solvent systems on a scale of few nanometer and more. Thanks to this coarse-grained model, we describe diffusive process which depends on system's history. Finally such a coarse-grained approach is important to reduce the number of physical parameters we have to deal with.

Appendix

1.A Thermodynamics

1.A.1 Comparisons with experimental results: semi-quantitative agreement

Polymer blend	c ($10^{-20}J$)	X_{PS}	$X_{PVME\ or\ PB}$	T_c (K)	T_c^{exp} (K)
PS-PVME (1)	$-1.85327(0.15\%)$	89	886	482.1	482
PS-PVME (2)	$-1.85519(0.25\%)$	200	886	423.1	424
PS-PVME (3)	$-1.85611(0.30\%)$	515	886	390.5	391
PS-PVME (4)	$-1.85645(0.32\%)$	1160	886	372.1	373
PS-PVME (5)	$-1.85668(0.33\%)$	1990	886	370.1	370
PS-PB (1b)	$-1.86795(1.32\%)$	23	49	426.1	427
PS-PB (2b)	$-1.86772(1.33\%)$	34	49	492.6	494

Table 1.1: Values of the parameters we used for calculating the binodal and spinodal lines displayed in Figures 1.A.1, 1.A.2 and 1.A.3 at pressure $P = 1$bar. The interaction energies are -1.9635×10^{-20}J (PS); -1.744×10^{-20}J (PVME) and -1.825×10^{-20}J (PB). c is slightly adjusted to fit the data. In the second column, we indicate in bracket the difference (in %) between the adjusted value c for each blends and the theoretical value $c = -\sqrt{ab}$. $T_c^{\rm exp}$ is the critical temperature obtained experimentally, while T_c is the one obtained from the model. The data regarding the polymer molecular weights are given in Table 1.2

Polymer blend	$M_w^{(a)}(PDI)$	$M_w^{(b)}(PDI)$
PS-PVME (1)	$1,0\times10^4(1.06)$	5.15×10^4(NC)
PS-PVME (2)	$2.04\times10^4(1.06)$	5.15×10^4(NC)
PS-PVME (3)	$5.1\times10^4(1.06)$	5.15×10^4(NC)
PS-PVME (4)	$1.1\times10^5(1.06)$	5.15×10^4(NC)
PS-PVME (5)	$2\times10^5(1.06)$	5.15×10^4(NC)
PS-PB (1b)	2.4×10^3(NC)	$2.6\times10^3(1.13)$
PS-PB (2b)	$3.5\times10^3(1.06)$	$2.6\times10^3(1.13)$

Table 1.2: Experimental molecular weight $M_w^{(a)}$ of the PS and experimental molecular weights $M_w^{(b)}$ of the PB or the PVME used to compare the experimental binodal curves and the ones obtained from our model (see Table 1.1 and Figures 1.A.1,1.A.2 and 1.A.3). The Polydispersity index (PDI) is also given unless it was not given in the original reference (NC).

We consider two different blends: Polystyrene (PS)/poly(vinyl methyl ether) (PVME) and Polystyrene/Polybutadiene (PB) blends studied in [67] and [68] respectively. Experimental data that we consider for comparing our model to experiments are cloud point curves. If a state of

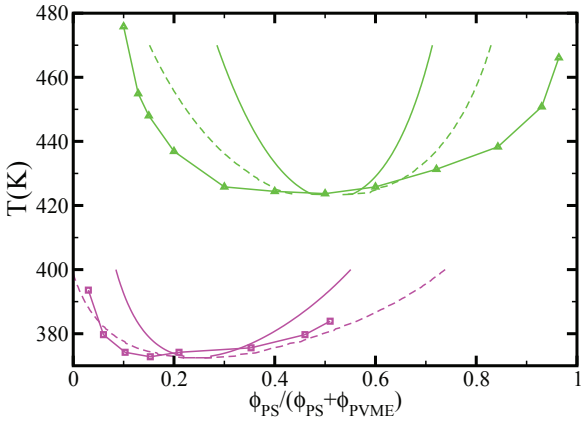

Figure 1.A.1: Spinodal and binodal curves of different PS/PVME blends as studied in reference [67], at pressure $P = 1$ bar. We take $\rho_0 = (\rho_0^{PS} + \rho_0^{PVME})/2 = 1.6525 \times 10^{28} m^{-3}$ where $\rho_0^{PS}$and ρ_0^{PVME} are pure PS and PVME close packing density obtained form PVT fits [70]. The solid lines represent the theoretical spinodal curve, the dotted lines represent the theoretical binodal curves while the point lines with the same color represent the experimental curves. The parameters are given in Tables 1.1 and 1.2. The parameter c is slightly adjusted in order to provide a better fit to the experimental data of the critical temperatures. For all curves, the molecular weight of PVME is $X_{PVME} = 886$. green curve (blend (2) in Tables 1.1 and 1.2): $X_{PS} = 200$; $T_c = 423.1$ K, experimental $T_c \approx 424$ K; magenta curve (blend (4) in Tables 1.1 and 1.2): $X_{PS} = 1160$, $T_c = 372.1$K, experimental value $T_c \approx 373$ K

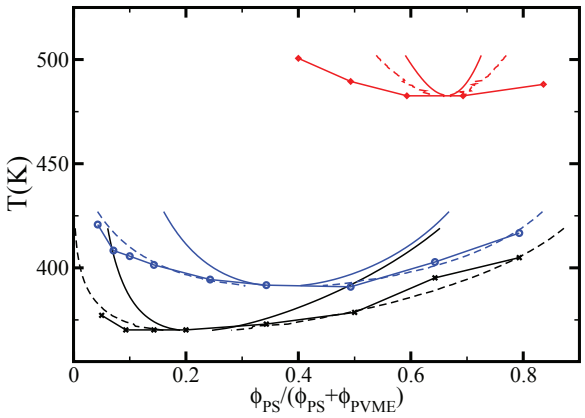

Figure 1.A.2: Spinodal and binodal curves of different PS/PVME blends at pressure $P = 1$bar as studied in reference [67]. We take $\rho_0 = (\rho_0^{PS} + \rho_0^{PVME})/2 = 1.6525 \times 10^{28} m^{-3}$ where $\rho_0^{PS}$and ρ_0^{PVME} are pure PS and PVME close packing density obtained from PVT fits [70]. The solid lines represent the theoretical spinodal curve, the dotted lines represent the theoretical binodal curves while the point lines with the same color represent the experimental curves. For all curves, the molecular weight of PVME is $X_{PVME} = 886$. red curve (blend (1) in Tables 1.1 and 1.2): $X_{PS} = 89$, $T_c = 482.1$ K, experimental $T_c \approx 482$ K; blue curve (blend (3) in Tables 1.1 and 1.2): $X_{PS} = 515$, $T_c = 390.5$ K, experimental $T_c \approx 391$ K; black curve (blend (5) in Tables 1.1 and 1.2): $X_{PS} = 1990$, $T_c = 370.1$ K (black), experimental value $T_c \approx 370$ K.

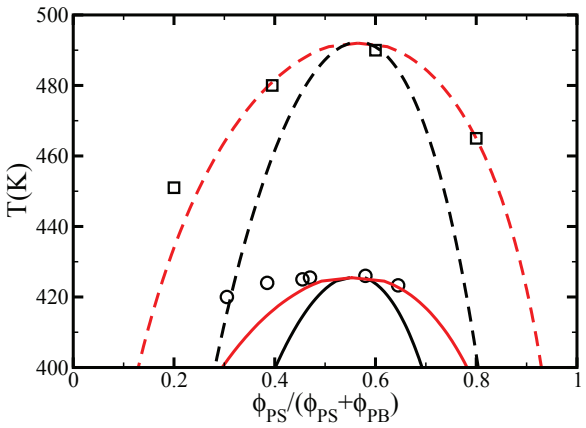

Figure 1.A.3: Spinodal and binodal curves of two different PS/PB blends at pressure $P = 1$bar as studied in reference [68].We take $\rho_0 = (\rho_0^{PS} + \rho_0^{PB})/2 = 1.604 \times 10^{28} m^{-3}$ where $\rho_0^{PS}$and ρ_0^{PB} are pure PS and PB close packing density obtained form PVT fits [70]. The parameters are given in Tables 1.1 and 1.2. The black curves correspond to the theoretical spinodals and red ones represent theoretical binodals. The squares and circles correspond to the experimental data. dashed line (blend (2b) in Tables 1.1 and 1.2): $X_{PS} = 34$, $X_{PB} = 49$ $T_c = 492.6$ K, experimental $T_c \approx 494$ K. solid line (blend (1b) in Tables 1.1 and 1.2): $X_{PS} = 23$, $X_{PB} = 49$, $T_c = 426.1$ K, experimental $T_c \approx 427$ K).

quasi-static equilibrium was reached, the experimental curve would correspond to binodal ones. We plotted in Figures 1.A.1, 1.A.2 and 1.A.3 both spinodal and binodal curves for PS/PVME and PS/PB blends. For computing binodal curves, we consider two sets of volume fractions $(\tilde{\phi}_A^1, \tilde{\phi}_B^1(\tilde{\phi}_A^1))$ and $(\tilde{\phi}_A^2, \tilde{\phi}_B^2(\tilde{\phi}_A^2))$ that correspond to the composition of both phase 1 and 2 in polymer A and B at temperature T. $\tilde{\phi}_B^k(\tilde{\phi}_A^k)$ are solutions of Eq.(1.3.8). These two sets are chosen such as the following equations are satisfied:

$$\begin{aligned} \left(\frac{\partial \overline{G}}{\partial \phi_A}(\tilde{\phi}_A^1, \tilde{\phi}_B^1(\tilde{\phi}_A^1))\right)_{T,P} &= \left(\frac{\partial \overline{G}}{\partial \phi_A}(\tilde{\phi}_A^2, \tilde{\phi}_B^2(\tilde{\phi}_A^2))\right)_{T,P} \\ \left(\frac{\partial \overline{G}}{\partial \phi_B}(\tilde{\phi}_B^1, \tilde{\phi}_A^1(\tilde{\phi}_B^1))\right)_{T,P} &= \left(\frac{\partial \overline{G}}{\partial \phi_B}(\tilde{\phi}_B^2, \tilde{\phi}_A^2(\tilde{\phi}_B^2))\right)_{T,P} \end{aligned} \tag{1.A.1}$$

The parameters and the critical temperatures obtained with the model and the experimental T_c are given in Table 1.1. These results depend only on the parameters a, b and ρ_0 which have been obtained by PVT fits [70]. The close packing density ρ_0 is taken as the average of the corresponding parameters of each component. We just consider polymers for which this parameter is found to be close from each other from PVT data. The curves are calculated under an applied pressure $P = 1$ bar. The parameter c has been slightly adjusted for each blends in order to obtain the right critical temperature. We could obtain a semi-quantitative agreement regarding the dependence of the critical temperature as a function of the molecular weight of polystyrene, which was varied between about 10^4 g/mole and 2×10^5 g/mole (see Table 1.1). We observe in Figure 1.A.1 and 1.A.2 that binodal curves reproduce experimental data satisfactorily. We note however, for all sets, a slight divergence between our model and experiments for high PS concentration part of the phase diagram, whereas matching regarding high PVME concentration part is much better. In Figure 1.A.3, we see that binodal curve

fits quite well the experimental data for the lower T_c curve. We observe that the fit with experimental data is especially accurate for high molecular weight polymers. The fit for the lower molecular weight polymers is not as good, though we have no interpretation for this.

1.A.2 Composition fluctuations distribution

By definition, we know that total composition fluctuations ($\delta\phi$) distribution P in a system of volume N is given by;

$$P(\delta\phi) \propto \exp\Big(- \frac{N\Delta\overline{G}}{T}\Big) \tag{1.A.2}$$

where $\delta\phi = \begin{pmatrix}\delta\phi_A \\ \delta\phi_B\end{pmatrix}$ with $\delta\phi_{A/B} = \frac{\delta N_{A/B}}{N}$. By using equation 1.3.12 of section 1.3 one finds:

$$P(\delta\phi_A, \delta\phi_B) \propto \exp\Bigg(- \frac{N}{2T}\big(\delta\phi_A, \delta\phi_B\big)\partial^2\overline{G} \begin{pmatrix}\delta\phi_A \\ \delta\phi_B\end{pmatrix} \Bigg) \tag{1.A.3}$$

It is worth considering the expression of composition fluctuations distribution $P(\delta_{A/B})$ for each component A and B. We define the former as:

$$\tilde{P}\big(\delta\phi_k\big) \propto \int d(\delta\phi_{k'}) P(\delta\phi_k, \delta\phi_{k'}) \tag{1.A.4}$$

where k and k' refer to both polymeric species.
An exact expression of $\tilde{P}$ can be obtained analytically. Indeed, with $\beta = \frac{N}{2T}$, one has:

$$\begin{aligned}\tilde{P}(\delta\phi_k) &\propto \exp\big(- \beta\partial^2_{\phi_k^2}\overline{G}\delta\phi_k^2\big) \int d(\delta\phi_{k'}) e^{-\beta\left(\partial^2_{\phi_{k'}^2}\overline{G}\right)\delta\phi_{k'}^2 - 2\beta\left(\partial^2_{\phi_k\phi_{k'}}\overline{G}\right)\delta\phi_k\delta\phi_{k'}} \\ &\propto \exp\big(- \beta\partial^2_{\phi_k^2}\overline{G}\delta\phi_k^2\big) \int d(\delta\phi_{k'}) e^{-\frac{1}{2\alpha}\delta\phi_{k'}^2 - iy\delta\phi_{k'}}\end{aligned} \tag{1.A.5}$$

with $1/(2\alpha) = \beta\big(\partial^2_{\phi_k\phi_{k'}}\overline{G}\big)$ and $y = -2i\beta\big(\partial^2_{\phi_k\phi_{k'}}\overline{G}\big)\delta\phi_k$. By making use of a "Hubbard-Stratonovitch" transformation one obtains:

$$\tilde{P}(\delta\phi_k) \propto \exp\big(- \beta\partial^2_{\phi_k^2}\overline{G}\delta\phi_k^2\big)\frac{1}{\sqrt{2\pi a}} e^{-\frac{\alpha}{2}y^2} \tag{1.A.6}$$

which yields for polymer $k = A/B$:

$$\tilde{P}(\delta\phi_k) \propto \exp\Bigg(- \frac{N}{2}\Bigg[\big(\partial^2_{\phi_k^2}\overline{G}\big) - \frac{\big(\partial^2_{\phi_k\phi_{k'}}\overline{G}\big)^2}{\partial^2_{\phi_{k'}^2}\overline{G}}\Bigg]\delta\phi_k^2\Bigg) \tag{1.A.7}$$

We write

$$\mathcal{L}_{k/k'} = \big(\partial^2_{\phi_k^2}\overline{G}\big) - \frac{\big(\partial^2_{\phi_k\phi_{k'}}\overline{G}\big)^2}{\partial^2_{\phi_{k'}^2}\overline{G}}$$

and we thus finally obtain:

$$\tilde{P}(\delta\phi_{A/B}) = \left(\sqrt{\frac{2T\pi}{N\mathcal{L}_{A/B}}}\right)^{-1} \exp\Big(-\frac{N}{2T}\mathcal{L}_{A/B}\delta\phi^2_{A/B}\Big) \tag{1.A.8}$$

By using notations introduced for matrix $\partial^2\overline{G}$ in equation(1.3.13), quantity $\mathcal{L}_{A/B}$ reads:

$$\mathcal{L}_{A/B} = a_{11} - \frac{a_{12}^2}{a_{22}} \ . \tag{1.A.9}$$

As it mentioned above, in the low temperature limit of interest, matrix coefficients a_{ij} are very close numerically, so $a_{11} \approx a_{22}$. By using this assumption, we get:

$$\mathcal{L}_{A/B} = \mathcal{L}_{B/A} \approx 2\,\frac{det(\partial^2\overline{G})}{Tr(\partial^2\overline{G})} \approx 2\,\lambda_2 \quad . \tag{1.A.10}$$

and finally, equation(1.A.8) becomes

$$\tilde{P}(\delta\phi_{A/B}) \propto \exp\big(-\frac{N}{T}\lambda_2\delta\phi^2_{A/B}\big) \tag{1.A.11}$$

1.A.3 Small angle neutron scattering in polymer blends

In a neutron scattering experiment an incident beam arrives on the studied sample and the same beam is scattered afterward. We assume that the sample is composed of two polymers 1 and 2. The amplitude of the diffused beam is expressed in the Fourier space as:

$$A(q) = \sum_{i=1}^{N_A} b_1 \exp(i\mathbf{q}.\mathbf{R}_i) + \sum_{j=1}^{N_B} b_2 \exp(i\mathbf{q}\mathbf{R}_j)$$

The quantity b_1 and b_2 are called diffusion length and can be positive or negative following the considered polymeric species. By definition, the scattered intensity is given by:

$$I(q) =< |A(q)|^2 > \tag{1.A.12}$$

Let's introduce the following quantity which correspond to a number of monomer per unit of volume $[m^-3]$ at a point $\mathbf{R}$ in space:

$$n_A(\mathbf{R}) = \sum_{i=1}^{N_A} \delta(\mathbf{R} - \mathbf{R}_i) = \rho_0\phi_A(\mathbf{R})$$

with ρ_0 the close-packing density. With such a quantity, the amplitude of the scattered beam reads:

$$A(q) = \int_V d^3\mathbf{R} \exp(i\mathbf{q}.\mathbf{R})(b_1 n_A(\mathbf{R}) + b_2 n_B(\mathbf{R})) \tag{1.A.13}$$

In terms of fluctuations:$\Delta n_i(\mathbf{R}) = n_i(\mathbf{R}) - < n_i >$ $(i = A, B)$, A reads:

$$A(q) = \int_V d^3\mathbf{R} \exp(i\mathbf{q}.\mathbf{R})(b_1 \Delta n_A(\mathbf{R}) + b_2 \Delta n_B(\mathbf{R})) \tag{1.A.14}$$

which gives:

$$\begin{aligned} I(q) = < \int_V d^3\mathbf{R} d^3\mathbf{R}' \exp\left(i\mathbf{q}.(\mathbf{R}-\mathbf{R}')\right) \Bigg(b_1^2 \Delta n_A(\mathbf{R}) \Delta n_A(\mathbf{R}') + \\ 2 b_1 b_2 \Delta n_A(\mathbf{R}) \Delta n_B(\mathbf{R}') + b_2^2 \Delta n_B(\mathbf{R}) \Delta n_B(\mathbf{R}) \Bigg) > \end{aligned} \tag{1.A.15}$$

In the zero wave length limit ($q = 0$), one obtains:

$$\begin{aligned} I(0) = \rho_0^2 < \int_V d^3\mathbf{R} d^3\mathbf{R}' \big(& b_1^2 \Delta\phi_A(\mathbf{R}) \Delta\phi_A(\mathbf{R}') \\ & + 2 b_1^2 b_2^2 \Delta\phi_A(\mathbf{R}) \Delta\phi_B(\mathbf{R}') \\ & + b_2^2 \Delta\phi_B(\mathbf{R}) \Delta\phi_B(\mathbf{R}') \big) > \end{aligned} \tag{1.A.16}$$

where $\Delta\phi_i(\mathbf{R}) = \phi_i(\mathbf{R}) - < \phi_i >$. In the case where both polymers have similar diffusion length, *i.e.* $b_1 = b_2$, one finds at temperature T:

$$I(0) \approx \frac{2}{\lambda_1} N T b_1^2 \approx \frac{\rho_0 T}{K_{bulk}} N b_1^2$$

which corresponds to the expression of the scattered intensity by a pure sample of dimensionless volume N and of bulk modulus K_{bulk}. We see that following this relation, the SANS intensity is directly proportional to the volume of the sample. One can refer to [71] for more details about calculations. The q dependance of the scattered intensity is also discussed in this reference.
Some results in the literature are given in term of an effective Flory Huggins interaction parameter $\chi_{eff}(P,T)$ and experimentally, most of the investigations regarding phase separation in polymer blends are performed thanks to neutron scattering in the small wave length limit. The relation

$$\chi_{eff}(T,P) = \frac{1}{2}\left(\frac{1}{\phi_A X_A} + \frac{1}{\phi_B X_B} - \frac{N(b_1 - b_2)^2}{I(0)} \right) \tag{1.A.17}$$

allows for obtaining an effective Flory interaction parameter with $I(0)$. One can show that in the low temperature limit, the scattered intensity reads:

$$I(0) \approx \frac{NT(b_1 - b_2)^2}{2\lambda_2} = \approx \frac{T\rho_0 N(b_1 - b_2)^2}{K_{osm}} \tag{1.A.18}$$

By using equations 1.A.17 and 1.3.17, we obtain:

$$\chi_{eff}(T,P) \approx (\phi_A + \phi_B)\left(\frac{2c-(a+b)}{T}\right) \tag{1.A.19}$$

By taking $\phi_A + \phi_B = 1$, which is valid in the low temperature or infinite pressure limit, we obtain the standard expression for the Flory-Huggins parameter [21].

1.B Derivation of Fick laws for diffusion

We propose here to derive Fick laws from our model.
In Equations 1.3.33, we have seen that flux are along chemical potential gradient. These equations can be formulated in a different way, e.i:

$$\begin{aligned}\vec{j}_A(\vec{r}) &= -\frac{\lambda_A}{T}\vec{\nabla}\mu_A = -\frac{\tilde{\lambda}_A}{T}\phi_A\vec{\nabla}\mu_A \\ \vec{j}_B(\vec{r}) &= -\frac{\lambda_B}{T}\vec{\nabla}\mu_B = -\frac{\tilde{\lambda}_B}{T}\phi_B\vec{\nabla}\mu_B\end{aligned} \tag{1.B.1}$$

where $\tilde{\lambda}_k = \lambda_k/\phi_k$, and let us remind that $\tilde{\lambda}_k$ is constant and do not depends on composition. The expression of the chemical potential for the species A is given in equation 1.B.2.

$$\begin{aligned}\mu_A = \left(\frac{\partial \overline{G}}{\partial \phi_A}\right)_{T,\phi_B,P} =& a\Big(3(\phi_A)^2 + 2\phi_A\phi_B\Big) + b(\phi_B)^2 + 2c\Big(2\phi_A\phi_B + (\phi_B)^2\Big) \\ &+ T\left(\frac{1}{X_A}\ln(\phi_A) - \ln(1-\phi_A-\phi_B) + \frac{1}{X_A} + \frac{\phi_A+\phi_B}{1-\phi_A-\phi_B}\right)\end{aligned} \tag{1.B.2}$$

We take $X_A = X_B = 1$ and $a = b = c$ for simplicity and we note $\phi_A + \phi_B = \alpha$ where quantity $\phi_A + \phi_B$ does not vary and α is smaller than one. By using such a notation, one can find that above equation 1.B.2 for μ_A reads:

$$\mu_A(\phi_A) = \Theta + T\ln(\phi) \tag{1.B.3}$$

where

$$\Theta = 3a\alpha^2 + \ln(1-\alpha) + \frac{\alpha}{1-\alpha} + 1$$

One hence obtains for current

$$\vec{j}_A(\vec{r}) = -\tilde{\lambda}_A\vec{\nabla}\phi_A \tag{1.B.4}$$

Following the same procedure, one has equivalently for species B:

$$\vec{j}_B(\vec{r}) = -\tilde{\lambda}_B\vec{\nabla}\phi_B \tag{1.B.5}$$

These expressions for currents correspond to first Fick law which says that current follows composition gradients. If inserting these expressions in equations dealing species volume fraction time evolution, one finds

$$\begin{aligned}\frac{\partial\phi_A}{\partial t} &= -\vec{\nabla}\cdot\vec{j}_A = \tilde{\lambda}_A\Delta\phi_A \\ \frac{\partial\phi_B}{\partial t} &= -\vec{\nabla}\cdot\vec{j}_B = \tilde{\lambda}_B\Delta\phi_B\end{aligned} \tag{1.B.6}$$

which is the second Fick law.

1.C Derivation of some basics for interface theory

We present calculations which allow for obtaining well known basics of surface theory [80]. We are particularly interested in giving an exact solution, in a mean field picture, of concentration profiles at interface between two coexisting phases.
In last section we have seen that total free energy in the system is given by

$$G = \rho_0 \int \left[\overline{G}(\phi_A,\phi_B,P,T) + \widetilde{a}\left\|\vec{\nabla}\phi_A\right\|^2 + \widetilde{b}\left\|\vec{\nabla}\phi_B\right\|^2 + 2\widetilde{c}\,\vec{\nabla}\phi_A\ \cdot\ \vec{\nabla}\phi_B\right]\ d^3x \tag{1.C.1}$$

where

$$\begin{aligned}\overline{G} = \frac{G}{N} =& a(\phi_A+\phi_B)\phi_A^2 + b(\phi_A+\phi_B)\phi_B^2 + 2c(\phi_A+\phi_B)\phi_A\phi_B \\ &+ T\left(\frac{\phi_A}{X_A}\ln\left(\phi_A\right) + \frac{\phi_B}{X_B}\ln\left(\phi_B\right)\right) \\ &- T(\phi_A+\phi_B)\ln\left(1-\phi_A-\phi_B\right) + \frac{P}{\rho_0}\end{aligned} \tag{1.C.2}$$

For simplicity we take $X_A = X_B = 1$ and by using $\phi_A + \phi_B = \alpha$ we obtain G, at $P = 0$, depending on one degree of freedom ($\phi_A = \phi$) only:

$$G = \rho_0 \int \left[\overline{G}(\phi) + \eta\left\|\vec{\nabla}\phi\right\|^2\right] d^3x \tag{1.C.3}$$

with $\eta = \widetilde{a} + \widetilde{b} + \widetilde{c}$, and

$$\begin{aligned}\overline{G} =& a\alpha\phi^2 + b\alpha(\alpha-\phi)^2 + 2c\alpha\phi(\alpha-\phi) \qquad (I) \\ &+ T\left(\phi\ln\left(\phi\right) + \phi\ln\left(\alpha-\phi\right)\right) \qquad (II) \\ &- T\alpha\ln\left(1-\alpha\right)\end{aligned} \tag{1.C.4}$$

To perform calculations, we consider that volume fraction is very close to the critical one(ϕ^c) i.e. $\phi \simeq \phi^c = \alpha/2$. This allows to define the field $\Psi = \phi - \phi^c$. By inserting field Ψ in term (I)

Equation 1.C.4, one finds

$$\begin{aligned}(I) &= a\alpha(\Psi+\phi^c)^2 + b\alpha(\phi^c-\Psi)^2 + 2c\alpha(\phi^c+\Psi)(\phi^c-\Psi) \\ &= A_1\Psi^2 + B_1\Psi + C_1\end{aligned} \tag{1.C.5}$$

with

$$\begin{aligned}A_1 &= \alpha(a+b-2c) \\ B_1 &= 2\alpha\phi^c(a-b) \\ C_1 &= \alpha(a+b+2c)\end{aligned} \tag{1.C.6}$$

By developing term (II) in the vicinity of $\Psi \simeq 0$ at fourth order, one finds:

$$\begin{aligned}(II) &= T\left(\phi\ln\Big(\phi\Big) + \Big(\alpha-\phi\Big)\ln\Big(\alpha-\phi\Big)\right) \\ &= T\left(\Big(\Psi+\phi^c\Big)\ln\Big(\Psi+\phi^c\Big) + \Big(\phi^c-\Psi\Big)\ln\Big(\phi^c-\Psi\Big)\right) \\ &\simeq T\left(A_2\Psi^2 + B_2\Psi^4 + \alpha\ln(\alpha) - \ln(2)\right) + \mathcal{O}\big(\Psi^5\big)\end{aligned} \tag{1.C.7}$$

where

$$\begin{aligned}A_2 &= 1/\phi^c \\ B_2 &= 1/6\phi^{c3}\end{aligned} \tag{1.C.8}$$

And finally, Equation 1.C.3 becomes

$$G = \rho_0 \int \left[-\frac{\overline{A}}{2}\Psi^2 + \frac{\overline{B}}{4}\Psi^4 + \frac{\overline{\eta}}{2}\left\|\vec{\nabla}\Psi\right\|^2\right] d^2x \tag{1.C.9}$$

where constant term have been removed and $\overline{A} = 2(-A_1 - TA_2)$, $\overline{B} = 4B_2T$ and $\overline{\eta} = 2\eta$. Moreover, we can omit the linear term because $\int \phi d^3x$ is fixed. By taking the second order term at zero, which vanishes at the blend critical temperature T_c, this yields to

$$T_c = -A_1/A_2$$

We now aim at finding $\Psi = \Psi(\vec{r})$ which minimizes 1.C.9, i.e. which satisfies:

$$\frac{\delta G}{\delta \Psi} = 0$$

This equation is equivalent to equation:

$$-\overline{A}\Psi + \overline{B}\Psi^3 - \overline{\eta}\Delta\Psi = 0 \tag{1.C.10}$$

whose solution, in one dimension (y), is

$$\Psi(y) = \sqrt{\frac{\overline{A}}{\overline{B}}} \tanh\left(\frac{y}{\xi}\right) \tag{1.C.11}$$

with $\xi = \sqrt{2\eta/\overline{A}}$. This solution is valid only if one considers that $d\Psi/dz = 0$ for $y = \pm\infty$. Quantity ξ is the width of the interfacial length or again bulk correlation length and behaves like

$$\xi \sim 1/\sqrt{T - T_c}$$

and so diverges when approaching T_c. Far from the interface, at equilibrium, phase composition, in the approximation $\Psi = \phi - \phi^c$ is $\Psi_0 = \pm\sqrt{\overline{A}/\overline{B}}$

In this part, we derived standard mean field results of surfaces theory from our model. At interface, the concentration gradient is smooth, and the typical distance on which the profile decreases is a function of the temperature. This distance is related to the bulk correlation length, and the latter diverges when approaching the blend critical temperature. Furthermore, these results can be mapped to the case of incompressible blends in the low temperature or infinite pressure limit ($\alpha = 1$). In this limit, standard results obtained with the Flory-Huggins model are recovered.

1.D Method for determining the time steps

In this Appendix we discuss the method used for determining the time step δt when solving dynamical equations of the model.

In order to determine δt, we consider the following. We note $\delta\phi$ a total density fluctuation with $\phi = \phi_A + \phi_B$. The probability density P to observe such a fluctuation on a scale ξ at temperature T is given by:

$$P(\delta\phi) \sim \exp\left(-\frac{1}{2}\frac{K_{bulk}\xi^3}{T}\delta\phi^2 \right) \tag{1.D.1}$$

We know that:

- $K_{bulk} \sim \frac{1}{2}T\rho_0\lambda_1$
- $\xi^3 = \frac{N_c}{\rho_0}$

hence we can deduce from previous distribution(Dissipation-Fluctuation theorem) that:

$$< \delta\phi > \sim \sqrt{\frac{T}{K_{bulk}\xi^3}} \sim \sqrt{\frac{2}{N_c\lambda_1}} \tag{1.D.2}$$

Thanks to equation 1.4.20, the variation of a composition fluctuation for species k on a time step δt is given by:

$$\delta\phi_k \sim \delta t\gamma\sqrt{\frac{\gamma^{-1}}{N_c\delta t}} \tag{1.D.3}$$

Moreover we have $\delta\phi \sim \sqrt{2}\delta\phi_k$. We thus obtain:

$$\delta t\gamma\sqrt{\frac{\gamma^{-1}}{N_c\delta t}} = \frac{1}{\sqrt{N_c\lambda_1}} \tag{1.D.4}$$

which gives:

$$\delta t = \theta\frac{\gamma^{-1}}{\lambda_1} \tag{1.D.5}$$

with θ a coefficient smaller than 1 equal to $0,1$ typically . In our case, we chose $\gamma^{-1} = \tau_{10\%}^{fast}$ as the shortest time scales on which species diffuse in the material.
Following this method, the time step can adapt itself to the changes of dynamics in out of equilibrium conditions. Furthermore, time step is a function of λ_1 which depends on the studied system (interaction parameters, chain sizes, temperature, pressure....). As already seen previously, $K_{bulk} \sim 10^9 Pa$ in polymeric liquids, one hence obtain:

$$\lambda_1 \sim 10^2$$

with $\rho_0 \sim 10^{28} m^{-3}$, $T \sim 4 \times 10^{-21} J$. The time step value is thus typically

$$\delta t \sim 10^{-3} \times \tau_{10\%}^{fast}$$

.

1.E Paires correlation function: size of morphologies

A pair correlation function, whose expression is given by Equation 1.E.1, is used here to compute the evolution of the typical size of domains forming. This function is:

$$g(r;t) =< (\phi_B(0) - \overline{\phi}_B)(\phi_B(r) - \overline{\phi}_B) >_t \tag{1.E.1}$$

where the averaging is performing all over the film and $\overline{\phi}_B$ is the average volume fraction of the B species. A discretised version of this function on a 2D square lattice in the direction y reads:

$$g_y(y;t) = \frac{1}{n_x}\sum_i^{n_x} g_{y_i}(y;t) \tag{1.E.2}$$

where:

$$g_{y_i}(y;t) = \frac{1}{n_y}\sum_j^{n_y}(\phi_B(i,j) - \overline{\phi}_B)(\phi_B(i,j+y) - \overline{\phi}_B) \quad . \tag{1.E.3}$$

Of course an equivalent function can be defined in the other direction by replacing y to x. You can see in Figure 1.E.1 the typical shape of the normalized pair correlation function at three different stages during a phase separation in a dynamically homogeneous polymer blends. The value of the first zero, which corresponds to the typical size of domains, moves toward longer distances when the time increases.

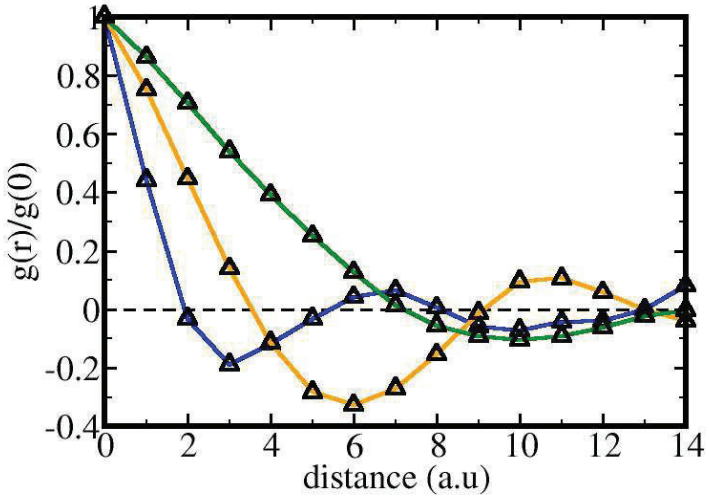

Figure 1.E.1: Normalized pair correlation functions at different stages of a phase separation (blue: t=10^2s, yellow; t=10^3s and green: t=6.10^3s) at fixed relaxation (1 s) in a polymer blend with symmetric composition. The first zero of the pair correlation function gives the average size of domains.

1.F Time correlation functions: composition fluctuations and relaxation times

Time auto correlation function of spatial composition fluctuations can be very useful to understand diffusion mechanisms of different molecular species. By making use of such a function, we can calculate the average terminal correlation time $< \tau_c >$ of composition fluctuations in the whole system. This quantity is related to the time that one has to wait for composition fluctuations to become uncorrelated. If a slow domain is surrounded by fast ones at a certain point in space, the decorelation of the composition fluctuation is fast because diffusion of monomers is driven by fast relaxation times. In contrast, if the slow dynamic heterogeneity is in contact with slow ones, which is also very probable, the decorelation of the composition fluctuation is slow. Thus $< \tau_c >$ is dominated by long relaxation times. The time correlation function in term of spatial composition fluctuation reads:

$$S_1^{\phi_B}(t_0; t_0 + t) =< (\phi_B(r; t_0) - \bar{\phi}_B(t_0))(\phi_B(r; t_0 + t) - \bar{\phi}_B(t_0 + t)) > \qquad (1.F.1)$$

where $< \cdot >$ corresponds to the spatial averaging all over the film and $\bar{\phi}_B$ is the film average volume fraction of B species. Time t_0 represents the specific time from which we compute function $S_1^{\phi_p} = S_1^{\phi_p}(t_0; t_0+t)$, and time t, the elapsed time from t_w. Average terminal correlation time is defined as:

$$< \tau_c >_{t_0} = \int_0^{+\infty} S_1^{\phi_B}(t_0; t_0 + t)dt \tag{1.F.2}$$

By fitting the function $S_1^{\phi_B}$ with a stretched exponential $\Big[f(t) \sim \exp\Big(- (\frac{t}{\tau})^{\beta}\Big)\Big]$ one finds:

$$< \tau_c >_{t_0} = \frac{\tau}{\beta}\Gamma\Big(\frac{1}{\beta}\Big) \tag{1.F.3}$$

where $\Gamma(z)$ is the gamma function.
Since monomeric relaxation times of a dynamic heterogeneity is related to its internal composition, it may be useful to compute the correlation function in term relaxation times. This function reads:

$$S_1^{\tau}(t_0; t_0 + t) = < (\tau(r; t_0) - \bar{\tau}(t_0))(\tau(r; t_0 + t) - \bar{\tau}(t_0 + t)) > \tag{1.F.4}$$

where $\bar{\tau}$ is the average relaxation time of the system.

Chapter 2

Dynamics in polymer blends close to and below the glass transition temperature: phase separation and rejuvenation

2.1 Résumé en français

Dans ce chapitre, nous étudions la dynamique dans les mélanges de polymères proche ou en dessous de T_g dont au moins une des composantes du mélange est en dessous du seuil d'enchevêtrement. Dans un premier temps, nous sommes intéressé au processus de séparation de phase dans le cas où le système est équilibré dans un état fondu homogène avant d'être trempé proche de T_g à des températures où il est immiscible : des domaines lents se forment en coexistence avec des domaines rapides. Nous montrons dans ce cas que la dynamique ne se ralentie pas instantanément, ce qui permet la formation rapide de petits noyaux de nucléation autour desquels les domaines se forment par la suite. Les domaines lents, riches en polymère haute T_g, vieillissent et grossissent au cours de la décomposition de phase, et en conséquent le temps de diffusion et de coalescence de ces domaines augmente au cours du processus. Nous montrons de façon semi quantitative qu'aux temps courts, la taille de ces domaines croît comme le logarithme du temps ce qui montre que nous avons à faire à un processus très lent. Aux temps longs, les domaines grandissent tout aussi lentement mais de façon chaotique. Nous attribuons ce comportement au fait de la différence importante de mobilité entre les deux phases et à la fusion partielle des domaines lents par la phase rapide.

Nous nous sommes intéressés dans un second temps au processus de rajeunissement de ces systèmes –i.e. la température est augmentée dans un régime où le système est fondu et homogène. Nous montrons dans ce cas que les domaines lents fondent plus vite que le temps écoulé pendant le processus de vieillissement pour les former. Ceci met en évidence une asymétrie temporelle entre les processus de vieillissement et de réchauffe. Nous montrons également de façon phénoménologique que la fusion des domaines lents résulte de mécanismes de facilitation qui

sont la conséquence de -1- la diffusion du polymère rapide en leur sein par l'interface -2- et de la diffusion du vide induit par des effets de pression osmotique.

2.2 Introduction

In this chapter, we apply the spatial model to the case of polymer blends. We are first interested in phase separation process close to or below the glass transition temperature of the blend. In a second step, we study the rejuvenation process after the system has been phase separated and aged close to or below T_g.
This section is organised as follow. We first present results of phase separation close to T_g, and rejuvenation in case of symmetrical blends composed of polymers with low molecular weight. At the end of this section, we study phase separation and rejuvenation in case of non-symmetric blends where one of the components is below the entanglement threshold. Finally, results regarding phase separation in dynamically homogeneous polymer blends are given in appendix 2.A.

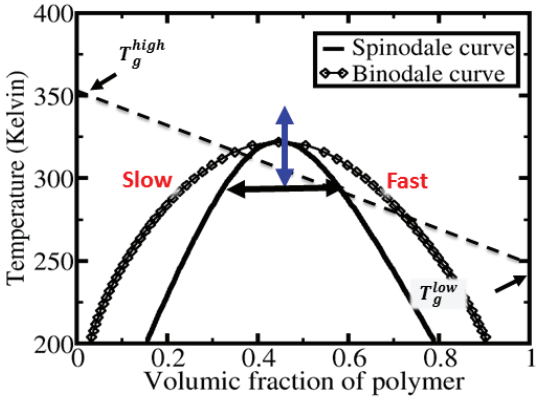

Figure 2.2.1: UCST phase diagram of a $X_A = X_B = 50$ blend as a function of the low T_g polymer volume fraction. Interaction parameters are $a = -2,32 \times 10^{-20}J$, $b = -1,595 \times 10^{-20}J$ and $c = -\sqrt{ab}$. The critical temperature is $T_c = 320K$. Low T_g polymer has a pure component glass transition temperature equal to $255K$ and the high T_g polymer has a pure component glass transition temperature equal to 355K. Dashed line represents the blend T_g variation as a function of the low T_g polymer volume fraction. After cooling the system from a homogeneous molten state (Blue arrow) down to temperature close to or below T_g, it phase separates and fast domains (rich in low T_g polymer) appear in coexistence with a slow ones (rich in high T_g polymer). By increasing again the temperature, the system remixes and rejuvenates (rejuvenation).

2.3 Phase separation and aging in polymer blends close to and below T_g

In case of polymer blends where components of different T_g's are mixed together, we first study phase separation processes close to the blend glass transition temperature. For that, we consider a blend composed of small chains having similar mass. At a given composition, the system is quenched from an homogeneous molten state down to T_g or below where it is unstable (See Figure 2.2.1). Hence a slow phase rich in high T_g polymer can be formed in coexistence with a fast one rich in low T_g component. We observe in Figure 2.3.1 and 2.3.3 that the dynamics is fast at the beginning of the process. At longer times however, relaxation time distribution widens and translates toward longer times and α-relaxation times increases with the aging time: the system follows the so-called Struik -i.e.

$$\tau_\alpha \sim t^\mu \tag{2.3.1}$$

with $\mu \sim 1$ as it has already been observed in the past in the context of pure polymeric glass forming liquids either by simulation technics or experimentally ([90, 41]). Finally, the slow contraction of the system is at the origin of the slowing down of the dynamics because of the reduction of the average free volume fraction in the system. Since dynamics is fast at the beginning of the process, small nucleating seeds appear quickly as it can be observed in Figure 2.3.2 and 2.3.4. Relaxation times of the phase rich in slow polymer correspond to longer times of the distribution, and dynamics of this phase slows down when the aging time increases. Hence,

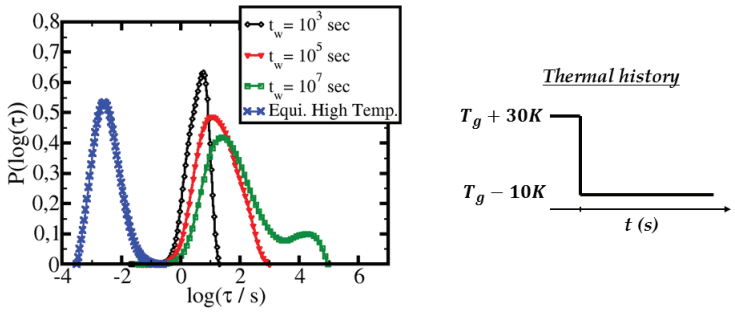

Figure 2.3.1: Distribution of relaxation times at different times $t_w = 10^3\text{s}; 10^5\text{s}; 10^7\text{s}$ during a phase separation at $T_g - 10K$. The system is initially equilibrated at $T_g + 30K$ and is composed of 30% of high T_g polymer and of 70% of low T_g polymer. Equilibrium distribution of relaxation times at $T_g + 30\text{K}$ is also displayed in the figure (blue curve).
During the phase separation, the distribution of relaxation times widens when t_w increases and translates toward longer times, it contracts at short times though. At the end of the process, the distribution spans many decades and is split in two parts: a first one at short relaxation times which is related to the phase rich in low T_g polymer and a second one at longer relaxation times related to the phase rich in high T_g polymer.

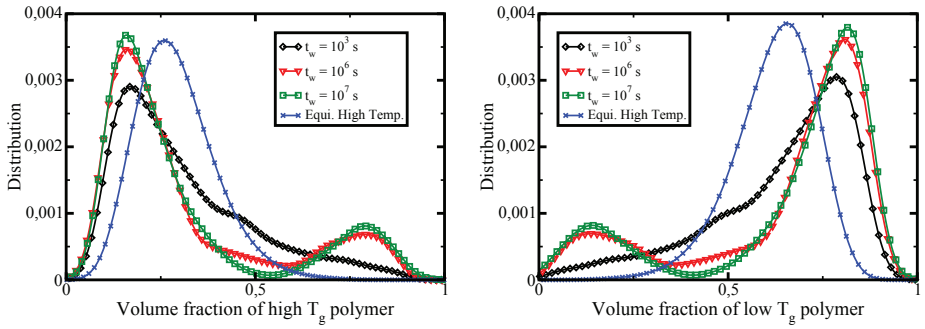

Figure 2.3.2: Distribution of low(Left) and high(Right) T_g polymer composition at different times $t_w = 10^3 s; 10^5 s; 10^7\text{s}$ during a phase separation at $T_g - 10K$. Thermal history of the system is that given in Figure 2.3.1. The system is composed of 30% of high T_g polymer and of 70% of low T_g polymer. Equilibrium distribution of relaxation times at $T_g + 30\text{K}$ is also displayed in the figure (blue curve).

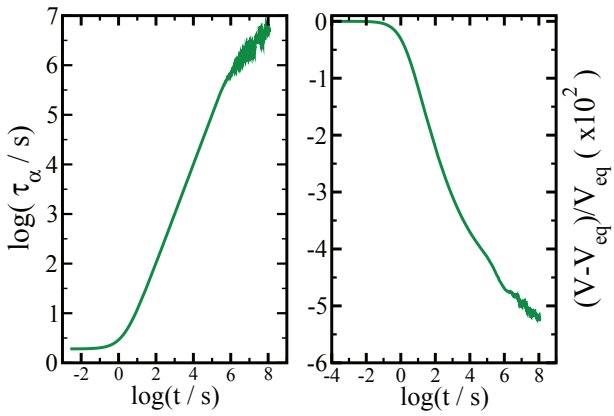

Figure 2.3.3: Evolution of α-relaxation times (Left) and volume (Right) after the temperature quench at $T_g - 10K$. Thermal history of the system is that given in Figure 2.3.1.
α-relaxation times increases linearly with the aging time t_w: $\tau_\alpha \sim t_w$. We see that the contraction of the sample is slow: the total volume decreases of 5% in 10^7s with respect to the initial equilibrium volume V_{eq} at $T_g + 30$K.

as it is visible in Figure 2.3.5 and Figure 2.3.4, domains rich in slow components are aging in the same time they are forming, which makes their diffusion and coalescence times very long. One can distinguish two distinct regimes in the slow growth process of forming morphologies.

a) Steady and logarithmic growth of domains at early stages

Growth of domains at short time scales is reported in Figure 2.3.5. Let us extract a growth law for domains size evolution. As it is shown in appendix 2.A the average size R of domains reads:

$$R^2 \frac{dR}{dt} \sim 2\frac{\lambda}{T} \times \eta a^3 \tag{2.3.2}$$

with λ a diffusion coefficient in Joules per surface unit, η the surface tension in Joules per meter, a the size of a monomer in meters and T the temperature in Joules. In the case of aging systems close to the glass transition, local diffusion coefficient λ depends on the history of the system and can be written as: $\lambda \sim a^2/\tau$ where τ is a monomeric relaxation time. We have seen that relaxation times grow linearly with time: $\tau \sim t$. Hence this leads to:

$$\frac{1}{a^3} \times \frac{dR^3}{dt} \sim 2\frac{\eta}{T} \times \frac{a^2}{\tau} \sim 2\frac{a^2\eta}{T} \times \frac{1}{t} \tag{2.3.3}$$

By integrating this equation, one finds:

$$\frac{1}{a^3} \times R^3(t) \sim \frac{1}{a^3} \times R^3(t_0) + 2\frac{a^2\eta}{T} \times \log(t/t_0) \tag{2.3.4}$$

where t_0 is a reference time. From this, we conclude that domains grow like the power 1/3 of the logarithm of the time. In Figure 2.3.5 we give the evolution of domains size between times $t = 10^4$s and $t = 10^6$s. We see that the numerical results match well the scaling law given in equation 2.3.4. Moreover, we superpose a linear curve (exponent 1) to the power law curve

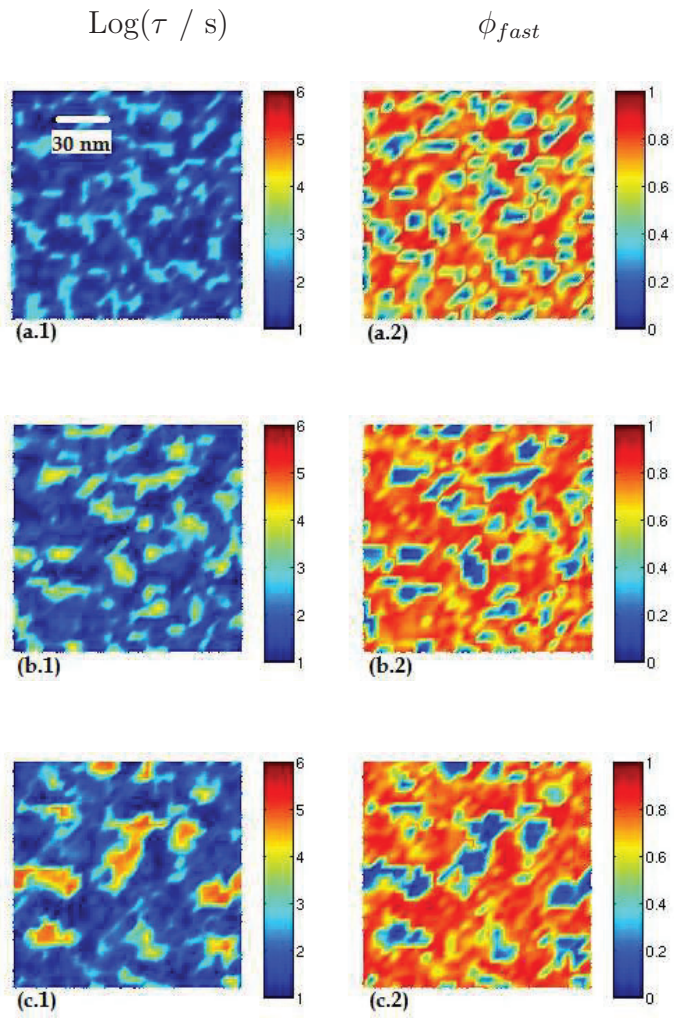

Figure 2.3.4: Snapshots of a phase separating system composed of 70% of low T_g polymer and of 30% of high T_g at three different stages during aging at $Tg - 10K$: (a) $t_w = 10^5$s, (b) $t_w = 10^6$s and (c) $t_w = 10^7$s. The system initially equilibrated at $T_g + 30K$ before aging. On the left column we give the relaxation times ($\log(\tau$ / s)) and on the right one the fast polymer volume fraction (ϕ_{fast}). We see that domains rich in high T_g polymer grow slowly and age during the process. They are in coexistence with a fast fluid phase rich in fast polymer.

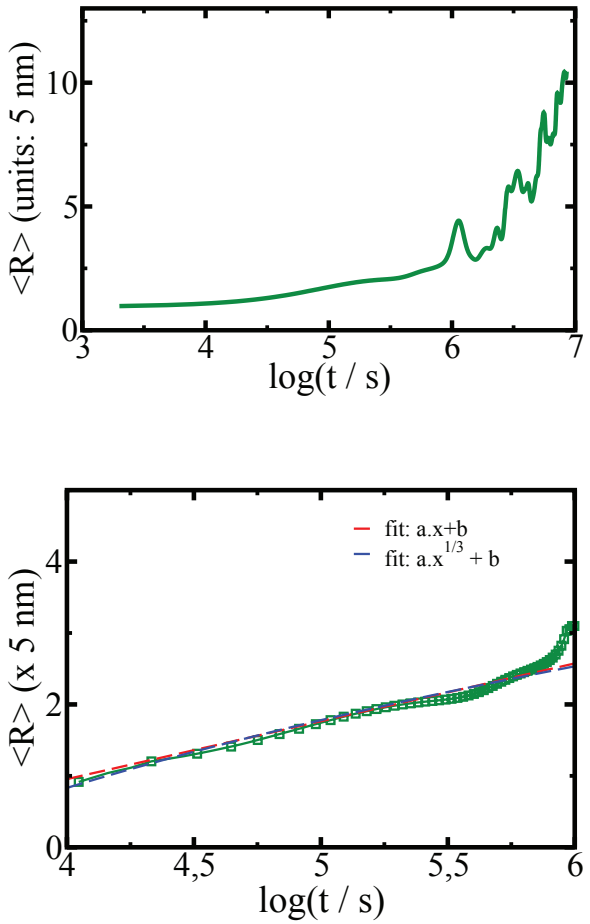

Figure 2.3.5: (UP) Average domains size evolution during the phase separation process at $T_g - 10K$ for a system composed of 70% of low T_g polymer and of 30% of high T_g. Thermal history of the system is that given in Figure 2.3.1.
We observe two regimes during the domains growth process: at the beginning of the process, domains grow in a regular way. At longer times scales, domains size grow in a rather chaotic way. (BOTTOM) Average domains size evolution at relatively short times scales during the phase separation process. The green curve represent data given by the simulation. The red curve represents a linear fit of simulation data, and the blue one a power law fit (exponent 1/3). Fits in the form of $(Log(t))^{\alpha}$ with $\alpha = 1$ and $1/3$ are very close from each other: domains grow like logarithm of the time.

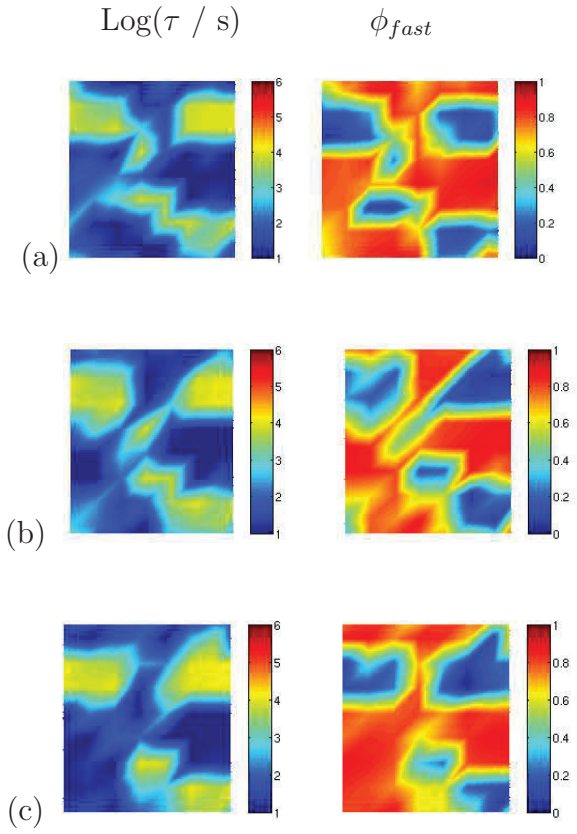

Figure 2.3.6: Snapshots representing a 15nm×15nm large area of the system represented on Fig.(2.3.4) at $t = 10^6$s (a), $t = 1.2 \times 10^6$s (b) and $t = 1.45 \times 10^6$s (c). For pictures (a), (b) and (c) we give relaxation times ($\log(\tau$ /s))[left column] and the fast polymer volume fraction (ϕ_{fast})[Right column]. We see that slow domains melt partially due to the fast phase which surround them. The size of slow domains can be reduced of a few nanometer because of melting mechanisms.

(exponent 1/3). As variable $\log(t)$ increases only by a factor 2 here, the power law and the linear curve are very close from each other. Though, one would see a significant divergence between them if variable $\log(t)$ varies by several decades, which is not the case here. Hence, on this time interval, growth regime can be assimilated to a purely logarithmic one.

b) Chaotic evolution of domains a late stage of the phase separation

At late stages (for $t > 10^6$s), we observe the existence of a chaotic regime during which the size of domains fluctuate on relatively small time scales. We attribute this effect to the partial melting of very slow domains by fast ones. For a sake of simplicity, let us call A the polymer with high T_g and B the polymer with the low one. Thermodynamically, at the interface between a slow and a fast domain, there is a flux of B polymer which goes out of the slow domain, while a flux of A polymer goes in. Since matter exchanges between two close regions are controlled by shortest relaxation times, the flux of B polymer at the interface is fast. As a consequence, fast monomers diffuse out in a much shorter time than the typical relaxation time

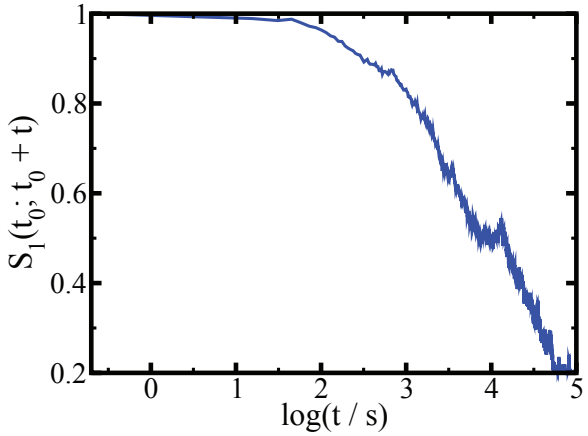

Figure 2.3.7: Evolution of the composition fluctuation auto-correlation function for the system represented in Figure 2.3.4 This function is calculated at time $t_0 = 10^6$s. We observe that 40% of composition fluctuations become uncorrelated 4000 seconds after $t_0 = 10^6$s in the whole system.

of the slow domains. Finally melting mechanisms are enhanced at late stage as compared to the early stage due to the large difference of mobility between the slow phase and the fast one. In order to give an example about melting process of slow domains by the fast fluid phase, we present three 15 nm large snapshots in Figure 2.3.6. The first of them is at time $t = 10^6$ s, the other one at time $t = 1.002 \times 10^6$ s and the last one at time $t = 1.0045 \times 10^6$ s. During the elapsed 4500 seconds between the first and the last snapshot, we do observe a local morphology changing on a shorter time scale than the relaxation time of the slow domains. As dynamics is conservative, the matter which was extracted from the slow domains which undergo the melting process moves apart until finding an other domains in the close environment. As shown in Figure 2.3.7 the rate of morphology changing at short time scales due to melting mechanisms is important in the whole system. Finally, the rather complex shape of obtained morphologies is also the consequence of melting mechanisms.

We have considered only systems composed in majority of fast polymer so far. It is worth considering phase separation in case of a system with opposite composition. Results regarding aging in these systems are given in appendix 2.B. As dynamics is fast at the beginning and also because dynamics slowing down is not instantaneous, phase separation occurs relatively quickly as one can see on composition distributions. However, the majority phase is composed of slow polymer and fast domains forming are trapped in the dominant phase which is aging. As a consequence, the diffusion time of fast domains is extremely long, and their size increase very slowly. This is the main difference between this situation and the previous one where the fluid phase is dominant. Indeed in the previous situation, the typical size of domains was about 50 nm after 10^7s while it is twice smaller in average in this present case.

2.4 Rejuvenation and high temperature remixing dynamics for aged and phase separated blends close to T_g

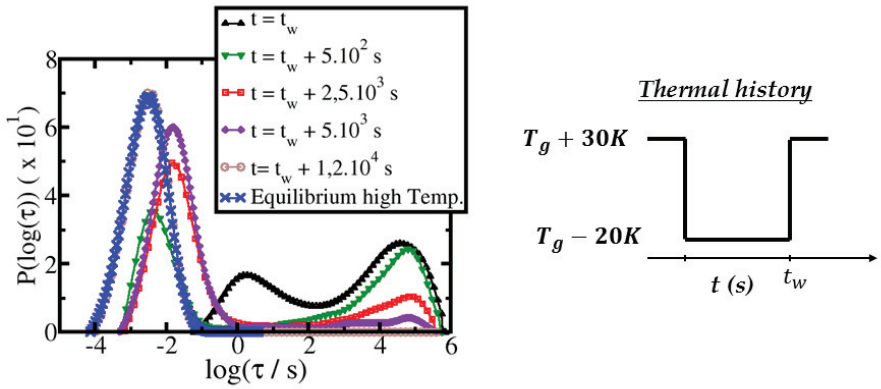

Figure 2.4.1: Distributions of relaxation times at different times during rejuvenation at $Tg + 30K$. The system has a symmetric composition and has been aged and phase separated for $t_w = 10^9$s at $T_g - 20K$ before rejuvenation. Rejuvenation occurs at times $t > t_w$. Black curve represents the dynamical state of the system at the end of aging. Faster relaxation times of the distribution become almost 100 times faster in the first 500 seconds of the process, then the proportion of slow relaxation times decreases. The relaxation time distribution matches the equilibrium distribution at $Tg + 30K$ in $1,25 \times 10^4$s.

After studying aging and phase separation in polymer blends close to T_g, we study the reverse process during which the temperature is increased again in a miscible range far above T_g. We see in Figure 2.4.3 that during rejuvenation the volume reaches its initial equilibrium value in slightly more than 10^4s after rejuvenation, while it takes 10^9 s to contract by 6% during aging (black curve). We can do the same statement about the evolution of the α-relaxation times. Hence, the system remixes and recovers its initial homogeneous molten state much faster than the time required to phase separate below T_g as one can see in Figure 2.4.1 and 2.4.2: there is a strong temporal asymmetry between the aging and the rejuvenation process. Note that such a temporal asymmetry had already been observed experimentally many years ago in pure polymeric liquids [90, 91, 92] and more recently by numerical simulations in pure Van der Waals glass forming liquids [41]. Spatial representations of the system (see Figure 2.4.4) and distribution of relaxation times during rejuvenation show us that the fast fluid phase accelerates significantly on short times scales as due to the temperature increase. In addition, small and slow isolated domains immersed in the fast fluid phase melt really quickly due to their small contact surface. As it can be seen in Figure 2.4.7 and Figure 2.4.5, the melting of bigger domains takes more times and is the consequence of inter penetration mechanisms of the very mobile polymer inside them from the interface (see Figure 2.4.7). Inter penetration mechanisms at the interface induce an increase of free volume in this region by osmotic effects. However, these effects take a certain time to take place, which explains why composition fluctuations become

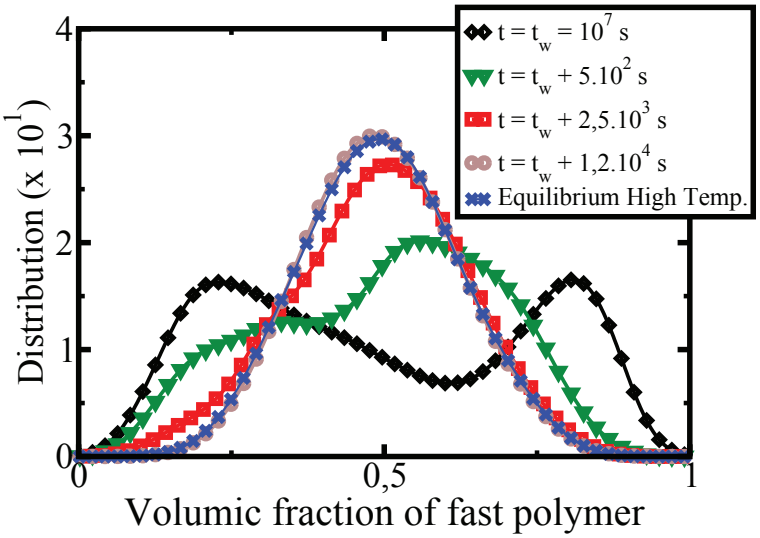

Figure 2.4.2: Distributions of low T_g polymer volume fraction during rejuvenation at $Tg+30K$. The system has a symmetric composition and its thermal history is that given in Figure 2.4.1. Black curve represents the phase separated state of the system at the end of aging. The low T_g polymer volume fraction distribution shows that the system remixes and recovers the equilibrium state at $Tg+30K$ in only $1,25\times10^4$ seconds during rejuvenation, while the system has been aged for 10^9 seconds before rejuvenation.

uncorrelated faster than relaxation times as it is shown in Figure 2.4.6. Since the free volume fraction is a good plasticizer for the system, the dynamics accelerates, which makes the inter penetration of monomers easier. In addition, the free volume diffuses toward the central region of the glassy structure which facilitates the their melting. As a conclusion, the combination of both interpenetration and free volume diffusion mechanisms makes that the melting glassy morphologies is a non linear self accelerating process driven by the dynamics of the mobile polymer they are in contact with. The mobility of the fast fluid phase is enhanced when the rejuvenation temperature T_{rej} increases. Hence, the subsequent melting of slow morphologies is faster when T_{rej} increases as it is plotted in Figure 2.4.8. Moreover, it can be observed in this Figure that the lower the aging temperature, the longer the rejuvenation time at fixed rejuvenation temperature. The rejuvenation kinetics depends also on the time during which the system has been aged before being reheated. Indeed on can see in Figure 2.4.8 that the shorter the aging time, the shorter t_{rej}. This essentially results from the fact that the dynamics of the slow domains forming during aging slows down with the time, which makes them longer to melt.

Finally, evolution of domains size and SANS scattered intensity during aging and rejuvenation are displayed in Figure 2.4.9 for a system mainly composed of fast polymer. During rejuvenation, we observe that the domains size reduction takes places in 40 second and that SANS scattered intensity drops by several order of magnitudes in the same time. As a reminder, at equilibrium, SANS scattered intensity $I(0)$ reads (for a homogeneous blend):

$$\frac{I(0)}{N(b_1-b_2)^2} \backsimeq \frac{T\rho_0}{K_{osm}}$$

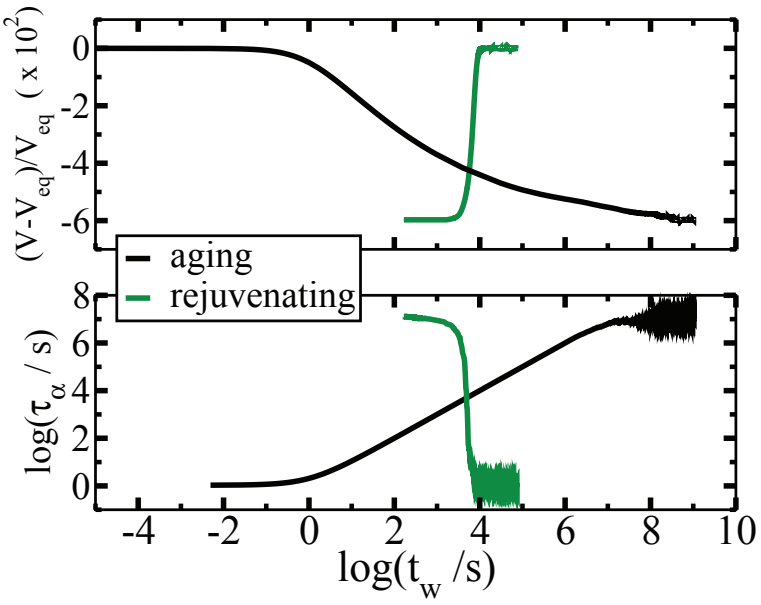

Figure 2.4.3: Evolution of the volume (UP) and the α-relaxation times (BOTTOM) during aging and rejuvenation for the system described in Figure(2.4.1) and Figure(2.4.2). The volume evolution is compared to the equilibrium volume (V_{eq}) at $Tg + 30K$. We observe a strong temporal asymmetry between aging and rejuvenation.

with $T \sim 4 \times 10^{21} J$, $\rho_0 \sim 10^{28} m^{-3}$, $K_{osm} \sim 10^7$Pa, one finds that $\frac{I(0)}{N(b_1-b_2)^2}$ is a quantity of order unity. N is the dimensionless volume of the sample ($V[m^3] = N/\rho_0$).

It is worth mentioning the case of systems composed of a majority of slow component as described in appendix 2.B. Like in previous case, a temporal asymmetry is observed between aging and rejuvenation. It is also observed in this case that faster domains acquire a high mobility very quickly at short time scales during the rejuvenation process. After that, high mobility domains begin to grow and to melt the lower mobility phase at interfaces. At longer times, high mobility domains are large enough so that they create a continuous path surrounding slower domains. This makes them easier to melt and the system recovers a complete miscibility as fast as the previous situation where the fast phase was in majority. Since both systems were aged and rejuvenated in equivalent conditions, although the way slow morphologies melt is different, we can conclude that rejuvenation kinetics does not depend on the macroscopic composition of the blend.

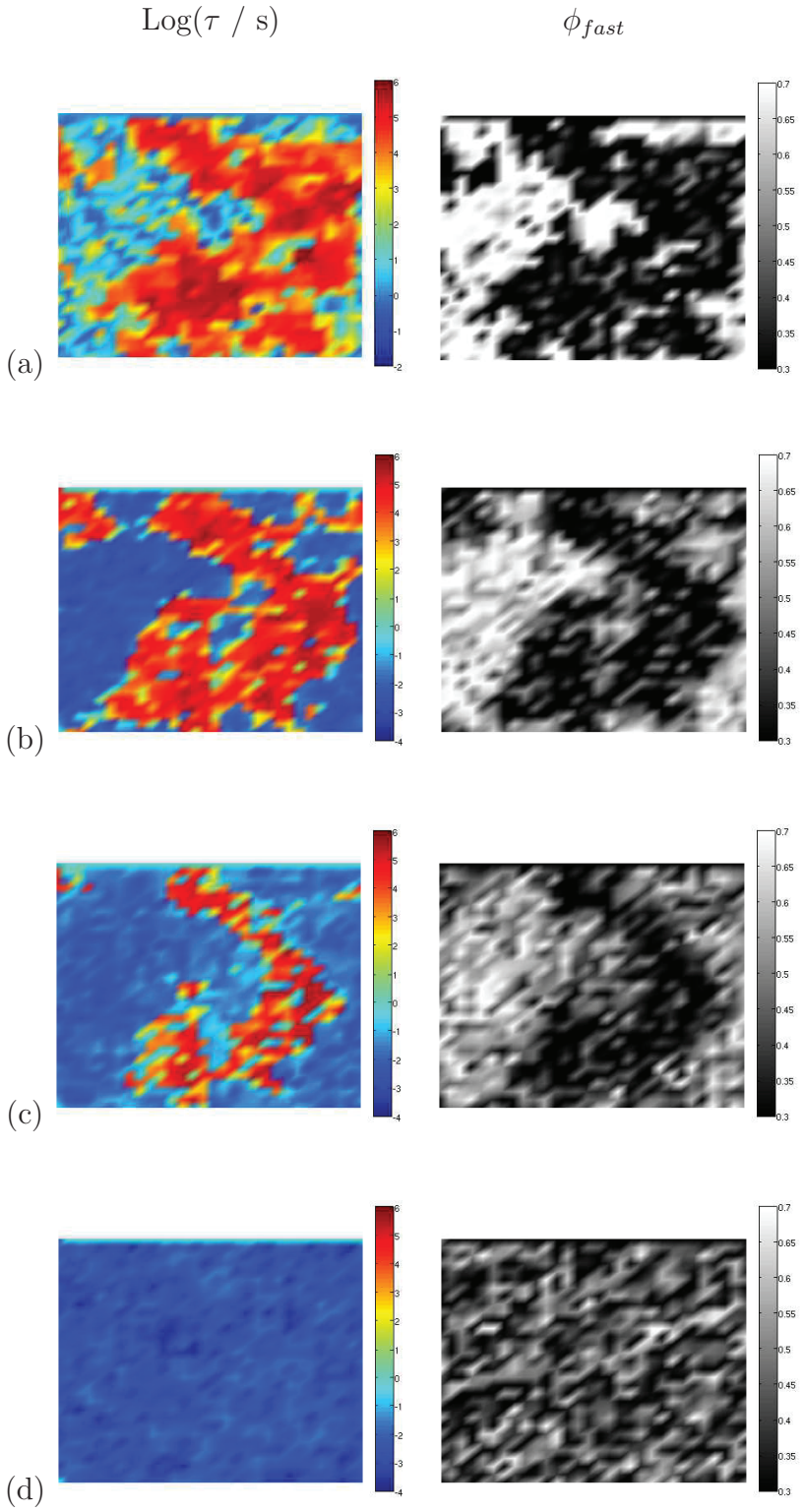

Figure 2.4.4: 120nm×120nm large Snapshots of the system described in Figure(2.4.1) and Figure(2.4.2) at times: $(a)t = t_w$; $(b)t = t_w + 500$s; $(c)t = t_w + 2500$s and $(d)t = t_w + 1,25 \times 10^4$s during rejuvenation at $Tg + 30K$. The system has a symmetric composition and has been aged and phase separated for $t_w = 10^9$s at $T_g - 20K$ before rejuvenation. Rejuvenation occurs at times $t > t_w$. On each snapshot, the left column represents the logarithm of relaxation times ($log(\tau/s)$), and the right one, the fast polymer volume fraction (ϕ_{fast}). Snapshot (a) represents the system before rejuvenation. A very large glassy morphology has been formed during the aging process at $T_g - 20K$, and the former takes $1,25 \times 10^4$ second to melt. At time $t = t_w + 1,25 \times 10^4$s, the system recovers a complete miscibility and is fluid.

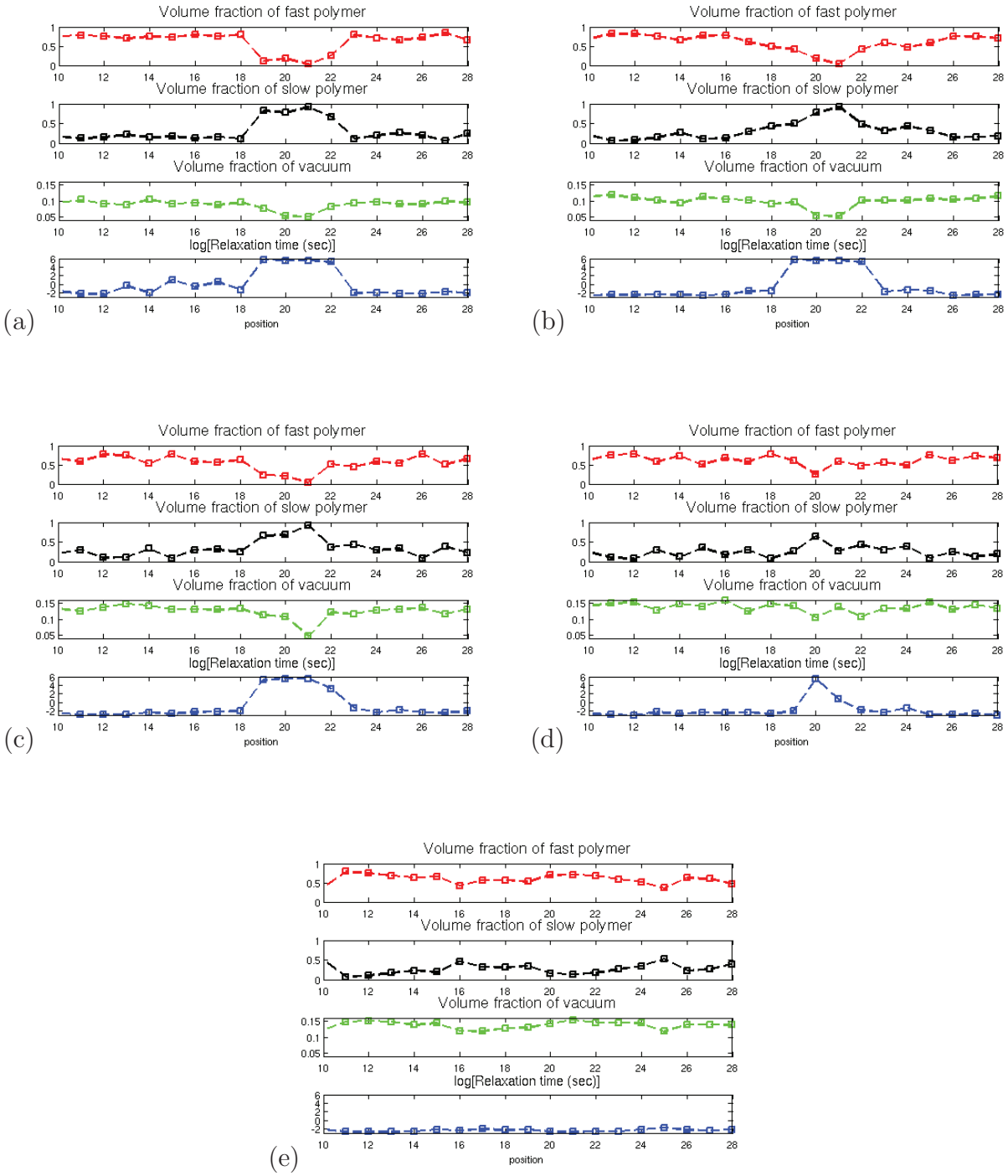

Figure 2.4.5: Profiles of fast polymer, slow polymer and vacuum volume fraction as well as relaxation times on a system's layer rejuvenating at $T_g + 30K$ at times (a)$t = 1s$, (b)$t = 1000s$, (c)$t = 2500s$, (d)$t = 4000s$ and (e)$t = 5000s$. The system is composed 70% of fast polymer and 30% of slow polymer and has been aged and phase separated for $t_w = 10^7$s at $T_g - 10K$ before rejuvenation. Rejuvenation occurs at times $t > t_w$. The layer intersects a slow domain between position 18 and 22. During rejuvenation, we see that fast monomers penetrate the slow domain and that slow monomers are leaving the domains through the interface. At short times, free volume fraction is low and the domain remains contracted. At longer times the free volume fraction increases at the interface of the domain due to osmotic pressure effects. Afterward, free volume diffuses into the domain and the later begins to plasticise. The central region of the domain melts at last.

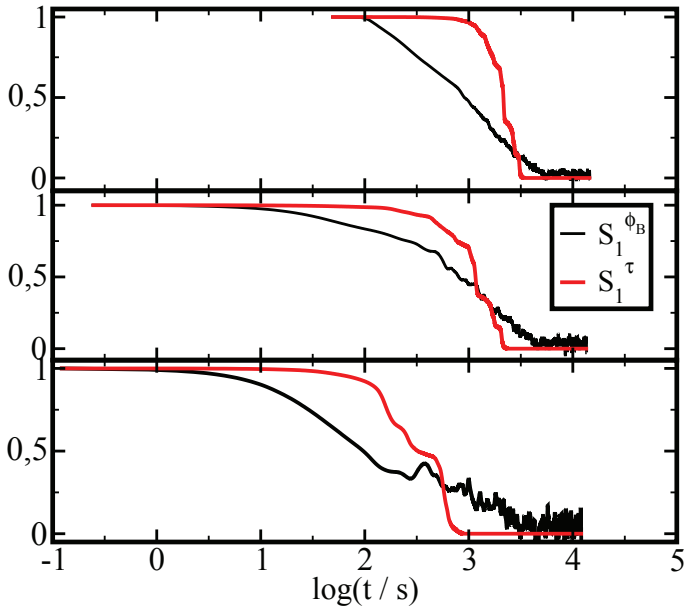

Figure 2.4.6: Evolution of composition (black curve) and relaxation times (red curve) fluctuations auto-correlation functions during rejuvenation computed at three different times: (a) 0s, (b) 2500s and 5000s after rejuvenation. The system is the same than the one described in Figure 2.4.5. We see that after 10^3s, 50% of composition fluctuations have become uncorrelated while relaxation times are still correlated.

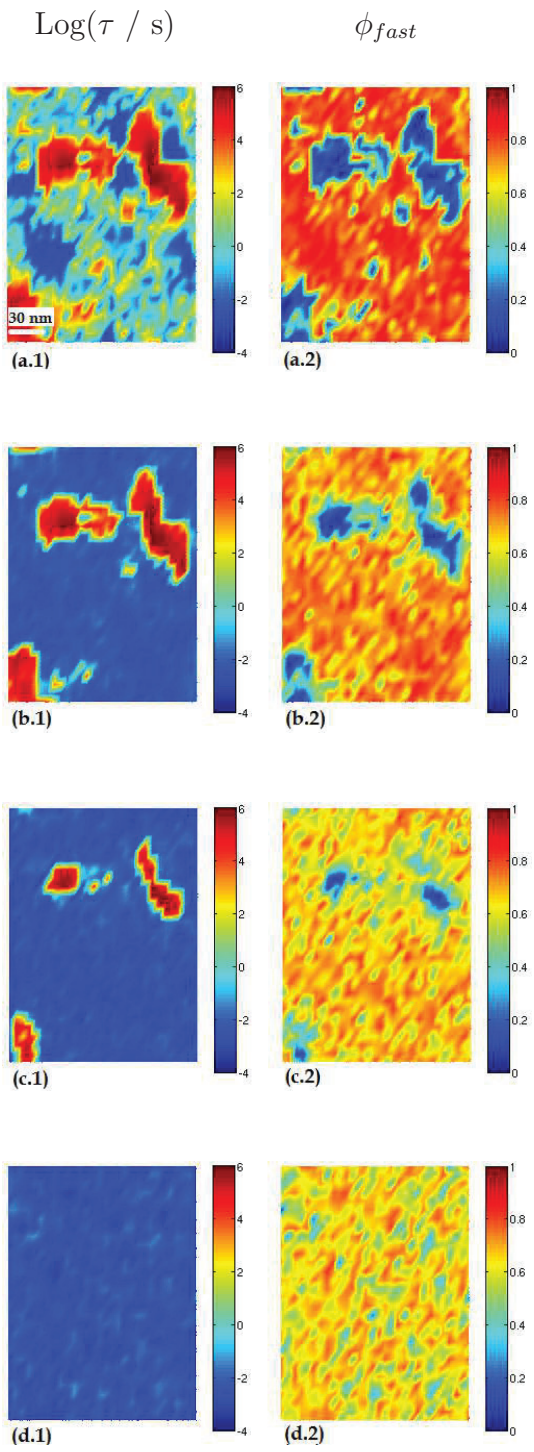

Figure 2.4.7: Snapshots of the system described in Figure 2.4.5 at different times ($t = t_w + 0\text{s}(a)$; $t = t_w + 1000\text{s}(b)$; $t = t_w + 2500\text{s}(c)$; $t = t_w + 7500\text{s}(d)$) during rejuvenation. left column corresponds to relaxation times $\log(\tau/s)$ and the right column corresponds to the fast polymer composition (ϕ_{fast}).
In the first 1000s after rejuvenation, size of domains in term of composition decrease: the fast polymer interpenetrate slow domains. 1000 seconds after rejuvenation however, glassy structures melt from the interface. The central regions of glassy domains melt at last, and 7000 s after rejuvenation, the system is molten and miscible.

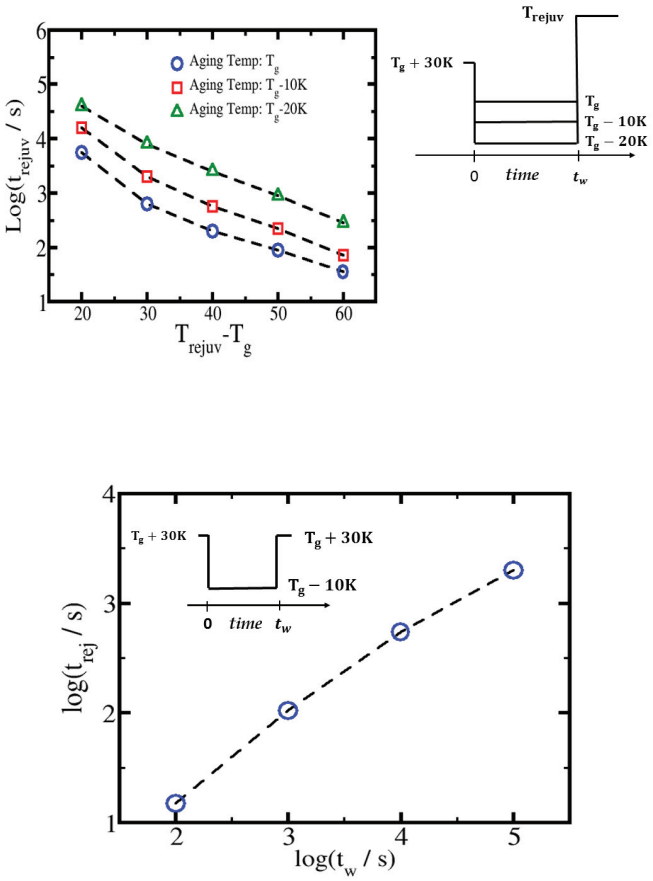

Figure 2.4.8: (Left) Evolution of the rejuvenation time t_{rej} as a function of the rejuvenation temperature. We consider a system with symmetric composition equilibrated at T_g+30K before aging. Then systems age for $t_w = 5 \times 10^7$s at three different temperatures:$T_g K$, $T_g - 10K$ and $T_g - 20K$. The rejuvenation temperature varies between $Tg + 20K$ and $Tg + 60K$.(Right) Evolution of the rejuvenating time (t_{rej}) as a function drying time in a polymer blend with a symmetric composition. The system was quenched from $T_g + 30K$ down to $T_g - 10K$ where it has been aged for various times $t_w = 10^2$s; 10^3s; 10^4s; and 10^5s. Then the system rejuvenates at $T_g + 30K$. Furthermore, we see on this log-log plot that the rejuvenating time behaves like $t_{rej} \sim t_w^{0.70}$. This is relevant with what has already been observed by Merabia et al. [88] in the case of pure polymer melts.

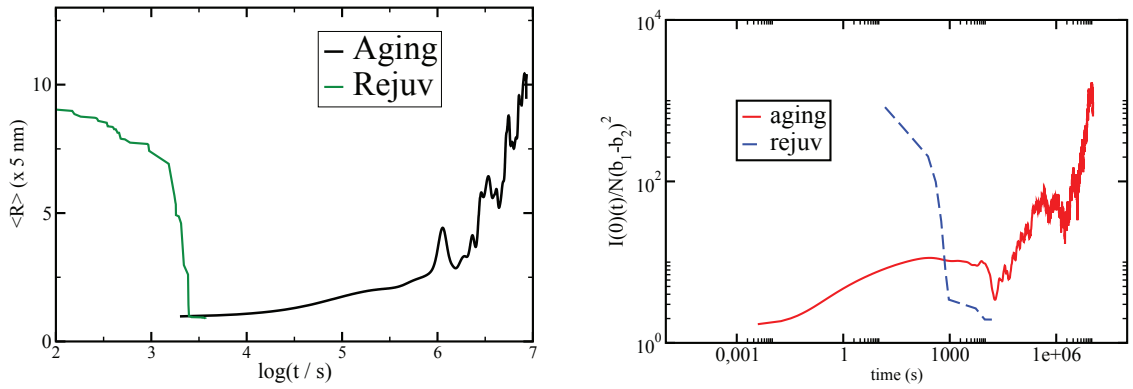

Figure 2.4.9: (Left) Evolution of typical domains size during aging and rejuvenation for the system studied in 2.4.7
Domains melt faster than the elapsed time required to form then during aging. (Right)Evolution of SANS intensity during aging and rejuvenation for the system studied in 2.4.7. Diffusion length b_1 for the low T_g polymer is $b_1 = 3,305 \cdot 10^{-15} m$ and diffusion length b_2 for the high T_g polymer is $b_2 = 1,066 \cdot 10^{-13} m$. These values are from reference [87].
Evolution of SANS intensity matches with the domains growth during aging, and the domains melting during rejuvenation. During rejuvenation, the SANS intensity decreases by several decades in 7000 seconds.

2.5 Conclusion

In this chapter, we have studied dynamics in polymer blends close to and below the glass transition temperature. First, we have considered the situation during which a phase separation takes place when the system is close to the glass transition temperature. As components of different T_g's are mixed together, domains of very different dynamics are forming during the phase separation. This is accompanied by a linear increase of α-relaxation times with the aging time and a slow mechanical contraction. Furthermore, relaxation times distribution translates towards longer times and widens when the time increases. Moreover, the Stokes Einstein law has been observed to be violated as a consequence of the widening of relaxation time distributions as discussed in appendix 2.C. The system is not frozen and the diffusion of polymeric species is possible on time scales shorter than α-relaxation times. At early stages of the phase separation process, we have observed that morphologies grow like the logarithm of the time in a steady way. At later stages however, a rather chaotic growth regime takes place which we attribute to the partial melting of slow domains by fast ones. In the chaotic regime, average domains size can be reduced by a few nanometers, and the shape of morphologies changes constantly in a random way. Finally, all these observations indicate that even if the system is aging close to T_g, we observe that morphologies grow, although the process is very slow (logarithmic). Moreover, heterogeneous dynamics allows for diffusive process to appear thanks to faster dynamic heterogeneities which makes the diffusion of polymer chains possible on short times scales: a glassy system is not "frozen".

The reverse process corresponding to rejuvenation has also been studied. During this process, the system recovers a homogeneous molten state after the temperature is increased again in a miscible range. We observe a strong temporal asymmetry between aging and rejuvenation *i.e.* the domains melt and the system recovers a complete miscibility in a much shorter time than the elapsed time to build them during aging. This is coherent with what has already been observed in the past in the context of pure polymeric system [90, 91, 92] [41]. The plasticization of large glassy domains results from a non linear cascade of events which are the consequence of an important acceleration of the fast fluid phase and the swelling of slow domains by facilitation mechanisms: -1- slow domains are quickly inter-penetrated by the fast component from the interface. This induces osmotic pressure effects which results in an increase of the free volume fraction in this region; -2- the free volume diffuses toward the center of the domains and the latter plasticise subsequently. We have seen that the rejuvenation kinetics depends strongly on the history of the system. Indeed, the longer the aging time, the longer the rejuvenation time and the higher the rejuvenation temperature, the shorter the rejuvenation time.

The case of blends with polymers of different chain sizes has been also studied (see appendix 2.D). We considered a polymer blend where long chains of 1000 monomers are mixed with small polymer chains of 50 monomers. Two situations have been considered: a first one where the small polymer chain is the fast component and a second one where the small chain is the slow

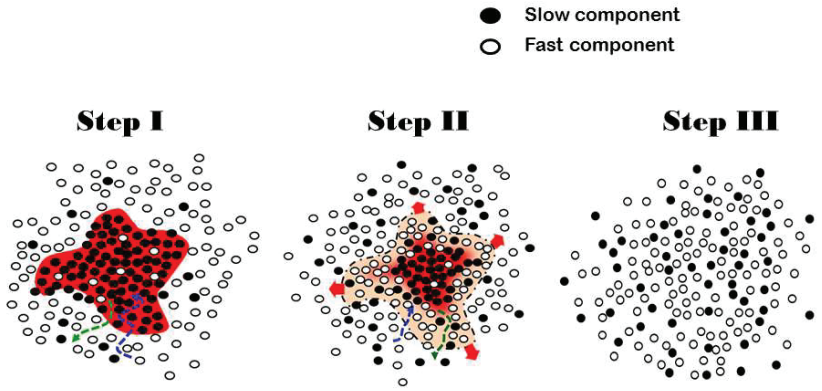

Figure 2.5.1: Schematic representation of the melting of a glassy nanostructure (Red) during rejuvenation. At very first times of the process (step I), fast monomers penetrate the slow structure from the interface (blue dotted arrow), and simultaneously, slow monomers, of which it is mainly composed, diffuse out of it (green dotted arrow). This engenders osmotic pressure effects which induce an increase of the free volume at the interface. Then, the free volume diffuses from the interface toward the center (step II) and the slow structure plasticises progressively. Plasticisation resulting from the free volume diffusion facilitates the penetration process of species inside the slow structure, and finally, at step III, the latter is completely melted and the system is miscible.

component. In both cases, the system is composed of 80% of small polymer chains, and it has been observed that the first system rejuvenates 100 times faster than the second one.

Appendix

2.A Phase separation in dynamically homogeneous polymer blends ("Standard case")

Phase separation takes place when a system is quenched from a single homogeneous phase into regions where the system is metastable.
During the phase decomposition process in molten polymer blends, domains are seen to be forming following several regimes [81]. One of them is the Ostwald rippening [89, 82, 83, 84, 85, 86]. In this regime, which is driven by the surface tension, average domain size $R(t)$ increases like $R(t) \sim t^{1/3}$. Ostwald ripening was confirmed by many experimental technics such as light or neutron scattering [22, 23, 24, 26, 25]. From a theoretical point of view, it is recovered by assuming that polymer mobility is independent of composition (homogeneous) and does not depend on the system's history. Here, we consider phase separation in dynamically homogeneous polymer blends *i.e.* at fixed relaxation times.

The "Ostwald ripening"

We consider a blends of polymers having the same degree of polymerisation: $X_A = X_B = 50$. We give in Figure 2.A.1 the UCST phase diagram that we consider here. The critical temperature is of the blend is $T_c = 320K$. Relaxation times $\tau = 1s$ are fixed in the whole system. The system is initially prepared at thermodynamic equilibrium at $T = 330K$ and it has symmetric composition. After equilibration, the system is quenched at $T = 270K$ inside the spinodal decomposition region. We give in Figure 2.A.2 the polymer B volume fraction distribution at times $t_w = 1s; 10^2s; 10^3s$ after the system was quenched. We observe that for times shorter than 1 second there is no phase separation in the system. At much longer times two peaks on both side of the distribution meaning that the system phase separates. Moreover, when the time increases, peaks representing rich phases in polymer A and B shift toward richer concentrations. Phases forming during the process are represented in Figure 2.A.4 where we give snapshots of the system at four different times t_w: (a) $t_w = 1s$, (b)$t_w = 10^2s$, (c)$t_w = 10^3s$ and (d)$t_w = 10^4s$ during the phase separation. In the first 1 seconds, system has not demixed yet as it is confirmed by polymer volume fraction distribution in Figure 2.A.2. Surface tension imposes that the domains acquire a circular shape on short distances. When time increases, the system tends to maximize the curvature radius of domains (increasing the radius of domains) in

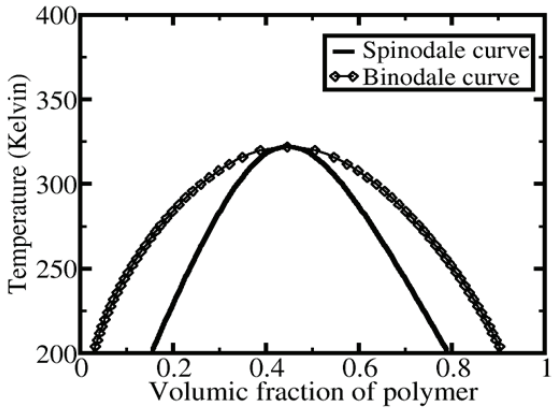

Figure 2.A.1: UCST phase diagram of a $X_A = X_B = 50$ blend. Interaction parameters are $a = -2,32 \times 10^{-20}J$, $b = -1,595 \times 10^{-20}J$ and $c = -\sqrt{ab}$. The critical temperature is $T_c = 320K$. We consider such a phase diagram to study spinodal decomposition when the dynamics is homogeneous in the blend.

order to minimize the excess of free energy due to domains forming. The size R of the domains increases during the process and their shape becomes much more circular. It is found that R grows like $t^{0.30}$ between time $t_w = 10^2 s$ and time $t_w = 10^4 s$. One can refer to Figure 2.A.3. This result is very satisfying regarding the Ostwald ripening which predicts an exponent 1/3. Let us now introduce a simple semi quantitative method which allows for obtaining the Ostwald ripening exponent. During a spinodal decomposition process, when the radius R of an existing sphere increases of δR, the change of energy, related to the surface tension η ($[\eta] = J \times m^{-1}$), is $\delta E \sim 8\pi\eta R\delta R$, and the quantity δN of penetrating monomers is $\delta N \sim a^{-3}4\pi R^2\delta R$. Hence, the chemical potential $\Delta\mu$ (per monomers) reads:

$$\Delta\mu = \frac{\delta E}{\delta N} \sim 2\frac{\eta a^3}{R} \tag{2.A.1}$$

We have seen that the flux j reads $j = \frac{\lambda}{T}\nabla\mu$ where μ is the chemical potential (per monomers) in Joules, T the temperature in Joules and λ is the diffusion coefficient where $[\lambda] = m^2 \cdot s^{-1}$. Hence we have $[j] = m \cdot .s^{-1}$. By using the above equation 2.A.1, we obtain:

$$\begin{aligned} j =& \frac{\lambda}{T} \times \frac{\Delta\mu}{R} \\ =& 2\tilde{\lambda}\frac{\eta a^3}{R^2} \end{aligned} \tag{2.A.2}$$

where $\tilde{\lambda} = \lambda/T$.
One can write:

$$\frac{dR}{dt} \sim j \tag{2.A.3}$$

we straightforwardly obtain

$$\frac{dR}{dt} \sim 2\tilde{\lambda}\frac{\eta a^3}{R^2} \tag{2.A.4}$$

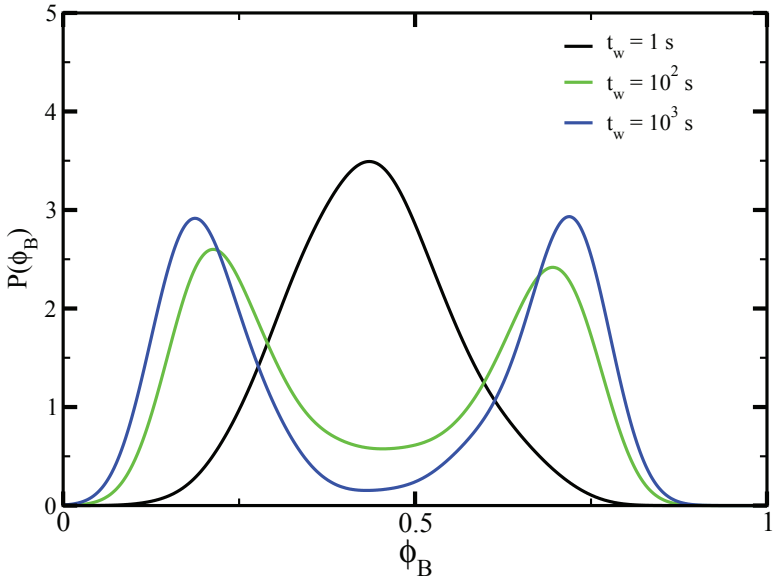

Figure 2.A.2: Distribution of B polymer volume fraction during a phase separation occurring in a polymer blend at $T = 270K$. We consider distributions at times $t_w = 1s; 10^2 s; 10^3 s$. Relaxation times are equal to one second and the blend composition is symmetric. Before phase separation, the system was initially prepared at $T = 330K$ in a miscible regime.

As $\tilde{\lambda}$ is a constant, we have:

$$R^3 \sim 2\tilde{\lambda}\eta a^3 \times t \tag{2.A.5}$$

Thanks to this simple semi-quantitative development, one finds the exponent 1/3 predicted by the Ostwald ripening in 3D. This exponent holds also in 2D [99].

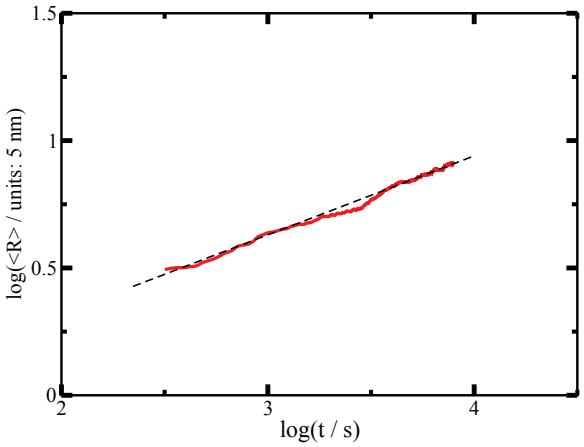

Figure 2.A.3: Evolution of the typical size R of domains during a phase separation in a dynamically homogeneous polymer blend. The system is initially prepared at $T = 330K$ at thermodynamic equilibrium and quenched from $T = 330K$ down to $T = 270K$. At this temperature, the system is unstable and spinodal decomposition occurs. Size R is found to grow like $R \sim t^{0.30}$ which is very closed to what is predicted by the Ostwald ripening.

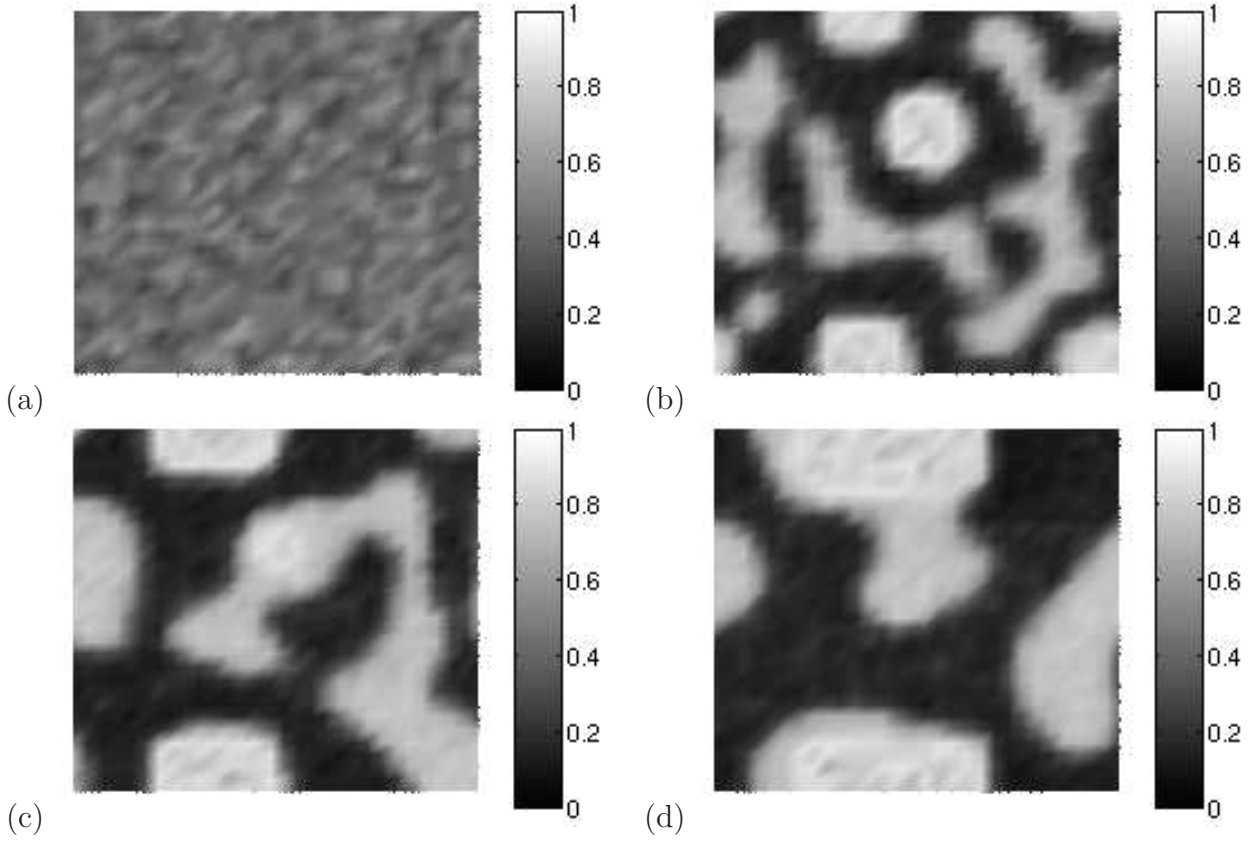

Figure 2.A.4: 300nm×300nm snapshots of the system during a phase separation at fixed relaxation times ($\tau = 1s$) at different times t_w: (a) $t_w = 1s$, (b)$t_w = 10^2s$, (c)$t_w = 10^3s$ and (d)$t_w = 10^4s$. The system is composed in equal proportion in polymer A and B and snapshots are given in term B polymer volume fraction. The system is initially equilibrated at $T = 330K$ in a miscible state. It is then quenched down to $T = 270K$.
One second after quenching the system, the blend has not phase separated yet. At longer times however, the phase separation occurs and domains grow until forming two clusters rich in A polymer (poor in B polymer). Between times $t_w = 10^2s$ and $t_w = 10^4s$, domains size R grow like $R \sim t^{0.30}$ (Cf Figure 2.A.3).

2.B Aging and rejuvenation in symmetrical polymer blends

In this appendix, we give results regarding aging and rejuvenation in polymer blends composed in majority of slow component.

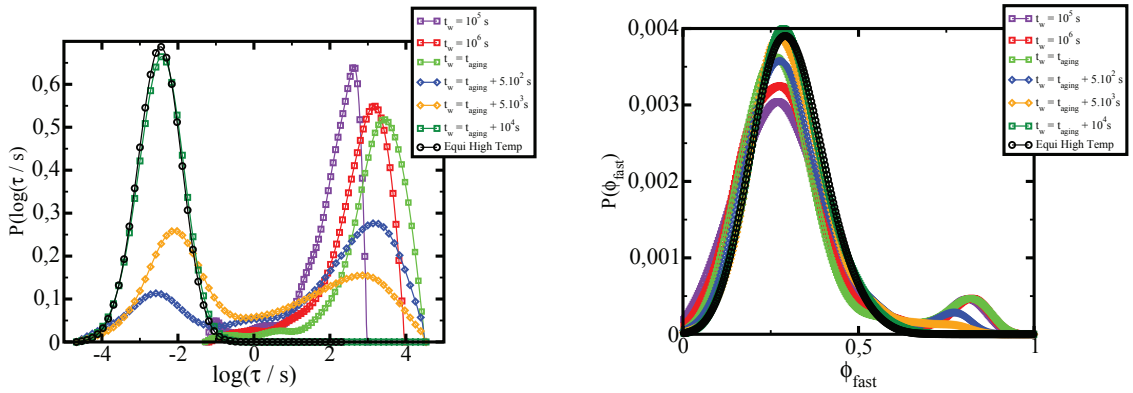

Figure 2.B.1: Distribution of relaxation times (Left) and fast polymer volume fraction (Right) at different times during aging and rejuvenation at $T_g + 30K$ for a system composed of 30% and 70% of fast and slow polymer respectively. The system was initially prepared 30K above T_g before aging. Then the system ages for $t_{aging} = 1 \times 10^7 s$ at $T_g - 10K$. Finally it is rejuvenated by increasing the temperature at $T_g + 30K$ at $t > t_{aging}$. During aging, the majority phase is rich in slow polymer, and a few fast domains build up. After aging, the system rejuvenates in a few thousands of seconds as one can see in Figure 2.B.2.

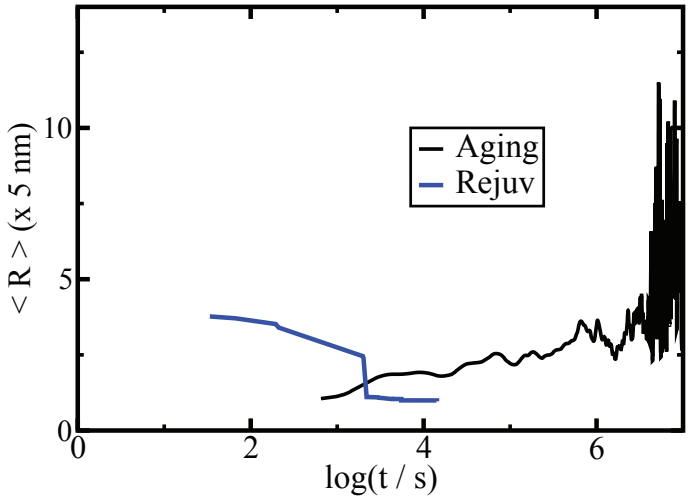

Figure 2.B.2: Evolution of average domains size during aging and rejuvenation for the system described in Figure 2.B.1. We see that growth process of morphologies is very slow: domains size is of 4-5 dynamic heterogeneities at $t_{aging} = 1 \times 10^7 s$. Domains melt in a few thousands of seconds during rejuvenation after the temperature was increased: there is a temporal asymmetry between aging and rejuvenation.

2.C Violation of the Stokes-Einstein relation for diffusion

Stokes-Einstein relation gives the diffusion coefficient D of a probe of size a as a function of the viscosity η and the temperature T of the material environment this probe diffuses in. This relation reads:

$$\frac{D\eta}{T} = \frac{k_B}{6\pi a} \tag{2.C.1}$$

Let us write:

$$\mathrm{Log}\Big(\frac{D\eta}{T}\Big) = \mathrm{Log}\Big(< \gamma > \tau_\alpha \Big) + \kappa \tag{2.C.2}$$

where κ is a numeric constant which depends on the probes size. Quantity $< \gamma >$ is the average relaxation frequency and represents the average diffusion coefficient of polymer chains which diffuse through fast dynamic heterogeneities, i.e. $D \sim \langle 1/\tau \rangle \approx 1/\tau_{fast}$.
We propose here to calculate quantity $\mathrm{Log}\Big(< \gamma > \tau_\alpha \Big)$ during a phase separation close to or below T_g. For that, we consider the same system as the one studied in part 2.3.
One observes in Figure 2.C.1 that the time evolution of the quantity $\mathrm{Log}\Big(< \gamma > \tau_\alpha \Big)$ is not constant meaning that the Stokes-Einstein law is not satisfied.
We see that quantity $\mathrm{Log}\Big(< \gamma > \tau_\alpha \Big)$ decreases first because of the sharpening of relaxation times distributions. Afterward, the same quantity increases because of widening of relaxation times distribution which translate toward longer times. Finally, evolution of quantity $< \gamma > \tau_\alpha$, which can be calculated experimentally, is a proof that dynamics becomes more and more heterogeneous as time increases during the aging process.

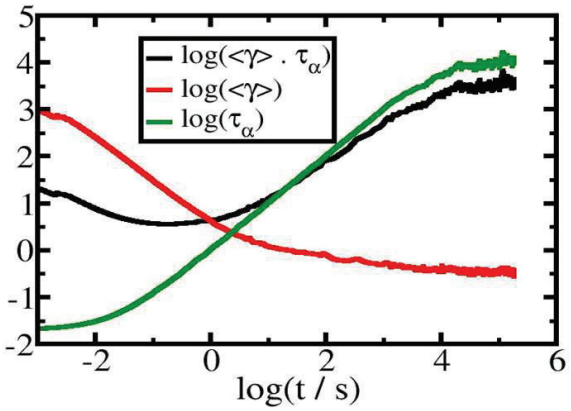

Figure 2.C.1: Evolution of $< \gamma >$, τ_α and $< \gamma > \tau_\alpha$ in a phase separating polymer blends at $T_g - 10K$. Blend composition is: 70% of low T_g polymer and 30% high T_g polymer and chains size are $X_A = X_B = 50$.
We observe that quantity $< \gamma > \tau_\alpha$ is not constant: the Stokes-Einstein relation is not satisfied. Quantity $< \gamma > \tau_\alpha$ first decreases at short times and it increases at long times. The increase of quantity $< \gamma > \tau_\alpha$ is a signature of the heterogeneous dynamics and the widening of relaxation times distribution. Diffusion of polymeric species is driven by fast relaxation times.

2.D Non symmetric phase diagrams: phase separation close to T_g and rejuvenation

We consider a non symmetric blends where the small polymer chain is either the fast (case I) or the slow component (case II). Small and large chains have a polymerisation degree of 50 and 1000 respectively. The phase diagram and the T_g of the blend are given in Figure 2.D.1. We study aging and rejuvenation in this system when it is composed of 80% of small chain. For this composition, equilibrium T_g is $260K$, whether it is in case I or II. In both cases the system is aged at T_g for 1.5×10^6s and is rejuvenated at $T_g + 40K$. Systems are prepared at equilibrium at $T_g + 40K$ before aging.

Small polymer chain: fast component

Snapshots of the system in terms of relaxation times and slow polymer volume fraction (small chains) at times $t = 10^3$s; 5×10^4s and10^6s during aging are given in Figure 2.D.3. We observe the presence of a few domains essentially composed of large chains. However, as the slow phase is in minority, the melting of slow domains by the fast fluid phase competes with the growth process. Hence, their does not increase much and fluctuates a lot. Evolution of α-relaxation times and volume during aging and rejuvenating are given in Figure 2.D.2. A temporal asymmetry is clearly observed. Indeed, the system rejuvenates in two seconds which is very fast as compared to the aging time. Snapshots during rejuvenation are given in Figure 2.D.4 at four different times. Domains composed of small chains accelerate very quickly and slower domains begin to melt. Two seconds after rejuvenation, the whole system has melted except for one isolated slow domain which is still in the process of melting.

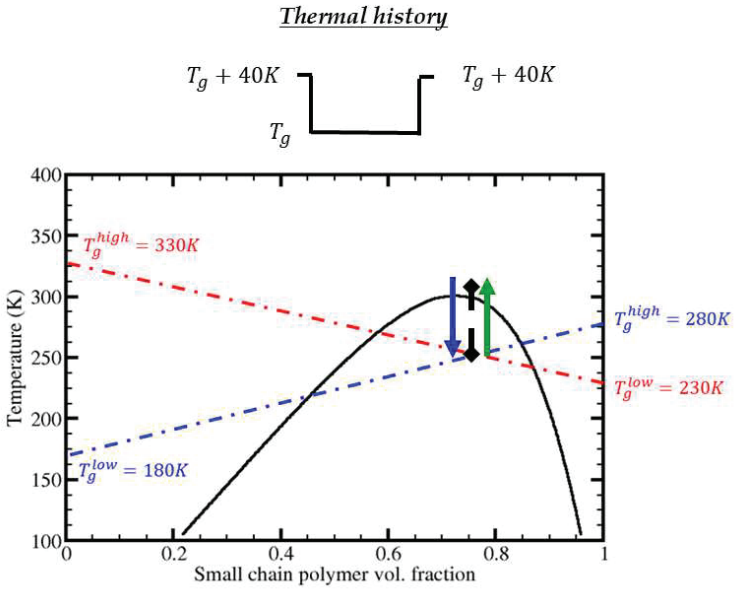

Figure 2.D.1: Phase diagram in case of an non symmetric polymer blend. Long chain length is $X_A = 1000$ and small chain length is $X_B = 50$ monomers. The blend critical temperature is $T_c = 300K$. Parameters are $a = -5.1426e\times10^{-20}J$, $a = -7.2e\times10^{-20}J$, $b = -4.8855e\times10^{-20}J$, $c = -\sqrt{ab}$ and $\rho = 10^{28}m^{-3}$. The left and the right hand side of the diagram corresponds respectively to the semi-dilute and the dilute phase and dotted lines represents the equilibrium glass transition of the blend when the small chain is the low T_g polymer (red dotted curve) and the when small chain is the high T_g polymer (blue dotted curve). Pure polymer Tg's are reported in the Figure for each considered situations.

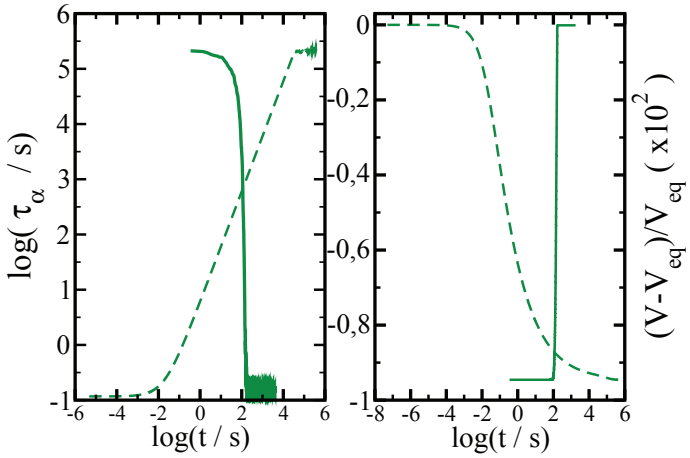

Figure 2.D.2: Evolution of α-relaxation times (left) and volume (right) during aging (green dotted curve) and rejuvenation (green full curve) for a system composed of 80% of low T_g polymer (small chain) volume fraction. During aging the system phase separates at T_g for 10^6s, and temperature is increased at $T_g + 40K$ during rejuvenation. The system is equilibrated at $T_g + 40K$ before rejuvenation. We see that relaxation times increase with the aging time. During this process, volume contracts slowly by almost 1% and the system rejuvenates in 100s: we observe a strong temporal asymmetry between aging and rejuvenation.

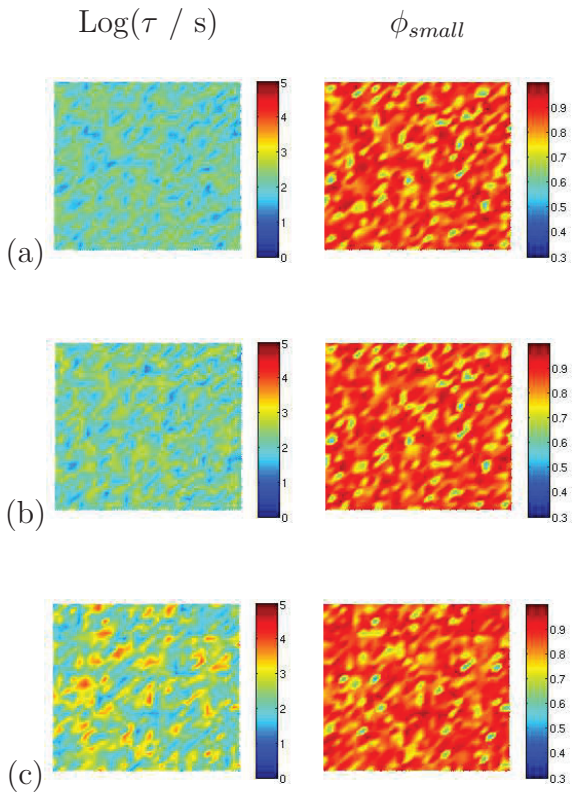

Figure 2.D.3: Snapshots in term of the logarithm of relaxation times(Left column) and small polymer chain volume fraction (Right column) at the three different times $t = 10^3$s(a); $t = 5 \times 10^4$s(b); $t = 10^6$s(c) of a phase separating non symmetric blends composed at 80% of small polymer chain. The large chain length is $X = 1000$ and the small chain length is $X = 50$. The system is aging for 10^6s at T_g and the small chain is the fast component. The left column represents the logarithm of relaxation times and the right one the small chain polymer volume fraction (ϕ_{small}). We observe some domains rich in long chain which appear during the phase separation process, However, their size does not increase much. Moreover relaxation times of these small domains are long.

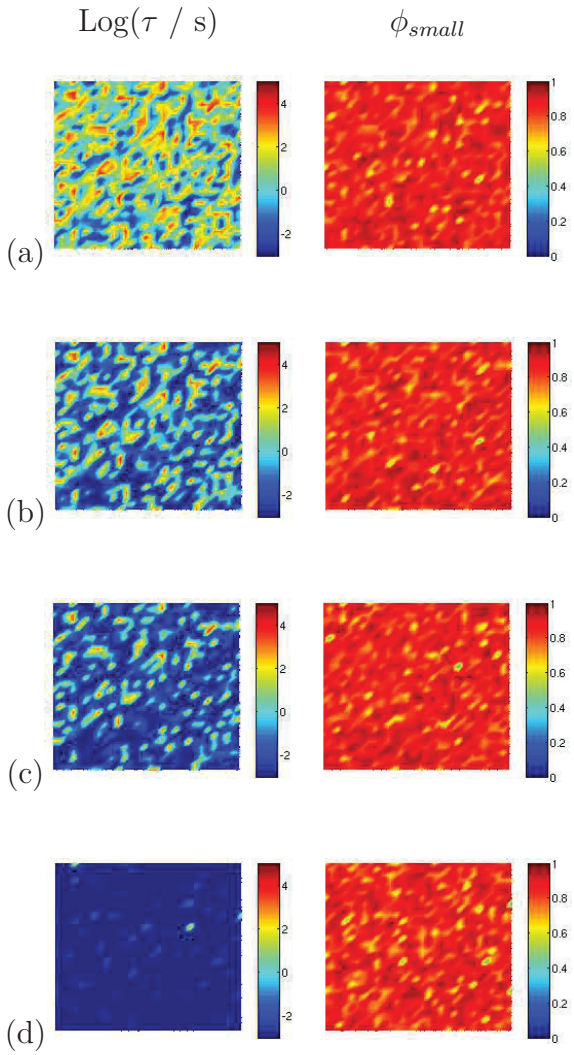

Figure 2.D.4: Snapshots of the system represented in Figure 2.D.3 during rejuvenation at $T_g + 40K$ after it has been aged at T_g for $\sim 10^6$s. Times are $t = 30$s(a); $t = 100$s(b); $t = 123$s(c) and $t = 200$s(d) after rejuvenation. The left column represents the logarithm of relaxation times and the right one the small chain polymer volume fraction (ϕ_{small}). Fastest domains are rich in small polymer chains and melt quickly the slow domains composed mainly of slow components. The system rejuvenates in 200 seconds.

Small polymer chain: slow component

Snapshots of the system in term of relaxation times and slow polymer volume fraction (small chains) at times $t = 10^3$s; 5×10^4s and 10^6s during aging are given in Figure 2.D.6. Like in previous situations, domains composed of large chains do not grow much during the aging process. They are immersed in a large slow phase composed of small chains with relaxation times longer than 100 s. Evolution of α-relaxation times and volume during aging and rejuvenating are given in Figure 2.D.5. Like in the previous situation, a temporal asymmetry is observed between aging and rejuvenation, however, rejuvenation kinetics is 100 time slower here. This comes from the fact: -1- when small chains are the fast ones, they penetrate easily and melt slow domains -2- the rejuvenating time is large when the majority phase is in a glassy state before rejuvenation.

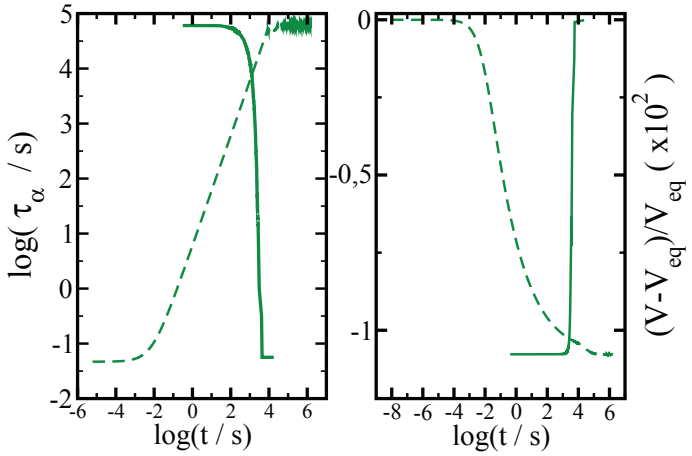

Figure 2.D.5: Evolution of α-relaxation times (left) and volume (right) during aging (green curve) and rejuvenation (black) for a system composed of 80% of small chain. The small polymer chain is the slow component. During aging the system phase separates at T_g for 10^4s, and temperature is increased at $T_g + 40K$ during rejuvenation . The system is equilibrated at $T_g + 40K$ before aging. We see that relaxation times increase with the drying time. During this process, volume contracts slowly by 1% and the system rejuvenates in 10^4s. These curves show that the system rejuvenates in longer times than in Figure 2.D.2 where the small polymer chain corresponds to the fast component.

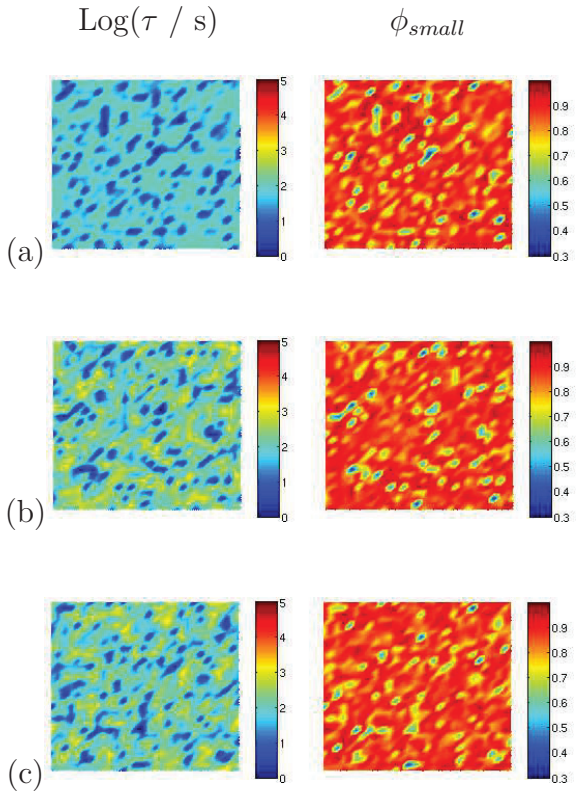

Figure 2.D.6: Snapshots at the three different times $t = 10^3$s(a); $t = 5\times10^4$s(b); $t = 10^6$s(c) of a phase separating non symmetric blends composed at 80% of small polymer chain. Chain length are $X = 1000$ regarding the large polymer chain and $X = 50$ regarding the small polymer chain. The left column represents the logarithm of relaxation times and the right one the small chain polymer volume fraction (ϕ_{small}). Unlike Figure 2.D.3, the small polymer chain corresponds to the slow component. Mobility of the large chain is reduced of a factor 10. We see the appearance of small isolated domains rich in large polymer chains. However their size remain small during the phase separation process.

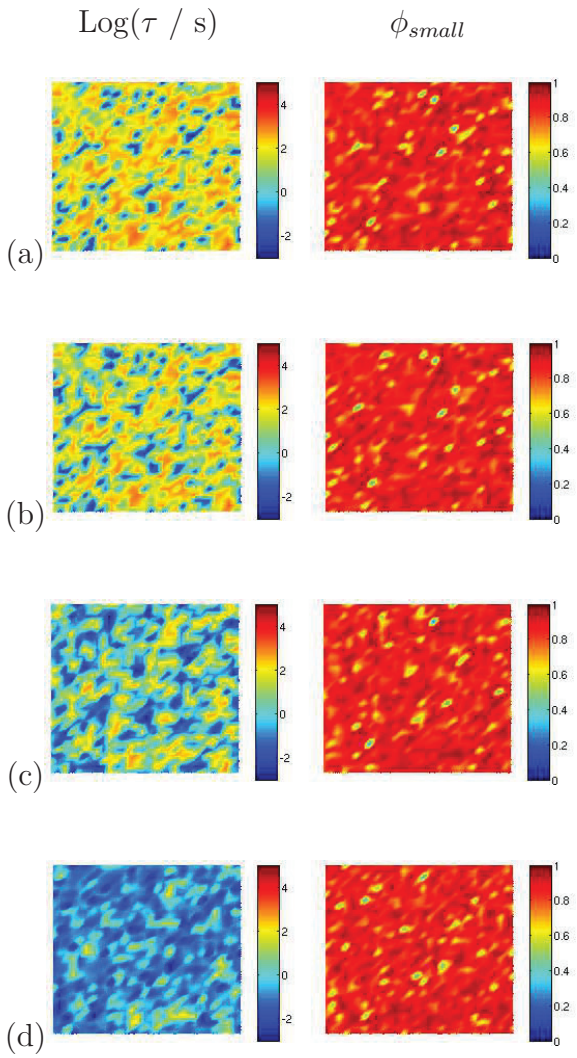

Figure 2.D.7: Snapshots of the system represented in Figure 2.D.6 during rejuvenation at $T_g + 40K$ after it has been aged at T_g for $\sim 10^6$s. Times are $t = 100$s(a); $t = 800$s(b); $t = 1,2 \times 10^3$s(c); and $t = 5,0 \times 10^3$s(d) after rejuvenation. The left column represents the logarithm of relaxation times and the right one the small chain polymer volume fraction (ϕ_{small}). Fastest domains are rich in long polymer chains which corresponds to the fast component. The melting of slow domains by long fast chains is longer than in the situation where the small chain is the fast component. The rejuvenating time of this system is longer as compared to previous situation because the majority phase is glassy before rejuvenation here.

Chapter 3

Dynamics in polymer-solvent systems close to and below the glass transition temperature

3.1 Résumé en français

Dans ce chapitre nous étudions la dynamique dans les systèmes polymère solvant lorsque le système se trouve bien en dessous de la T_g du polymère pur. Nous nous sommes plus précisément intéressés aux phénomènes de séchage et de gonflement dans les films polymère solvant dits minces (de taille inférieur à 500 nanomètres-1 micron) et épais (de taille supérieur à 1 micron). Le système est initialement équilibré avec un réservoir de solvant ayant une activité donnée. Durant le séchage, l'activité est baissée ce qui fera évaporer le solvant. Dans le cas des films minces, nous observons que l'évaporation du solvant est la conséquence de -1- une diffusion rapide du solvant via les zones à dynamique rapide au temps courts et -2- d'une séparation d'échelle de temps entre la diffusion du solvant et la contraction du système au temps longs. Nous observons une accélération de la dynamique globale du système résultant de l'augmentation du volume libre lors de la diffusion rapide du solvant. Pendant la contraction du système en revanche, le système vieillit du fait de la réduction du volume libre. Nous montrons également que des films séchés à très basse activité (atmosphère sèche) peuvent être séchés completement. En revanche, dans certaines conditions, ils peuvent être le siège de cavités grandes de quelques nanomètres qui se forment pendant le processus de vieillissement du film. Dans le cas de films épais nous observons plus de séparation d'échelles de temps ce qui fait que le mécanisme de diffusion du solvant et de contraction du système se superposent. En conséquent une croûte lente sèché se forme proche de l'interface avec le réservoir, alors qu'une grande quantité de solvant reste piégée dans le fond du système. Durant le gonflement, l'activité du réservoir est augmentée après séchage, ce qui impose la pénétration du solvant dans le système. Nous montrons dans ce cas que le solvant diffuse tout d'abord de façon fickienne par les zones rapides dans le film. Ce processus est accompagné d'un ralentissement de la dynamique globale du système du fait de la réduction du volume libre. Au temps longs, nous observons que le solvant diffuse de par un

processus cas II. Ce dernier est la conséquence de la dilatation progressive du système résultant d'effets de pression osmotique exercés par les molécules de solvant au sein de la matrice. Enfin, à la fin du processus de gonflement, le système est fluide et à l'équilibre avec le réservoir.

3.2 Introduction

In this Chapter, we consider the drying and the swelling of polymer-solvent films at temperatures far below the pure polymer glass transition temperature. For that, we apply the spatial model described in the introduction to the case of polymer solvent films in contact with a solvent reservoir . In what follows, parameter α introduces in equation 1.4.4 of the introduction is equal to 10^{-3}. This is for modelling the relatively low mobility of the polymer chain as compared to solvent molecules. In Figure 3.2.1 we give a schematic representation of applied transformations in term of activity during drying and swelling at constant temperature. The T_g of the solution is also displayed (red curve). Initially the system can either be in a molten or a glassy state before drying. As solvent volume fraction decreases during drying, the system goes below its glass transition temperature and ages. After drying, the activity can be increased again and the system swells subsequently due to solvent penetration. We first discuss the thermodynamics of compressible polymer-solvent system in contact with a solvent reservoir in section 1.A. We then present in section 3.4 results regarding solvent diffusion in dynamically homogeneous systems. In section 3.5, we present results regarding thin/thick films drying. The specific situation of drying at very low activity will be also studied in section 3.6. Finally, we study thin/thick films swelling in section 3.7.

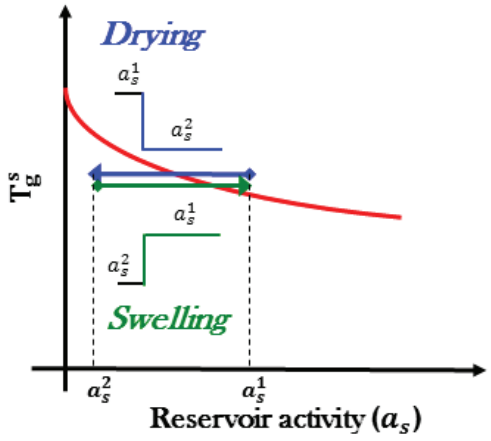

Figure 3.2.1: Representation of transformations experienced by the system during drying or swelling in our model. A schematic representation of the evolution of the glass transition temperature evolution as a function of reservoir activity is also given (red curve). Blue and green arrows represent instantaneous activity variation during drying (blue) from activity a_s^1 down to a_s^2 and swelling from activity a_s^2 up to a_s^1(green) at fixed temperature. The system can either be prepared in a molten or a glassy state before drying (above T_g or at T_g). The activity drop makes that the solvent quantity diminishes in the film and consequently the system undergoes the glass transition temperature (aging). During the revers process, molecules penetrate the system.

3.3 Thermodynamics of polymer-solvent systems in contact with a pure solvent reservoir

The equilibrium, at pressure P and temperature T, between the reservoir of pure solvent and the polymer-solvent mixture is given by

$$\begin{aligned} \left(\frac{\partial G}{\partial N}\right)_{(N_s,N_p,P,T)} &= 0 \\ \left(\frac{\partial G}{\partial N_s}\right)_{(N,N_p,P,T)} &= \mu_s^{res}(P,T) \end{aligned} \tag{3.3.1}$$

where G is the free energy given by relation 1.3.7 where the molecular mass for the solvent X_s is put equal to one. The first expression gives the volume of the polymer-solvent mixtures while the second one, describes the equilibrium between the chemical potential of the solvent in the reservoir $\mu_s^{res}(P,T)$ and in the polymer-solvent mixture. By solving this set of equations we obtain $\phi_s^{eq} = N_s/N$ and $\phi_p^{eq} = N_p/N$ as a function of pressure P and temperature T. Let us now discuss the chemical potential of the solvent in the reservoir $\mu_s^{res}(P,T)$. $\mu_s^{res}(P,T)$ is obtained from G when reduced to one component by imposing $N_p = 0$, and by writing:

$$\begin{aligned} \left(\frac{\partial G}{\partial N}\right)_{(N_s,N_p=0,P,T)} &= 0 \\ G(N, N_p = 0, N_s, P, T) &= N_s \mu_s^{res}(P,T) \end{aligned} \tag{3.3.2}$$

If we impose $N_s = 1$, which has no consequence on the physics since the latter depends only on the ratio N_s/N, relations (3.3.2) become

$$\begin{aligned} & x^4 - x^3 - \frac{T + P/\rho_0}{2a} + \frac{P}{2a\rho_0} = 0 \\ & G(1/x, N_p = 0, N_s = 1, P, T) = \mu_s^{res}(P, T) \end{aligned} \tag{3.3.3}$$

where $x = 1/N$. Thus, the chemical potential $\mu_s^{res}(P,T)$ is obtained as follow : we plot $G(1/x, N_p = 0, N_s = 1, P, T)$ as a function of x. The obtained curves are characterized by 1 or 2 minimums whose the values $G(1/x, N_p = 0, N_s = 1, P, T)$ give the chemical potential $\mu_s^{res}(P,T)$ since they are solutions of the second equation of (3.3.3). In figure (3.3.1), we plot such curves for different pressures at fixed temperature. The minimums can be obtained either for small x which corresponds to a gas phase noted x_g, or for large x related to a liquid phase and noted x_l. The more stable phase is that having the lower chemical potential and the reservoir chemical potential μ_s^{res} is given by this minimum. When the two minimums are equal -i.e. when $G(1/x_l, N_p = 0, N_s = 1, P, T) = G(1/x_g, N_p = 0, N_s = 1, P, T)$- both phases are in coexistence: the system is at the equilibrium saturation pressure $P_{sat}(T)$. We note $\mu_s^{res}(P_{sat}(T)), T)$ the corresponding solvent chemical potential. In order to express the evolution of $\mu_s^{res}(P,T)$ we can use the activity $a_s(P,T)$, defined by

$$\mu_s^{res}(P,T) = \mu_s^{res}\Big(P_{sat}(T), T\Big) + T \ln\Big(a_s(P,T)\Big) \tag{3.3.4}$$

By using the following for the chemical potential potential: $\mu_s^{res}(P,T) = C + T \ln P$, valid in the gas state, and the standard perfect gas equation of state, one obtains

$$a_s(P,T) = \frac{P}{P_{sat}(T)} \tag{3.3.5}$$

where the saturated state has been taken as the reference state. In figure (3.3.2) we plot the evolution of $a_s(P,T)$ using relation 3.3.4 as a function of P/P_{sat} at fixed temperature. This figure shows that the expression (3.3.5) is a good approximation of the evolution of the activity $a_s(P,T)$. Thus if $a_s = 0$ which is equivalent to $P = 0$ the thermodynamic equilibrium corresponds to the pure polymer while if $a_s = 1$ the thermodynamic equilibrium corresponds to the pure solvent.

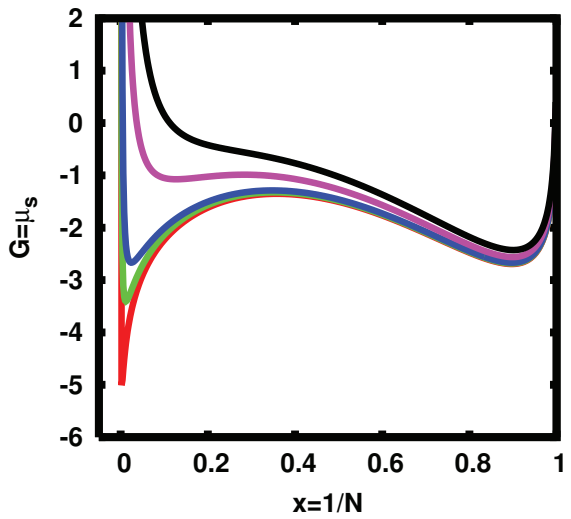

Figure 3.3.1: Evolution of $G(N, N_s = 1, N_p = 0, P, T) = \mu^{res}(P, T)$ as a function of $x = 1/N$ for different pressures P at fixed temperature $T = 300$K. The energy parameter a solvent-solvent is equal to -2.5×10^{-20}J and $\rho_0 = 10^{28}\text{m}^{-3}$. We have plotted in red $P = 10^5$Pa, in green $P = 5 \times 10^5$Pa, in blue $P = P_{sat} = 1.04 \times 10^6$Pa, in purple $P = 5 \times 10^6$Pa and in black $P = 10^7$Pa.

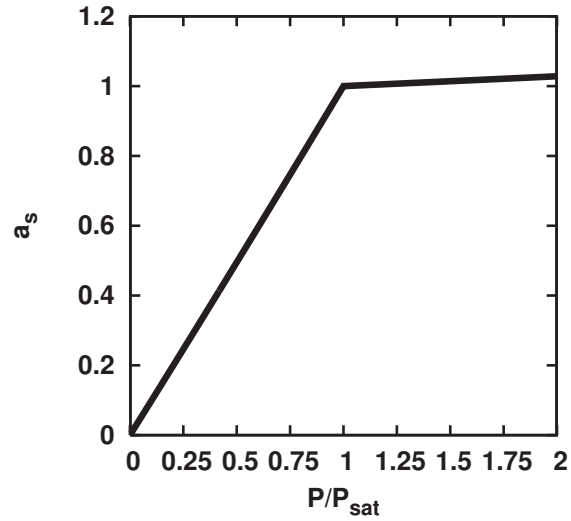

Figure 3.3.2: Evolution of the activity $a_s(P, T)$ calculated from Eq. (3.3.4) as a function of P/P_{sat} for $T = 300$K. The energy parameter a (solvent-solvent interaction) is equal to -2.5×10^{-20}J and $\rho_0 = 2 \times 10^{28}\text{m}^{-3}$.

3.4 Standard Fickian diffusion in polymer-solvent systems

In this section, we study solvent diffusion during drying and swelling in case of dynamically homogeneous polymer-solvent system: there is no coupling between composition fluctuations and the glass transition temperature (constant diffusion coefficient independent of composition). In Figure 3.4.2, we plot the evolution of film average solvent volume fraction as a function of the square root of time in case of drying and swelling. At the beginning of the drying and swelling process, the evolution is clearly linear: the diffusion process is Fickian, i.e. during drying:

$$< \phi_s >_{drying} (t) \sim < \phi_s > (0) - \alpha_{dry}\sqrt{t} \tag{3.4.1}$$

and during swelling:

$$< \phi_s >_{swelling} (t) \sim < \phi_s > (0) + \alpha_{swell}\sqrt{t} \tag{3.4.2}$$

Here, $\alpha_{dry/swell}$ is a positive parameter with $[\alpha_{dry/swell}] = s^{-1/2}$. These are given in Table 3.1. Regarding drying curves, final average solvent volume fraction value, corresponding to equilibrium, diminishes when decreasing the activity. During drying and swelling, we see that all systems are converging toward equilibrium in the same time: the diffusion process does not depend on the history of the system. Diffusion time is equal to a few hundred of seconds here. For a given history, evaporating (for drying) and penetrating (for swelling) rates are the same. They are given in Table 3.1 . We see that the lower the activity during drying, the higher the solvent evaporation rate. During swelling on the other hand, the penetrating rate is higher for the system which has been dried at activity $a_s = 0.25$ than for the one which has been dried at activity $a_s = 0.35$.

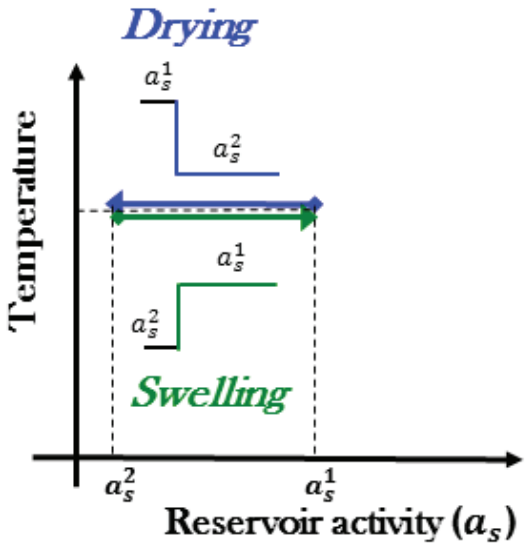

Figure 3.4.1: Schema illustrating transformation imposed to the system during drying and swelling at constant temperature. There is no coupling between the system glass transition temperature and the thermodynamic: dynamics is homogeneous. The systems dries following an activity drop from a_s^1 down to a_s^2. By applying the opposite transformation, the system swells.

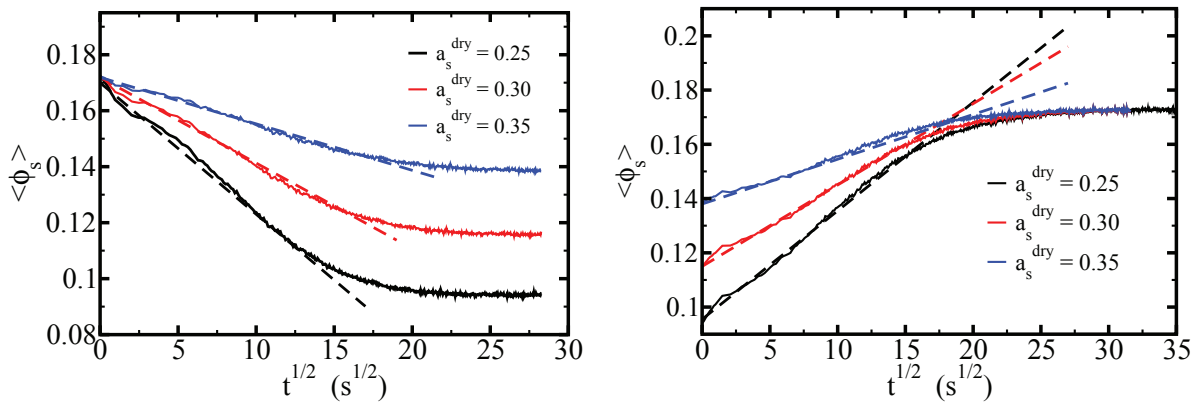

Figure 3.4.2: Fickian diffusion during drying(LEFT) and swelling(RIGHT) of a 15×15 cells film. Dynamics is homogeneous and relaxation times are equal to 1s. The system is prepared at activity $a_s = 0.42$ and $T = 330$K and systems are dried at three different activity $a_s = 0.35; 0.30$and 0.25. For all systems, after drying, the activity is increased again at initial activity $a_s = 0.42$. Whether it is during drying or swelling, all systems relax to equilibrium in the same time scales: the solvent diffusion does not depend on the history of the system. Finally, for a given history, evaporation or penetration rates of solvent molecules are equals, and are higher when the gap between the initial and the final state is large. Parameters of the system are $a = -2.5 \times 10^{-20}J$, $b = -2 \times 10^{-20}J$ and $c = -2.5 \times 10^{-20}J$. Polymer chain size is $X = 100$ and $\rho_0 = 10^{28}m^{-3}$

	$a_s^{init} \rightarrow a_s^{dry}$	$\alpha_{dry}(s^{-1/2})$
Drying	$0.42 \rightarrow 0.25$	4.10×10^{-3}
	$0.42 \rightarrow 0.30$	3.06×10^{-3}
	$0.42 \rightarrow 0.35$	1.66×10^{-3}
	$a_s^{dry} \rightarrow a_s^{init}$	$\alpha_{swell}(s^{-1/2})$
Swelling	$0.25 \rightarrow 0.42$	4.12×10^{-3}
	$0.30 \rightarrow 0.42$	3.02×10^{-3}
	$0.35 \rightarrow 0.42$	1.64×10^{-3}

Table 3.1: Table resuming the values of the solvent molecules evaporation or penetration rate in case of Drying or Swelling in a 15×15 cells film. Relaxation times equal to 1s. The systems are equilibrated at at activity $a_s^{init} = 0.42$ and at temperature $T = 330$K. they are then dried at activity $a_s^{dry} = 0.35; 0.30$and 0.25. FInally, they are swelled at activity $a_s = 0.42$. As diffusion is independent of the system's history, solvent molecules evaporation or penetration rate for every systems are equals for a given transformation. Parameters of the system are $a = -2.5 \times 10^{-20}J$, $b = -2 \times 10^{-20}J$ and $c = -2.5 \times 10^{-20}J$. Polymer chain size is $X = 100$ and $\rho_0 = 10^{28}m^{-3}$

3.5 Drying of polymer-solvent films close to T_g at non zero activity

In the course of thin films drying, the solvent volume fraction drops rapidly by 3% as one can see in Figure 3.5.1. During this process, solvent molecules diffuse through path all over the film. This process is faster than α-relaxation times, thus the polymer does not contract and average polymer volume fraction keeps a constant value $< \phi_p > \sim 0.749$. As a consequence, the free volume fraction increases by almost 2%, and since it is a good plasticiser for the system, the dynamics accelerates slightly as it can be observed in Figure 3.5.2. At the end of the fast evaporation process the solvent volume fraction is homogeneous in the whole film and is solution of equation:

$$\begin{aligned} &\Big(\frac{\partial \overline{G}}{\partial \phi_s}\Big)_{T,P,\phi_p^{init}\approx 0.749} = T\ln(a_s = 0.15) \\ \Rightarrow \quad &\phi_s(\phi_p \approx 0.744, a_s = 0.15) = 0.119 \end{aligned} \tag{3.5.1}$$

This corresponds to an intermediate thermodynamical state during which the solvent volume fraction adapts itself to the initial polymer volume fraction ($< \phi_p > \sim 0.749$), given the drying activity $a_s = 0.15$. At times of the same order of α-relaxation times, the system begins to contract in a homogeneous way in order to reduce the excess of free energy resulting from fast evaporation process. The slow contraction of the system drives the solvent evaporation, and the subsequent free volume reduction makes results in the slowing down of the dynamics. Note that during the aging process, α-relaxation times increase linearly with the drying time, which is equivalent with what has been observed in polymer blends. However, the evolution of α-relaxation times does not necessarily follows the struick Law, but can increase more slowly than the drying time in some circumstances as shown in Figure 3.A.1 of appendix 3.A. The reason is that the Struick law is only valid when the difference between the initial and the final state is large, which is not the case for a system drying at relatively high activity as compared to the initial one. A spatial representation at different stages of a thin film drying given in Figure 3.5.4 shows us in particular that the solvent volume fraction is homogeneous in the whole film during the process of contraction. Finally, during this regime, the system tries to converge towards a final equilibrium state not accessible on experimental time scales: the system is still out of equilibrium even after a long drying time. Despite this, as one can see in Figure 3.5.3, the drying of thin films is more efficient when the drying activity decreases.

During the fast evaporation process, solvent diffusion coefficient is $D_{fast} \sim 1/\tau_{fast}$. Thus, the required time t_{diff} so that molecules diffuse on distance L is

$$t_{diff} \sim L^2 \times D_{fast}$$

As long as the thickness of the film (L) is small enough so that $t_{diff} < \tau_\alpha$, there is a separation

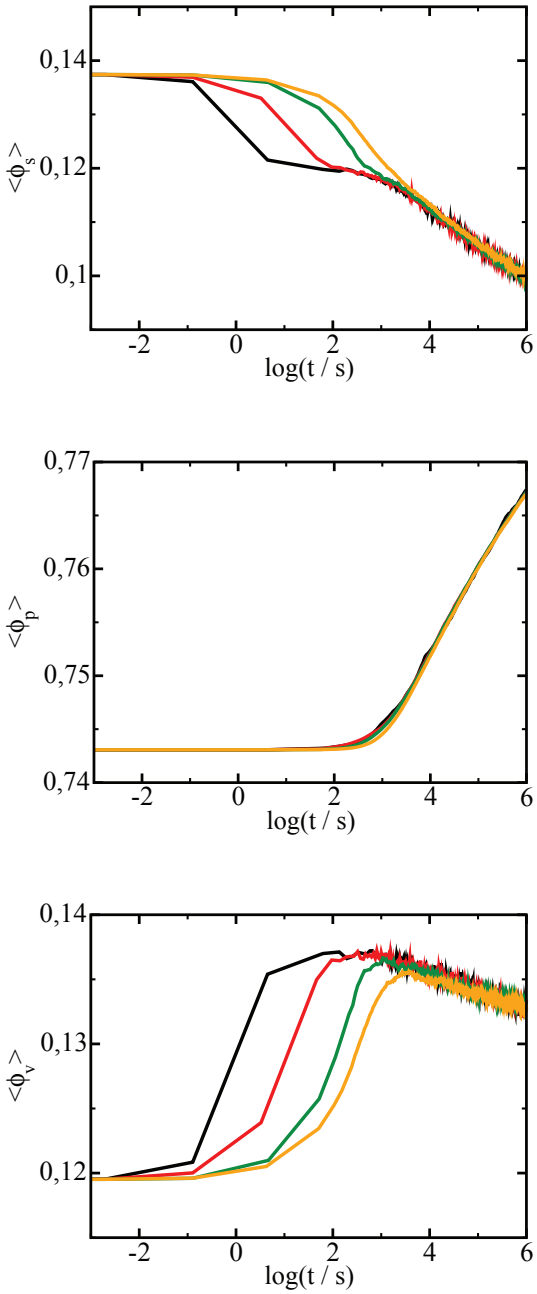

Figure 3.5.1: Evolution of the average solvent(UP),polymer (MIDDLE) and vacuum(BOTTOM) volume fraction during drying. The averaging is performed over the whole film. All systems were initially prepared at equilibrium at $a_s = 0.35$ and $T = 310K$. Then the system dries following a drop of activity at $a_s = 0.15$. The width of the film is maintained constant here (50 cells) but we vary its depth N:$N = 2; 10; 30; 50$ (black, red, green and orange curves respectively).
We observe a net separation of times scales between the fast evaporation process and the contraction of the system. Separation of time scales is more pronounced when considering very thin films.

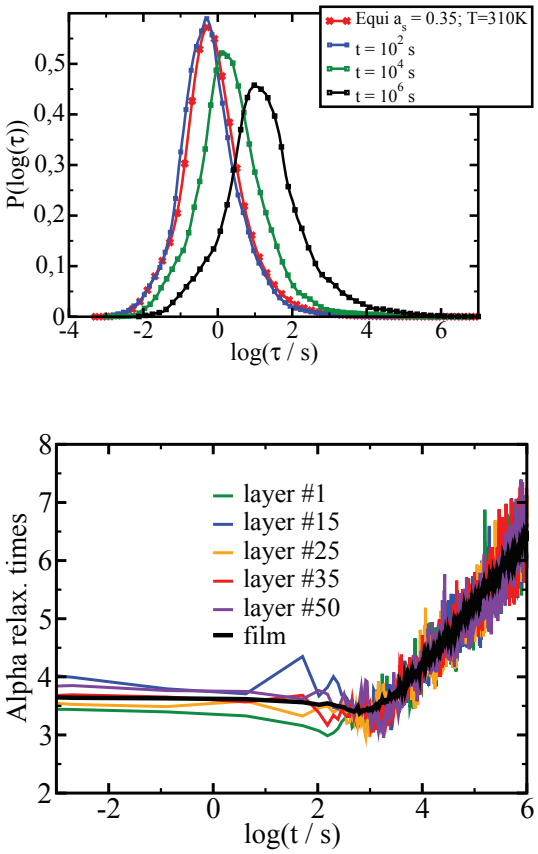

Figure 3.5.2: (UP) Distribution of relaxation times at different times: $t = 1s$, $t = 10^3 s$ and $t = 10^4 s$ and evolution of (BOTTOM)α-relaxation times during drying at activity $a_s = 0.15$ and $T = 310K$. Equilibrium distribution at activity $a_s = 0.35$ is also displayed (red curve). For the first $10^2 s$ of the drying process, solvent diffuse by means of fastest relaxation times and the free volume increases by almost 2% which slightly accelerates the dynamics. At much longer times however, as a consequence of the free volume reduction during the film contraction, the system is aging: the distribution translates towards longer relaxation times and widens, and α-relaxation times increase.

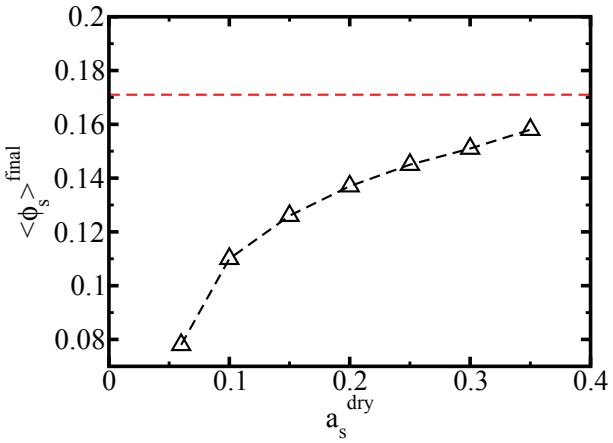

Figure 3.5.3: Evolution of the final average solvent volume fraction as a function of drying activity. Red horizontal curve represents the initial equilibrium value before drying. All systems have been prepared at activity $a_s = 0.42$ and at temperature $T = 330$K after being dried for 10^7s at activity a_s^{dry}.

of time scales between the solvent diffusion and the film contraction. For much thicker films however, the time scales separation observed in Figure 3.5.1 is no longer present. Indeed in this case, both the solvent diffusion and the mechanical relaxation mechanisms overlap, which gives rise to a large gradient of solvent concentration with respect to the films thickness, as well as an inhomogeneous contraction of the system as shown in Figure 3.5.5. As a consequence of the breaking down of the time scales separation, at long times the film is much more contracted close to the free surface and the dynamics of layers in this region is much slower than those deeper in the film: a 500-1000 nm thick (from the interface) glassy crust build up close to the free surface as it is visible in Figure 3.5.6 and Figure 3.5.5. The evaporation of solvent molecules is then considerably slowed down due to the glassy crust, and a large part of them remain trapped in the bottom of the film, though the solvent volume fraction decreases slightly in this region at long times. Note that waiting for much longer times does not allow to dry a larger number of layers. Finally, there is a critical thickness above which the system cannot be dried completely. We estimate this critical thickness to be about 500 dynamic heterogeneities large. Note that this is the case for unentangled polymers as studied here.

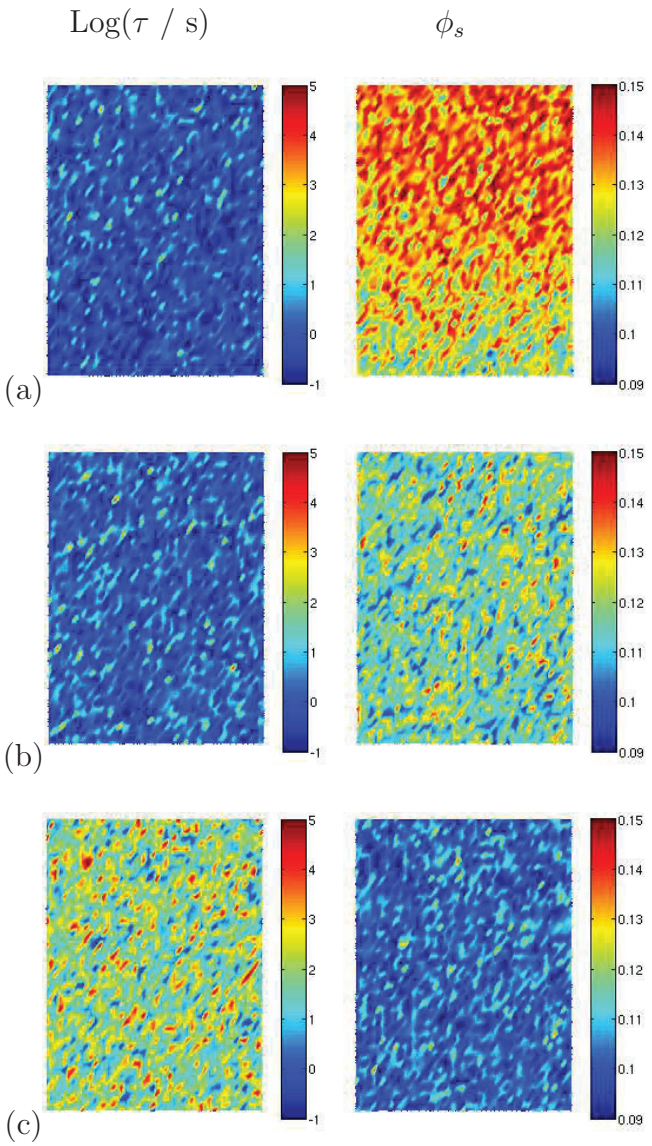

Figure 3.5.4: Snapshots of a 50×50 film drying activity $a_s = 0.15$ at different times: $t = 80s$ s (a), $t = 4 \times 10^3$ (b) and $t = 10^6 s$ (c). Initially the system is prepared at activity $a_s = 0.35$ and temperature $T = 310K$. The left column represents the logarithm of relaxation times and the right one the solvent volume fraction ϕ_s. The reservoir is located at the bottom of each picture. At the very first time of the process, the solvent evaporates quickly the matrix through fast subunits. We see that layers at the film/reservoir interface are the first to dry. Layers deeper in the film takes a longer time to dry because the distance over which the solvent has to diffuse before reaching the film/reservoir interface is larger. At longer times, the system contracts homogeneously and ages. Finally, during this process, the solvent evaporation, which is driven by the contraction of the system, is slow.

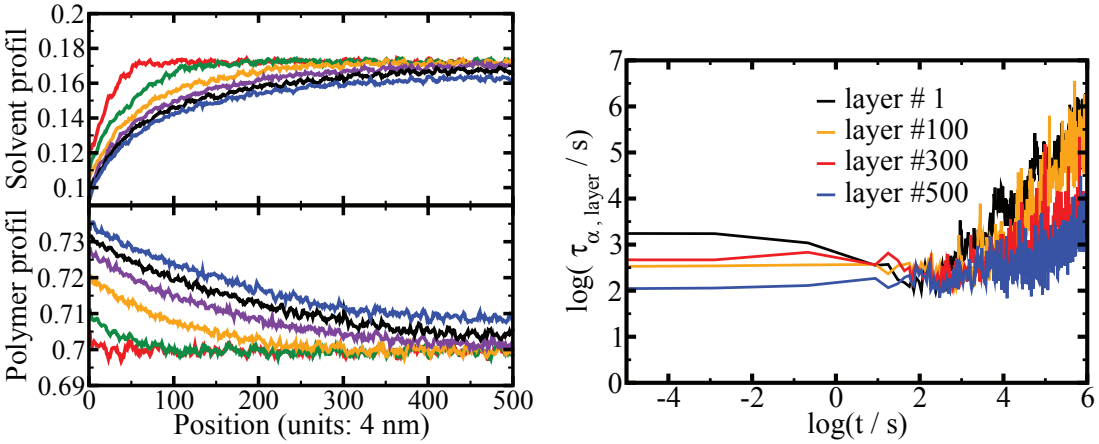

Figure 3.5.5: (Left) Evolution of a solvent(top) and polymer average volume fraction (bottom) in a $2\mu m$ thick film drying at activity $a_s = 0.08$. Curves correspond to times (red) $t = 10^2$s, (green) $t = 10^3$s, (orange) $t = 10^4$s,(purple) $t = 10^5$s,(black) $t = 5,5 \times 10^5$s and (blue) $t = 10^6$s during the drying process. Even after a long drying time, a large quantity of solvent molecules remains trapped in the bottom of the film while layers at the film/reservoir interface are dried. Moreover, layers close to the film/reservoir interface are more contracted as compared to layers in the bottom of the film: as a consequence of the break down of time scales separation, the contraction of the system is inhomogeneous and a glassy crust appears at the film/reservoir interface. (Right): Evolution of α-relaxation times for layers number 1,100,300 and 500. The dynamics remains relatively fast in the bottom of the film as compared to the region close to the reservoir.

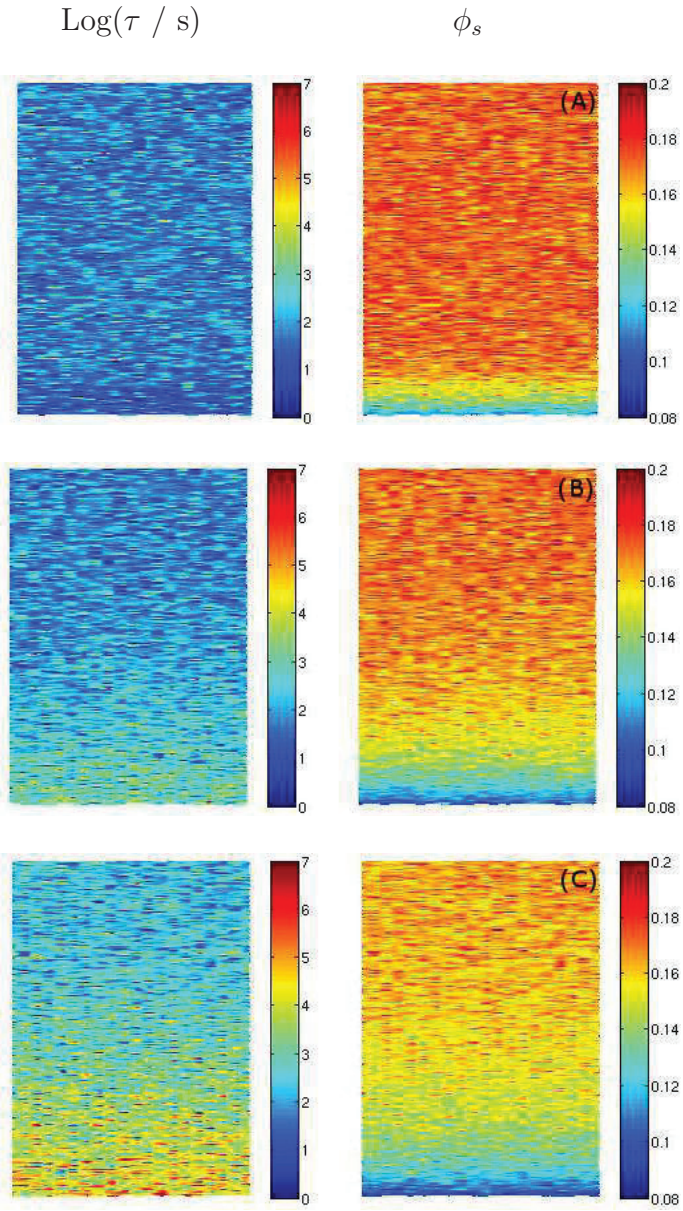

Figure 3.5.6: Snapshot of a $1\mu m \times 100nm$ (Depth×Widht) film drying at activity $a_s = 0.08$ at times: (A) $t = 10^2$s , (B) $t = 4, 4 \times 10^4$ and (C) $t = 10^6$s. The left column represents relaxation times [$\log(\tau/s]$ and the right column represents solvent volume fraction ϕ_s. The reservoir is located at the bottom of each pictures (A) , (B) and (C) and is not represented here. At time 10^6 s, a large quantity of solvent remains trapped in the bottom of the system while the region close to the film/reservoir interface is dried. The matrix contracts in this region, bringing to the formation of a very slow crust (see FIG 3.5.5).

3.5.1 Conclusion on film drying close to T_g at non zero activity

We have studied thin and thick films drying close to the glass transition temperature at non zero activity. Drying at zero activity (dry solvent atmosphere) will be discussed later on. Regarding thin films situation, as it represented in Figure 3.5.7, we have first noted a separation of time scales during the process of drying. At short times scales, solvent diffuses through fast path with dynamics much faster than α-relaxation times: the system does not contract. At the end of this fast evaporation process, the system reaches an intermediate homogeneous state in which the solvent quantity adapts to the initial polymer volume fraction given the drying activity. At longer times, the solvent evaporation is driven by the homogeneous contraction of the system which is kinetically controlled by α-relaxation times. Finally, the system ages because of the free volume reduction during the matrix contraction.
On the one hand, we have seen that drying is more efficient when the imposed drying activity is low. On the other hand, in the case of relatively low activity drying, dynamics slightly accelerates at short time scales. This is due to the free volume fractions which increases in a significant way during the fast evaporation process, and which tends to plasticise the system. Study on thick films drying shows that the film contraction overlaps the solvent evaporation process: there are no longer time scales separation in the system as a whole. At long times, the contraction of the system is inhomogeneous and a glassy crust of 400-500nm is forming close to the free surface, while a large quantity of solvent remains trapped in the bottom of the films. Note that waiting for much longer times does not allows to dry a larger number of layers. The drying process is slowed down due to the presence of the glassy crust and we did not observe significant solvent evaporation at long times. Finally, there is a critical thickness in between thin and thick films situation from which the system cannot be dried completely. We estimate this critical thickness to be about 500 dynamic heterogeneities large.

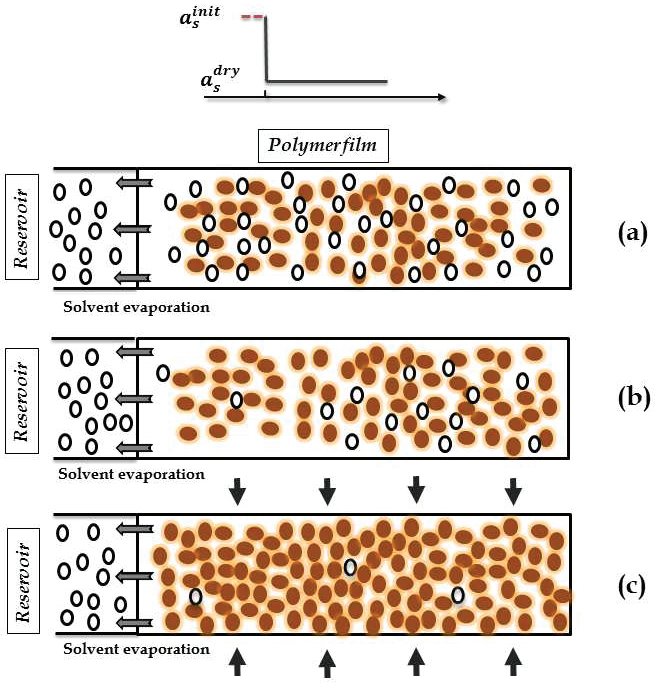

Figure 3.5.7: Schema of thin film drying after a drop of activity from a_s^{init} down to $a_s^{dry} < a_s^{init}$ of the solvent reservoir. Before drying (a), a large quantity of solvent dilutes the polymer which is swollen. At the first instants of drying(b), solvent molecules quicly evaporate. As the matrix is not contracted yet, the free volume increases in the system. At longer times(c), the polymer contracts and the solvent slowly evaporates the system.

3.6 Drying of polymer-solvent films close to T_g at very low activity

3.6.1 Prediction of cavity formation

After discussing about non zero activity drying in section 3.5, we discuss the case of drying at very low activity. We give in Figure 3.6.1 the phase space of the system in term of solvent and polymer volume fraction. The phase space is a square triangle defined by $1 > \phi_s \geq 0; 1 > \phi_p \geq 0; \phi_s + \phi_p < 1$. In Figure 3.6.1, the red part corresponds to the unstable region with $\lambda_2 < 0$ and Blue curve corresponds to the equilibrium line which satisfies:

$$\left(\frac{\partial G}{\partial N}\right)_{\phi_s,\phi_p,P,T} = 0 \tag{3.6.1}$$

Finally, the white part of the phase space in between the red part and the equilibrium line corresponds to the stable region with $\lambda_2 > 0$. We propose to study the difference between systems dried either at low activity or at non zero activity by looking at trajectories $(\phi_s(t), \phi_p(t))$ followed by these systems in the phase space.

We consider the situation where systems are prepared in equivalent conditions, and where equilibrium solvent volume fraction is large before drying. Regarding the phase space given

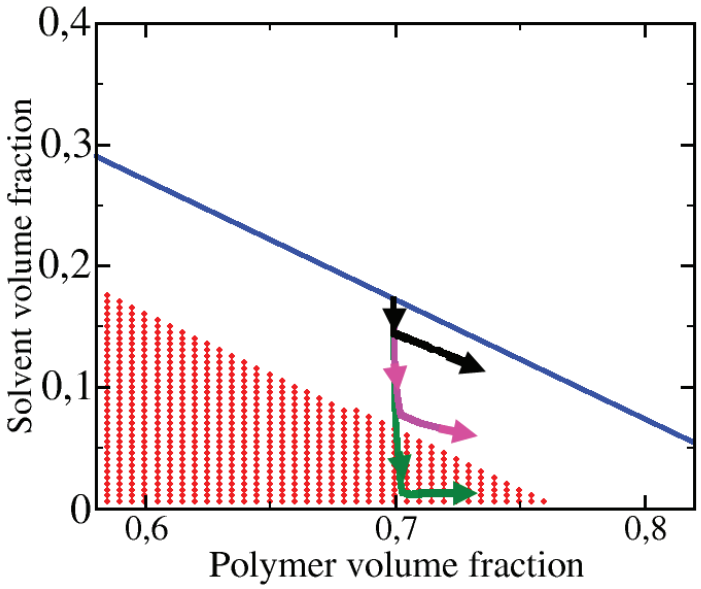

Figure 3.6.1: Trajectories $(\phi_s(t), \phi_p(t))$ in the phase space in term of polymer (ϕ_p) and solvent (ϕ_s) volume fraction at $T = 330$K. Parameters of the system are $a = -2.5 \times 10^{-20}J$, $b = -2 \times 10^{-20}J$ and $c = -2.25 \times 10^{-20}$, $X = 100$ and $\rho_0 = 10^{-28}m^{-3}$. Red part corresponds to the unstable region ($\lambda_2 < 0$) and the blue line corresponds to the equilibrium curve. The white region in between the red part and the equilibrium line corresponds to the stable region ($\lambda_2 > 0$). Trajectories are for systems (10×10 film) drying at activity $a_s = 0.15$ (Black trajectory), $a_s = 0.045$ (Magenta trajectory) and $a_s = 0.01$ (Green trajectory). All systems were first equilibrated in equivalent equilibrium conditions ($a_s^{init} = 0.42$ and T=330K) before drying. We see that trajectories of systems drying at activity higher than $a_s = 0.045$, remain always in the stable region. In contrast, systems drying at lower activity undergo the unstable region: thermodynamic instabilities appear in the system.

in Figure 3.6.1, we see that when the system is dried at activity higher than or equal to $a_s = 0.045$, the trajectory $(\phi_s(t), \phi_p(t))$ remains always in the stable region. First, the solvent volume fraction decreases while the polymer volume fraction remains constant. In a second step, the system begins to contract and trajectory moves slowly toward higher polymer volume fractions. At lower activities, in contrast, the trajectory of the system cross the unstable region (Green trajectory). This suggests that for systems prepared in equivalent conditions at equilibrium, thermodynamic instabilities may appear during drying if the activity is too low (below $a_s = 0.045$ here). Let us describe Figure 3.6.2 in order to understand thermodynamic instabilities which occur during drying at low activity. In this figure, polymer chemical potential and polymer free energy are plotted at two different fixed solvent volume fraction: a first one (situation I) where $\phi_s = 0.17$ and a second one (situation II) where $\phi_s = 0.005$. Initial equilibrium polymer volume fraction ($\phi_p = 0.70$) is also displayed in this Figure (Blue dotted line). In situation I, the system is stable and at thermodynamic equilibrium. In situation II, where the system is dried but not contracted, the derivative of the chemical potential is negative and the free energy is such that $\partial^2 G/\partial\phi_p^2 < 0$ in the vicinity of $\phi_p = 0.70$: the system is unstable. In these conditions, phase separation takes place by creating domains rich in polymer, in coexistence with domains poor in polymer. We assimilate a domain poor in

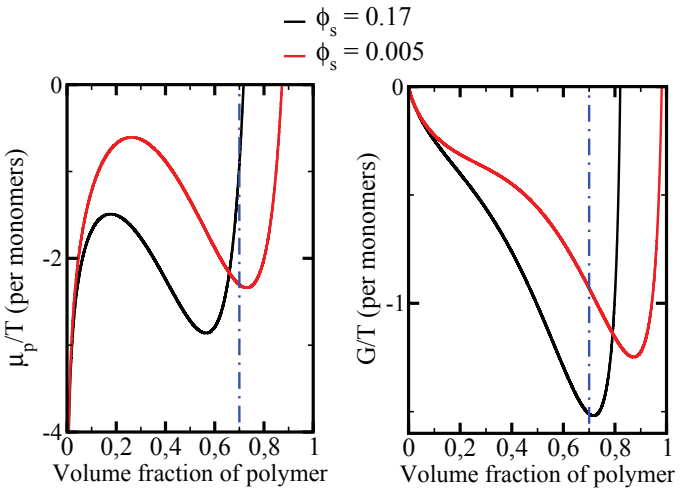

Figure 3.6.2: Dimensionless polymer chemical potential μ_p (Left) and free energy G (Right) per monomers at fixed solvent volume fraction ϕ_s. Blue line indicates the position of the initial equilibrium volume fraction. At $\phi_s = 0.17$ the system is at equilibrium at $a_s^{init} = 0.42$ and $T = 330$K. However, for $\phi_s = 0.005$ and $\phi_p = 0.70$, the derivative of the polymer chemical potential is negative and the free energy is such that $\partial^2 G/\partial\phi_p^2 < 0$ in the vicinity of $\phi_p = 0.70$: the system is unstable and a phase separation occurs.

polymer to a cavity.

Let us now discuss the kinetics of the formation of cavities. We have seen that the exchange kinetics between two close sites is controlled by faster relaxation times. SInce the free volume fraction inside the cavity is large, relaxation times are very fast, while, domains surrounding the cavity are rich in polymer and are slow: according to our dynamics ansatz, the phase separation kinetics is controlled by the relaxation times of the cavity. Hence, a cavity will form in a few time steps, and the relaxation times of domains surrounding the cavity, which fill up in polymer, will become very long in the same time (some of them have relaxation times larger than $10^{11} - 10^{12}$s). As a consequence, cavities appear very quickly and they freeze the system. As an illustration of this, we give a spatial representation in term of logarithm of relaxation times and total composition of a cavity in Figure 3.6.3. In next section, we will expose a new ansatz for calculating relaxation times in order to avoid such situations. We will see that cavities usually appear in systems composed of a large quantity of solvent before drying. Nevertheless, if the initial equilibrium solvent volume fraction is sufficiently low, the trajectory of the system remains in the stable region: the system can be completely dried and aged still remaining homogeneous.

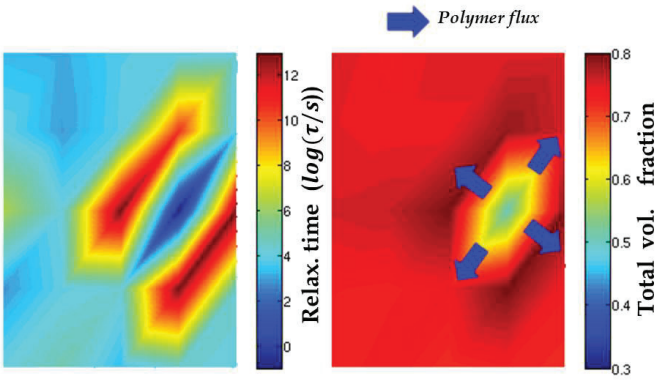

Figure 3.6.3: Representation of a cavity forming in term of the logarithm of relaxation times and the total volume fraction $\phi_s + \phi_p$ during drying at low activity $a_s = 0.01$ and temperature $T = 330$K. The snapshot is 20×20 nm large. We see that the relaxation times within the cavity (τ_{fast}^{cavity}) are fast due to the high free volume fraction inside. Following the dynamics ansatz discussed in Chapter I, the flux of polymer between the cavity and surrounding cells (Blue arrow) is driven by τ_{fast}^{cavity}. Hence, polymer volume fraction of neighboring cells becomes very large in a few time steps, and their relaxation times increase by many decades in the same time: the system becomes frozen.

3.6.2 New ansatz for calculating kinetic coefficients

We expose here the algorithm used to calculate kinetic coefficients in case of drying at very low activity during which cavities appear. The general formulation of this ansatz is the following.

$$\text{if } \mu_s(j) - \mu_s(i) > 0 \quad \rightarrow \quad \gamma_s^{i,j} = \gamma(i) \tag{3.6.2}$$

$$\text{if } \mu_p(j) - \mu_p(i) > 0 \quad \rightarrow \quad \gamma_p^{i,j} = \alpha\gamma(i) \tag{3.6.3}$$

where couple (i,j) refers to a site i in contact with a site j, and $\gamma_k(m) = 1/\tau_k(m)$. Following this scheme, mater exchanges between two neighboring sites is controlled by the relaxation time of the site having the lower chemical potential. Finally, when a cavity is forming, the polymer chemical potential is lower outside the cavity than inside. Hence, the polymer flux is controlled by long relaxation times of domains surrounding the cavity. Hence, this new ansatz guarantees the stability of the system when a cavity appear during drying.

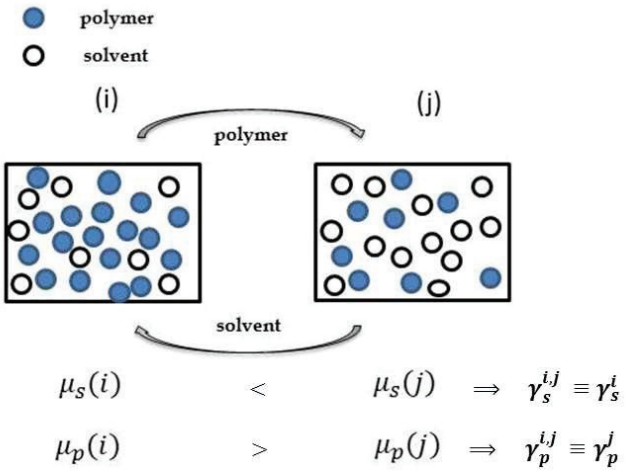

Figure 3.6.4: Schematic representation of a cell i and j with different polymer and solvent composition. For each species, kinetic coefficient driving the exchanges between both sites is equal to the relaxation frequency of the cell having the lowest chemical potential. Both species do not have equal kinetic coefficients following this ansatz.

3.6.3 Low activity drying without cavity formation

We consider a 10×10 cells large film. The systems are equilibrated at activity $a_s = 0.21$ and temperature $T = 325$K. They are then dried at three different activities: $a_s = 0.01; 0.005; 0.001$. Trajectories followed by these systems in the phase space are given in Figure 3.6.6. According to initial equilibrium conditions, none of these trajectories $(\phi_s(t), \phi_p(t))$ cross the unstable region of the phase space during the drying process: cavities will not appear.

Evolution of the film average solvent and polymer volume fraction as well as α-relaxation times are given in Figure 3.6.5. We observe that solvent quantity drops by more than 8% in the first ten milliseconds of the process. Then, the solvent volume fraction reaches a constant value which decreases when the drying activity decreases. Solvent volume fraction slightly decreases at long times though, but this is not significant. During the fast solvent evaporation process, we observe that α-relaxation decrease by 4 decades and distribution of relaxation translates towards faster relaxation times (see Figure 3.6.7). The softening of the material results from the large free volume increase (6-7%) which accelerates the dynamics in a significant way. Note that an equivalent phenomenon has already been observed in case of drying of thin films at non zero activity, but in lower proportions. In Figure 3.6.5, we see that almost immediately after the system has softened, the system contracts and ages as show in Figure 3.6.5. Finally, a spatial representation of the system drying at $a_s^{dry} = 0.001$ is given in 3.6.8.

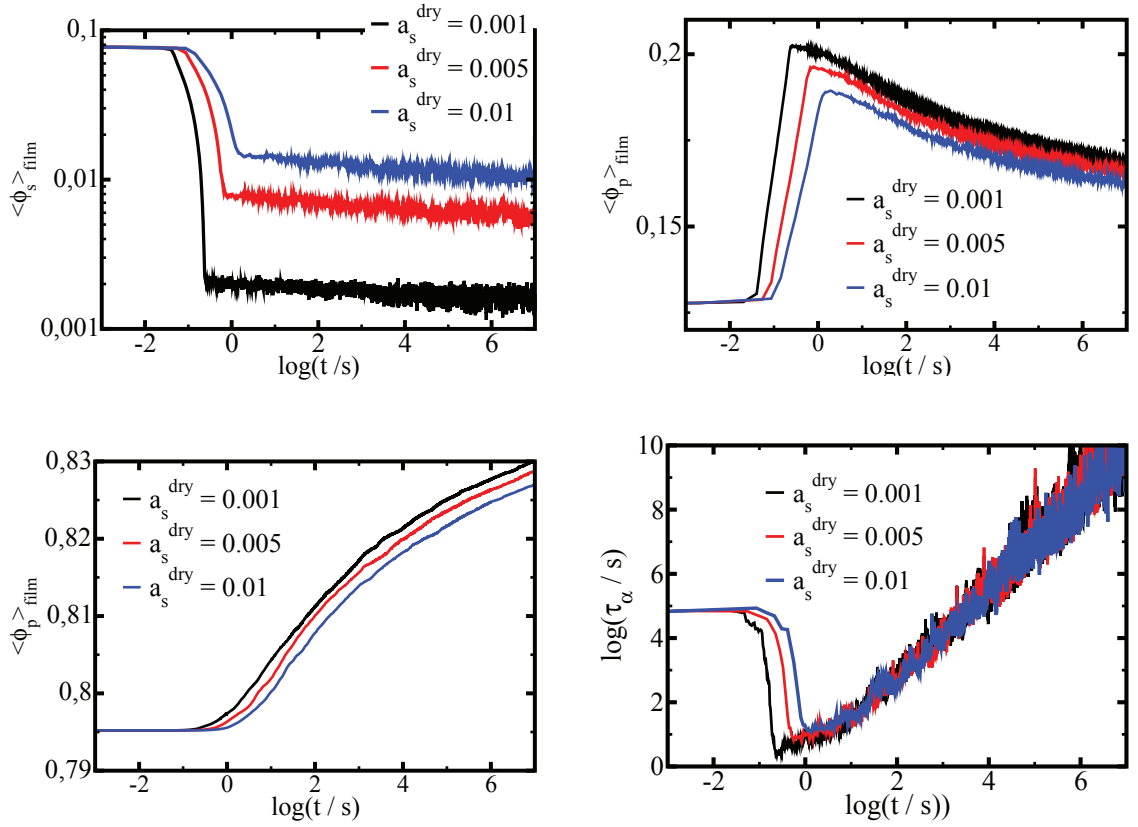

Figure 3.6.5: Evolution of the average solvent, free volume and polymer volume fraction and α-relaxation times during a 10×10 film drying at activity $a_s^{dry} = 0,01;\quad 0.005\quad$ and $\quad 0,001$. Systems were all first equilibrated at activity $a_s = 0.22$ and T=325K. Solvent volume fraction drops rapidly to a low constant value which decreases with respect to the drying activity. During the fast evaporation process, the free volume fraction increases in an important way (6-7%) and dynamics accelerates by more than 4 decades: the system softens as due to the large free volume increase. At longer times, the system contracts and the dynamics slows down with drying time. Finally, the acceleration of the dynamics is more pronounced at low drying activity.

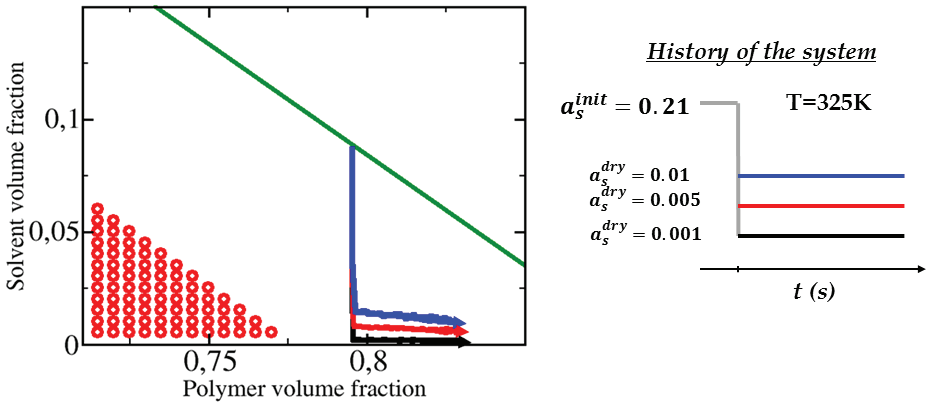

Figure 3.6.6: Trajectories $(\phi_s(t), \phi_p(t))$ in the phase space in term of polymer (ϕ_p) and solvent (ϕ_s) volume fraction at $T = 325$K. Parameters of the system are $a = -2.5 \times 10^{-20}J$, $b = -2 \times 10^{-20}J$ and $c = -2.25 \times 10^{-20}$. $X = 100$ and $\rho_0 = 10^{-28}m^{-3}$. Red part corresponds to unstable region($\lambda_2 < 0$) and the green line is the equilibrium curve. Trajectories are for systems (10×10 film) drying at activity $a_s = 0.01$ (blue trajectory), $a_s = 0.005$ (red trajectory) and $a_s = 0.001$ (Black trajectory). All systems were first equilibrated in equivalent equilibrium conditions ($a_s^{init} = 0.22$ and T=325K) before drying. We see that trajectories do not undergo the unstable region: no cavity appear in the systems during drying.

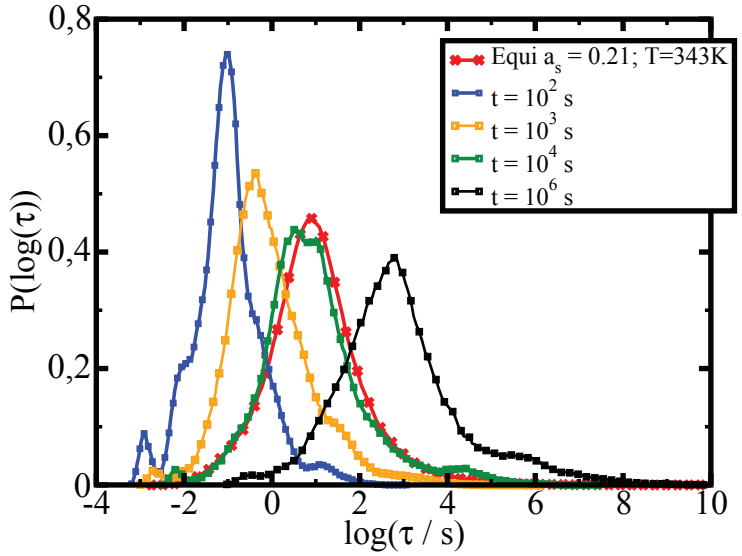

Figure 3.6.7: Distribution of relaxation times at different times during drying at activity $a_s = 0.005$. At shirt times scales, dynamics accelerates and distribution shift toward faster relaxation times. At longer times, the system is dried and is aging due to matrix contraction: distribution translates toward longer times.

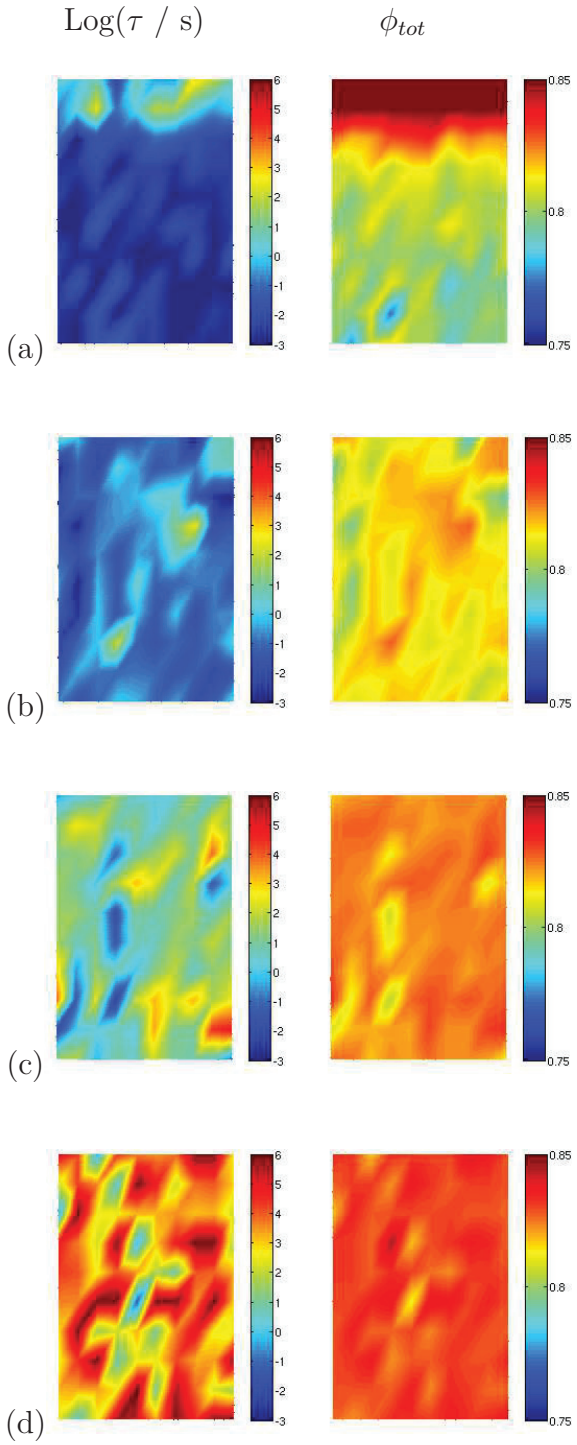

Figure 3.6.8: Snapshots at different times: $t = 10^{-1}$s (a), $t = 10^{2}$s (b), $t = 10^{4}$s (c),$t = 10^{6}$s (d) during the drying of a 10×10 film (40nm×40nm) at activity $a_s^{dry} = 0.001$. On each picture, the left column represents the logarithm of relaxation times and the right one, the total composition $\phi_{tot} = \phi_s + \phi_p$. At short times scales, total composition decreases due to fast solvent evaporation and relaxation times decreases. At longer times scales, the system is almost empty of solvent and the polymer contracts and ages. During the drying process, the system remains homogenous in term of total composition in the whole film: no cavity appear.

3.6.4 Low activity drying with cavity formation

We consider a 10×10 film equilibrated at activity 0.42 and at temperature $T = 290$K. The system is then dried at activity $a_s = 0.01$. Here, the initial solvent fraction at equilibrium is high enough so that the trajectory $(\phi_s(t), \phi_p(t))$ of the system cross the unstable region of the phase space. Evolution of solvent, polymer and free volume fraction as well as α-relaxation times are given in Figure 3.6.9. Equivalently to previous cases, solvent volume fraction drops rapidly to a low constant value and the dynamics accelerates. Afterwards, the system contracts and ages. Note that the acceleration of the dynamics during the fast evaporation process is slightly more pronounced here than in previous case. Indeed, during this process, the free volume fraction increases by more than 10% here instead of by $6 - 7\%$ in the previous case. After the solvent has completely evaporated, domains with low composition appear in the system as shown in Figure 3.6.10. We assimilate these domains to cavities. Relaxation times of a cavity are very fast due to the large free volume fraction inside. However, thanks to the new dynamics ansatz described in previous section, the polymer diffusion between the inner and the outer part of the cavity is controlled by the relaxation times of slow surrounding domains. As a consequence, the cavity becomes empty on very long times which makes them stable in time. Note that these cavities have the size of a dynamics heterogeneity (3-5 nm). Finally, one needs to integrate a surface tension term in the free energy of the system to observe the nucleation of cavities. This will be done in a further extension of the model.

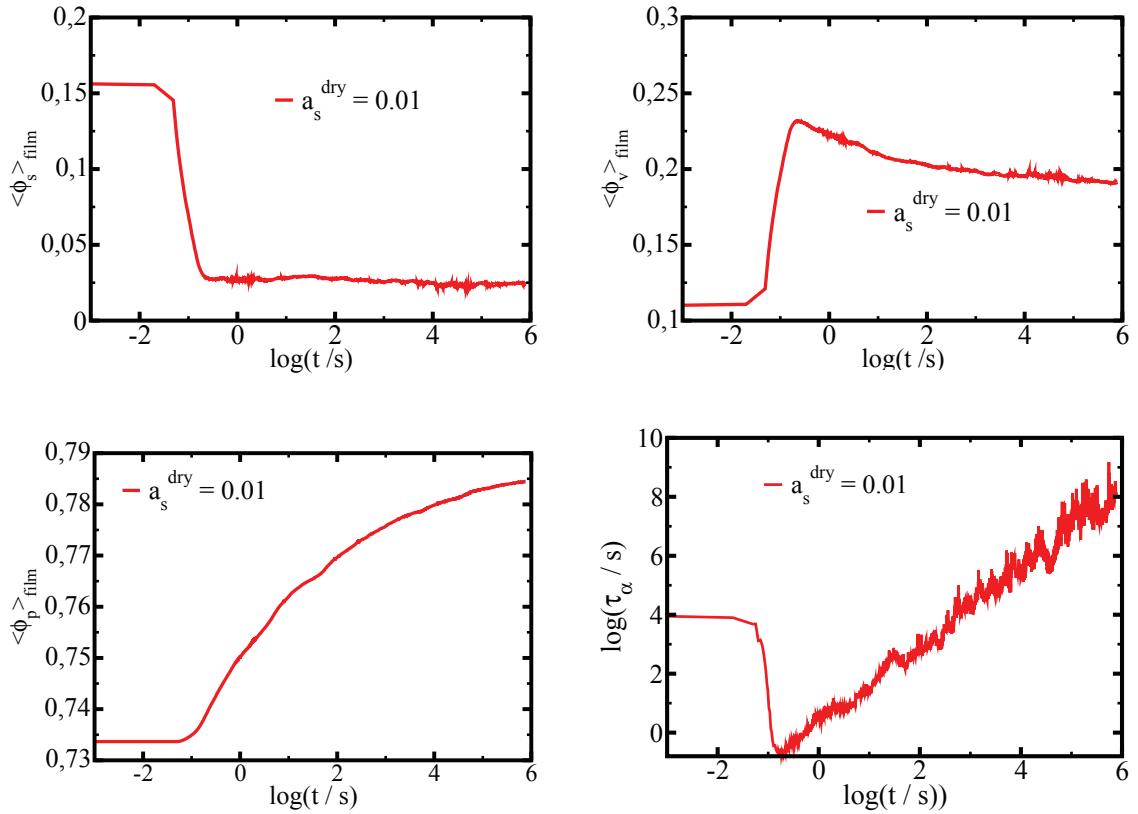

Figure 3.6.9: Evolution of the average solvent, free volume and polymer volume fraction and α-relaxation times during a 10×10 film drying at activity $a_s^{dry} = 0,01$. The system was initially equilibrated at activity $a_s = 0.42$ and T=290K. Solvent volume fraction drops rapidly to a low constant value, though it decreases slightly at long times. At short times, the free volume fraction increases in an important way (10%) and the dynamics accelerates by 5 decades. Afterward, system contracts and the dynamics slows down.

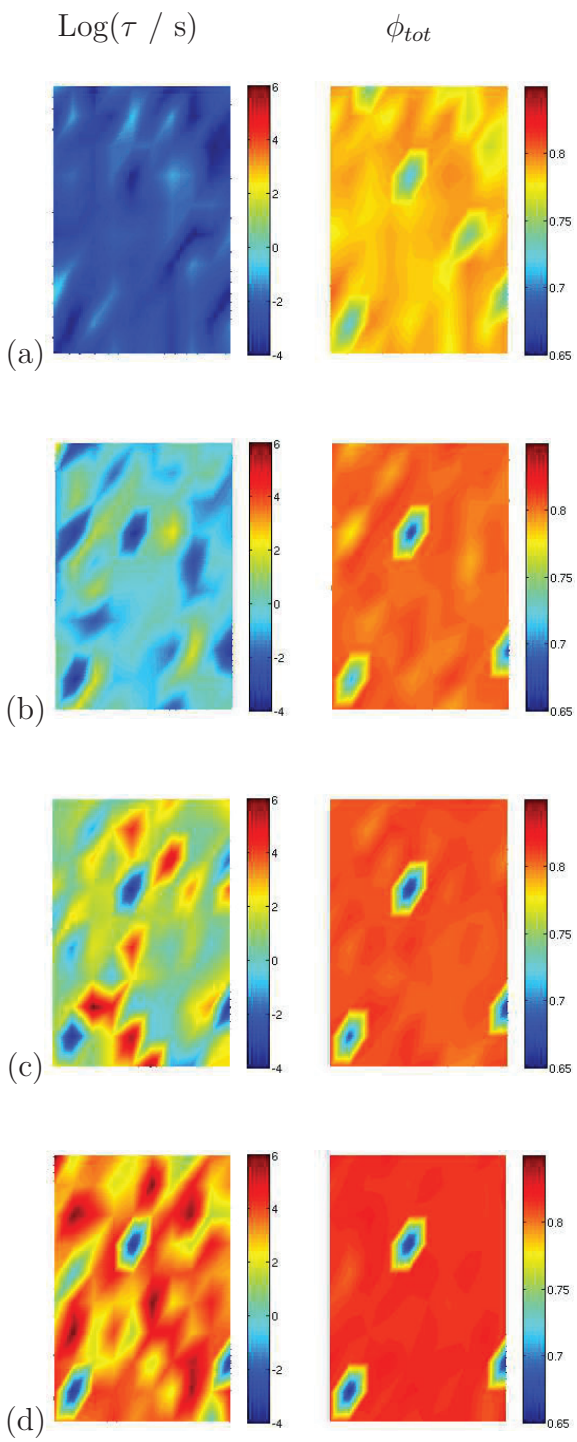

Figure 3.6.10: Snapshots at different times: $t = 5 \times 10^0$s (a), $t = 10^2$s (b), $t = 10^4$s (c),$t = 10^6$s (d) during the drying of a 10×10 film (40nm×40nm at activity $a_s^{dry} = 0.01$. On each snapshot, the left column represents the log of relaxation times and the right one the total composition $\phi_{tot} = \phi_s + \phi_p$. At short times scales, total composition decreases due to the fast solvent evaporation and the system softens. At longer times scales, the system is almost empty of solvent and the polymer contracts and ages. After the fast solvent evaporation process, some domains with low composition appear: cavities are forming. They become more and more empty when the time increases and relaxation times within cavities are fast. Since a surface tension term is not included in the free energy of the system, cavities can not grow and their size is equal to a dynamic heterogeneity. Finally, according to the ansatz discussed in section 3.6.2, cavities are long lived.

3.6.5 Conclusion on low activity drying

Drying of polymer-solvent films at very low activity may exhibit very interesting features. Our model is able to predict that cavities may appear or not following the initial equilibrium conditions before drying. Indeed, in the system we have considered, when the initial solvent volume fraction is larger than 10%, such instability appear (situation I) during drying. However, for lower solvent concentration, the system remains homogeneous (situation II). Wether it is in case I or case II, the solvent evaporates strongly on very short time scales and the dynamics accelerates significantly. This a consequence of a very large increase of the free volume fraction which softens the systems considerably. Afterward, the solvent volume fraction reaches a final constant value and the system start contracting: the free volume fraction decreases and the systems ages. Hence, as a consequence of the softening of the material, and the very fast solvent evaporation process taking place at short times, one can explain how a thin film can be dried completely. Finally, after waiting for longer times, one obtains a completely dried and aged system, almost pure of polymer. In situation I, the drying phenomenology is equivalent, except that we observe some cavities forming after the fast evaporation process. These cavities long lived, and become more and more empty when time increases. The cavity formation can be avoided by considering the following process:
first the activity can be dropped instantaneously at $a_s = 0.045$ or higher. Afterward the reservoir activity must be decreased at relatively slow rate so that the system follows a trajectory parallel to the unstable region, until reaching a solvent volume fraction lower than a few percent. Finally, the reservoir activity can then be dropped again at very low values.

3.7 Swelling of polymer-solvent films close to T_g

In this section, we study the thin and thick glassy polymeric films swelling. To do so, we start from the situation where the system has been partially dried before swelling. The procedure is the following: The system is equilibrated at certain activity and then dried at non zero activity. Finally, during swelling, the activity of the reservoir is raised again and the solvent penetrate the system. Note that at the initial stage of the swelling process, the system is in an out of equilibrium situation: the value of the osmotic stress is positive which results from the process of contraction during drying (see Figure 3.7.2).
As it is represented in Figure 3.7.1, solvent molecules diffuse first inside glassy matrix through fast dynamic heterogeneities: the film average solvent volume fraction increases like

$$< \phi_s >_{film} (t) \sim t^{1/2}$$

This process is faster than α-relaxation times and consequently the matrix is still contracted. A subsequent free volume reduction is then observed (See Figure 3.7.3) due to penetrating solvent molecules which fill up empty spaces which results in a slowing down of the dynamics of the system as one can see in Figure 3.7.4. At the end this process, the system reaches a plateau regime at time $t_{pI} \sim 2,5 \times 10^5 s$ during which the solvent volume fraction is homogeneous in the whole film (see Figure 3.7.5) and is solution of equation:

$$\begin{aligned} &\Big(\frac{\partial \overline{G}}{\partial \phi_s}\Big)_{T,P,\phi_p^{init} \approx 0.766} = T\ln(a_s = 0.35) \\ \Rightarrow \quad &\phi_s(\phi_p \approx 0.766, a_s = 0.35) = 0.117 \end{aligned} \tag{3.7.1}$$

Like for drying, this corresponds to an intermediate thermodynamical state where the solvent adjust itself to the initial polymer volume fraction given the activity of the reservoir. In this regime, solvent molecules exert an osmotic pressure in the sample as shown in Figure 3.7.2: the osmotic stress is negative meaning that a positive pressure must be applied on the system to keep its volume constant. At the induction time $t_{ind} = 2.03 \times 10^7 s$, solvent molecules melt the polymer under the osmotic pressure it exerts as shown in Figures 3.7.3 and 3.7.5, and we see that: -1- the solvent volume fraction $< \phi_s >_{film}$ increases linearly with time, i.e. $< \phi_s >_{film} (t) \sim t$ (See Figure 3.7.1), and -2- solvent molecules penetrate the matrix in the form of an invariant front moving at constant velocity as it is shown in Figures 3.7.5. Hence, the combination of observations -1- and -2- shows that the system swells by means of a case II diffusion process. We can see as well that layers dilate on the passage of the case II front and they accelerate due to the large solvent quantity which penetrates them (see Figure 3.7.4). Finally, after the front has propagated all over the film at time $t_{pII} = 2,08 \times 10^7 s$, the whole system is at equilibrium with the reservoir. This corresponds to the second plateau regime in which the polymer is diluted, and the dynamics of the system as a whole is fast as shown in Figure 3.7.4.
A clear separation of time scales between the first and the second plateau regime can be ob-

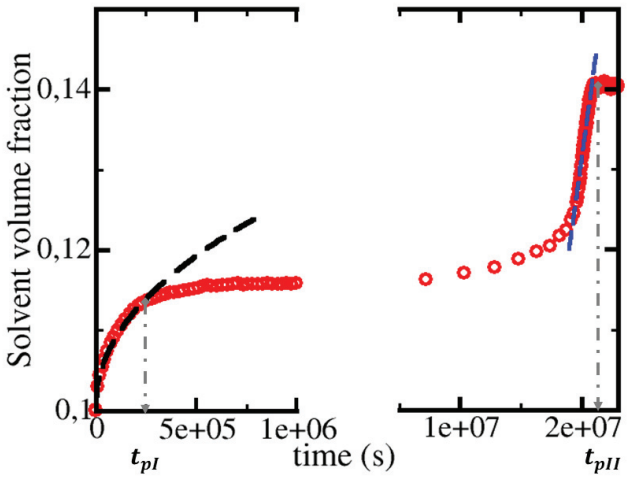

Figure 3.7.1: Evolution of film (50×50 cells) average solvent volume fraction as a function of time during swelling at activity 0.35. The system is that described in Figure 3.7.3. For clarity, time axe has been cut off. At short times, before reaching the first plateau regime at time t_{pI}, average solvent volume fraction increases like the square root of time (Black dashed curve fit), meaning that the molecules of solvent diffuse in a Fickian way through fast path. Then, after the first plateau regime, the average solvent volume fraction increases linearly with time which is the signature of a case II diffusion process. At the end of the case II process at time t_{pII}, the system is in the second plateau regime and film average solvent fraction admit a constant value corresponding to that of the final equilibrium state.

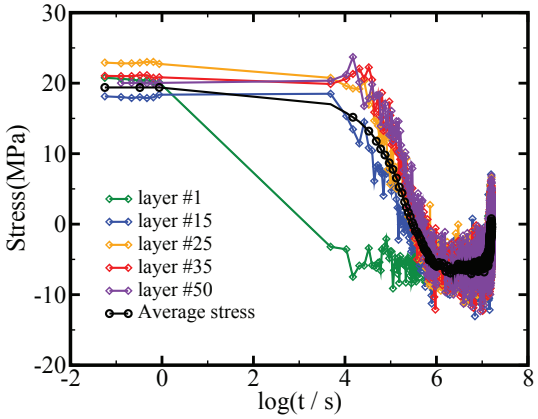

Figure 3.7.2: Evolution of the average osmotic stress on layers 1,15,25,35 and 50 during the swelling of a 50x50 film at activity $a_s = 0.35$ and temperature $T = 310$K. The system was dried at activity 0,15 for 10^6s before swelling. The black curve represents the evolution of the film average osmotic stress. The swelling of layers results from osmotic pressure effect apply by solvent molecules within the matrix. Finally, after swelling the osmotic stress relaxes to zero.

served in Figure 3.7.3. In particular, like it is the case during drying, the separation of time scales is more pronounced when considering very thin films, whereas it is no longer observed in the case of very thick films. Indeed, as it can be observed in Figure 3.7.7 the Fickian front which first takes place does not have the time to reach the bottom of the films before the induction time $t_{ind} \sim 2 \times 10^5$s, and consequently, the latter continues to propagate ahead of the case II front. Note that a specific method presented in Appendix 3.C has been developed to obtain a dried homogeneous thick film before swelling. A spatial representation (see Figure 3.7.9) of the system shows us that the front moves in the direction normal to the film/reservoir. The system is then shared in two parts: a highly swollen one at equilibrium with the reservoir, and a glassy one in which the Fickian front propagates. The interface between both regions is called the "Fickian foot". Finally, it can be seen in Figure 3.7.8 that the osmotic stress in layers located deeper in the glassy region is positive ($< \sigma > \sim 30$MPa) and remains constant at the beginning of the swelling process: these layers are still equilibrating with the low solvent volume fraction resulting from drying.

Let us now highlight the physical mechanisms responsible for the Fickian foot propagation. At the Fickian foot, solvent molecules quickly penetrate the glassy layers located beyond through fastest subunits as given in Figure 3.7.10. In addition, thanks to the facilitation mechanism, fastest subunits can exchange their excess of solvent with long lived subunits which undergo the melting process. This makes that α-relaxation times decrease and thus, the dilatation of layers self accelerates in a catastrophic way. Finally, according to the dynamics ansatz, the solvent flux propagation at the film/reservoir interface and at the Fickian foot are mainly driven by relaxation times (noted τ_{fast}) of the swollen region behind the case II front. Consequently, the quantity of solvent required so that the Fickian foot moves of a distance L between two times t and $t' > t$ is exactly balanced by the reservoir: the solvent penetration rate in the film is constant, and so is the front velocity. See Figure 3.7.16 as an illustration of

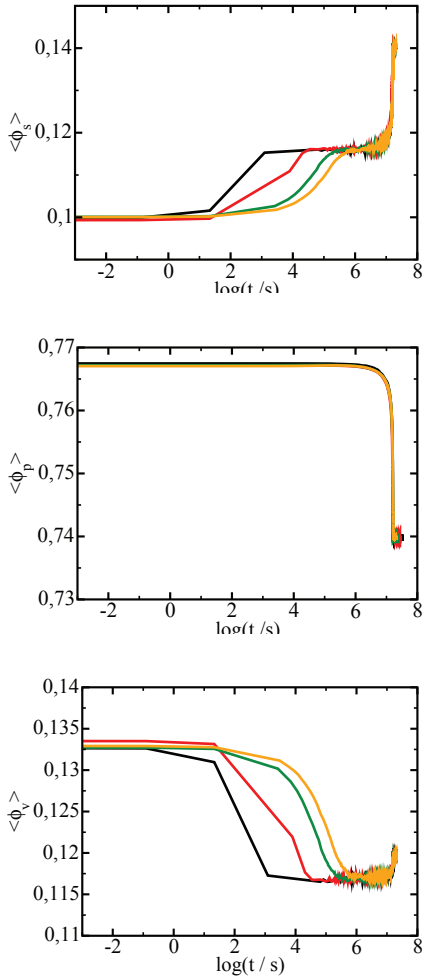

Figure 3.7.3: Evolution of the average solvent(a), polymer(b) and vacuum(c) volume fraction during swelling. The averaging is performed over the whole film. All systems were initially prepared at equilibrium at $a_s = 0.35$ and $T = 310K$ and then dried for $10^6 s$ at activity $a_s = 0.15$. We report the subsequent evolution of solvent polymer and vacuum volume fraction after the reservoir activity was increased at $a_s = 0.35$. The width of the film is maintained constant here (50 cells) but we vary its depth (N) from $N = 2; 10; 30; 50$ (black, red, green and orange curves respectively).
We observe a net separation of times scales between the fast diffusion process of solvent though fast path and the case II diffusion process. The times scales separation is more pronounced when considering very thin films.

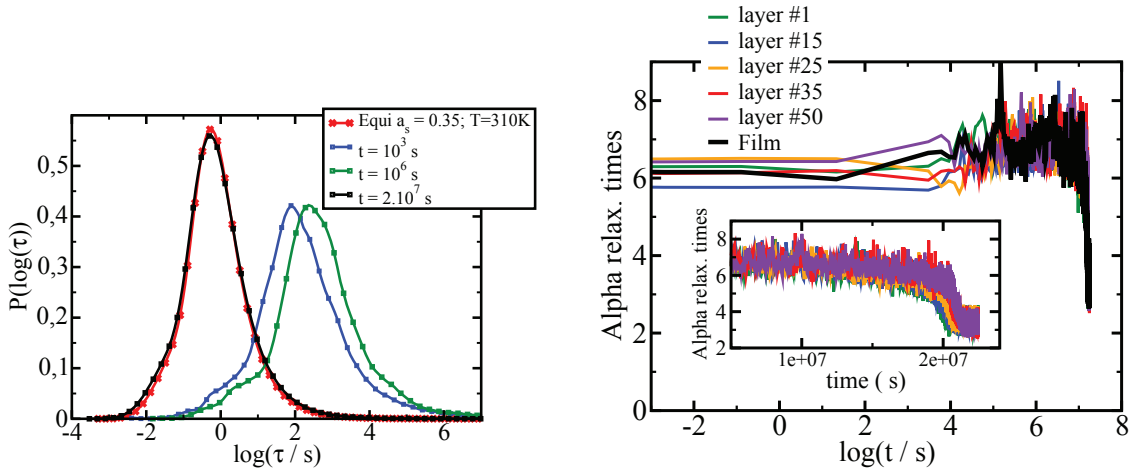

Figure 3.7.4: (Left) Distribution of relaxation times at different times $t = 10^4 s, 10^6 s$and$2, 2 \times 10^7 s$ and (right) evolution of α-relaxation times during swelling at activity $a_s^{swell} = 0.35$ at $T = 310K$. The system was first dried at activity $a_s = 0.15$ for $10^6 s$. We observe that during swelling, the distribution of relaxation times shifts slightly towards longer times, and that α-relaxation times increases before the induction time. We attribute the slowing down of the dynamics to the free volume reduction during the penetration of solvent molecules during the Fickian diffusion process. After the induction time however, case II process takes place and the matrix swells layers by layers: the dynamics accelerates. Finally, in the second plateau regime, the system has completely swollen and the distribution of relaxation times superposes to the equilibrium distribution (red curve) at activity $a_s = 0.35$: the system is in its final dynamical state.

this.

This model, by its coarse grained nature, has been designed to take also into account the history of the system regarding the solvent diffusion. We hence propose to look at the influence of drying time and swelling activity on case II diffusion (front velocity and induction time). To that purpose, considered systems have either been dried at different activities or for different times and then swelled at various activities in both cases. We can see first in Figures 3.7.11 and 3.7.12 that the induction time depends on the way the system has been dried: the longer the drying time, the longer the induction time, and the lower the drying activity, the longer the drying time. Although the swelling activity range is rather small, one can also notice that the induction time decreases when the swelling activity increases whatever the drying conditions. We attribute this effect to the osmotic pressure which increases when the swelling activity increases as it is explained in appendix 3.B. Regarding the front velocity, it can be observed that the latter does not depends on drying conditions (drying time and drying activity), but in contrast it depends strongly on swelling conditions. This is a consequence of the fact that the Fickian foot propagation kinetics is mainly driven by the dynamics of the swollen region behind the front at equilibrium with the reservoir as it has been explained above.
The influence of the plasticisation power of solvent molecules on case II diffusion has also been studied. To that purpose, two different blend T_g's has been considered where one of them

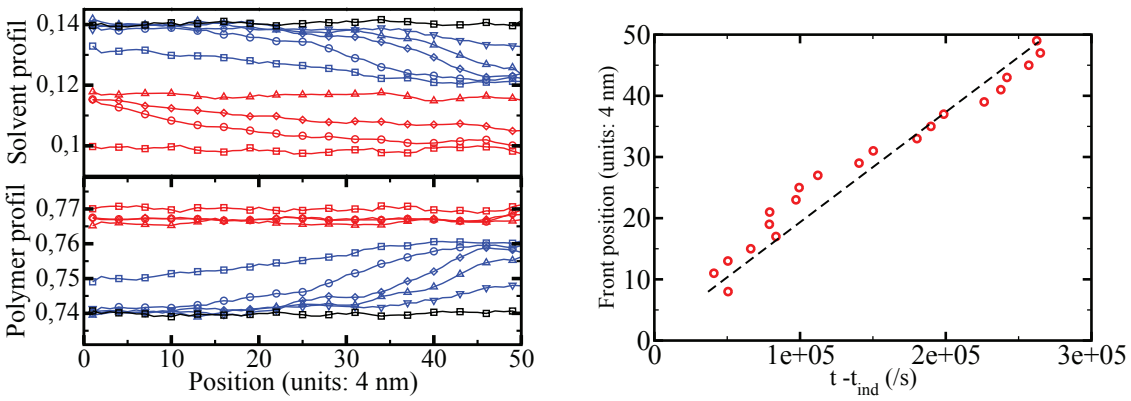

Figure 3.7.5: (Left) solvent and polymer average volume fraction profile at different times during swelling at activity $a_s = 0.35$ and $T = 310$K. Red curves correspond to volume fraction profiles before the induction time $t_{ind} = 2,03 \times 10^7$s: ($\square$: $log(t/s) = 0$), ($\circ$: $log(t/s) = 2.45$), ($\diamond$: $log(t/s) = 5$), ($\triangle$: $log(t/s) = log(t_{pI})$). From the induction time, layers swell progressively (blue curves) and solvent propagates as a front: ($\square$: $t = 1,95 \times 10^7$s), ($\circ$: $t = 2,038 \times 10^7$s), ($\diamond$: $t = 2,045 \times 10^7$s), ($\triangle$: $t = 2,05 \times 10^7$s), ($\triangledown$: $t = 2,06 \times 10^7$s). The front is invariant and its velocity is constant as one can see on the Right panel: the system is swelling thanks to a case II diffusion process. Layers behind the front are at equilibrium with the reservoir, and at the end of the front propagation, the homogeneous final equilibrium state is reached (black curve: ($\square$: $t = t_{pII}$)): the whole system is equilibrated with the reservoir. Finally, the front velocity V_{front} is estimated to be $V_{front} \sim 8,0 \times 10^{-4}$nm.s^{-1}.

decreases faster than the other with respect to the solvent volume fraction as given in Figure 3.7.13. We notably observe in Figure 3.7.14 that at fixed swelling activity, the case II front propagates faster when the solvent is a good plasticiser as compared to the case where it is a weak plasticiser. Moreover, one can notice a significant reduction of the induction time when the solvent is a good plasticiser for the system. Hence, in addition to osmotic pressure effects, the effect of the plasticisation power of penetrating solvent molecules and their ability to accelerate polymer chains has an important influence on case II diffusion.

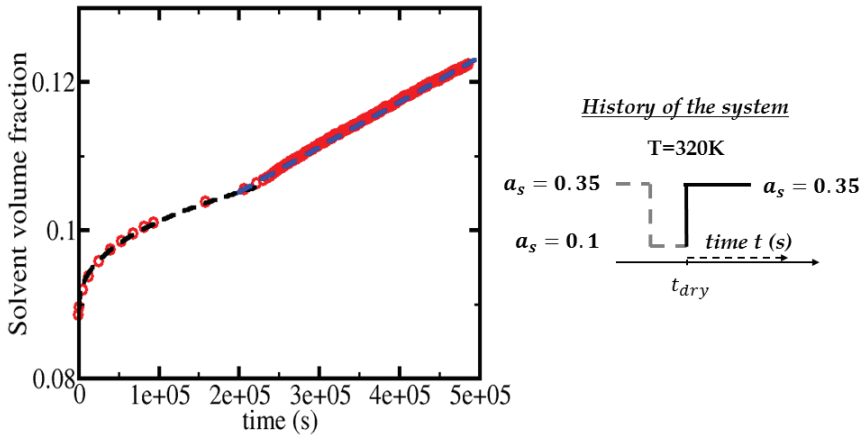

Figure 3.7.6: (Left) Evolution of film average solvent volume fraction during swelling at $a_s = 0.35$ at $T = 320$K . The system has been frist dried at activity $a_s = 0.10$ for $t_{dry} = 5 \times 10^4$s. Before the induction time $t_{ind} = 2 \times 10^5$s, the solvent volume fraction increases like the square root of time (black dashed curve):$< \phi_s >_{film} (t) =< \phi_s >_{film} (0) + \alpha\sqrt{t}$ with $\alpha = 1,23 \times 10^{-4} s^{1/2}$. From time t_{ind}, the solvent volume fraction increases in a linear way: $< \phi_s >_{film} (t) \sim t$ (blue dashed curve): a case II diffusion process takes place in the system.

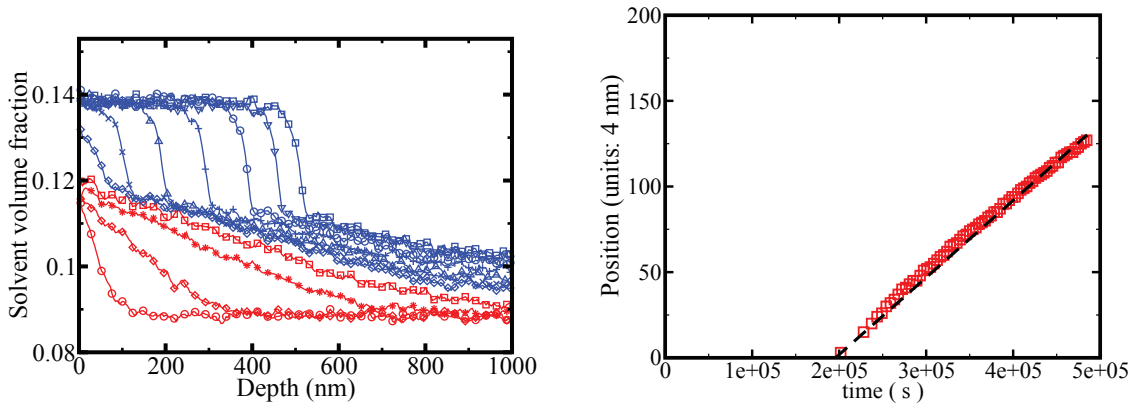

Figure 3.7.7: (Left) Average solvent volume fraction profile at different times during the swelling of a $1\mu m$ thick film at $a_s = 0.35$ and temperature $T = 320$K. The system has been first dried at activity $a_s = 0.10$ for 5×10^4 s at the same temperature. Red curves correspond to profiles before the induction time: ($\circ$: $log(t/s) = 2.72$), ($\diamond$: $log(t/s) = 3.90$), ($*$: $log(t/s) = 4.77$), ($\square$: $log(t/s) = 5.11$). Blue curves correspond to profiles after the induction time: ($\diamond$: $t = 2.202 \times 10^5$s), ($\times$: $t = 2.475 \times 10^5$s), ($\triangle$: $t = 2.899 \times 10^5$s), ($+$: $t = 3.482 \times 10^5$s), ($\circ$: $t = 4.0913 \times 10^5$s) ($\triangledown$: $t = 4.479 \times 10^5$s) and ($\square$: $t = 4.866 \times 10^5$s). Before the induction time, solvent molecules penetrate the matrix in a Fickian way through fast path. At the induction time, a case II solvent front takes place and the large Fickian front keeps to propagates ahead. (Right) Position of the case II solvent front as a function of time. The intersection between the time axis and the linear black curve corresponds to the induction time. The later is equal to 2.0×10^5s. From time the induction time, the front position increases linearly with time: the case II front moves at constant velocity $V_{front} = 1.80 \times 10^{-3}$nm.s^{-1}.

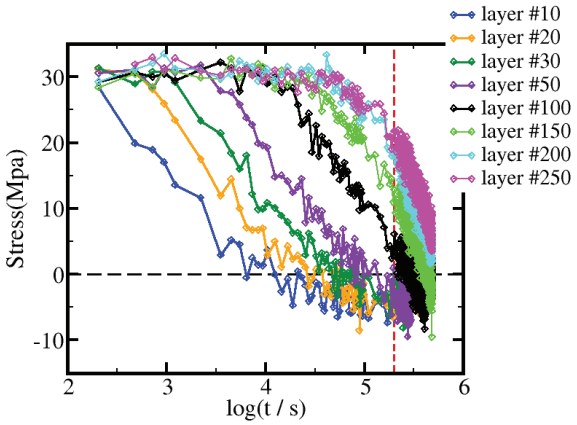

Figure 3.7.8: Evolution of the average osmotic stress on layers 10,20,30,50,100,150,200 and 250 during the swelling of a 250 layers thick film ($1\mu m$) at activity $a_s = 0.35$ and temperature $T = 330$K. Vertical red dashed line indicates the position of the induction time on the time axis. Regarding layers near the free surface, the osmotic stress becomes negative before the induction time: solvent molecules exert an osmotic pressure in layers. After the induction time, the case II diffusion front appears and the osmotic stress relaxes to zero (mechanical relaxation of layers) as the front propagates. Layers located deeper in the film keep on contracting (constant positive value of the osmotic stress) during the first decades of the process. However, the osmotic stress inside these layers decreases when the Fickian front reaches them.

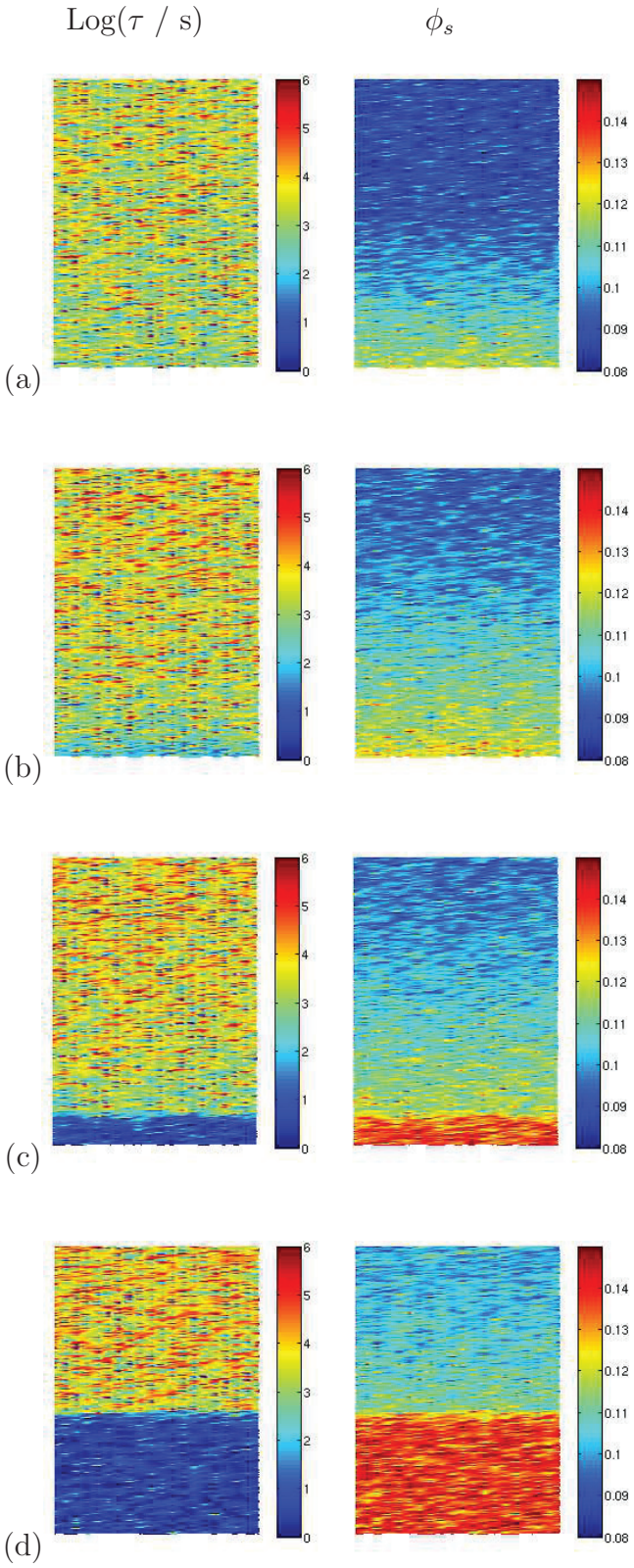

Figure 3.7.9: Snapshots at $t = 6.10 \times 10^3$ s (a), $t = 1.8 \times 10^5$s (b), $t = 2.61 \times 10^5$s (c), $t = 4.51 \times 10^5$s (d) during the swelling of a $1\mu m \times 80nm$ film at activity $a_s = 0.35$. The system has been first dried at activity $a_s = 0.10$ and $T = 320$K for 5×10^4 s. The left column represents the logarithm of relaxation times and the right one the solvent volume fraction ϕ_s. The reservoir is located at the bottom of each picture. In Figures (c) and (d), we observe the case II solvent front moving at constant velocity $V_{front} = 1.80 \times 10^{-3}$nm.s^{-1} in the direction normal to the free surface. The induction time is $t_{ind} = 2 \times 10^5$s. Snapshot (b) represents the system just before the induction time.

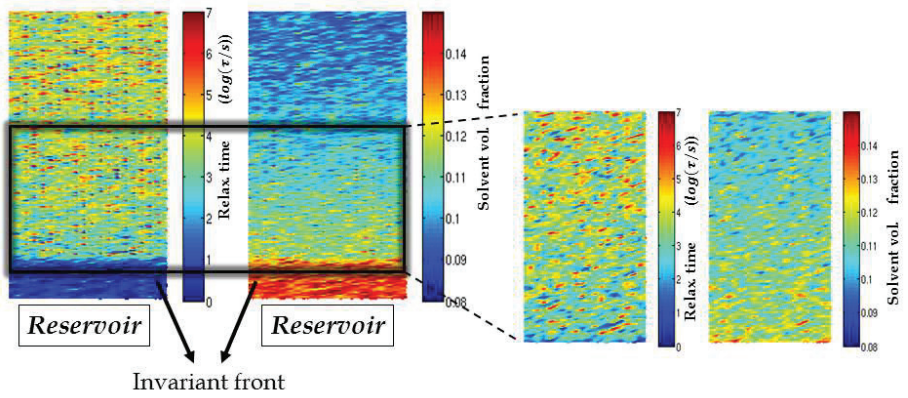

Figure 3.7.10: Representation of a $1\mu m \times 80nm$(Thickness×width) large film (left) at time $t_w = 3.1 \times 10^5$s during swelling at activity $a_s^{swell} = 0.35$ at $T = 320$K. A case II front Induction time is 2×10^5s. Figure on the right hand side represents a $400nm \times 80nm$(Thickness×width)large zoom of the system ahead the case II front (black frame on the left picture). We observe that the solvent molecules penetrate through fast dynamic heterogeneities in layers right ahead the front.

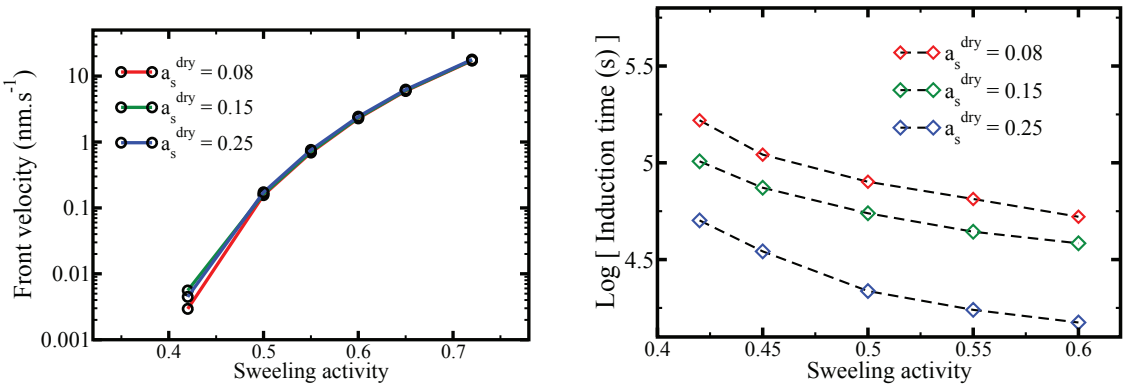

Figure 3.7.11: (Left)Evolution of the case II front velocity and (Right) the induction time as a function of the reservoir swelling activity a_s^{swell} for systems which were dried for 3×10^4s at temperature T=320K and at activity $a_s^{dry} = 0.25$, $a_s^{dry} = 0.15$ and $a_s^{dry} = 0.08$.

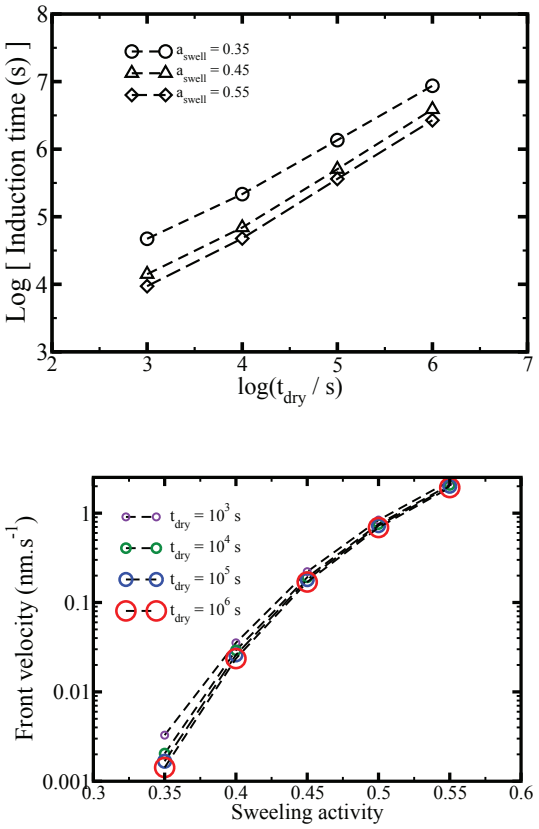

Figure 3.7.12: (Up) Evolution of the induction time as a function of drying time t_{dry} for systems swelling at different activities: $a_{swell} = 0.35$(circles); $a_{swell} = 0.45$(triangle); $a_{swell} = 0.55$(diamond). (Bottom) Evolution of the front velocity during swelling as a function of the swelling activity at different drying times.

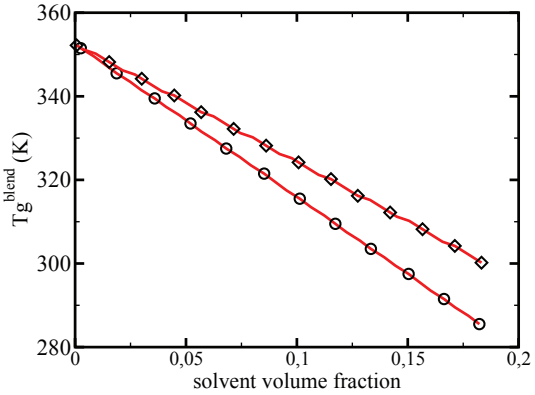

Figure 3.7.13: Evolution of two equilibrium solution glass transition temperatures T_g^{blend} as a function of solvent volume fraction. Regarding the curve with circle points, we have $\Delta T_g = T_g^{bulk} - T_g^{blend} = 37$K, and regarding the curve with diamonds points we have $\Delta T_g = T_g^{bulk} - T_g^{blends} = 27$K (diamonds) for $\phi_s = 10\%$: the curve with circle represents the blend T_g variation in case where the solvent is a good plasticiser for the system and the other curve in case where the solvent is a weak plasticiser for the system.

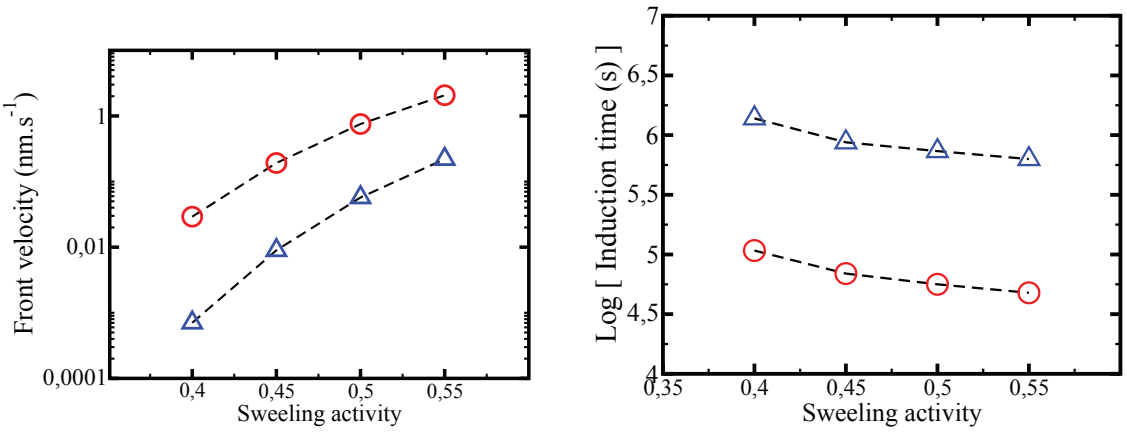

Figure 3.7.14: Evolution of the front velocity (Left)and the induction (Right) as a function of swelling activity when considering solvent molecules with different plasticisation power as explained in Figure 3.7.13.

3.7.1 Conclusion on thin and thick films swelling

In previous sections, we have studied the swelling of thin and thick polymer films. Before swelling, films are dried at non zero activity. Regarding thick films swelling, a method has been developed in order to obtained homogeneously dried films of a few microns thick.
In the case of thin films swelling, a time scales separation is observed during the swelling process. The solvent molecules penetrate first the matrix in a Fickian way through fast dynamic heterogeneities. During this process, the solvent volume fraction increases until reaching the first plateau regime: thermodynamically, the solvent volume fraction adjust itself to the initial polymer volume fraction given the swelling activity. In this plateau regime, which may last for several decades, the solvent free volume fraction is homogeneous in the whole film, and solvent molecules exert an osmotic pressure in the contracted sample. At the induction time, closest layers from the free surface swell as a consequence of osmotic pressure effects, and a case II front takes place: the fornt propagates at constant velocity in the direction normal to the film/reservoir interface, and the film average solvent volume fraction increases linearly with time. Behind the case II front, the solvent volume fraction is at equilibrium with the reservoir and the system is plasticised in this region. Finally, at the end of the case II front propagation, the whole system is at equilibrium with the reservoir: the system is in the second plateau regime. We have seen that the higher the swelling activity, the shorter the elapsed time to reach the second plateau regime. In thick films, the situation is slightly different from a phenomenological point of view. Indeed, like for thin films situation, a Fickian front penetrates first the system, and a case II front takes place at the induction time. However, the system is thick enough so that the Fickian front keep to propagate ahead the case II front, and the intermediate plateau regime is not longer observed: there is no time scales separation in the system as a whole.

The induction time depends on drying conditions (drying activity and drying time), which is not the case for the case II front velocity. Nevertheless, the latter increases strongly with respect to the swelling activity and seems to depend mainly on the final thermodynamical state. The influence of solvent plasticisation power on case II diffusion has also been studied. We have seen that both the induction time and the front velocity depend on the plasticisation power of the solvent: the stronger the solvent plasticisation power, the shorter the induction time and the larger the front velocity. Schematization of thin films swelling is given in Figure 3.7.15.

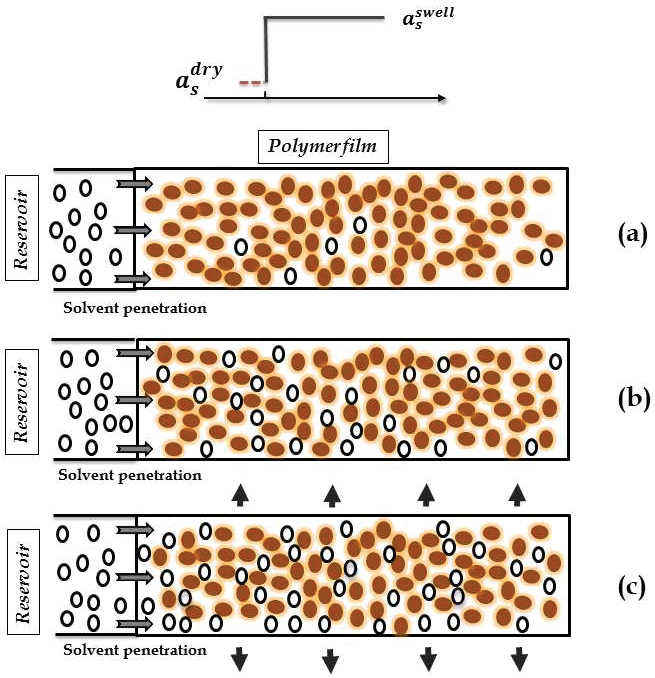

Figure 3.7.15: Schema of thin film swelling after an increase of activity from a_s^{dry} up to $a_s^{swell} > a_s^{dry}$ of the solvent reservoir. Right after the increase of the activity(a), the matrix is contracted and contains a few solvent molecules. At the first moment of the solvent penetration(b), solvent molecules diffuse through empty spaces. At longer times(c), the matrix swells due to osmotic pressure effects induced by solvent molecules. During the swelling process, a large quantity of solvent penetrates the system and dilutes the polymer chains.

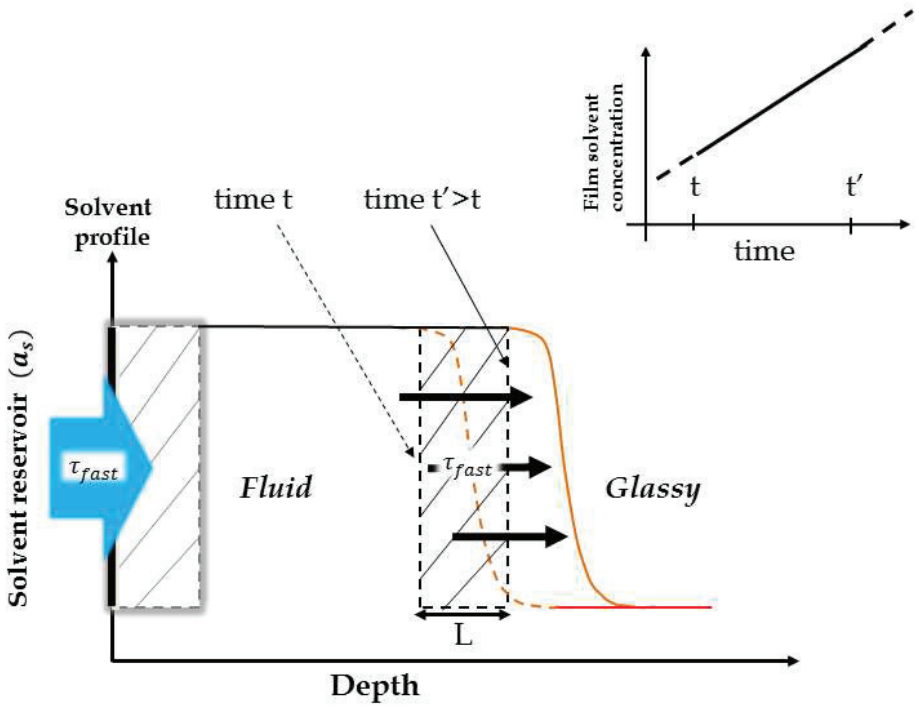

Figure 3.7.16: Schema representing a case II solvent front at time t and $t' > t$. Dashed area corresponds to solvent quantity entering the system between both times t and t'. Upstream the front, dynamics is fast and typical relaxation time is τ_{fast} while downstream the front the film is glassy. Due to the dynamics ansatz, the propagation of the foot ahead the front is driven by τ_{fast}. The solvent penetration kinetics at the film/reservoir interface is also driven by τ_{fast}. Thus, the quantity of solvent required so that the invariant front moves of a distance L between t and t' is is exactly balanced by the reservoir: the solvent penetration rate in the system is constant, and so is the front velocity.

Appendix

3.A Effect of activity on drying

In this section, we look at the effect of the activity in the drying process. Evolution of α-relaxation times is given in Figure 3.A.1 for systems dried at activity $a_s^{dry} = 0.35$ $(magenta)$, 0.30 $(purple)$, 0.25 $(orange)$, 0.15 $(green)$; 0.06 $(black)$). We note that dynamics accelerates significantly at short times regarding the system dried at activity $a_s^{dry} = 0.06$. This is caused by the relatively large increase of free volume fraction resulting from the fast evaporation process. Finally, the acceleration of the dynamics is more pronounced when drying activity is low. The reason is that the increase of the free volume fraction during the fast evaporation process is more important when the drying activity is low. Furthermore, at long times, α-relaxation times increase linearly with time for the system drying at lower activity, while dynamics slowing down is less pronounced for the system drying at higher activity. The reason is that the difference between the initial and the final state is relatively small in this case: the dynamics evolution does not follows the Struick law.

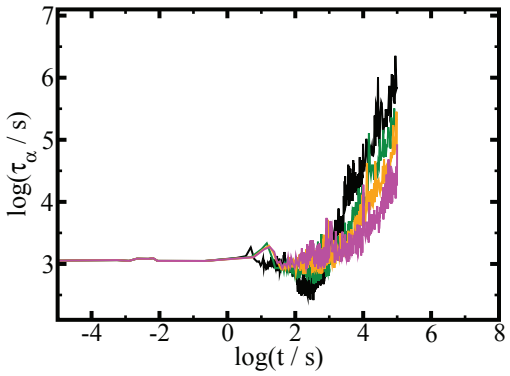

Figure 3.A.1: Evolution of α-relaxation times in a 50×50 cells film drying at activity $a_s^{dry} = 0.35(magenta); 0.30(purple); 0.25(orange); 0.15(green); 0.06(black))$ for 10^5s. The system is first equilibrated at activity $a_s = 0.42$ and $T = 330$K. We see that the dynamics accelerates slightly at short times. This results form the increase of the free volume fraction before the matrix contraction. The dynamics acceleration is less pronounced when drying activity increases. It is no longer observed at the higher drying activity though. Finally, at long times, the dynamics slows down. α-relaxation times increase more slowly than the waiting time for the system drying at higher activity.

3.B Effect of activity on swelling

In this part, we look at the influence of swelling activity a_s^{swell} on swelling kinetics.
We consider systems dried in strictly equivalent conditions (drying time: $t_{dry} = 10^6$s and drying activity: $a_s = 0.10$) and then swelled at different activities comprised between $a_{swell} = 0.35$ and $a_{swell} = 0.55$. Evolution of times t_{pI} and t_{pII} as a function of swelling activity is given in Figure 3.B.1. First, we see that time t_{pI} does not depend on the swelling activity. This is explained by the fact that all systems follow the same history during drying: their dynamical state at the end of drying is equivalent. Second, the time t_{pII} increases by almost one decade between $a_{swell} = 0.31$ and $a_{swell} = 0.55$. As seen in section 3.5, the film average osmotic stress is negative before the induction time. It can be observed in Figure 3.B.1 that the higher the swelling, the higher the osmotic pressure that solvent molecules exert in the sample before the induction time. As a consequence, the induction time, and also the time t_{pII} decreases with the swelling activity .

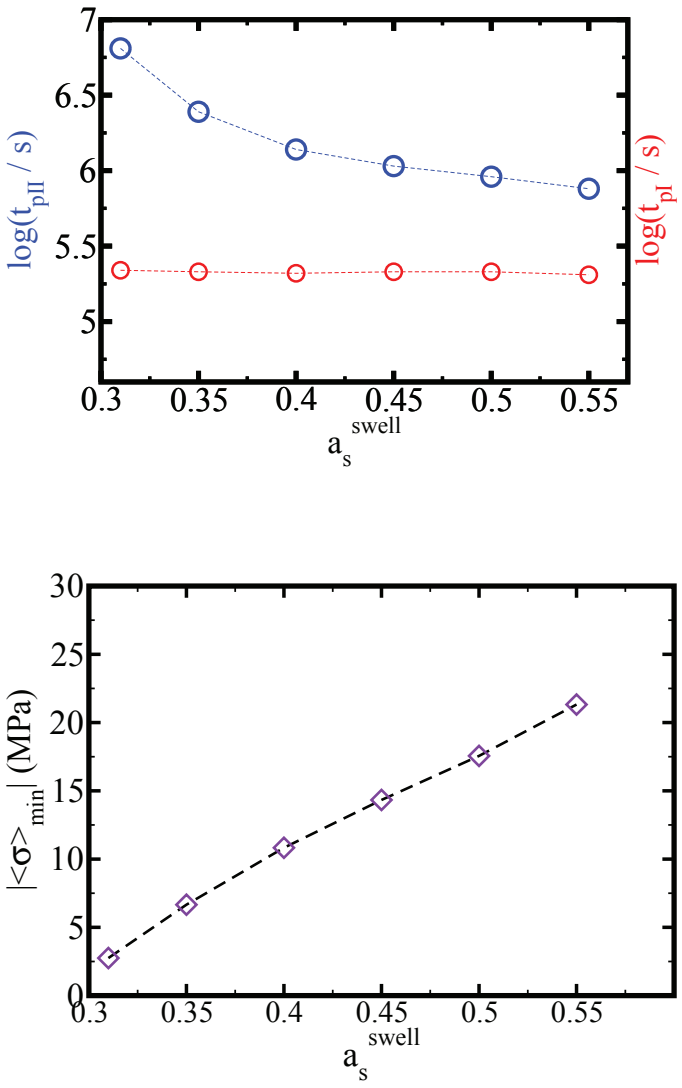

Figure 3.B.1: (UP) Evolution of t_{pI} and t_{pII} as a function the swelling activity. All 50×50 cells systems were first dried for 10^6s at activity $a_s = 0.1$ at temperature $T = 320K$. The time t_{pI} does not depend on the imposed final activity. However, the time t_{pII} varies significantly with the swelling activity: the lower the swelling activity, the longer the total swelling time t_{pII}. (BOTTOM) Evolution of absolute value of the film average osmotic stress $< \sigma >_{min}$ before the induction time. We see that the higher the swelling activity, the higher the osmotic pressure. This explains why the system swells faster at higher swelling activity than at lower swelling activity.

3.C Numerical method for studying thick films swelling

We have seen that it is impossible to completely dry a film of a few micrometers thick on reasonable observation times. Indeed a very slow crust is forming close to the free surface, which prevents the solvent contained in the bottom of the film to evaporate. We have then developed a method designed for obtaining homogeneous dried thick films.

- - **Step 1**: A 10×10 cells large film is equilibrated at activity a_s^{init} and at constant temperature. It is then dried at activity a_s^{dry} for a time t_{dry}.
- - **Step 2**: We cut off the connection with the reservoir and we consider periodic boundary conditions. The activity of the reservoir is maintained at a_s^{dry} for a time $t_{inter,1}$
- - **Step 3**: Thin films are stuck together in order to form a larger one of the desired size. The activity of the reservoir is maintained at a_s^{dry} for a time $t_{inter,2}$. We consider periodic boundary conditions.
- - **Step 4**: The reservoir is plugged again and activity is raised from a_s^{dry} up to a_s^{swell}.

This method is illustrated in Figure 3.C.1. Times $t_{inter,1}$ and $t_{inter,2}$ are taken equal to drying times t_{dry} so slower density fluctuations can relax. At the end of step 3, we obtain a dried thick film and homogeneous in term of solvent volume fraction.

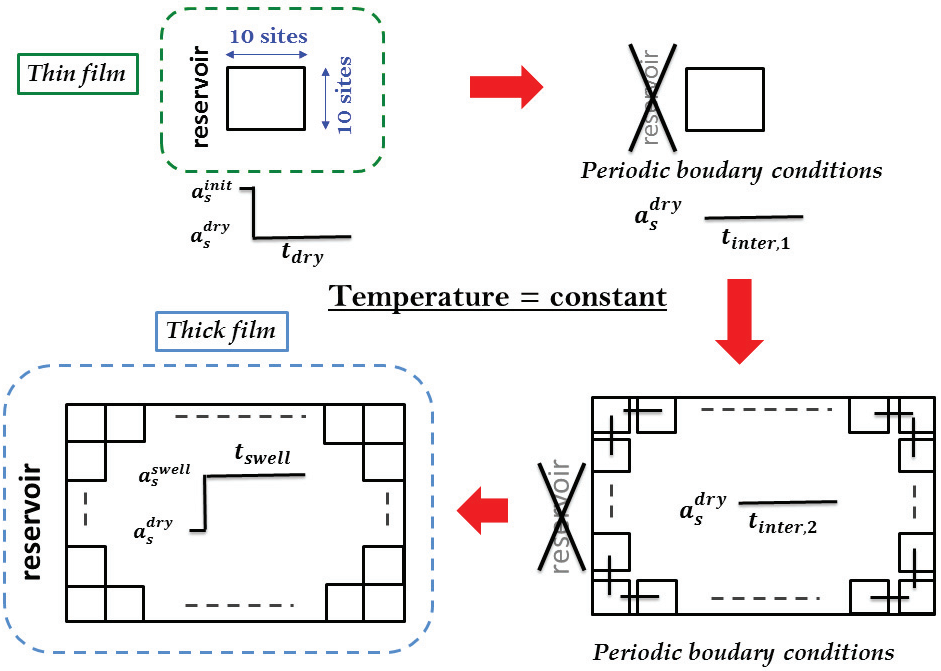

Figure 3.C.1: Schematic representation of the method developed to obtain homogneous and dried thick films. At last step, the reservoir activity is increased from a_s^{dry} up to a_s^{swell}. Thanks to this method, one can study solvent penetration mechanisms in thick and glassy polymer solvent systems.

General conclusion

In this work, we consider molecular diffusion mechanisms in polymer blends or polymer-solvent systems close to or below the glass transition temperature. In case of polymer blends, below their entanglement threshold, we have studied phase separation mechanisms occurring close to the blend glass transition, and also rejuvenation mechanisms during which the system mixes again and recovers a homogeneous molten state. In case of polymer-solvent systems, we have been interested in drying and swelling processes when the system is far below the glass transition temperature of the pure polymer.

Experiments have put in evidence that dynamics is extremely heterogeneous on a scale of dynamic heterogeneities of a few nanometers (3-5nm). Moreover, probes diffusion experiments have shown, in the context of pure glass forming liquids, that heterogeneous dynamics allows for small probes (smaller than a dynamic heterogeneity) translational diffusion through fast dynamic heterogeneities. In case of binary systems, we argued that heterogeneous dynamics is the consequence of composition fluctuations, and we assumed the existence of a large spatial distributions of relaxation times in these systems. In addition, we considered that the α-relaxation time, which controls the macroscopic stiffness of the system, is the consequence of the percolation of a small fraction of slower dynamic heterogeneities. Following these assumptions, the relaxation of the system takes place through the superposition of slowly relaxing structural changes occurring at large scale which control the mechanics of the system, and fast diffusion processes through very mobile dynamic heterogeneities. Finally, we describe a facilitation mechanisms which controls the relaxation process of slow composition fluctuations by a diffusion process of monomers and free volume.

We have developed a spatial diffusion model which we apply to the case of polymer blends in contact with a thermal bath, and polymer solvent system in contact with a thermal bath and a solvent particles reservoir. In both situations, we solved a 2D coarse grained spatial model which integrates the spatial nature of dynamical heterogeneities on a scale of 3-5nm. The latter corresponds to the spatial resolution of the model. A thermodynamical model describing binary systems, has been designed in order to implement the thermodynamical forces which drives the evolution of the dynamics of the system. Driving forces are equal to the gradient of chemical potential. This thermodynamical model has been confronted to experiment. It is also able to describe equilibrium situations in polymer-solvent system in contact with a pure

solvent reservoir. Finally, we have seen that this model can give results regarding the variation of Small Angle Neutron Scattering (SANS) intensity as a function of pressure, and that the Flory Huggins model can be recovered in the limit of the low temperatures or high pressures. Dynamics follows from an Onsager principle and composition fluctuations modelling the thermal noise are written in a Langevin scheme. The model is discretised Following and the evolution of the composition on a given site i is governed by following equations:

$$\begin{aligned}\frac{\partial \phi_A(i)}{\partial t} &= \sum_{<j>} \gamma^{(i,j)} \Big(\mu_s^{(j)} - \mu_A^{(i)} + \delta\phi_A^{i,j} \Big) \\ \frac{\partial \phi_B(i)}{\partial t} &= \sum_{<j>} \gamma^{(i,j)} \Big(\alpha(\mu_B^{(j)} - \mu_B^{(i)}) + \delta\phi_B^{i,j} \Big)\end{aligned} \tag{3.3.1}$$

with γ a relaxation frequency $[\gamma] = s^{-1}$, $\delta\phi_A = \beta\sqrt{2\gamma^{-1}/N_c\delta t}$ and $\delta\phi_B = \beta\sqrt{2\alpha\gamma^{-1}/N_c\delta t}$ where β is a random number distributed following a gaussian distribution of variance unity. This random term, which holds for the thermal noise, gives rise to composition fluctuations in the system. μ is a dimensionless chemical potential per monomers and $N_c \sim 400 - 500$ is the dimensionless volume of a given site. Finally, $< \cdot >$ denotes the summation over all next neighboring sites. Note that these are "bulk" equations, and that a supplementary term $\gamma^i \times (\ln(a_s) - \mu^i)$, where a_s is the solvent reservoir activity (depending on reservoir chemical potential μ_{res} (dimensionless): $a_s = \exp(\mu_{res})$), must be added to take into account the interaction between the reservoir and the film in case of polymer-solvent systems.
Since we mix a slow component A (of glass transition temperature T_g^{slow}) with a fast one B (of glass transition temperature T_g^{fast}), the glass transition temperature of the solution depends explicitly on system's composition: $T_g^{blend} = T_g^{blend}(\phi_A, \phi_B; T_g^{slow}, T_g^{fast})$. Then, by means of a WLF law, we compute the monomeric relaxation times which depend on the composition:

$$\tau(\phi_A, \phi_B) = \tau_{WLF}(T - T_g^{blend}(\phi_A, \phi_B; T_g^{slow}, T_g^{fast}))$$

Hence, by coupling composition fluctuations and the glass transition, we obtain a large spatial distribution of relaxation times at the scale of dynamical heterogeneities: a site which contains a large quantity of slow (resp. fast) component is slow (resp. fast). Finally, the above expression for WLF-like relaxation times takes into account the free volume fraction. Kinetic coefficients which control the matter exchange between a given site and its next neighbor, is taken as the shortest relaxation times between these two sites:

$$\gamma^{i,j} = max\Big(\gamma(i)\ ;\ \gamma(j)\Big) \tag{3.3.2}$$

which is basic assumption of the model.
The volume of the system is also assumed to be changing layers by layers which contract or swell homogeneously and independently from each other. The thermodynamical force which drives the evolution of the volume N (dimensionless) of a site on a given layer composed of n_{layer} sites reads: $\frac{1}{n_{layer}} \sum_{layer} \frac{\partial G}{\partial N}$ which is zero at equilibrium. The deformation kinetics of the entire layer

is controlled by α-relaxation times (τ_α^{layer}). By considering the additional contraction/dilation term in dynamical equations, we obtain:

$$\begin{aligned}
\frac{\partial \phi_A(i)}{\partial t} &= \sum_{<j>} \gamma_A^{(i,j)} \Big[\Big(\mu_A^{(j)} - \mu_A^{(i)} \Big) + \delta\phi_A^{i,j} \Big] \\
&\quad + \phi_A(i) \frac{N_c^{2/3}}{\tau_\alpha^{layer} n_{layer}} \sum_{layer} \frac{\partial G}{\partial N} \\
\frac{\partial \phi_B(i)}{\partial t} &= \sum_{<j>} \gamma_B^{(i,j)} \Big[\Big(\mu_B^{(j)} - \mu_B^{(i)} \Big) + \delta\phi_B^{i,j} \Big] \\
&\quad \phi_B(i) \frac{N_c^{2/3}}{\tau_\alpha^{layer} n_{layer}} \sum_{layer} \frac{\partial G}{\partial N}
\end{aligned} \tag{3.3.3}$$

In conclusion, following this model, the relaxation of a given site is the consequence of non linear diffusion mechanisms between itself and its next neighbors, and of the mechanical relaxation of the layer it belongs to.

Let us first discuss the case of polymer blends. We have considered symmetric blends composed of low molecular weight polymers with two different T_g's, and non-symmetric blends composed of long chains and much shorter ones (below the entanglement threshold). In non symmetric blends the small chain is either the fast or the slow component. For polymer blends with symmetric and low molecular weight, it has been observed that during a phase separation close to or below T_g, the α-relaxation time increases linearly with time, and that slow and fast domains build up in the system. Hence, dynamics does not slow down instantaneously, and formation of domains is possible. At early stages, domains's size is found to grow like the logarithm of the time. During this process, domains rich in slow component age and the growth kinetics slows down. At later stages, the growth process is very slow but becomes chaotic. We attribute this effect to the partial melting of slow domains by the fast fluid phase as due the large difference of mobility between both phases. Finally, after sufficiently long times, one can obtain morphologies of a few tens of nanometers in size. However, this depends on the relative composition of the system in terms of slow and fast polymer. We have seen that in systems composed mainly of the fast component, domains may become relatively large. Since the fluid phase is in majority, the diffusion of domains is possible which allows the coalescence and formation of larger ones. However, when the system is composed mainly of slow components, diffusion of fast domains forming is not possible: the slow phase build continuous rigid network which ages.

When studying the revers process -i.e. when the temperature is increased again into a homogeneous molten state- we have seen that the melting of glassy nano-morphologies takes place in much shorter times than the elapsed time to form them during aging: there is a strong temporal asymmetry between aging and rejuvenation. We have shown than the melting of slow domains results from the facilitation mechanism due to the presence of the mobile polymer which surround them. Regarding non-symmetrical blends, domains rich in long chains do not

grow much and their size fluctuates a lot due to the presence of the fluid phase which tends to melt them.

Let us now discuss the polymer-solvent systems, and first the process of drying of thin/thick films

We considered a system initially equilibrated close to the solution T_g. Three different situations of drying have been studied. We first discuss the situation where the system is initially composed of a large fraction of solvent, and is drying a non zero activity (a_s^{dry}). In this case, the system's trajectory during drying remains always in the stable region of the phase space: no thermodynamic instabilities appear. We have seen also in the case of thin films with different thickness, that the drying process is decomposed in two distinct steps. A first one, during which solvent molecules evaporate from the system by diffusing through fast path in times shorter than α-relaxation times. During this process, the matrix does not contract ($\phi_p = \phi_p^{init}$) and consequently, the free volume fraction increases in the system: a subsequent acceleration of the dynamics is observed. At longer times, solvent molecules evaporation is driven by the slow contraction of the system: as a consequence of the free volume reduction, the system ages and imprison solvent. In the case of drying at very low activity however, the film can be dried completely. This is the consequence of the large solvent evaporation and of the acceleration of the dynamics. Finally, the polymer contracts and ages. At long times, one obtains a very stiff and homogeneous matrix almost empty of solvent. In certain circumstances, cavities may appear during films drying at very low activity. Cavities appear the fast evaporation process as a consequence of thermodynamic instabilities. Wether it is in the case of drying at non zero activity or very low activity, the separation of time scales between the fast evaporation process and the contraction of the sample is more pronounced when considering very thin films. Regarding films of more than $1\mu m$ thick, the time scales separation is no longer observed. A glassy crust of a few hundreds of nanometer build up at the free surface and large quantity of solvent remains trapped in the bottom of the film.

When considering swelling of thin polymer-solvent films, we have seen that the solvent penetrates first the system through fast path in a Fickian way. During this process the matrix remains contracted ($\phi_p = \phi_p^{init}$) and the free volume fraction decreases. A subsequent slowing down of the dynamics is then observed. At longer times, the systems swell under the action of the osmotic pressure that solvent molecules exert and the solvent penetrates following a case II diffusion process.

We have seen, through these results, that the same general physical model is able to describe the phase separation close to T_g and the rejuvenation mechanisms in case of polymer blends, and also the drying and the swelling of polymer-solvent films. The physics which governs these systems is the same, such as osmotic pressure effect or the plasticising effect of free volume. These effects are the direct consequence of the compressibility. We have seen also that this non

linear diffusion model takes also into account the history of the system. For instance, in case of polymer blends we have seen that the rejuvenation time varies by several order of magnitude depending on the conditions. It is also the case for polymer-solvent systems where the induction time depends on the drying time or the drying activity before swelling.
This coarse grained model allows for recovering time scales comparable to experimental situations, and for studying systems, wether it is for polymer blends or polymer solvent system, where the dynamics adapts itself to imposed physical conditions. Finally, it is able to cover a large spectrum of dynamical quantities just by adapting the history of the system.

Regarding perspectives, a next step in the model's development would be to define an evolution equation for the stress tensor coupled to diffusion equations in order to take into account the mechanical relaxation in a more realistic way than what has been done here. In polymer blends, it is worth confronting our model to neutron scattering experiments in order to validate mechanisms responsible for the dynamics close to and below T_g. The influence of chains size on growth process of glassy morphologies could be also evidenced by this technic. Finally, the obtained results regarding phase decomposition processes may pave the way for creating nanostructured long lived polymer materials with desired morphologies. In polymer-solvent systems, from a fundamental point of view, it could be interesting to investigate the drying dynamics of polymer solvent films of various thickness for several solvent species. In addition, the influence of chains size on drying processes may be a field which could be explore. Indeed, when drying polymer films composed of very long entangled chains, the reorganisation time of the latter by reptation processes is very long. Thus, the coupling between diffusion and contraction processes may take place on much larger time scales than in case where the film is composed of short chains or oligomers. Finally, the presence of cavities when drying a polymer-solvent films in a dried atmosphere should be also investigated by neutron scattering experiments.

Conclusion générale

Dans ce travail, nous avons regardé les mécanismes de diffusion dans les mélanges de polymères et polymères solvant proche de ou en dessous de T_g. Dans le case des mélanges de polymères, sous le seuil d'enchevêtrement, nous avons étudions en particulier les mécanismes de séparation de phase, et aussi les mécanismes de réchauffe durant lesquels le système se remélange au-dessus de T_g. Dans le cas des mélanges polymère solvant, nous avons étudié les processus de séchage dans le cas où le système est sous la T_g du polymère pure.

Nous avons développé un model spatiale adapté pour les deux systèmes. Ce modèle coarse grainé est résolu sur un réseau carré et intègre le caractère hétérogène de la dynamique à l'échelle d'une hétérogénéité dynamique. Cette dernière correspond à la résolution spatiale du système (3-5nm). Un modèle thermodynamique a été conçue pour calculer les forces permettant de piloter l'évolution de la dynamique du système. Ces dernières sont égales au gradient de potentiel chimique. La dynamique suit le principe d'Onsager et les compositions de fluctuations sont écrite dans un schéma de Langevin. Ce modèle est ensuite discrétisé. L'évolution de la composition à un site i est donné par les équation suivantes:

$$\begin{aligned}\frac{\partial \phi_A(i)}{\partial t} &= \sum_{<j>} \gamma^{(i,j)} \Big(\mu_s^{(j)} - \mu_A^{(i)} + \delta\phi_A^{i,j} \Big) \\ \frac{\partial \phi_B(i)}{\partial t} &= \sum_{<j>} \gamma^{(i,j)} \Big(\alpha(\mu_B^{(j)} - \mu_B^{(i)}) + \delta\phi_B^{i,j} \Big)\end{aligned} \tag{3.3.4}$$

avec γ une fréquance de relaxaiton $[\gamma] = s^{-1}$, $\delta\phi_A = \beta\sqrt{2\gamma^{-1}/N_c\delta t}$ et $\delta\phi_B = \beta\sqrt{2\alpha\gamma^{-1}/N_c\delta t}$ où β est une nombre aléatoire qui suit une distribution gaussienne de variance unité. De plus μ est un potentiel chimique par monomères sans dimension et $N_c \sim 400 - 500$ est the volume adimensionnée d'un site.
Comme nous mélangeons une composante lente A (T_g^{slow}) avec une composante rapide B (T_g^{fast}), la température de transition de la solution dépend explicitement de la composition: $T_g^{blend} = T_g^{blend}(\phi_A, \phi_B; T_g^{slow}, T_g^{fast})$. Ensuite par le biai de la loi WLF, nous calculons les temps de relaxation monomérique:

$$\tau(\phi_A, \phi_B) = \tau_{WLF}(T - T_g^{blend}(\phi_A, \phi_B; T_g^{slow}, T_g^{fast}))$$

En conclusion, en couplant les fluctuations de composition et la température de transition

vitreuses, on obtient une distribution spatiale des temps de relaxation: les temps de relaxation sur un site riche en composante lente (resp rapide) est long (resp. court). Enfin, l'expression ci-dessus des temps WLF prend en compte le volume libre. Les coefficients cinétiques qui contrôlent les échanges de matière entre un site et un de ses proches voisins dépendent donc de la composition locale et est pris comme le plus court des deux:

$$\gamma^{i,j} \sim 1/\tau_{WLF} = max\Big(\gamma(i)\ ;\ \gamma(j)\Big) \tag{3.3.5}$$

Ceci est une hypthèse de base du modèle.
Le volume du système peut également changer. La relaxation mécanique est calculée couche par couche. La force thermodynamique qui pilote l'évolution du volume N (sans dimension) d'un site sur une couche composée de n_{layer} sites est:$\frac{1}{n_{layer}} \sum_{layer} \frac{\partial G}{\partial N}$ qui est nulle à l'équilibre. La cinétique de déformation est contrôlé elle par les temps de relaxation α de la couche (τ_α^{layer}). En insérant le terme de contraction/dilation dans l'équation dynamique, on obtient:

$$\begin{aligned}
\frac{\partial \phi_A(i)}{\partial t} &= \sum_{<j>} \gamma_A^{(i,j)} \Big[\Big(\mu_A^{(j)} - \mu_A^{(i)} \Big) + \delta\phi_A^{i,j} \Big] \\
&\quad + \phi_A(i) \frac{N_c^{2/3}}{\tau_\alpha^{layer} n_{layer}} \sum_{layer} \frac{\partial G}{\partial N} \\
\frac{\partial \phi_B(i)}{\partial t} &= \sum_{<j>} \gamma_B^{(i,j)} \Big[\Big(\mu_B^{(j)} - \mu_B^{(i)} \Big) + \delta\phi_B^{i,j} \Big] \\
&\quad \phi_B(i) \frac{N_c^{2/3}}{\tau_\alpha^{layer} n_{layer}} \sum_{layer} \frac{\partial G}{\partial N}
\end{aligned} \tag{3.3.6}$$

En conclusion, suivant ce modèle, la relaxation d'un site est la conséquence de mécanismes de diffusion non linéaires entre le site lui même et ses proches voisins, et de la relaxation mécanique de la couche à laquelle il appartient.

Nous avons considéré des mélange symétriques composés de polymères de mêmes masses ayant deux T_g différentes, et des mélanges de polymères composés de longues chaines et de chaines courtes (sous le seuil d'enchevêtrement). Dans ce dernier cas, la petite chaine est soit la composante rapide ou la composante lente. Pour les mélanges symétriques, il a été observé que les domaines lents se forment logarithmiquement . Pendant ce processus, les domaines riches en composante lente vieillissent ce qui rend leur temps de diffusion et de coalescence très longs. En conséquence le processus de croissance est lent. Aux temps longs, l'évolution de la taille des domaines est chaotique. On explique ceci par des effets de fusion partielle des domaines lents par la phase rapide du fait de la grande différence de mobilité entre les deux phases. Nous avons vu également que si le système est principalement composé de composante rapide, les domaines peuvent atteindre des tailles de quelques dizaines de nanomètres. Ceci provient du fait que la phase majoritaire fluide facilite la coalescence des domaines. A l'inverse, lorsque la phase majoritaire est la phase lente, la diffusion des domaines rapides qui se forment est bloquée à

cause de la phase majoritaire qui vieillit et qui forme un réseau rigide et dur. En conclusion, on peut dire qu'en considérant des mélanges symétriques composés de polymères de petite masses ayant des T_g différentes, il est possible d'obtenir des matériaux polymérique nanostructures très stables dans le temps. La croissance des morphologies obtenues correspondant à la phase minoritaire sera plus rapide quand la phase majoritaire est rapide. Lorsque l'on étudie le processus de réchauffe -i.e quand la température dans un domaine où le système est fondu homogène- nous avons vu que les nano-morphologie fondent plus vite que le temps nécessaire pour les former pendant le vieillissement. Nous avons montré que les domaines lents fondent grâce au mécanisme de facilitation du fait de la présence du polymère rapide en leur contact. En ce qui concerne les mélanges asymétriques, nous avons vu que les domaines riches en longues chaines grandissent peu et leur tailles fluctue beaucoup du fait de la présence de la phase rapide qui tend à les fondre. Dans le cas où la phase rapide est composée en la majorité de chaines courtes, le system se ré-homogénéise plus rapidement que dans le cas opposé.

Lors du séchage de films minces et épais, trois situations différentes ont été étudiées. Lorsque le système est initialement composé d'une relativement grande quantité de solvant, et sèche ensuite à activité non nulle (a_s^{dry}), le système reste toujours dans la partie stable de l'espace des phases: aucune donc aucune instabilité n'apparaît. Dans ce cas, le séchage se produit en deux étapes distinctes: une première durant laquelle le solvant s'évapore en diffusant par les zones rapides en des temps plus courts que les temps de relaxation α. En conséquence, pendant ce processus, le system ne se contracte pas et la fraction volumique de vide augmente. On observe donc une accélération de la dynamique. Au temps long, l'évaporation des molécules de solvant est piloté par la contraction lente du système. En conséquence de la réduction du volume libre, le système vieilli et la dynamique se ralentie: du solvent reste emprisonné dans le système. Dans le cas du séchage à très basse activité en revanche, le film peut être séché complétement. Ceci s'explique par la combinaison de l'évaporation rapide du solvant et de l'accélération importante de la dynamique aux temps courts. Enfin, comme dans le cas du séchage à activité non nulle, après l'évaporation rapide du solvant, le polymère se contracte et vieillit, et au temps longs, on obtient une matrice rigide et vide en solvant. Dans certaines circonstances, le système peut être le siège de la formation de cavités lorsqu'on séche le film à très basse activité. Elles apparaissent après le processus d'évaporation rapide du solvant dans le cas où la fraction initiale de solvant est relativement importante. Elles résultent d'un phénomène de séparation de phase qui tend à former des domaines vides en matières en coexistence avec des domaines très dense en polymère. La séparation d'échelles de temps entre le processus d'évaporation rapide du solvant et la contraction du système est plus prononcée pour des films de faible épaisseurs. En ce qui concerne les films d'épaisseur supérieur à un micron, cette séparation d'échelles de temps n'est plus observée. Une croûte vitreuse se forme proche à la surface du films. La diffusion des molécules de solvant est donc très ralentie et une grande fraction du solvant reste piégée dans le fond du film.

Dans le cas du gonflement de films minces, le solvant pénétre le film de façon Fickienne par les zones rapides. Pendant ce processus qui est plus rapide que les temps de relaxation α, la

matrice reste contractée et la fraction volumique de vide diminue. Ceci est à l'origine d'un ralentissement de la dynamique pendant ce processus. Au temps longs, le système gonfle sous l'effet de la pression osmotique que les molécules de solvant elle exercent au sein de la matrice. Le solvant diffuse ensuite par un processus cas II.

Le même modèle physique permet de décrire la séparation de phase proche de T_g et les mécanisme de réchauffe dans les mélanges de polymères, ainsi que le séchage et le gonflement de films polymère solvant. La physique qui gouverne ces systèmes est la même et se traduit de notamment dans les effets de pression osmotiques ou encore l'effet plastifiant du vide. Ces effets sont des conséquences direct de la compressibilité. Ce modèle prend aussi en compte l'histoire du système. Dans le cas des mélanges de polymères, la cinétique de rajeunissement varie de plusieurs ordres de grandeurs suivant les conditions physiques imposées durant le vieillissement ou la réchauffe. C'est également le cas pour les mélanges polymère solvant où le temps d'induction dépend du temps de séchage avant gonflement. La vitesse du front ne dépend pas de façon significative du temps de séchage, mais dépend fortement de l'activité de gonflement. Enfin, ce modèle coarse grainé permet d'accéder à des échelles de temps comparable à l'expérience.

En termes de perspectives, une prochaines étape dans le développement du modèle serait de de définir une équation d'évolution du tenseur des contraintes couplé aux équations de la diffusion afin de prendre en compte la relaxation mécanique de façon plus réaliste. Dans les mélanges de polymères, il serait intéressant de confronter notre modèle à des expérience de diffusion de neutrons afin de valider notre approche microscopique de la dynamique à la transition vitreuse. L'influence de la taille des chaînes sur les processus de croissance des morphologies vitreuses pourrait être mise en évidence par cette même technique. Enfin, les résultats obtenus concernant la séparation de phase proche de Tg dans les mélanges de polymères ouvre la voie pour créer des matériaux de polymères nanocomposites stables dans le temps. Dans les systèmes polymères-solvant, d'un point de vue fondamental, il pourrait être intéressant d'étudier la dynamique de séchage de films en fonction de leurs épaisseurs et du type de solvant. De plus, l'influence de la taille des chaînes sur le processus de séchage pourrait être un champ d'exploration intéressant. En effet, lors du séchage de films composés de chaînes longues enchevêtrées, le temps de réorganisation de ces dernières par le mécanisme de reptation est très long. En conséquence, le couplage entre la diffusion et la contraction du système se fera sur des échelles de temps beaucoup plus grandes que lorsque que l'échantillon est composé de chaînes courtes ou d'oligomères. Enfin la présence de cavités lors du séchage de films à atmosphère sèche pourrait être étudier par diffusion de neutron.

Bibliography

[1] J. Cranks *J. of Polymer Science* **1951**, *XI*, 151

[2] Kee D.D., Liu Q ,J. Hinestroza *The Chemical Journal of Chemical Engineering* **2005**, *83*, 913

[3] Hopfenberg, H.B. Holley, R.H. et Stannet V. *Polym. Eng. Sci.* **1969**, *9*, 242

[4] Hopfenberg, H.B. Nicolais, L. et Drioli E. *Polymer* **1976**, *17*, 195

[5] Alfrey, T. Gurnee, E.F. et Lloyd W.G. *J. Polym. Sci.* **1966**, *12*, 249

[6] G.F. Billovits, C.J. Durning *Macromolecules* **1994**, *27*, 7630

[7] T.P. Gall, R.C. Lasky, E.J. Kramer *Polymer* **1990**, *31*, 1491

[8] C.Y. Hui, K.C Wu, R.C Lasky, E.J. Kramer *J. Appl. Phys* **1987**, *61*, 5137

[9] P.J. Mills, C.J Palmstrøm, E.J. Kramer *Journal of material science* **1986**, *21*, 1479

[10] R.C Lasky,C.Y. Hui, E.J. Kramer *Polymer* **1988**, *29*, 1131

[11] R.C Lasky, C.Y. Hui, E.J. Kramer *Polymer* **1988**, *29*, 673

[12] Thomas, N.L. and Windle A.H. *Polymer* **1978**, *19*, 255

[13] Thomas, N.L. and Windle A.H. *Polymer* **1982**, *23*, 529

[14] Dubreuil A.-C and al. *Macromolecules* **2003**, *36* 5157

[15] Dubreuil A.-C and al. *Polymer* **2003**, *44*, 337

[16] Doumenc A.-C and al. *J. Chem. Eng. Data* **2005**, *50* 983

[17] Saby-Dubreuil A.-C and al. *Polymer* **2001**, *4*, 371

[18] S. Peter, H. Meyer, J. Baschnagel *J. Chem. Phys*, **2009**, *131*, 14903

[19] D.E. Bornside, C.W. Macosko, L.E. Scriven *J. Appl. Phys* **1989**, *66*, 5185

[20] Doi M., Edwards S.F. *Polymer Dynamics* (Clarendon Press, Oxford) **1986**

[21] De Gennes, P.-G. "Scaling Concept in Polymer Physics", Cornell University Press, Ithaca **1979**

[22] T. Hashimoto, T. Takebe, S. Sueshiro *Polym. J.* **1986**, *18*, 123

[23] T. Hashimoto in *Currents Topics in Polymer Science* **1987**, Eds. Carl Hanser Verlag, Munich

[24] T. Hashimoto *Phase Transition* **1988**, *12*, 47

[25] B. Crist, A.R. Neirikar *Macromolecules* **1995**, *28* 890

[26] F.M. Mirabella, J.S. Barley *J. Polym. Sci. partB: polym. phys* **1994**, *32*, 2187

[27] J.D. Ferry *Viscoelastic properties of polymers* (John Wiley and Sons, Inc. 1980).

[28] U. Tracht, M. Wilhelm, A. Heuer, H. Feng, K. Schmidt-Rohr, H.W. Spiess, *Phys. Rev. Lett.* **2001**, *81*, 2727

[29] K. Schmidt-Rohr, H . W . Spiess, *Phys. Rev. Lett.* **1991**, *66*, 3020

[30] S. A. Reinsberg, X. H. Qiu, M. Wilhelm, H.W. Spiess, M.D. Ediger, *J. Chem. Phys.* **2001**, *114*, 7299

[31] M. D. Ediger, C. A. Angell, S.R, Nagel *J. Phys. Chem.* **1996**, *100*, 13200

[32] M.T. Cicerone, P.A. Wagner, M.D. Ediger *J. Phys. Chem.* **1997**, *101*, 8727

[33] M.T. Cicerone, F.R. Blackburn, M.D. Ediger, *Macromolecules* **1995**, *28*, 8224

[34] C. Y. Wang, M.D. Ediger *J. Macromolecules* **1997**, *30*, 4770

[35] Hwang Y., Inoue T., Wagner P.A., Ediger M.D., *J. Polym. Sci. , Part B: Polymer Physics* **2000**, *38*, 68-79

[36] D. Long, F. Lequeux *EPJ E* **2001** *4*, 371

[37] Long D. *Eur. Phys. J E* **2002**, *8*, 245-246

[38] S. Merabia , D.R. Long, *Eur. Phys. J. E.* **2002**, *9*, 195

[39] *Soft Matter* **2013**, *9*, 3173

[40] S. Merabia , P. Sotta, D. Long, *Eur. Phys. J. E.* **2004**, *15*, 184

[41] S. Merabia , D.R. Long, *J. Chem. Phys.* **2006**, *125*, 234901

[42] M. Souche, D.R. Long *Europhysics Letter* **2007**, *77*, 48002

[43] Paul, D.R. Newman, S., eds, "Polymer Blends", vols1 and 2, Academic Press, New York, **1978**

[44] Flory, P.J. *J. Chem. Phys* **1941**, *9*, 660-661

[45] Flory, P.J. "Principles of Polymer Chemistry", Cornell University Press, Ithaca, **1953**

[46] Huggins, M.L. *J. Chem. Phys* **1941**, *9*, 440-449

[47] Huggins, M.L. *J. Phys. Chem* **1942**, *46*, 151-158

[48] Kohlman, R.S. Joo, J. Epstein, A.J. Mark, J.E. In *Physical Properties of Polymers Handbook* American Institute of Physics, New-York, 1996

[49] Flory, P.J. Orwoll, R.A. Vrij, A. *J. Am. Chem. Soc.* **1964**, *86*, 3507-3514

[50] Flory, P.J. Orwoll, R.A. Vrij, A. *J. Am. Chem. Soc.* **1964**, *86*, 3515-3520

[51] Flory, P.J. *Discussions of the Faraday Society* **1970**, *49*, 7-29

[52] Li, H. Jiang, S. Sun, Z. An, L. *J. Polym. Sci.: Part B: Polym. Phys* **2008**, *46*, 452-459

[53] Ruzette, A.-V.G. Mayes A.M. *Macromolecules* **2001**, *34*, 1894-1907

[54] Prigogine, I. "The Molecular Theory of Solutions", North-Holland Publishing Co, Amsterdam, **1957**

[55] Prigogine, I. Trappeniers, N. Mathot, V. *Discuss. Faraday Soc.* **1953**, *15*, 93-107

[56] Prigogine, I. Trappeniers, N. Mathot, V. *J. Chem. Phys.* **1953**, *21* 559-560

[57] Prigogine, I. Mathot, V. Trappeniers, N. *J. Chem. Phys.* **1953**, *21* 560-561

[58] Merabia, S. Long, D. *Macromolecules* **2008**, *41*, 3284-3296

[59] Eichinger, B.E. Flory, P.J. *Trans. Faraday Soc.* **1968**, *64*, 2035-2052

[60] Eichinger, B.E. Flory, P.J. *Trans. Faraday Soc.* **1968**, *64*, 2053-2060

[61] Eichinger, B.E. Flory, P.J. *Trans. Faraday Soc.* **1968**, *64*, 2061-2065

[62] Eichinger, B.E. Flory, P.J. *Trans. Faraday Soc.* **1968**, *64*, 2066-2072

[63] Israelachvili, J.N. In *Intermolecular and Surface Forces*, Academic Press, London, **1992**

[64] Landau, L. Lifchitz, E.M. *Statistical physics, 3rd Edition, Part 1:Volume 5*, Elsevier Amsterdam **1980**, Chapter VII, paragraph *76*: Van der Waals Formula

[65] Kurata, M. "Thermodynamics of Polymer Solutions", Harwood Academic Publishers, London, **1982** sections *1.3.2* to *1.3.4*, p. 26-41

[66] Tompa, H., *Polymer Solutions*, Butterworths scinetific publications London **1956** section *2.12*: "Conditions of stability for ternary systems", p.43-48

[67] Nishi, T. Kwei, T.K. *Polymer* **1975**, *16*, 285-290

[68] Roe, R.J. Zin, W.C. *Macromolecules* **1980**, *13*, 1221-1228

[69] Benoît, H. Benmouna, M. *Macromolecules* **1984**, *17*, 535-540

[70] Masnada E. M., Julien G. , Long D. R. *J. Polym. Sci.: Part B: Polym. Phys* **2013**

[71] Mélange de polymère et polymère-solvant. Thermodynamique et dynamique à l'approche de la transition vitreuse, Université Claude Bernard Lyon I, 2010

[72] T.G. Lombardo, P.G. Debenedetti, F.H. Stillinger, *J. Chem. Phys.* **2006**, *125*, 174507

[73] De Groot S.R., Mazur P. *Non-Equilibrium Thermodynamics* (Dover Publications, New York) **1984**

[74] J. Colmenero, A. Arbe *Soft Matter* **2007**, *3*, 1474

[75] S. K. Kumar, S. Shenogin, R. Colby *Macromolecules* **2007**, *40*, 5759

[76] A. Alegia, J. Colmenero, K.L. Ngai, C.M. Roland *Macromolecules* **1994**, *27* 4486

[77] F. Alvarez, A. Alegria, J. Colmenero *Macromolecules* **1997**, *30* 597

[78] A. Arbe, A. Alegria, J. Colmenero S. Hoffman, L. Willner, D. Richter *Macromolecules* **1999**, *32* 7572

[79] T.P. Lodge, T.C. McLeish *Macromolecules* **2000**, *33*, 5278

[80] Safran S.A. *Statistical Thermodynamics of Surfaces, Interfaces, and Membranes* (Addison-Wesley Publishing Company) **1994**

[81] L. A. Utracki *Polymer Blends Handbook* (Kluwer Academic Plublishers) **2003**, Netherlands

[82] J. W. Cahn, *Acta. Met.* **1961**, *9*, 795

[83] J.W. Cahn, J. E. Hilliard, *J. Chem. Phys* **1959**, *31*, 658

[84] J. W. Cahn *Acta. Met.* **1966**, *14*, 1685

[85] H. E. Cook *Acta. Met.* **1970**, *18*, 297

[86] G. Brown, A. Chakrabarti *Phys. Rev. A* **1992**, *46*, 4829

[87] B. Hammouda, M. Benmouna *J. Polym. Sci.: PartB Polym. Phys* **1995**, *33*, 2359

[88] Hétérogénéités dynmaique dans les liquides surfondus. Transition vitreuse dans les films minces et en volume. Propriétés mécaniques des elastomeres chargés, Université Paris XI, 2004

[89] P.G. de Gennes *J. Chem. Phys* **1980**, *72*, 4756

[90] A.J. Kovacs, J.J. Aklonis, J.M. Hutchinson, A.R. Ramos, *J. Polym. Sci: Polm. Phys. Ed.* **1979**, *17*, 1097

[91] A.J. Kovacs, Fortschr *Hochpolym.-Forch.* **1979**, *3*, 394

[92] A.J. Kovacs *J. Polym. Sci* **1958**, *30*, 131

[93] Fujara F., Geil B., Sillescu H. and Fleischer G.l *Z.Phys.B.*, **88** (1992) 195

[94] Chow T.S. *Macromolecules*, **1980**, *13*, 362-364

[95] A. Sariban, K. Binder *Macromolecules* **1988**, *21*, 711

[96] K. Binder *J. Chem. Phys* **1983**, *79*, 6387

[97] P. Pincus *J. Chem. Phys* **1981**, *75*, 1996

[98] T. S. Chow *Macromolecules* **1980**, *13*, 362

[99] A. S. Bray *Adv. Phys.* **1994**, *43*, 357